DOE/CE/23810-75

INVESTIGATION INTO THE FRACTIONATION OF REFRIGERANT BLENDS

Final Technical Report
March 1994 - December 1995

Frank R. Biancardi
Harvey Michels
Tobias Sienel
Dennis Pandy

UNITED TECHNOLOGIES RESEARCH CENTER
411 Silver Lane
East Hartford, CT 06108

January 1996

Prepared for
The Air-Conditioning and Refrigeration Technology Institute
Under
ARTI MCLR Project Number 660-52300

Mr. Steven Szymurski - Program Manager

This program is supported, in part, by U.S. Department of Energy (Office of Building Technology) grant number DE-FG02-91CE23810: Materials Compatibility and Lubrication Research (MCLR) on CFC-Refrigerant Substitutes. Federal funding supporting this program constitutes 93.57% of allowable costs. Funding from non-government sources supporting this program consists of direct cost sharing of 6.43% of allowable costs, and significant in-kind contributions from the air-conditioning and refrigeration industry.

DOE/CE/23810-75

DISCLAIMER

The U.S. Department of Energy's and the air-conditioning industry's support for the Materials Compatibility and Lubricants Research (MCLR) program does not constitute an endorsement by the U.S. Department of Energy, nor by the air-conditioning and refrigeration industry, of the views expressed herein.

NOTICE

This report was prepared on account of work sponsored by the United States Government. Neither the United States Government, nor the Department of Energy, nor the Air-Conditioning and Refrigeration Technology Institute, nor any of their employees, nor of any of their contractors, subcontractors, or their employees, makes any warranty, expressed or implied, or assumes any legal liability or responsibility for the accuracy, completeness, or usefulness of any information, apparatus, product or process disclosed or represents that its use would not infringe privately-owned rights.

COPYRIGHT NOTICE

(for journal publications submissions)

By acceptance of this article, the publisher and/or recipient acknowledges the right of the U.S. Government and the Air-Conditioning and Refrigeration Technology Institutes, Inc. (ARTI) to retain a non-exclusive, royalty-free license in and to any copyrights covering this paper.

Investigation into the Fractionation of Refrigerant Blends

TABLE OF CONTENTS

TABLE OF CONTENTS (CONT'D.)

LIST OF TABLES

LIST OF FIGURES

LIST OF FIGURES (CONT'D.)

LIST OF FIGURES (CONT'D.)

LIST OF FIGURES (CONT'D.)

LIST OF FIGURES (CONT'D.)

ABSTRACT

As a means of complying with current and impending national and international environmental regulations restricting the use and disposal of conventional CFC and HCFC refrigerants which contribute to the global ozone depletion effects, the HVAC industry is vigorously evaluating and testing HFC refrigerant blends. While analyses and system performance tools have shown that HFC refrigerant blends offer certain performance, capacity and operational advantages, there are significant possible service and operational issues that are raised by the use of blends.

Many of these issues occur due to the fractionation of the blends. Therefore, the objective of this program is to conduct analyses and experimental tests aimed at understanding these issues, develop approaches or techniques to predict these effects and convey to the industry safe and reliable approaches.

As a result, analytical models, verified by laboratory data, have been developed that predict the fractionation effects of HFC refrigerant blends when (1) exposed to selected POE lubricants, (2) during the system charging process from large liquid containers, and (3) during system startup, operation and shutdown within various system components (where two-phase refrigerant exists), and during selected system and component leakage scenarios.

Model predictions and experimental results are presented for HFC refrigerant blends containing HFC-32, HFC-134a, and HFC-125 and the data are generalized for various operating conditions and scenarios.

BACKGROUND

Under the provisions of the Montreal Protocol, the CFCs and HCFCs, the backbone refrigerants for the air conditioning and refrigeration industry products for the last five decades are being phased out or usage is being capped, starting in 1996 because of their deleterious effect on the global ozone layer. The HVAC industry has aggressively pursued alternatives, especially new HFC single component compounds and blends as replacements for CFC and HCFCs. The level of activity devoted to insuring that safe, environmentally acceptable refrigerants and enhanced systems are utilized has increased significantly and include corporate, industry, and government sponsored efforts.

Among the new HFC refrigerants that are being evaluated, are a substantial number of refrigerant blends as substitutes for HCFC-22 in residential building air conditioning and heat pump applications. Analytical predictions and system tests have indicated there are certain performance, capacity and operational advantages and potential size and weight improvements. However, these blends can introduce significant possible service and operational issues, many of which occur due to the fractionation of the blends. Fractionation can result in increased safety hazards if the more volatile component is flammable and a leak occurs. Fractionation can have impact on the component and system design, especially those where two-phase flow occurs, such as the heat exchangers, expansion valve, compressor sump and other system components. Furthermore, fractionation can occur during charging of the system, and by the presence of the system lubricant. All of the above fractionation effects can also change performance during cooling or heating operation or can cause unacceptable higher system pressures.

Therefore, the subject program is aimed at understanding these issues, developing models that can predict these effects, techniques to overcome these potential harmful situations, and conveying to the industry safe and reliable approaches for utilizing these refrigerant blends. To validate the modeling techniques and fractionation predictions, experimental data was obtained and compared to the analytical results.

SCOPE

A four-technical task program has been defined to conduct the necessary analyses and confirming experimental tests to understand and describe fractionation effects in blends and produce useful analytical models and explanations of the physical phenomena. The program activities are organized into the following tasks, including a preprogram project review and development of detailed work plan, (Task 0), four technical tasks, (Tasks 1.0 through 4.0) and a separate report, presentation and program management task (Task 5.0).

Task 0.0 Project Review and Detailed Work Plan

Task 1.0 Lubricant Solubility Effects on Fractionation of Blends
- 1A Model Development and Review of Prior Activity/Results
- 1B Experimental Verifications

Task 2.0 Fractionation Effects from Successive Charges
- 2A Model Preparation
- 2B Bench Scale Verification Testing

Task 3.0 Fractionation Effects within System Components
- 3A Model Development and Revisions
- 3B Experimental Verification

Task 4.0 Fractionation Effects During System Leaks
- 4A Dynamic Model Development and Enhancements
- 4B Experimental Verification

Task. 5.0 Reports, Presentation and Program Management

Upon completion of the entire four-task program for Blend A (HFC-32/HFC-134a), additional effort was included in the program. This additional effort included (a) developing a refrigerant/lubricant solubility and prediction fractionation results based upon R407C (which consists of HFC-32, HFC-125 and HFC-134a), a three component blend rather than the original two-component blend "A" and comparing the model results to test data, (b) modifying the storage tank filling fractionation results for R407C, and (c) conducting Task 3 and Task 4 effort based upon R407C rather than Blend "A". The experimental and modeling tasks were to be extended for R407C and significant additions to the test facility and instrumentation data systems were to be included to gain further insight into the fractionation effects which occur within major system components, especially the heat exchangers and compressor sump, where two-phase effects and hence significant fractionation can occur.

MAJOR RESULTS AND CONCLUSIONS

A model for predicting the solubility properties of refrigerant/lubricant mixtures has been developed based on the applicable theory for the excess Gibbs energy of non-ideal solutions. The model is based on the Wohl suffix equations and used for mixtures where one component is a POE lubricant. The Wohl suffix approach was selected after an extensive study of models for describing non-ideal liquid effects. Some experimental single refrigerant/lubricant experimental data is necessary for development of the computer model.

The computer code developed (NISC) was used to predict dewpoint and bubble point conditions over a range of temperatures for refrigerant blend compositions representative of three-component R407C (HFC-32/HFC-125/HFC-134a) and two-component Blend "A" (HFC-32/HFC-134a) together with a POE-ISO 68 lubricant and compared to experimental data, provided by the manufacturer, in UTRC tests or from other sources.

The experimental results compare favorably (within 10% or better based on saturation pressure) for the R407C and lubricant at low liquid mass fractions (≤30%) and high liquid mass fractions (≥75%), especially at low temperatures (40°C or less). The model results for the Blend "A" refrigerant are generally less consistent with experimental data, especially at low refrigerant/high lubricant concentrations.

The computer model results were used for inclusion in the dynamic system modeling efforts to predict fractionation in the system compressor sump and accumulator. The NISC model appears to be a consistent reliable approach for predicting solubility and miscibility of HFC refrigerant blends and POE lubricants and should be generalized over a wider range of blends and lubricants than those studied during the program.

To predict the fractionation effects when charging HVAC systems from large tanks with non-azeotropic refrigerant blends (such as R407C and Blend "A"), two types of models were developed. In the preliminary or static model, no heat transfer effects within the tank were assumed to occur during the liquid charging process nor were time increments of discharge included. The heat transfer effects, tank configuration, time of discharge, and other factors were then included in the transient model. Both models indicated minor fractionation results except when the tank initial charge contains more than 80% vapor. Experimental data were then obtained to verify the model results for Blend "A" (a blend of HFC-32 and HFC-134a, containing 25% and 75% by weight). The experimental data were compared with the transient model and the fractionation which occurred was in excellent agreement, and the absolute fractionation changes in composition of component quantities was found to be a weak function of the time allowed for the discharge process. Time of discharge will affect the extent of discharge by an additional one or two points. Models developed for system filling from tanks of R407C provided the same results, i.e., more fractionation occurs during the discharge process if the percentage of liquid remaining in the tank were 10% (by wt) of the more volatile component.

Minor differences between the fractionation results for the static and dynamic models were found during the program.

A lumped parameter dynamic model was developed during the program and used to predict startup, operational, and shutdown trends for a split-system heat pump. The dynamic model provides valuable insight into the fractionation behavior of zeotropic refrigerant blends and helped identify system design features and components that can impact fractionation effects.

Different leakage scenarios can be simulated by the dynamic model developed and highlight potential system performance and capacity impacts. The dynamic model can predict refrigerant composition throughout the system and especially two-phase flow in the various components, as well as pressure, temperature and mass flow with time and during various leakage conditions and when withdrawing liquid or vapor.

The 0% temperature glide assumption appeared to more closely match measured system performance, pressure, temperature and refrigerant composition efforts. The opposite extreme of 100% temperature glide was found to be a less accurate prediction of operation, performance, and capacity trends.

Refrigerant Blend (R407C) containing HFC-32, HFC-125 and HFC-134a appears to be much less sensitive to fractionation than Blend A (containing only HFC-32 and HFC-134a).

An important operational consideration is that Blend A has a greater potential for flammable HFC-32 concentrations when the system is idle at low temperatures and especially during startup.

The modeling results also indicated that significant liquid in the accumulator or elsewhere in the system will change the circulating charge composition and can impact system performance. Test results obtained in the program (as well as elsewhere) substantiate this observation.

No extremes in temperature or pressure result from fractionation within the system. Furthermore, the model indicates that oil in the system absorbs some refrigerant and contributes to fractionation since HFC-134a is preferentially stored by the POE lubricant. However, the overall fractionation effect is small and impacts capacity and performance changes slightly.

However, there are design approaches which can accelerate composition change and these can provide beneficial system performance or capacity impacts. Test data developed by other researchers appear to also substantiate these observations as well.

The experimental tests to measure composition changes throughout the split-system HP system can provide an indication of fractionation, where it occurs, and how extensive in terms of composition change.

The test results confirm the observations developed by the dynamic system modeling that the circulating blend composition can be impacted severely by system leaks during shutdown (depending upon location) and much less so by leakage during system operation. The vapor leaks are generally much higher in HFC-32 concentration and therefore can be of concern due to flammability considerations.

The test data for R407C indicates less severe fractionation effects than for Blend A and essentially no performance changes or impacts after leakage during normal operation and subsequent successive recharges with the original charging composition.

Leakage during system-off or startup leaks will impact performance even when recharged with the original blend composition because of the preferential leakage of the more volatile blend component (HFC-32) of Blend A or R407C.

The heat exchanger circuit instrumentation and data obtained during the two-phase flow which occurs in the evaporator or condenser can clearly show the onset of two-phase flow and fractionation effects within that component.

SUMMARY

As a result of the comprehensive analytical and experimental efforts undertaken during this program, system operational, service and performance and capacity issues due to fractionation of selected HFC refrigerant blends being considered for HCFC replacement can be explained.

The regimes where fractionation effects are significant due to liquid charging from large and small cylinders during initial filling and during service conditions have been identified. The fractionation effects can be minimized if the storage tanks are maintained at high capacity levels and not allowed to approach 10% or less of liquid. Charging at nominal room temperatures at any reasonable rate will also likely not produce major composition changes in the charging fluid.

The presence of a POE lubricant will impact fractionation and tend to absorb different refrigerant blend components at different rates, but the effects on system operation, performance, and capacity during steady-state are generally small (or negligible), impacting capacity and performance by at most a few percent.

System design techniques are available to overcome these shortfalls and possible performance and/or capacity reductions.

The fractionation effects are generally most severe during startup where lighter components of the refrigerant blend can be separated and if a leak occurs, can result in a flammable mixture. Vapor leaks during steady-state operation are likely to be less sensitive to these safety issues with R407C because of the presence of HFC-125. R407C tends to behave more like a binary blend, but also shows generally much less tendencies toward leak scenarios that can become flammable. Finally, if after a leak occurs and the system is recharged with the initial blend composition, the performance (in terms of capacity and efficiency) will return to levels at those experienced during normal operation.

When fractionation occurs, and assuming vapor side leakage is not encountered, excessive excursions in system pressure or temperature are unlikely to occur unless substantial charge removal has occurred; as would be anticipated with current HVAC systems using HCFC and CFC single component refrigerants.

Models have been developed and verified using experimental data to predict the fractionation of refrigerant blends, (1) due to the presence of POE lubricant in the system, (2) due to liquid filling from a large or small storage tank at a range of likely temperatures, and change rates, and (3) during startup, shutdown, normal operation and various leakage scenarios likely to be encountered for split-system heat pump operation.

INTRODUCTION

National and international environmental concerns relative to the ozone-depletion effects of certain chemicals including chlorine containing CFC and HCFCs widely used in building heating and cooling systems has resulted in the banning of CFCs after 1995 and HCFC phaseout in the next century.

While zero-chlorine containing HFC refrigerants have been identified as potential substitutes or alternatives for CFC-11 and -12, candidate replacements for HCFC-22, the most widely used refrigerant in residential heating and cooling systems in the U.S. (and probably worldwide), have focused on refrigerant blends. Many of the suggested blends are zeotropic in nature, i.e., their vapor and liquid phase will exist at different mass fractions at given pressure and temperature conditions.

This tendency to fractionate has introduced concerns in the HVAC industry as the ultimate viability of zeotropic blends for refrigerant use because of potential deterious effects on performance, safety, service and operability.

Early drop-in tests when substituting two-and-three-HFC component blends as candidates for replacement to HCFC-22 have not clarified the impact of fractionation on HVAC residential systems. Soft-optimization efforts have shown that different heat exchangers, valving, and components may be required in the blends that fractionate.

To provide a better understanding of fractionation results in central HVAC residential sized systems that heat and cool, ARTI initiated this program with UTRC. The earliest efforts were focused on a two-component blend (such as Blend A) to determine if the fractionation effects could be modeled and the models could also be verified with experimental data.

Once the model potential was proven and verified, a second phase to include a three-component refrigerant blend was incorporated in the program. Analysis and tests were then conducted for the R407C type refrigerant blends.

The results, conclusions, and insights provided by this work are extensive and useful. To provide a reasonable approach to transferring this knowledge to the HVAC industry personnel interested in fractionation effects, this report has been organized along the efforts undertaken to explain different fractionation issues.

Therefore, in Task 1, the results, models, correlations for the fractionation produced when refrigerant blends are mixed together with lubricants are described first. The results for both Blend A and R407C refrigerants are presented in this section. Tasks 2, 3, and 4 are described separately as well with data, analysis and comparisons with experimental results shown for Blend A and R407C in each Task section.

Appendix A, B.1 and B.2, contain extensive equations and approaches used for the solution-theory model, and for the Blend A test data (B.1) and R407C test data (B.2) for those interested in all of the test conditions and details obtained in the program.

TASK 1. SOLUBILITY EFFECTS ON FRACTIONATION OF BLENDS DUE TO PRESENCE OF A LUBRICANT

Background

The addition of lubricants to refrigerants, either single component hydrofluorocarbons or the newer multicomponent blends, is necessary to reduce bearing friction and to minimize gas leakage at gaskets and fittings. The primary considerations in choosing a lubricant are its chemical compatibility with the refrigerant type and the required viscosity for the service application. In the case of refrigerant blends, a new problem arises since the individual refrigerant components may exhibit different solubilities in the lubricant. These different component solubilities can give rise to fractionation (distillation) effects in the evaporator or compressor sump which differ from the vapor-liquid equilibrium conditions in the absence of a lubricant. These effects are the result of several possible solution characteristics:

1) Refrigerant/lubricant mutual solubility limitations may result in a two-liquid phase region under certain conditions of composition and temperature.

2) Solubility of refrigerant in the lubricant held in the compressor (sump) may affect the equilibrium composition of the evaporator vapor and the lubricity characteristics of the lubricant.

3) Solubility of lubricant in refrigerant blends may result in composition shifts owing to refrigerant-lubricant interactions.

The inclusion of refrigerant/lubricant interactions may thus impact both cycle analysis and system performance. If these interactions are significant (non-ideal solution behavior), they may result in detrimental performance and lower system operating efficiency.

Analysis of Applicable Theory

In Task I of the program, an analysis of applicable theory for predicting the solubility of refrigerant-oil mixtures was carried out. Models based on both non-ideal solution theory and on an equation-of-state have been examined. The former require a large amount of experimental VLE data; the latter model involves the difficult task of describing the PVT behavior of two substances with drastically different boiling points. UTRC has mainly based the analysis on solution theory models. Several solution theory models have been described in the literature which relate non-ideal behavior, as measured for example by the excess Gibbs energy, to composition, temperature and pressure of the mixture (Ref. 1). A solution theory model for refrigerant/lubricant mixtures can be parameterized using limited data sets for the solubility of refrigerant/lubricant pairs. Owing to the large size differences between refrigerant and lubricant molecules, the model must account for differences in their effective molar volumes. In addition, the model should also be capable of predicting immiscible regions. Finally, the model should rely mainly on data for binary refrigerant/refrigerant and refrigerant/lubricant pairs. Ternary mixture interaction parameters are difficult to extract from experimental solubility data and the most useful model will be based on a theoretical description of the interaction parameters that minimizes the need for ternary or quaternary mixture data. Solution theory models are generally

reliable under the temperature and pressure conditions normally encountered in HVAC system operation.

UTRC has examined experimental solubility data for HFC-32/POE, HFC-125/POE and HFC-134a/POE mixtures. The POEs examined were mainly pentaerythritol esters, of both branched and straight chain formulations, with average molecular weights ranging from 500-800. Experimental data for mixtures of these lubricants with HFC-32, HFC-125 and HFC-134a were obtained from literature reports (Refs. 2-7), from manufacturer's tabulations (Refs. 8 and 9) and from experimental data collected in our laboratory. Altogether twenty sets of solubility data were analyzed. These data were reduced to pressure-composition isotherms, as required for rigorous thermodynamic solution, modeling.

Mathematical Model for Solubility of RefrigerantlLubricant Mixtures

The vapor-liquid equilibria of a mixture can be described in terms of the component fugacities in the liquid and vapor phases (Ref. 1). At equilibrium, we have

$$f_i^v = y_i P_T \phi_i^v = f_i^\ell = x_i \gamma_i P_i^v \phi_i^* \mathcal{F}_i^\ell \qquad (1)$$

where
- y_i = vapor phase molar composition of component i,
- P_T = total system pressure at temperature T,
- ϕ_i^v = vapor phase fugacity coefficient which, for moderate pressure, can be estimated from second virial coefficient data,
- x_i = liquid phase molar composition of component i,
- γ_i = liquid phase activity coefficient,
- P_i^v = vapor pressure of pure component i at temperature T,
- ϕ_i^* = fugacity coefficient for pure i at the system T and P,
- $\mathcal{F}_i^\ell$ = Poynting factor for compressibility of the liquid phase.

For $\phi_i^v = \gamma_i = \phi_i^* = \mathcal{F}_i^\ell = 1.0$, this analysis reduces to ideal solution behavior (Raoult's Law). Choosing a fixed value of the system temperature, the fugacity coefficients are evaluated in terms of the vapor phase virial expansion as follows:

$$\ln \phi_i^v = \frac{P_T}{RT}[2\sum_j y_j B_{ij} - B_{mix}]; \qquad B_{mix} = \sum_i \sum_j y_i y_j B_{ij} \qquad (2)$$

Correspondingly, for pure component i, we have

$$\ln \phi_i^* = \frac{B_{ii} P_T}{RT} = Z_{ii} - 1 \qquad (3)$$

The Poynting factor is normally negligible for moderate pressures, but may be estimated from molar volume data for pure liquid component i :

$$\ln \mathcal{F}_i^\ell = \int_{P_i^V}^{P_T} \frac{V_i^\ell}{RT} dP = \frac{V_i^\ell (P_T - P_i^V)}{RT} \qquad (4)$$

Finally, we combine the fugacity coefficients and Poynting factor into a correction term, F_i,

$$F_i = \exp\left[\frac{B_{ii} P_T}{RT} + \frac{V_i^{\ell}(P_T - P_i^V)}{RT} - \frac{P_T}{RT}\left(2\sum_j y_j B_{ij} - B_{mix}\right)\right] \quad (5)$$

The vapor-liquid equilibria for component i (Eq. 1) can then be written as

$$y_i P_T = x_i \gamma_i P_i^V F_i \quad (6)$$

The correction term, F_i , can be evaluated from liquid density and second virial coefficient data for pure refrigerants. One convenient source is the tabulation given in the NIST REFPROP database.[10] The difficult part of this analysis is the representation of the liquid phase activity coefficients, γ_i. These liquid activity coefficients may be extracted from experimental data or estimated using group additivity models such as UNIFAC (Ref. 11). The latter approach is difficult at present due to limited knowledge of the chemical formulations of the POEs and the lack of reliable functional group interaction parameters.

Preliminary evaluation of the non-ideal behavior of HFC-32/POE, HFC-125/POE and HFC-134a/POE binary mixtures indicated both positive and negative deviations from ideal solution behavior. Many of the proposed forms for liquid phase activity coefficients cannot mathematically represent such behavior. The Wilson model (Ref. 12) for the excess Gibbs energy, for example, is not applicable over the entire refrigerant/lubricant composition range. Various modifications of the Wilson model have been proposed, including those described in the literature as the Heil (Ref. 13), NRTL (Ref. 14), and T-K (Ref. 15) equations. All of these equations represent local composition models in an attempt to incorporate effects of molecular size as well as mixture concentration. Their derivations, however, are mainly empirically based, and can lead to computed solution parameters that lack physical meaning.

After an extensive study of models for describing non-ideal liquid phase effects, the Wohl [3]-suffix equations (Ref. 16) were chosen. Using the Wohl [3]-suffix expansion, the excess Gibbs energy can be represented as:

$$\frac{g^E}{RT\sum_j^n x_j q_j} = 2\sum_{\substack{i,j \\ i\neq j}}^{n} a_{ij} z_i z_j + 3\sum_{\substack{i,j \\ i\neq j}}^{n} a_{iij} z_i^2 z_j + 6\sum_{\substack{i,j,k \\ i\neq j\neq k}}^{n} a_{ijk} z_i z_j z_k \quad (7)$$

where z_i = generalized volume fraction (q-fraction) = $\dfrac{x_i q_i}{\sum_j^n x_j q_j}$; q_i = effective volume of species i upon collision. The a_j, a_{iij}, a_{ijk} are the interaction parameters describing binary and ternary interaction strengths. For binary pairs, this leads to the following form for the liquid phase activity coefficients:

$$\ln \gamma_1 = z_2^2 [A_{12} + 2z_1 (\frac{q_1}{q_2} A_{21} - A_{12})] \; ; \quad \ln \gamma_2 = z_1^2 [A_{21} + 2z_2 (\frac{q_2}{q_1} A_{12} - A_{21})] \qquad (8)$$

A_{12} and A_{21} are defined as follows:

$$A_{12} = q_1 (2a_{12} + 3a_{122}) \; ; A_{21} = q_2 (2a_{12} + 3a_{112}) \qquad (9)$$

We note that $A_{12} \neq A_{21}$ in this analysis. Eq. (8) was utilized to reduce the experimental solubility data for the six binary pairs: HFC-32/HFC-125, HFC-32/HFC-134a, HFC-125/HFC-134a, HFC-32/POE-ISO 68, HFC-125/POE-ISO 68 and HFC-134a/POE-ISO 68.

The analogous forms to Eq. (8) for ternary and quaternary mixtures have been developed and are shown in Appendix A. This Wohl [3]-suffix model has been developed into a Non-Ideal Solution Code (NISC) that, in its present form, describes HFC-32/HFC-125/HFC-134a/POE-ISO 68 mixtures over the entire composition range.

Discussion of Results

In this study UTRC analyzed in detail a POE-ISO 68 formulated as mixed esters of pentaerythritol with both straight and branched chain acids since structural and thermophysical property data are available for this POE. Data were collected from several sources (Refs. 2-9) on the solubility of the binary pairs: HFC-32/POE, HFC-125/POE, and HFC-134a/POE. In addition, refrigerant/lubricant solubility data for twelve different POE formulations, ranging in molecular weight from 525 to 1500, were examined in some detail. These included all of the mixtures reported by Henderson (Ref. 4), Cavestri (Ref. 5), Martz and Jacobi (Ref. 6), and Grebner and Crawford (Ref. 2), as well as data supplied by the manufacturers (Refs. 8 and 9). There are scatter in the data from these separate sources, which covered a temperature range of 0°-80°C. UTRC relied most heavily on the data supplied by the POE manufacturers which seemed internally to be more consistent. Data on the refrigerant pairs: HFC-32/HFC-125, HFC32/HFC-134a, HFC-125/HFC-134a, were also collected from several sources and compared with the predictions of the CSD equation-of-state model in REFPROP (Ref. 10). In addition, laboratory measurements of R-32/R-134a/POE mixtures were carried out at UTRC over the temperature range of 20-50°C. All experimental data have been analyzed within the Wohl [3]-suffix model.

Using the solution theory model described above, we have analyzed the P-T-X solubility data for binary mixtures to extract the liquid phase activity coefficients. As shown in Fig. 1.1, HFC-32 exhibits both positive and negative deviations from an ideal solution (g=1.0), illustrating the difficulty in modeling HFC/POE mixtures, which exhibit such behavior as a common characteristic. Few data are available for HFC-32/POE and HFC-125/POE mixtures since HFC-32 requires special handling owing to its flammability characteristics and HFC-125 is currently not used as a single component refrigerant. Henderson (Ref. 4) has reported data for several HFC-32/POE mixtures for both low refrigerant concentrations: 0-30 weight percent, and for high refrigerant concentrations: 80-100 weight percent. HFC-32 shows immiscibility regions with several of the mainly straight chain POEs for high refrigerant concentration mixtures. The HFC-32/HFC-125, HFC-32/HFC-134a, and the HFC-125/HFC-134a binary pairs exhibit small

deviations from ideal liquid phase behavior. For internal consistency, these refrigerant pairs were also analyzed using the Wohl [3]-suffix model.

The non-ideal liquid behavior of the refrigerant/lubricant binary pairs is illustrated in Figure 1.2 where we represent the logarithm of the activity coefficients of HFC-32, HFC-125 and HFC-134a (components 1) as functions of the q-fraction of POE-ISO 68 (component 2). A straight line fit indicates that the [3]-suffix form, represented by Eq. (8), is a satisfactory representation. The parameters for the data fit are the A_{ij} and the q-ratios. We find that measuring concentration in molar units is not satisfactory, since the refrigerant and lubricant molecules exhibit large size and volume differences. Figure 1.3 illustrates that the q-ratio is poorly represented as 1.0, which would be the case for molecules of similar size. Further, identifying the q-ratio as the molar volume ratio of the molecules, which would be an appropriate choice for small molecule/polymer solutions, is also unsatisfactory. HFC/POE mixtures have properties somewhere between these two limiting cases and the q-ratios must be treated as adjustable parameters. Experimental data for the binary pairs: HFC-32/POE, HFC-125/POE and HFC-134a/POE were all least-squares reduced to the functional form represented by Eq. (8) for the temperature range: 0°- 60°C. The activity coefficients, γ_i, indicated a temperature dependence over this range but the q-ratios were relatively constant with temperature. This is physically reasonable since the q-ratios are a measure of the relative size of the refrigerant and lubricant molecules, which should be nearly temperature independent. The coefficients, A_{ij}, are often taken to be either independent of temperature (athermal-solution behavior) or inversely proportional to temperature (regular-solution behavior). Neither limit is accurate for the refrigerant/lubricant pairs under study and we have chosen to fit the A_{ij} to the empirical form: $A_{ij}(T) = a + b/T$.

The optimum refrigerant/lubricant q-ratios were found to be:

$$\frac{q_{HFC-32}}{q_{POE}} = 0.28 \qquad \frac{q_{HFC-125}}{q_{POE}} = 0.62 \qquad \frac{q_{HFC-134a}}{q_{POE}} = 0.58$$

There are three refrigerant/refrigerant q-ratios that can be derived from the above data.

$$\frac{q_{HFC-32}}{q_{HFC-125}} = 0.45 \qquad \frac{q_{HFC-32}}{q_{HFC-134a}} = 0.48 \qquad \frac{q_{HFC-125}}{q_{HFC-134a}} = 1.07$$

These refrigerant/refrigerant q-ratios can be compared with ratios of the molecular structure parameter, r, of the UNIQUAC[11] solution theory model:

$$\frac{r_{HFC-32}}{r_{HFC-125}} = 0.59 \qquad \frac{r_{HFC-32}}{r_{HFC-134a}} = 0.63 \qquad \frac{r_{HFC-125}}{r_{HFC-134a}} = 1.07$$

The UNIQUAC r-parameters are interpreted as a measure of the size of a molecule. These r-ratios indicate good agreement with the q-ratios derived from our optimum fit of experimental refrigerant/lubricant data. The internal consistency and physically meaningful interpretation of solution parameters in the Wohl model is evident. This situation is in contrast to modified

Wilson solution theory models, where fitted refrigerant/lubricant interaction parameters can even change sign, depending on the exact form of the Wilson model equations.

Comparison of Calculated and Experimental Solubility Data

Calculated solubility data for three refrigerant/lubricant mixtures: 1) HFC-134a/POE, 2) Blend A/POE, and R-407C/POE, are shown in Figs. 1.4-1.6, respectively. The data are presented as P-X diagrams for several isotherms. Experimental data from several tabulated sources (Refs. 6, 8 and 9) are shown on Figs. 1.4 and 1.6 for HFC-134a/POE and R-407C/POE mixtures, respectively. In Fig. 1.7, we illustrate our experimental data for the mixtures 90/10, 36/64 and 10/90 (refrigerant blend/POE) for Blend A, a 25/75 blend of R-32/R-134a. The solid lines are calculated from our ternary solution theory model. Agreement in the refrigerant rich region (90/10) is excellent over the temperature range that was examined. The measured temperature dependence of the data in the lubricant rich region (10/90) suggest that equilibrium was not fully achieved in these runs. At the lower temperatures, an observed gradual downward drift in the pressure probably corresponded to incomplete mixing. The intermediate region data were taken with a large volume vessel and corrections were applied to the composition of the charged mixture to properly account for the large amount of refrigerant that was present in the vapor phase.

Predicted Fractionation Effects Using NISC

The fractionation effects arising from selective solubility of the individual components of a refrigerant blend into the lubricant are illustrated in Fig. 1.8. For the pure refrigerant case (x_{mass}=1.0), the vapor mass fraction is determined solely by the relative volability of the refrigerant components. Such data are available from REFPROP or similar refrigerant mixture codes. As the mass fraction of lubricant is increased in the liquid phase, we see only a small lubricant effect in Blend A/POE mixtures until a POE mass fraction of ~ 0.1 is reached. For R-407C/POE mixtures, however, the NISC model predicts significant selective fractionation of R-32 into the vapor phase below a POE mass fraction of ~ 0.2. This lubricant effect is temperature dependent and appears to be most severe under low temperature vapor-liquid equilibrium conditions. These data suggest that the heavier refrigerant components (R-125 and R-134a) are preferentially held in the lubricant and that the vapor phase is enriched in the lighter, more volative refrigerant components. Much more experimental evidence must be obtained, however, before any general conclusions can be drawn. The performance of the Wohl [3]-suffix model in describing the solubility of HFC-32/HFC-125/HFC-134a/POE mixtures is clearly satisfactory. Further improvements in the NISC model through adjustment of the ternary interaction parameters, are currently being undertaken in other programs at UTRC.

References

1. See for example: J. M. Prausnitz, R. N. Lichtenthaler and E. G. de Azevedo, Molecular Thermodynamics of Fluid-Phase Equilibria, 2nd Ed., Prentice-Hall, NJ (1986).

2. J. J. Grebner and R. R. Crawford, ASHRAE Trans. 99-1, 380 (1993).

3. Corr, F. T. Murphy, B. E. Gilbert and R. W. Yost, ASHRAE Trans. 99-2, 1123 (1993).

4. R. Henderson, Solubility, Viscosity and Density of Refrigerant/Lubricant Mixtures, Final Tech. Rpt. DOE/CE/23810-34, Spauschus Assoc., April 1994.

5. R.C. Cavestri, Measurement of Viscosity, Density and Gas Solubility of Refrigerant Blends in Selected Synthetic Lubricants, Final Tech. Rep. DOE/CE/23810-46, Imagination Resources, May 1995.

6. L. Martz and A. M. Jacobi, Refrigerant-Oil Mixtures and Local Composition Modeling, ACRC TR-68, U. of Illinois, October 1994.

7. M. Yokozeki, Solubility and Viscosity of Refrigerant-Oil Mixtures, Proc. Int. Ref. Conf., Purdue (1994).

8. P-T-X Diagrams for R-134a, R-410A and R-407C mixtures with Castrol Icematic POEs, private data communication, Castrol, Inc. (1994).

9. P-T-X Diagrams for R-134a, R-410A and R-407C mixtures with ICI Emkarate POEs, private data communication, ICI (1995).

10. Gallagher, M. McLinden, G. Morrison and M. Huber, NIST Thermodynamic Properties of Refrigerant and Refrigerant Mixtures Database (REFPROP), NIST Standard Reference Database 23, Version 4.0 (1994).

11. Fredenslund, J. Gmehling, M. L. Michelsen, P. Rasmussen and J. M. Prausnitz, Ind. Eng. Chem. Process Des. Dev. 16, 450 (1977).

12. M. Wilson, J. Am. Chem. Soc. 86, 127 (1964).

13. F. Heil and J. M. Prausnitz, AIChE J. 12, 678 (1966).

14. Renon and J. M. Prausnitz, AIChE J. 14, 135 (1968).

15. Tsuboka and T. Katayama, J. Chem. Engr. Japan, 8, 181(1975).

16. Wohl, Trans. AIChE, 42, 215 (1946).

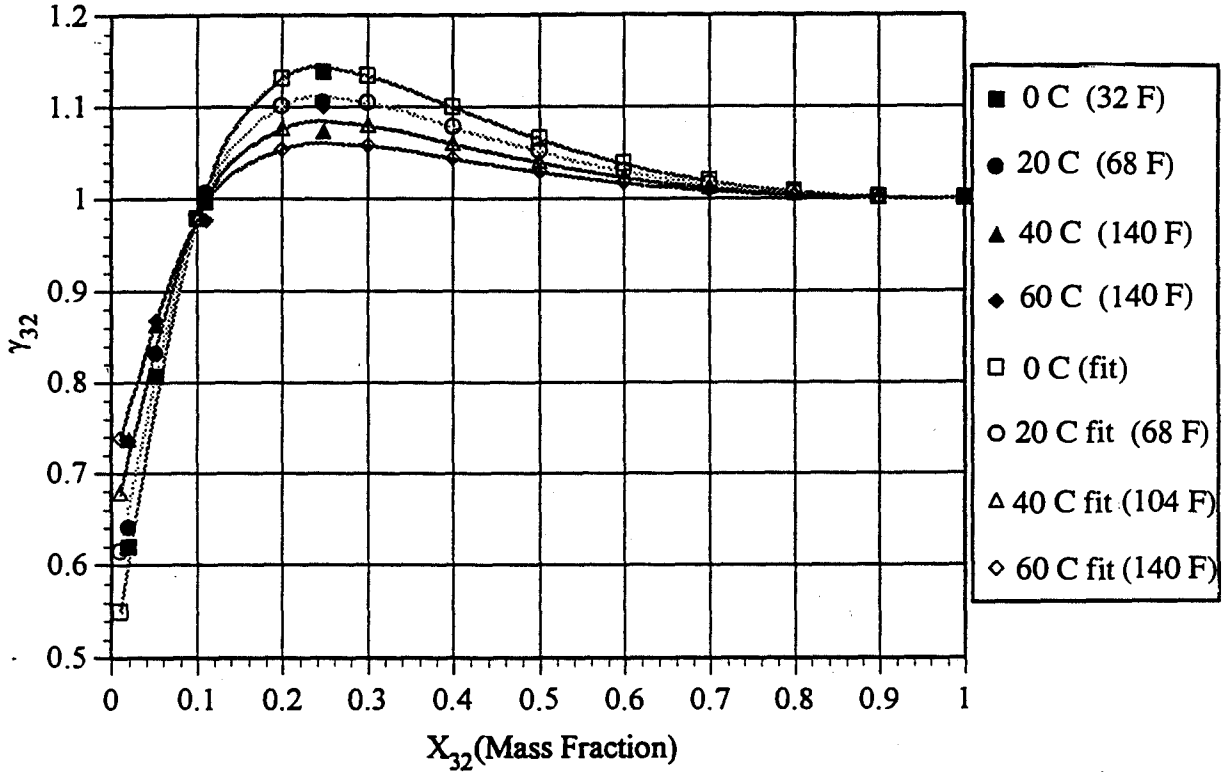

Fig 1.1 Liquid Phase Activity Coefficient for HFC-32/POE-ISO 68 Mixture

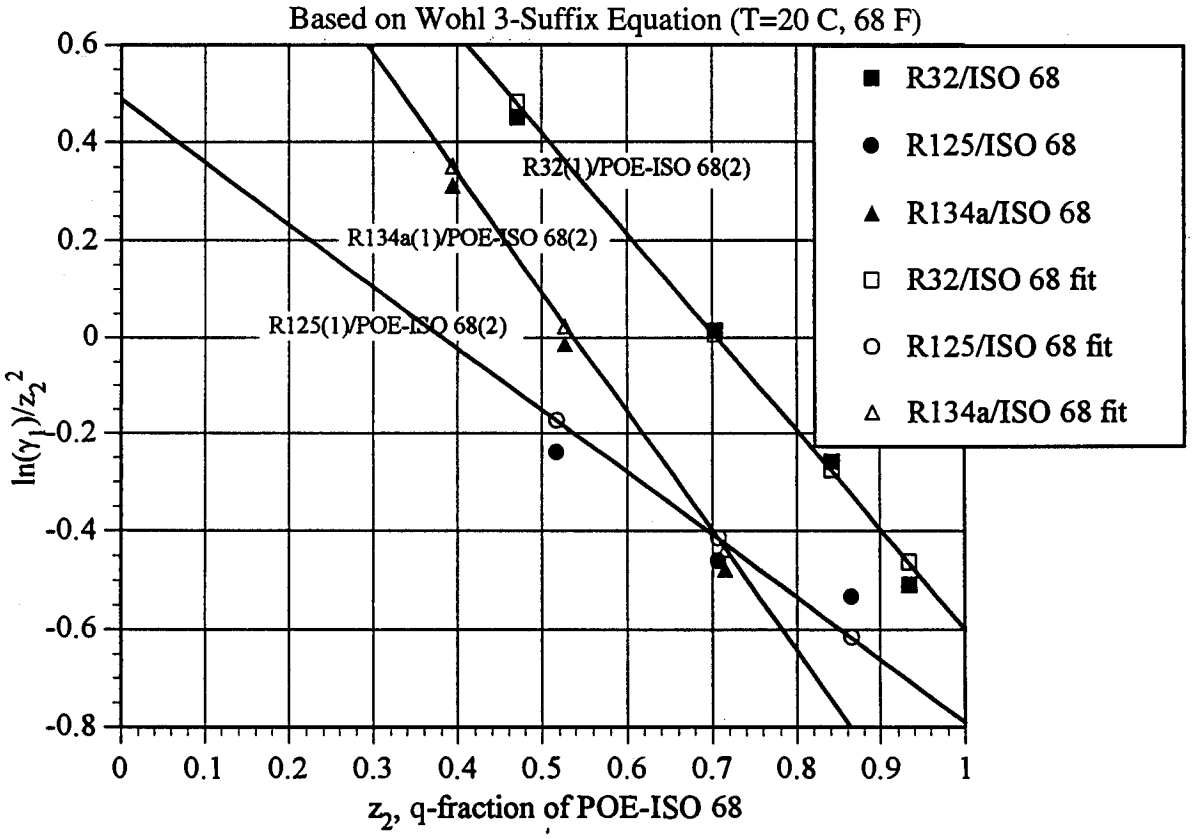

Fig. 1.2 Binary Activity Coefficients for HFC-32/HFC-125/HFC-134a/POE-ISO 68 Mixtures Based on Wohl 3-Suffix Equation (T=20 C)

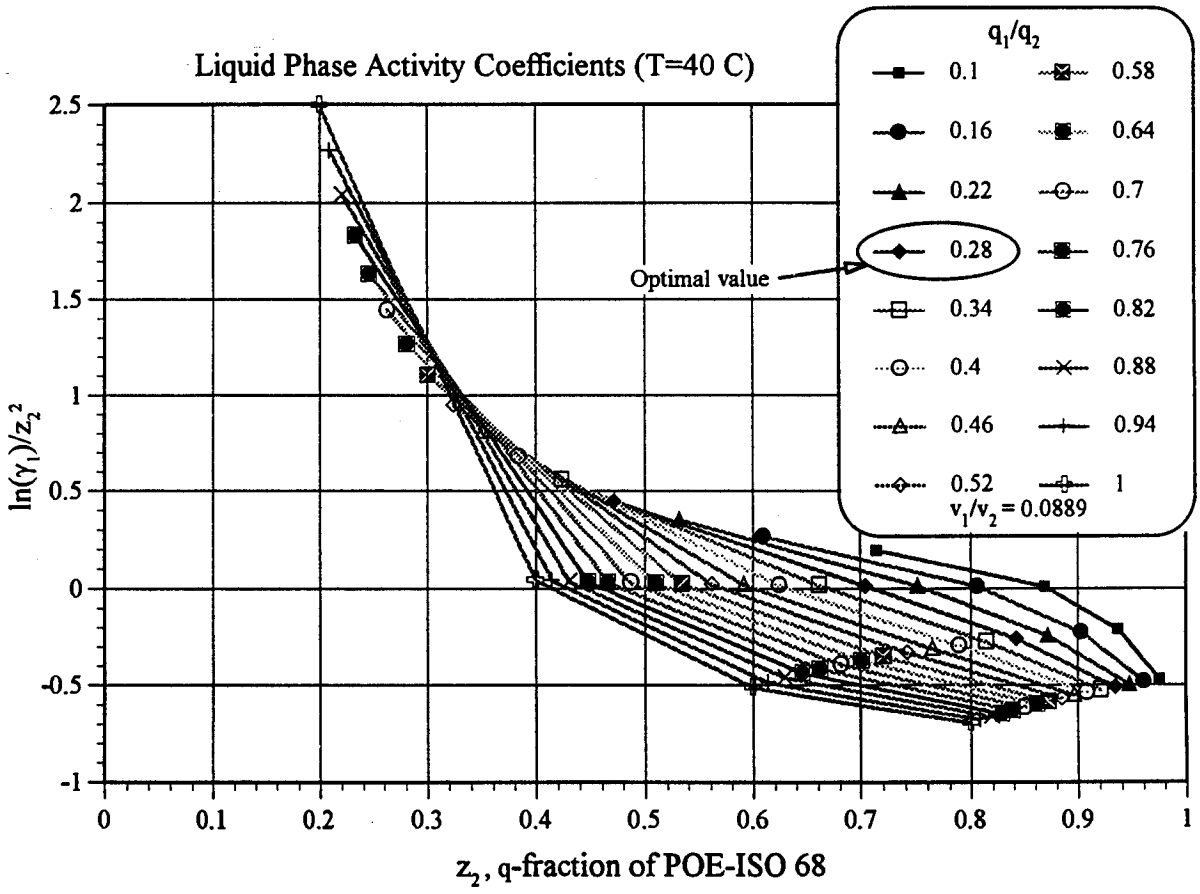

Fig. 1.3 Experimental HFC-32(1)/POE-ISO 68(2) Liquid Phase Activity Coefficients (T=40 C)

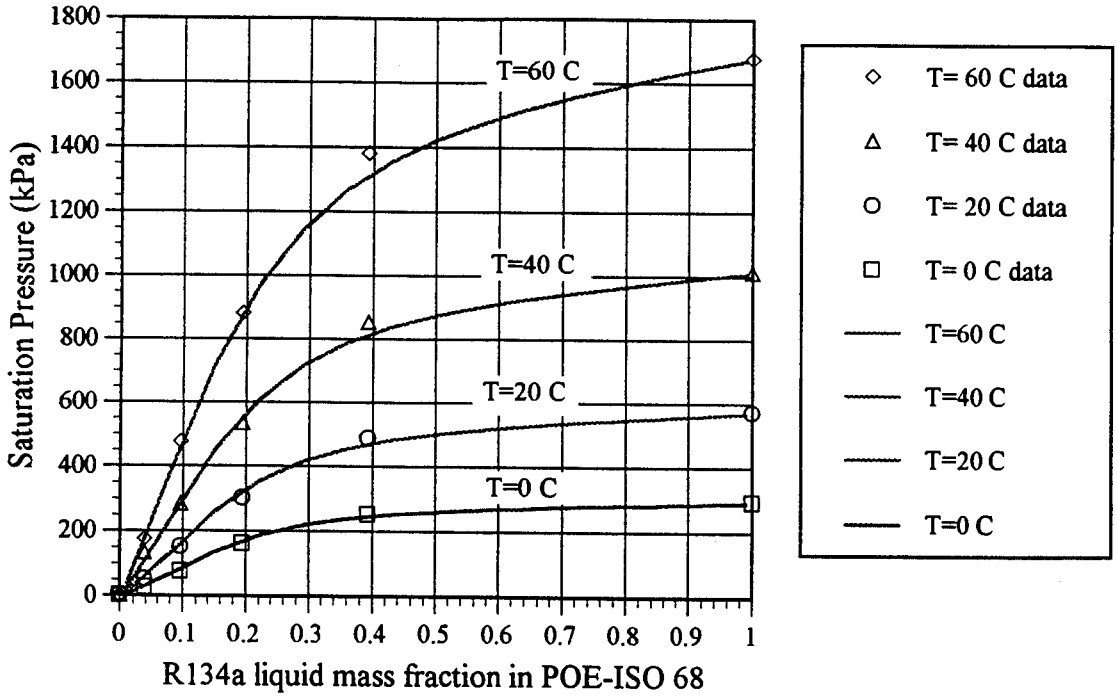

Fig. 1.4 R134a Experimental Data vs. NISC Predictions

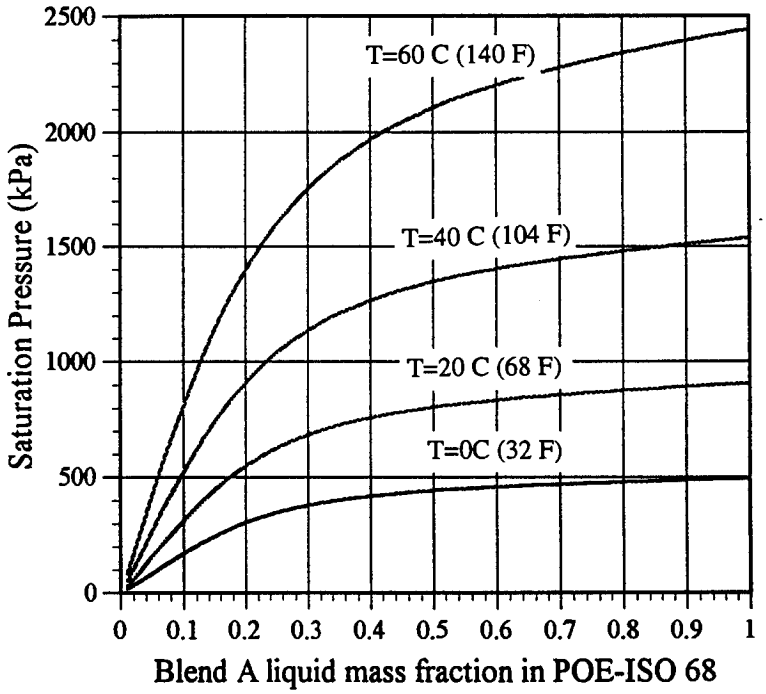

Fig. 1.5 Blend A NISC Predictions

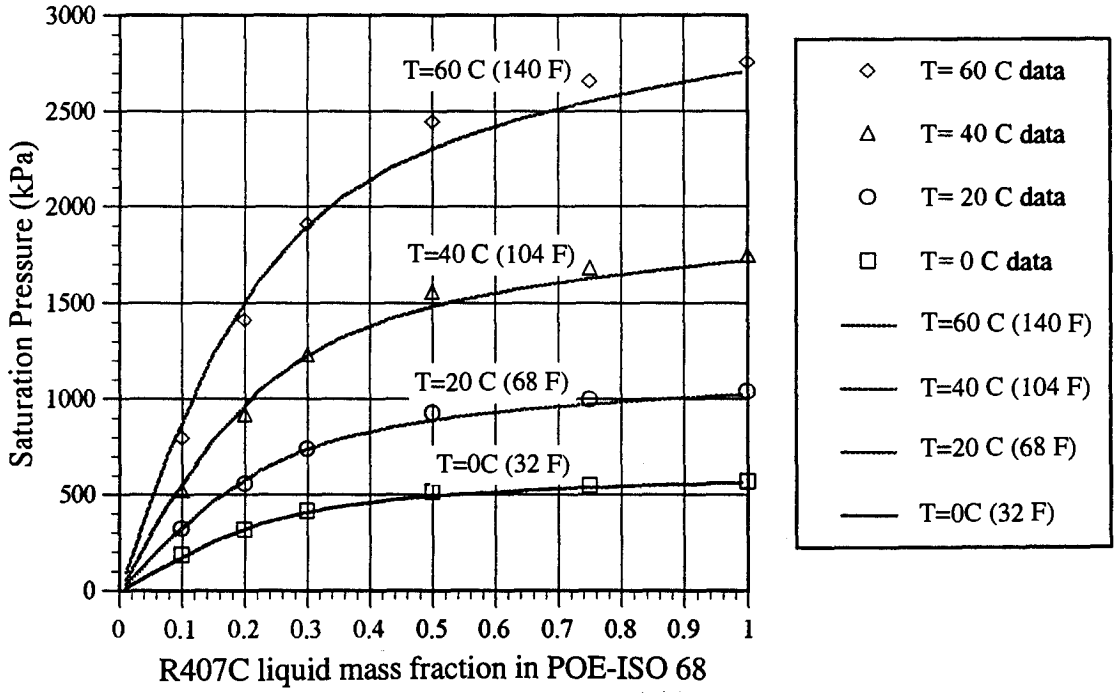

Fig. 1.6 R407C Experimental Data vs. NISC Predictions

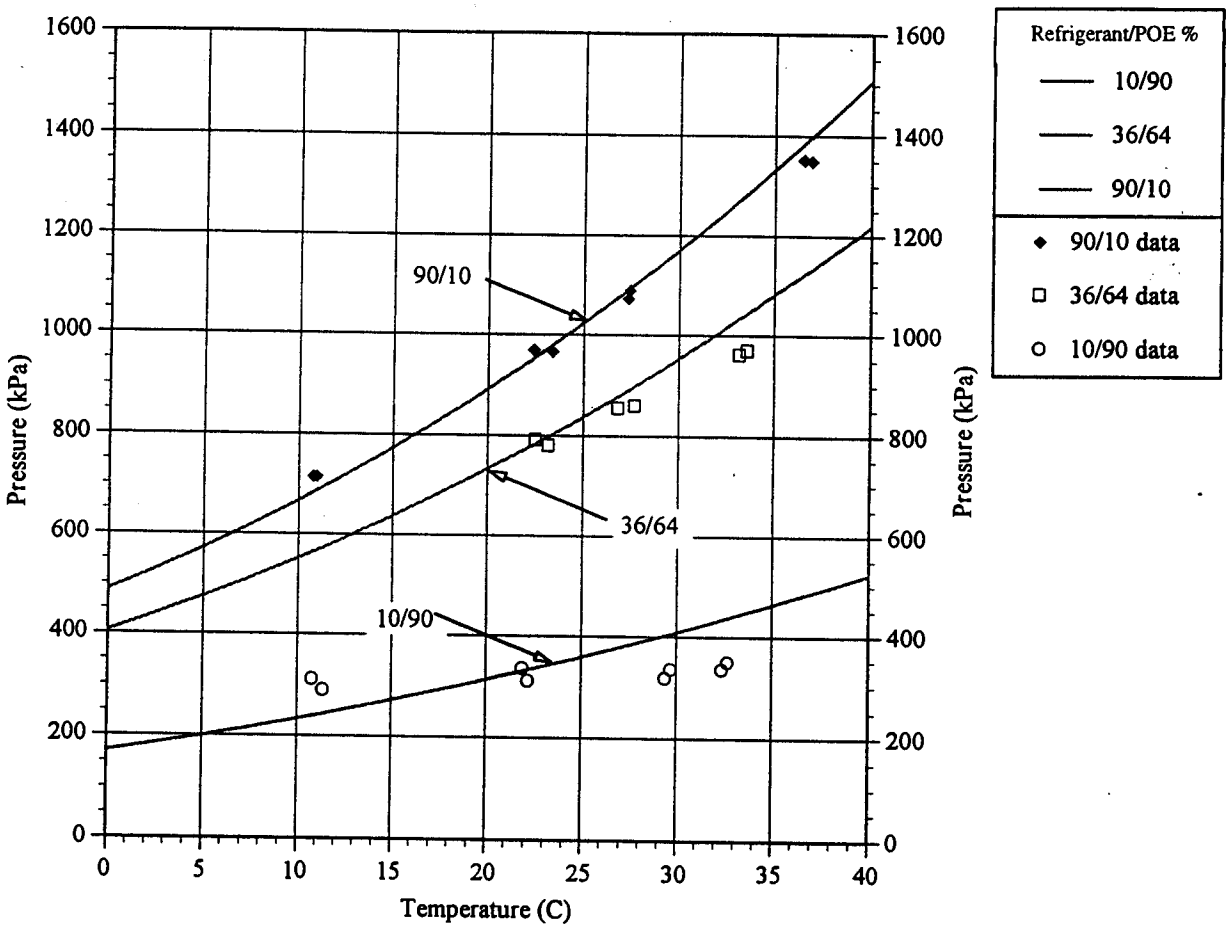

Fig. 1.7 Comparison of Experimental and NISC Predictions for Blend - A/POE-ISO 68 Mixtures

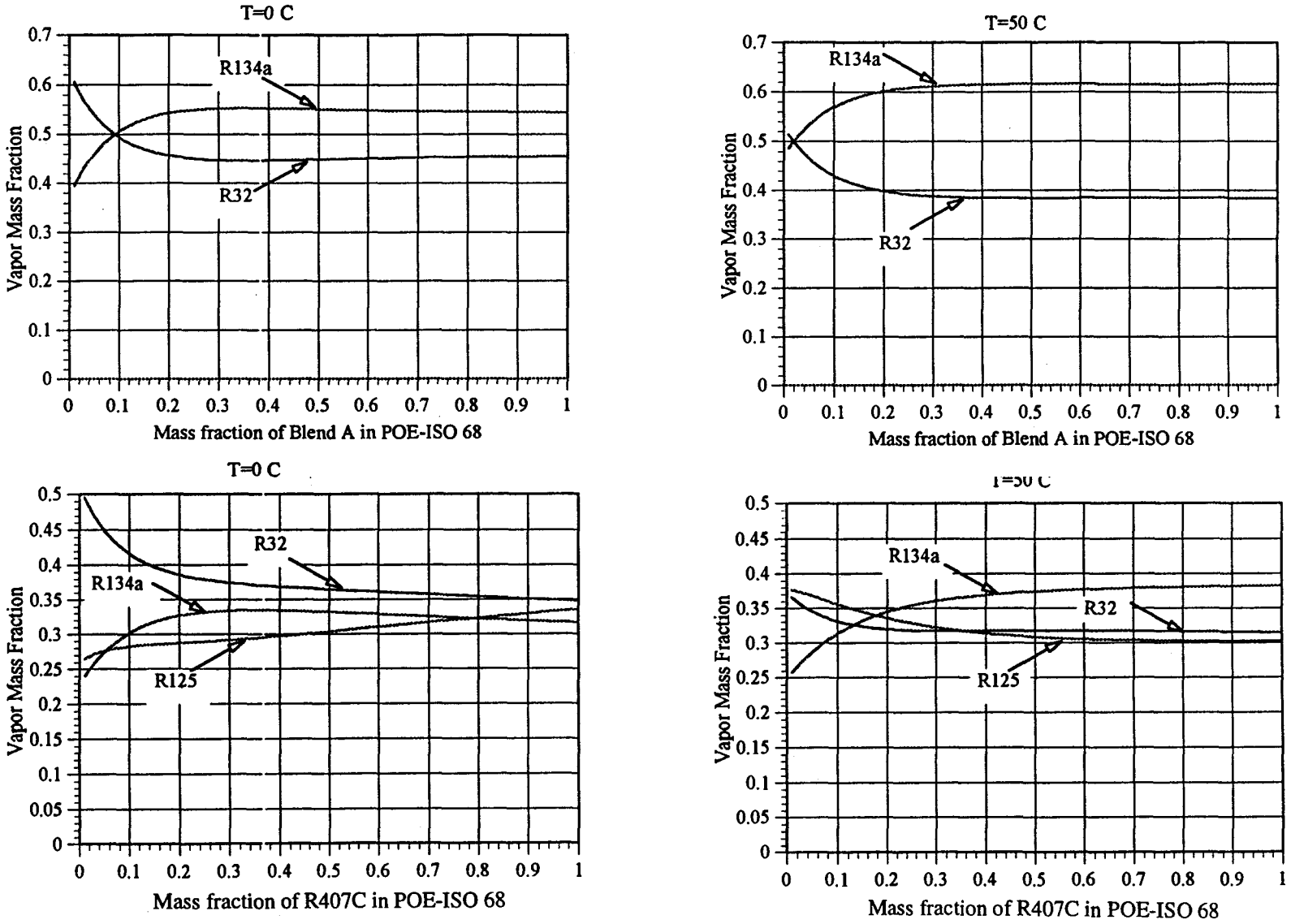

Fig. 1.8 Equilibrium Vapor Composition Above Blend A and R407C/POE-ISO 68 Mixtures

TASK 2 - FRACTIONATION EFFECTS DURING SYSTEM FILL FROM A LARGE STORAGE TANK

Background

Residential HVAC systems are typically sold with the refrigerant partially charged. As the systems are produced, refrigerant from a large storage tank is generally used to charge each unit. In addition, service personnel periodically top-off or totally recharge the systems from smaller cylinders in the course of maintenance. Both of these scenarios may present problems when a nonazeotropic blend of refrigerants is used as the charge. As the amount of charge in the storage or charging tanks is depleted, the composition of the remainder will change. The questions to be answered are: to what degree does the composition change, and what are the important parameters affecting the composition shift.

The objective of this program task was to develop analytical models that predict fractionation effects under various conditions and then to experimentally validate the models using test data obtained in the program.

In the sections which follow, the two different analytical models will be described and results will be presented for each model over a range of parameters as noted above. Fractionation results from tests with Blend A (R32/R134a) will be presented and compared with the model results. Model results will be shown for R407C. Finally, the test set up and procedures used in the Task 2 experimental program will be described and presented.

Analytical Evaluations

Two models were constructed to determine the fractionation properties of the two mixtures studied. The first model, a static model, was used to determine the composition shift under slow leak conditions. The second model, a transient model, was used to determine the fractionation under fast discharge conditions. A large, typically 500 gallon, tank for refrigerant storage was used as the model basis.

Static Equilibrium Model and Sample Results

This model predicts the effect of fractionation in a tank with no thermal effects. Liquid is discharged in roughly equal volume fraction steps, the size of which depended on the number of discharge steps chosen. After each discharge step, the mass remaining in the tank once again comes to equilibrium The procedure used to calculate the fractionation effects is described below.

1) First the initial concentration is fractionated into liquid and vapor compositions, depending on the specified initial liquid volume fraction

2) Next, the liquid volume to be discharged is calculated based on an estimate of the total liquid volume to be discharged and the number of discharge steps.

3) The discharged liquid is removed in an instantaneous step (i.e. no transient fractionation or thermal effects). The mass of each refrigerant removed is kept track of and subtracted from the total refrigerant mass, which yields a new total composition.

4) The volume of the liquid removed is filled with vapor boiled off from the liquid phase. The volume of liquid required to fill this vapor volume is estimated in an iterative process based on the old liquid and vapor densities.

5) The new quality is estimated and new liquid and vapor compositions are found. The final discharge step quality is found by iteration, until the total volume balances with the input volume (500 gallons). The final discharge step quality is used to find the new liquid and vapor compositions.

6) Steps 2-5 are repeated until the total number of steps has been completed.

Static Model Results for Blend A

The number of discharge steps has an effect on the final composition remaining in the tank, as shown (for Blend A) in Figure 2.1 a. A finite number of steps would be analogous to a storage tank being used to charge a number of units on a final assembly line. An infinite (or very large) number of steps would approach a constant small leak in a storage tank. A summary of the results of the first model for Blend A are shown in Figs. 2.1a and 2.1b. As shown in Fig. 2.1a, the number of discharge steps does not have a large effect on the final liquid composition. Figure 2.1b shows the liquid and total concentration as a function of the vapor volume fraction of the tank. The discharge was stopped at 90% vapor volume. The figure shows two important results of the static model. First is that the composition can shift to about 1 percent less R32 (from 25% to 24% by mass). Second is that the slope of the composition change becomes much more rapid the closer the tank comes to being totally empty of liquid. So, while a 10% liquid charged tank may have an acceptable composition shift, a 5% liquid charged tank may not.

Static Model Results for R407C

For 407C, the number of discharge steps used was set to 100. Figure 2.2a shows the liquid and total concentration as function of the vapor volume fraction of the tank. The discharge was again stopped at 90% vapor volume. The figure shows several interesting results. First is that the composition can shift to about 1 percent less R32 (from 23% to 22% by mass), which can be expected from the Blend A results. Second, the R125 composition closely follows the R32 trends. This would seem to indicate that the three component mixture of R407C is behaving more like a two component mixture of R134a and a R410 type blend. As also seen in the Blend A results, the slope of the composition change again becomes much more rapid the closer the tank comes to being totally empty of liquid. Figures 2.2b and 2.2c show the liquid mass fractions of R32 and R125 as a function of both vapor volume and ambient temperature. These results indicate that less fractionation occurs at lower temperatures.

Transient Model and Sample Results

The transient model incorporates a lumped parameter thermal circuit to model the transient thermal effects of liquid discharge. The change in temperature affects the phase equilibrium and composition of the blend. The sample tank geometry used in the analysis is shown in Fig. 2.3.

This geometry also corresponds to the experimental test tank. The thermal circuit is shown in Fig. 2.4. The thermal mass is divided into four wall nodes (top, bottom, liquid side, and vapor side) and two fluid nodes which are constrained to have the same temperature. The liquid and vapor side nodes change in size as the liquid level drops during the course of the simulation.

The procedure used to calculate the fractionation effects is described below.

1) First the initial mass is fractionated into liquid and vapor compositions.

2) A specified mass of liquid is discharged.

3) The amount of liquid vaporized is estimated.

4) An energy balance is performed on the tank to determine the heat removed by the discharge process and the amount of vaporization.

5) The thermal circuit shown in Figure 2.4 is solved.

6) The new specific volumes are found and a new total volume is found.

7) If the new volume is different from the previous total volume, the amount of vaporization is revised ...back to step 4.

8) The clock is incremented, and if the final time has not been reached, return to step 2.

Comparison of Test Results and Model Predictions

The next three sets of figures show simulation results compared to experimental results (the reader is referred to the next section for a description of the test plan, measurement techniques, and specific measurements). The experimental test matrix and results are shown in Tables 2.1 and 2.2. Figure 2.5 shows the results of a fast discharge at room temperature. The liquid volume fraction starts at 96% and has dropped to 10% at the end of the test. The fluid temperature drops about 6 degrees F over the course of the discharge. The liquid composition drops from 25.2% R32 to about 24.3% R32 over the course of the test. The three experimental data points are shown as crosses on the chart, and fall close to the predicted composition levels. Figure 2.6 shows a faster discharge at an elevated temperature. The faster discharge was possible in this case, due to the increased pressure difference between the discharge tank and the dump tank. In

this case, the liquid volume fraction drops to 6% from 94%. The R32 liquid composition drops from 25.2% to about 23.6%. Once again, the experimental data points are in very good agreement with the predicted values. The final experimental comparison is shown in Fig. 2.7. This test is a slow discharge at an elevated temperature, with a different initial composition. The simulation results show a drop in liquid R32 concentration from 23.4% to about 22.1%. The experimental results show a little bit less composition shifting, but still very close to the predicted results. An interesting side note to all three of the previous figures is that all show that as both the liquid and vapor R32 concentrations drop, the total R32 concentration increases. This is because as the liquid mass drops, more of the total mass is made up of vapor (the vapor mass fraction increases). Because the vapor always has a much higher concentration of R32, the total R32 concentration also increases.

The final set of charts, shown in Fig. 2.8, shows the results of a set of parametric studies to determine the factors which influence fractionation when discharging liquid from a tank. Three parameters were chosen: tank size, speed of discharge, and ambient temperature. The effect of tank size on the amount of composition shifting seems to be zero. The speed of discharge has a greater, but still negligible, effect on the composition shift. This is partly due to the fact that the liquid and vapor phases are always assumed to be in equilibrium in the model. The final parameter, temperature, seems to have the greatest effect. Three different ambient temperatures were chosen: 62F, 72F, and 92F. The greatest amount of composition shifting took place at the highest temperature (close to half a percent more R32 at the end of discharge at 62F than at 92F)

Comparisons of the static model results with the dynamic model results for Blend A indicated only small differences in the results from the static (isothermal) and dynamic models. In the interests of time, only the static model was run for the R407C phase of this contract.

Experimental Draw Down Test Configuration and Test Procedure

This section describes the experimental facility and test procedure to determine the impact on fractionation when liquid R32/R134a is drawn from a container under various conditions. The results from these tests were compared to analytical predictions in the previous section.

Experimental Design

The experimental test set up consists of a small holding tank which discharges through a sampling section into a receiving tank. The basic layout is shown in Figure 2.9a and described in detail below.

The holding tank, which consisted of a scroll compressor shell, including the central cylinder, had a total volume of about 2 gallons. The refrigerant blend was mixed in a 60 lb tank to the proper proportions and gravity-transferred to the scroll shell and filled to capacity. Gravity transfer was used to minimize any fractionation during the transfer process. One of the existing ports on the base of the shell was used to draw out liquid, the other port was used for a thermocouple. Fast-responding thermocouples were used to measure liquid and gas temperatures. A pressure transducer was mounted near the top of the case. A sight glass at the level of the discharge port was used to determine the lower limit of the liquid level. An in-line sight glass at the exit of the vapor line at the top of the tank was used to determine when the tank

is full. Other sight glasses on both sides of the switching valves were used to monitor the quality of the refrigerant and to insure that no gas bubbles were present in the liquid line.

The receiving tank (25 lb) was used to collect the liquid discharged from the holding tank. The tank was vacuumed and chilled with liquid nitrogen (using copper tubing wrapped around the tank), which provided a pressure drop across the metering valve to regulate flow.

A metering valve (Nupro SS-4BMRG) was used to adjust discharge flow, with an in-line sight glass upstream of the valve.

A liquid sampling section (using Hoke Multimite 7900 series 5-way valves), as shown in Fig. 2.9a, was used to take liquid samples for the gas chromatograph (GC). Each connecting piece was made up of a 5 in. section of 1/4 in. tubing for a volume sample of approximately 2 ml, used with 150 ml gas sampling cylinders.

Finally, a gas sampling section, as shown in Fig. 2.9b, was used to take gas samples for the GC. A quick-disconnect (Nupro QC6 series for minimal volume loss at disconnect) was used for the gas sampling cylinders.

Liquid and Gas Sampling Procedure

Figure 2.9b shows the sampling bottle arrangement used to draw liquid and gas samples for the gas chromatograph (GC). This arrangement was connected to the liquid or gas port on the rig (Fig. 2.9a) and then vacuumed through the vacuum valve. The sampling valve was then opened and the cylinder filled to approximately 50 psig. The gas sampling port was located at the top of the rig through a short piece of tubing and sight glass. A quick disconnect was used to minimize the amount of gas lost when switching sampling cylinders. Heating tape was wrapped around the tubing to raise its temperature above that of the tank, to eliminate any chance of condensation which would bias the results (increasing the fraction of R32 in the sample). The line was purged by briefly opening it to the atmosphere to assure that a "fresh" representative sample of gas from the main cylinder would fill the sampling cylinder.

Various options for liquid sampling were considered before the final design was selected. Simply drawing liquid from the tank or its discharge line with a "T" into the sampling bottle was not considered satisfactory. Liquid drawn off in this manner would be likely to fractionate, since more of the higher volatility component (R32) would fill the sampling bottle first. The approach taken was to trap a known volume of liquid in the exit line as it was discharging the tank. This sample (or "slug") of pressurized liquid would then be diverted to the vacuumed sampling bottle. This would guarantee that the entire volume of liquid would enter the gas phase without fractionation. This method also guarantees that a "fresh" liquid sample is analyzed at each time step. To implement this technique, it was necessary to design an arrangement which would allow capturing liquid samples quickly and accurately, without interrupting the drawdown. This was especially important for the rapid drawdown tests, since the time interval between samples could be very short. These liquid samples would have to be extracted into the sampling cylinders at the end of each test. Various manifold arrangements were considered, but the final arrangement consists of two 5-way valves in series. Initially both valves are set to position 1. At the next sample point, the bottom valve (in Fig. 2.9a) is rotated to position 2, followed by the top

valve. This traps a 2 ml sample of liquid in the connecting manifold. This procedure is repeated for each data point. At the completion, the samples are transferred to the gas sampling cylinders by connecting the gas sample bottles to the liquid sample port and rotating the valves in such a manner as to fill the bottles one at a time. The valves are rated at 2000 psi, ensuring that no leakage takes place.

Alternate Liquid Sampling Procedure

In the second liquid sampling procedure, a vacuumed test cylinder with a pressure gauge was used to collect a gas sample directly from the liquid line by flash-vaporization. The flow was shut off at the five way valve during the sampling procedure. A tee in the liquid line was used to attach the vacuumed cylinder. Before the cylinder was attached, the line was purged to remove any stagnant liquid present in the tee by quickly opening and closing the shut-off valve. The cylinder was next attached and the valve was opened slightly to allow vapor to fill to approximately 50 psig. This pressure was below saturation for the mixture, so there was no chance of two phases forming in the sample cylinder. The cylinder was next removed and carried to a GC for analysis.

Data Acquisition

Fast-response thermocouples were place near the top and bottom of the scroll compressor shell to measure gas and liquid temperatures, respectively. A pressure transducer was mounted on the side of the case to collect pressure data. A high-speed data acquisition system was used to collect 100 data point bursts of temperature and pressure data, which was then averaged and displayed.

Experimental Test Results

This section describes the results of the experimental verification tests. A total of seven tests were performed, with three liquid samples and two vapor samples being taken over the course of each of the tests. The tests are described in Table 2.1.

Test	Description
1	Fast drawdown at room temperature
2	Fast drawdown at room temperature (repeat)
3	Slow drawdown at room temperature
4	Fast drawdown at high temperature
5	Slow drawdown at high temperature
6	Slow drawdown at med-high temperature
7	Slow drawdown at med-high temperature (repeat)

Table 2.1. Experimental Test Matrix

The data collected in the tests is summarized in Table 2.2 below.

Test #	Ambient Temperature, F	Discharge Rate	Liquid Weight Fraction (weight/initial weight)	Liquid R32 Concentration %	
1	72	4.65 lbm/min	0.89 0.44 0.19	(n/a) 24.45 24.04	
2	74	4.32 lbm/min	0.90 0.50 0.19	25.21 24.77 24.42	
3	74	0.05 lbm/min	0.89 0.47 0.12	(n/a) 24.68 24.02	
4	113	7.89 1bm/min	0.89 0.44 0.13	25.20 24.40 23.59	
5	110	0.06 lbm/min		23.99 23.66 23.19	
6	Varied (7F-110)	0.15 lbm/min	0.80 0.47 0.16	22.25 22.73 22.76	(21.13)* (20.93) (21.17)
7	94	0.13 lbm/min	0.88 0.48 0.13	23.42 22.96 22.52	(22.11) (21.53) (21.06)
0* - composition data from second liquid sampling method					

Table 2.2 Test Results

Liquid Sample Technique Observations

During the course of the tests, many observations on obtaining accurate data were made, and modifications to the test rig to implement improvements were performed. In an effort to determine the accuracy of different liquid sampling techniques, two liquid samples were taken at the same time, using different methods during the last two tests. The first sample was taken using the standard liquid capture method used throughout the study. The second sample was taken using a separate procedure described above.

The results of the second sampling procedure indicated a consistently higher fraction of R134a in the sample bottle (see numbers in parentheses in Table 2.2). This was found to have been caused by the purging of the liquid line in the tee. When the tee was purged, R32 was preferentially removed from the line due to fractionation effects. This left a much higher R134a

concentration in the liquid line. So, when the sample cylinder was attached, even though R32 was again preferentially removed, the R134a concentration remained higher than that in the line. On the whole, this method was not found to be a satisfactory method for liquid sampling.

Summary

Both the more detailed transient model and the static model indicate that when liquid blend filling from a storage tank occurs, the fractionation effects are relatively small. That is, the composition will shift by 1% or less (from 25% to 24% R32 for Blend A), when the tank is discharged to no less than a 10% liquid level. The fractionation effects increase exponentially as the liquid level drops further. This result was predicted for both the Blend A studies and the R407C studies. In addition, the experimental results appear to confirm these results for Blend A. For R407C, the model results additionally predicted that the R125 concentration follows the same trends as the R32 concentration as fractionation occurs.

Major Conclusions

- A straightforward model can accurately predict the composition shifting, which occurs when liquid-filling from a tank containing a nonazeotropic blend.
- Composition shifting will be minimal when the tank is discharged to a liquid level of no less than 10%. Further charging will result in much higher composition shifts.
- Both Blend A and R407C appear to behave similarly. R407C actually appears to behave like a binary mixture of R134a and R410A, as the R32 and R125 concentrations closely track each other.

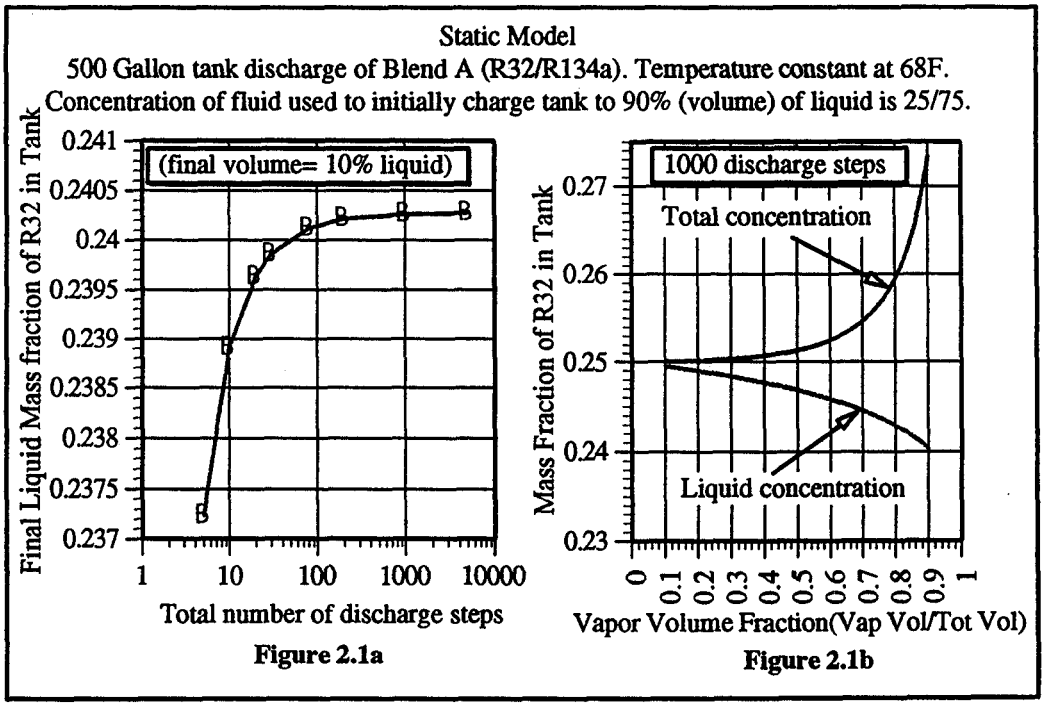

Fig 2.1 Static Model - 500 Gallon Tank Discharge of Blend A (R32/R134a).

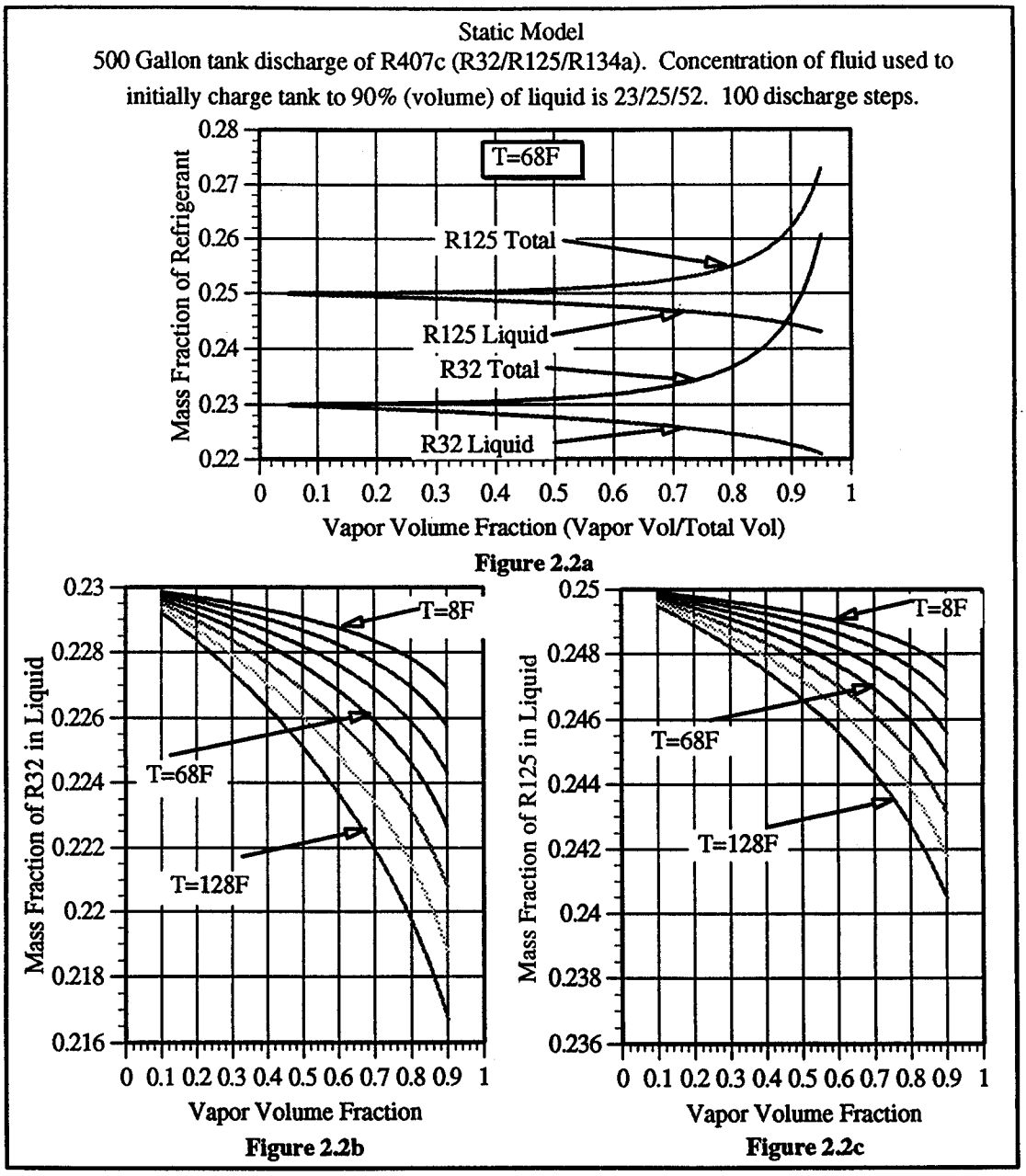

Fig. 2.2 Static Model - 500 Gallon Tank Discharge of R407C (R32/R125/R134a).

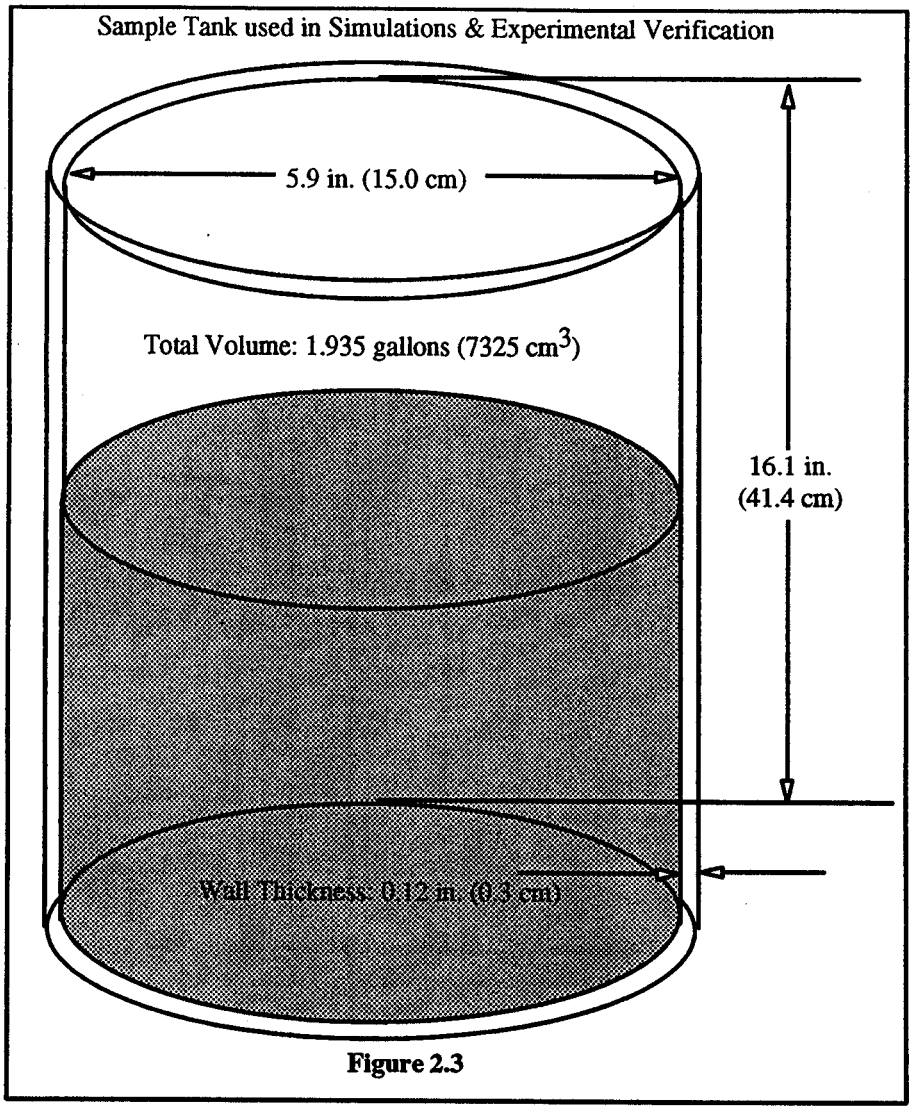

Fig. 2.3 Sample Tank used in Simulations and Experimental Verification

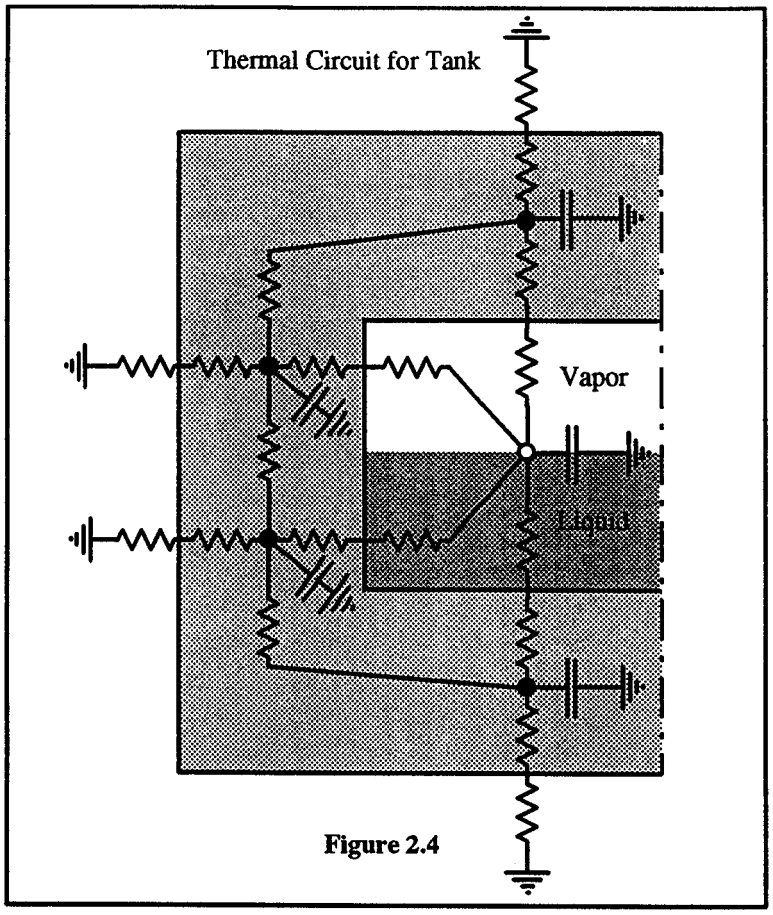

Fig. 2.4 Thermal Circuit for Tank

1.935 gallon tank discharge of R32/R134a. Ambient Temperature remains constant at 72F. Concentration of fluid used to initially charge tank to 96% (volume) of liquid is 25.2/74.8. Liquid is discharged at a constant mass discharge rate. Final vapor volume fraction is approximately 90%.

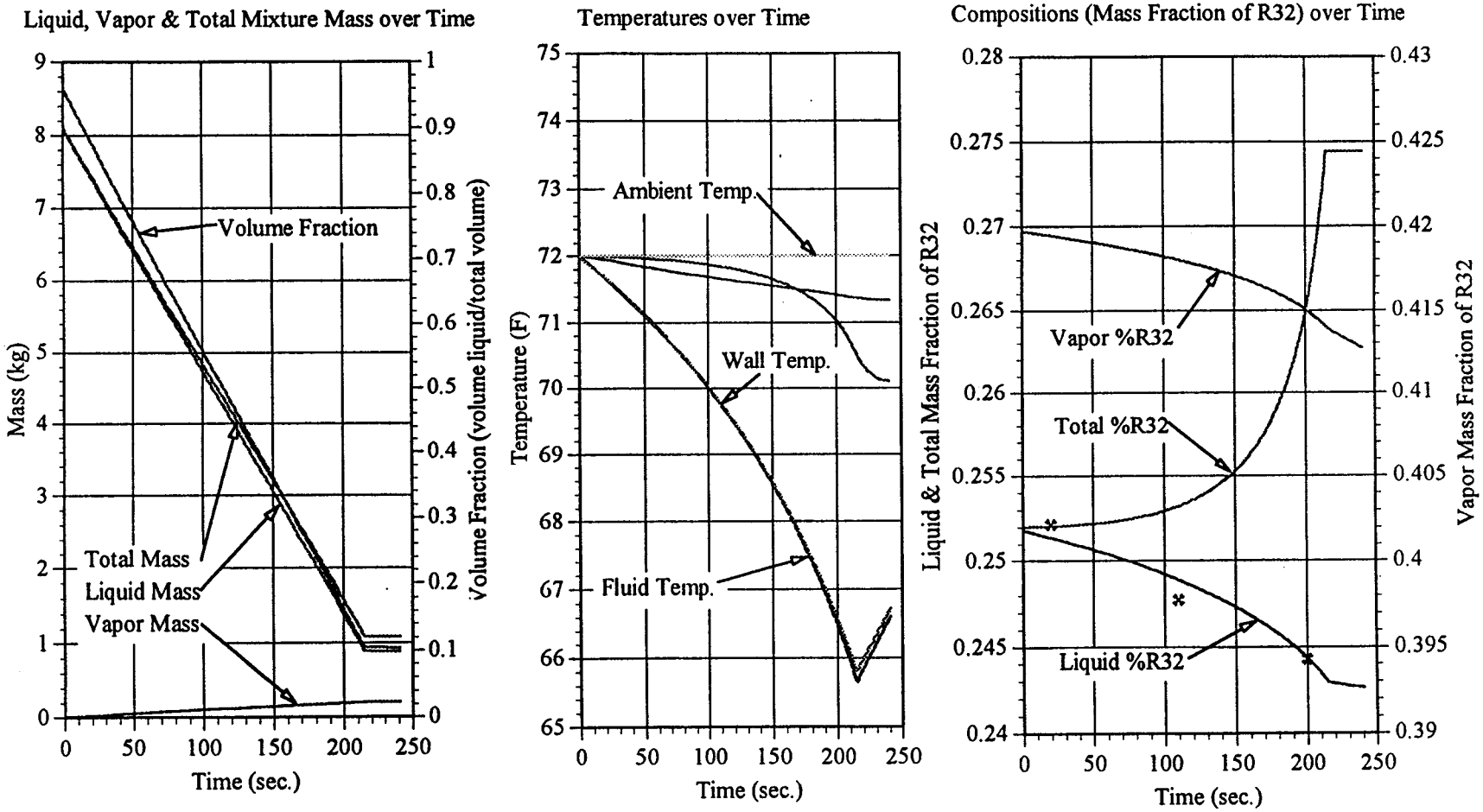

Figure 2.5

× - Experimental Test Data Point

Fig. 2.5 ARTI Task 2 - Discharge Tests 1 and 2 - Transient Model

1.935 gallon tank discharge of R32/R134a. Ambient Temperature remains constant at 113F until t=110s, when it drops to 72F. Concentration of fluid used to initially charge tank to 96% (volume) of liquid is 25.2/74.8. Liquid is discharged at a constant mass discharge raze. Final vapor volume fraction is approximately 94%.

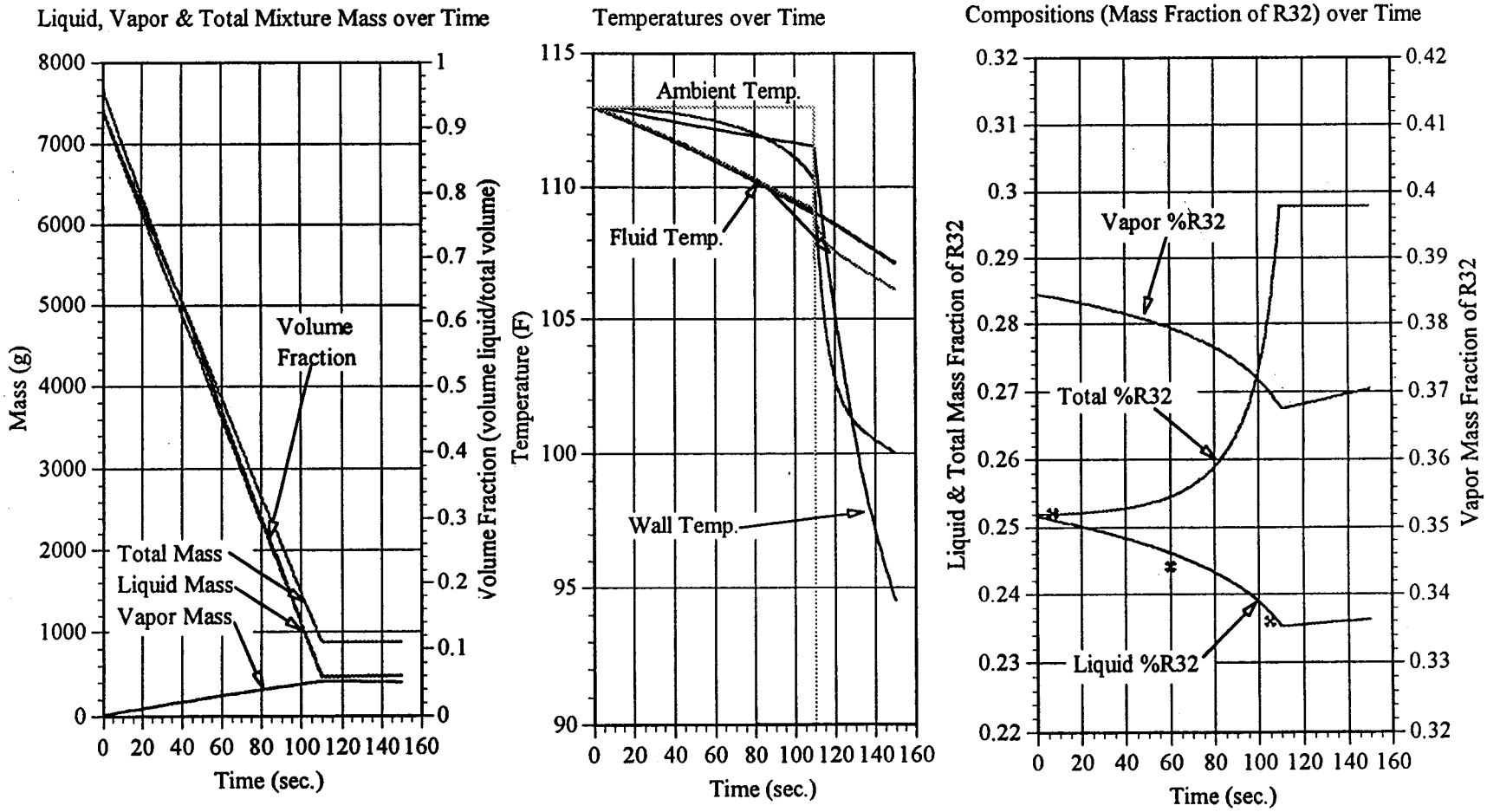

Figure 2.6

× - Experimental Test Data Point

Fig. 2.6 ARTI Task 2 - Discharge Test 4 - Transient Model

1.935 gallon tank discharge of R32/R134a. Ambient Temperature remains constant at 94F. Concentration of fluid used to initially charge tank to 96% (volume) of liquid is 23.45/76.55. Liquid is discharged at a constant mass discharge rate. Final vapor volume faction is approximately 93%.

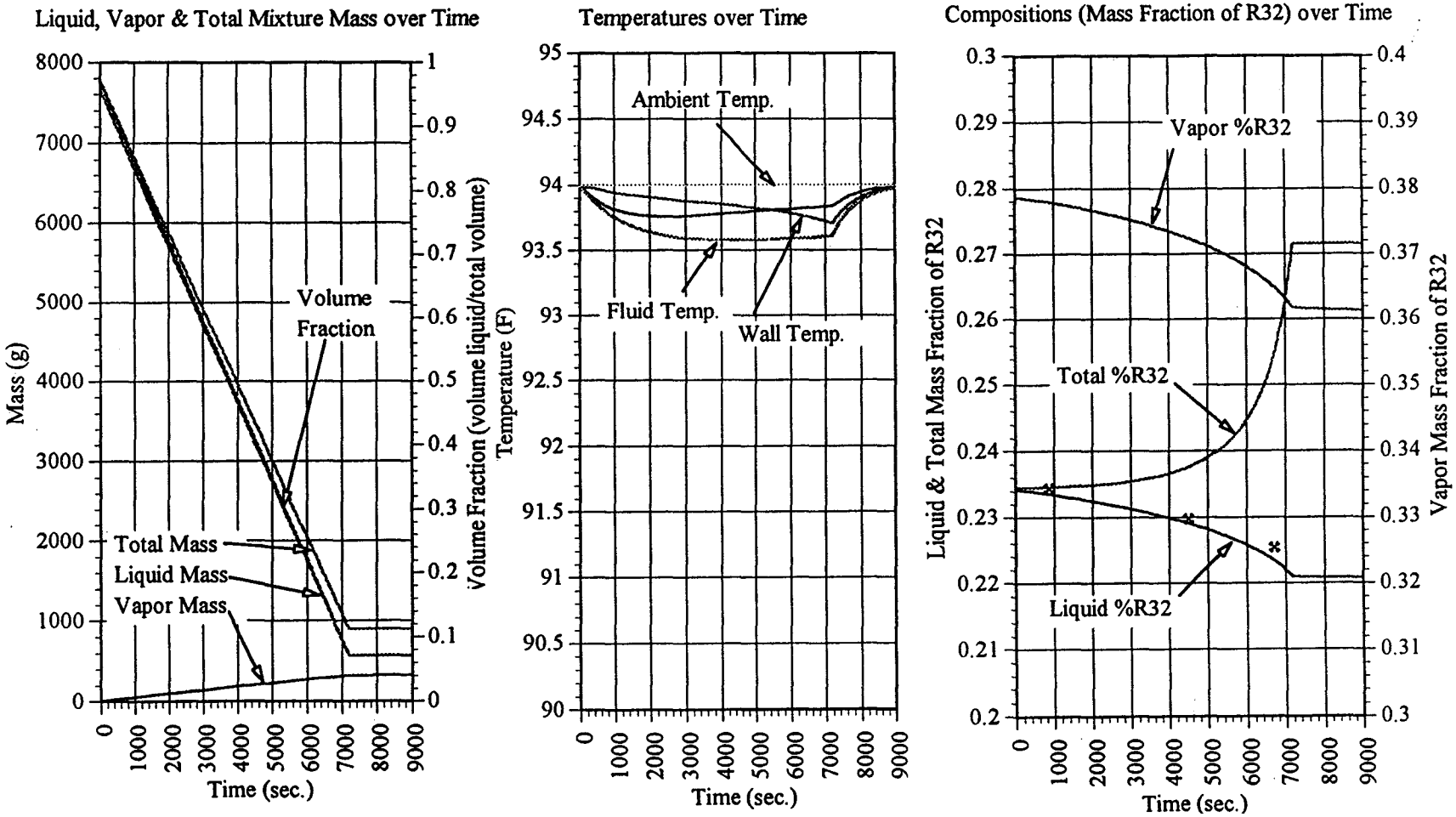

Figure 2.7

× - Experimental Test Data

Fig. 2.7 ARTI Task 2 - Discharge Test 7 - Transient Model

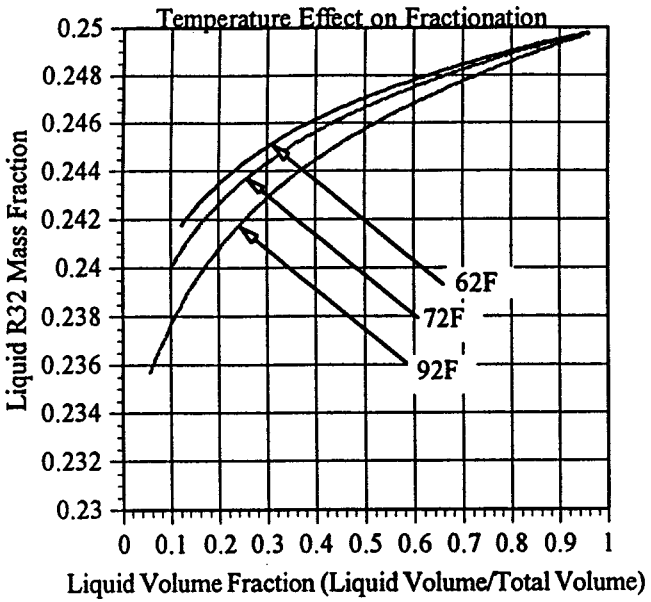

2 gallon tank
R32/R134a at 25/75
initially 96% liquid

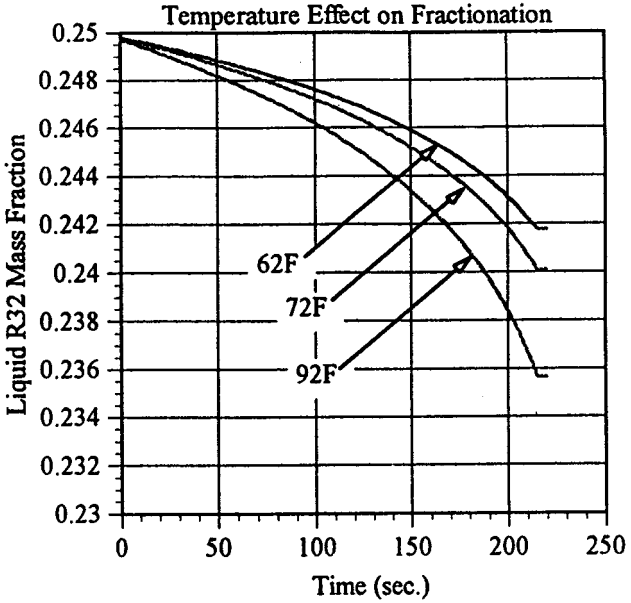

Figure 2.8

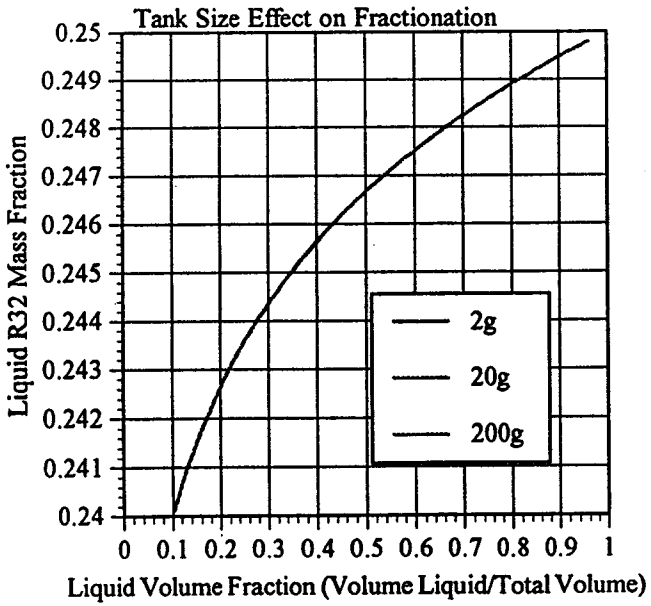

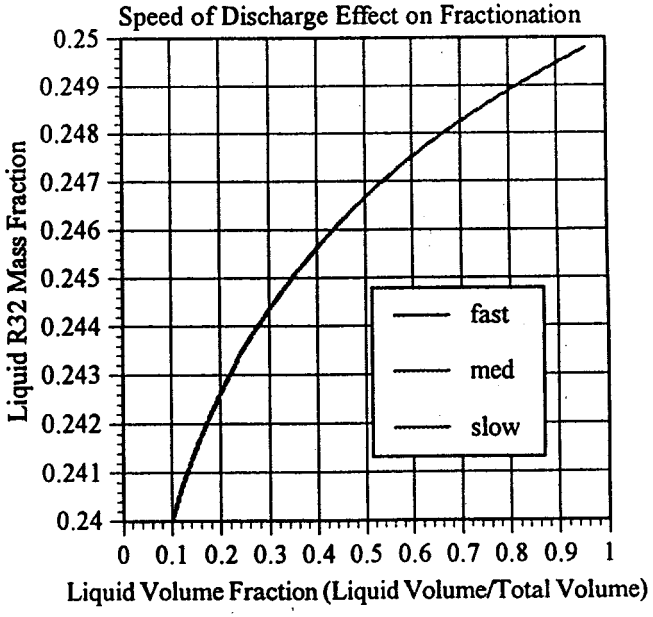

Fig. 2.8 ARTI Task 2a Part 2 - Transient Model

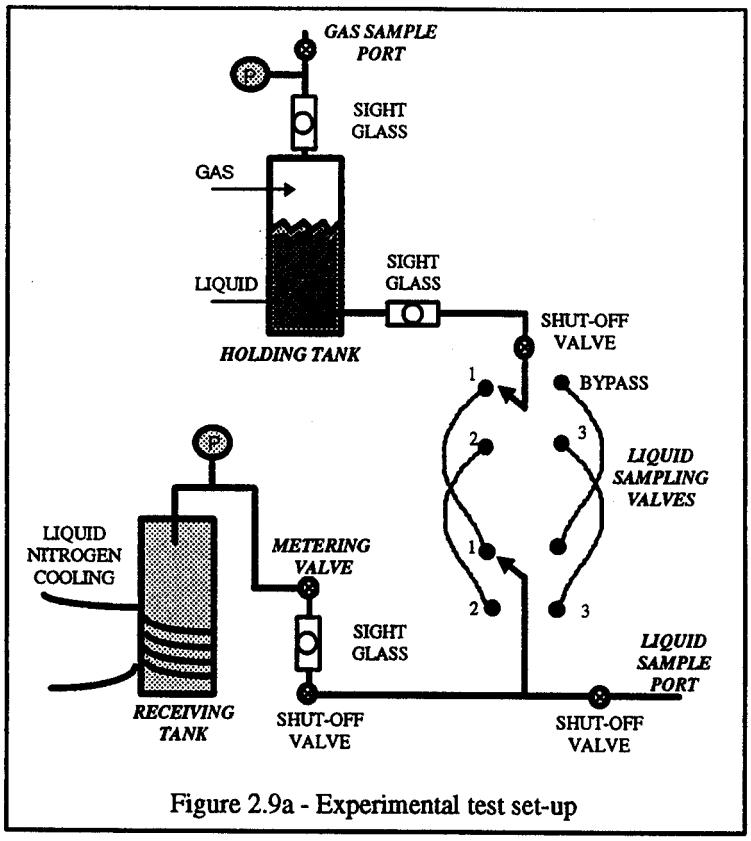

Figure 2.9a - Experimental test set-up

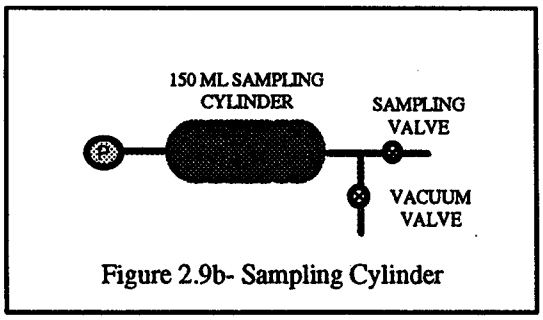

Figure 2.9b- Sampling Cylinder

Fig. 2.9 Experimental Test Set-up

TASK 3. MODELING OF FRACTIONATION EFFECTS WITHIN SYSTEM COMPONENTS

The objective of this task was to develop a computer model capable of predicting a zeotropic refrigerant composition shift within the two phase components of a system during start-up, normal operation, and after shut-off. The two-phase components of the system being the condenser, expansion valve, evaporator, accumulator, and compressor sump. In addition, the effect of composition shifts on the performance for the individual components and overall system was to be estimated.

Background and Physical Process Description

In considering an approach for such a model, it is important to have a good physical description of the process being modeled. Inspection of a phase diagram for a zeotropic mixture reveals that the gas and liquid phases have differing mass compositions for a given pressure and temperature (Fig. 3.1). The liquid and gas phase compositions depend on the total mass of each component present in a discrete volume, as well as the temperature, pressure being a function of temperature for the specified volume. For a refrigeration system, volume is fixed, but the mass and temperature vary with each discrete location. In the most rigorous analysis, a system could be divided into a great many sub-volumes, as is typical for computational fluid dynamics (CFD) analysis. Local heat, mass, and momentum transfer could then be used to determine the composition and state in each sub-volume. For the sub-volumes in the two-phase region, mass and density would be used to determine the liquid to gas mass fraction or quality. Then a routine such as REFPROP could be used to calculate the liquid and gas phase mass fractions.

In addition to local fractionation between the gas and liquid phases, bulk fractionation can take place, due to preferential migration of one refrigerant component to the surrounding sub-volumes. Assumptions about mass transport across a sub-volume surface in the two phase region are critical to explaining bulk composition shift. If liquid and gas migrate at equal rates, as would be true for a small liquid particle suspension, then the bulk composition must remain constant because all components are moving together. Composition shifting is only between the liquid and gas phase in the local volume. If, however, the gas migrates faster than the liquid, as would be true for large liquid particle suspension or a liquid pool and gas interface, then bulk composition change can be the result of spatial slip between the liquid and gas phases. In the extreme, such slip can be likened to pool boiling distillation. Each sub-volume acts like a boiler, becoming richer in the less volatile component.

To consider the consequence of bulk fractionation, assume that the condenser and evaporator of a refrigeration system are single volumes at constant temperature and pressure, with liquid and gas phases of differing composition. If in addition, it is assumed that the liquid leaving the condenser has the same overall composition as the gas leaving the evaporator (required for steady state operation), then the overall composition in the evaporator will differ from that in the condenser (Fig. 3.1). The exact degree of that difference will depend on the evaporator and condenser qualities. If the condenser and evaporator were considered as multiple volumes with varying pressure and temperature, the slip described in the above paragraph could account for differing bulk compositions in the condenser and evaporator.

If there is no slip between the gas and liquid phase, then the constant bulk composition assumption becomes a necessary condition. Given constant pressure and bulk composition in a sub-volume, the temperature must vary as the sub-volume quality varies from liquid to gas (Fig. 3.2). Note that the liquid and gas compositions vary considerably with quality, but that the bulk composition remains constant.

Model Approach

Because fractionation is dependent on both energy and mass migration, an accurate prediction can only be made by starting from a known initial condition and integrating to a selected end condition. At the same time, practical computer run time must be considered. This dictates a simplified model and relatively long integration time steps. Such requirements are typically met with a lumped parameter system representation. This was the selected approach for the model development of the fractionation evaluation. Unique to this application is the prediction of the zeotrope thermodynamic properties for a varying refrigeration and lubricant blend composition. This is accomplished by incorporating the refrigerant blend and oil models developed in Task 1 and 2 of this program.

The HVAC system selected for modeling and analysis is a 2.5 ton, split system residential heat pump. This heat pump formed the basis for the experimental test rig used in Task 4 efforts to measure fractionation effects. Basic components for this system include compressor, four-way valve, vapor line, indoor coil, indoor coil orifice, liquid line, outdoor coil orifice, outdoor coil, suction accumulator, and compressor sump (Fig. 3.3). The system is modeled as four discrete volumes: evaporator, accumulator, condenser, and compressor sump. This represents a minimum number, but it was believed to be a good starting position, given the potential to add more volumes at a later time, if required. Vapor and liquid line volumes are added to the appropriate coil volume, when calculating effective evaporator and condenser volumes during heating or cooling operating modes. These volumes are then subdivided into superheat, saturated, and subcooled sections as a function of vapor to liquid mass ratios. The heat transfer coefficient is unique for each subdivided section, and is currently kept constant for all refrigerant compositions. The pressure in each volume is a function of the refrigerant composition, mass, and enthalpy. These values are calculated from mass and energy convection through the volume, energy conduction through the coil walls, and the compression process adding energy.

Model Process Description and Assumptions

- **Circulation** of the refrigerant blend through the system begins with a constant volumetric flow model for the compressor. Vapor phase refrigerant from the compressor sump is transported to the condenser volume. Refrigerant flow out of the condenser can be gas, liquid, or two phase, depending on the mass and energy of refrigerant in the condenser volume. The flow rate out is a function of pressure difference across the expansion orifice. Similarly, flow from the evaporator to the accumulator is a function of refrigerant quality, line diameter and pressure drop. The accumulator and compressor sump are currently assumed to have equal pressure and gas phase composition. Only gas phase refrigerant is assumed to enter the compressor. Oil in the compressor sump is assumed to remain in the sump. The amount of liquid refrigerant absorbed by the oil is based on assumed liquid phase equilibrium with the sump gas phase (see Task 1 results).

- **Heat Transfer** is calculated by the LMTD method, with air side inlet conditions specified. With the compressor off, refrigerant and air temperatures are assumed to be equal. Liquid refrigerant is only present in the colder coil or absorbed in the compressor oil. Turning on the compressor reduces the pressure in the accumulator, which causes the liquid refrigerant to boil. The necessary heat of vaporization lowers the accumulator refrigerant temperature and vapor pressure. At the same time, refrigerant discharged by the compressor has increased in temperature due to compression work and compressor inefficiency. Typically, only gas phase is initially present in the condenser, but the compressor mass flow is greater than what the expansion valve can pass under such conditions, so the refrigerant mass in the condenser increases. Heat transfer to the condenser air is based on coil surface area, gas phase heat transfer coefficient and LMTD. Exiting air and refrigerant temperatures are based on this heat exchange. When sufficient mass is present in the condenser, a liquid phase develops. On the basis of typical condenser performance, 20% of the coil surface area is allocated for desuperheat and the remainder is assumed saturated, and having a unique heat transfer coefficient. Once the coil reaches a specified quality, a subcooled region is allocated on the basis of calculated subcooled liquid volume. A unique subcooled heat transfer coefficient is specified for this subcooled region, while the remaining coil area is divided 20%/80% superheat/saturated.

  The evaporator is partitioned into saturated and superheated regions as a function of overall evaporator quality. LMTD is again used to calculate heat transfer between the refrigerant and air. If superheat is not present, then saturated refrigerant is transported to the accumulator. From the accumulator, only gas phase is assumed to enter the compressor or sump. Unique heat transfer coefficients are specified for the accumulator. Sump temperature is calculated from accumulator and compressor discharge temperatures. A simple Euler integration of this overall process is performed until steady state operation develops.

- **Slip** that exists between the gas and liquid phases is a key parameter for each modeled system volume. As previously discussed, such slip can account for a change in entering and exiting bulk composition. Another effect is refrigerant temperature glide. For this simple lumped parameter model, pressure in the saturated region of each system volume is assumed constant. If there is no slip, temperature must change with refrigerant quality (100% temperature glide). If temperature is constant (0% temperature glide), the liquid and gas phase each have a constant and unique composition and a maximum amount of slip must occur, such as in pool boiling. Rather than attempt to predict the amount of slip present in each component, slip is treated as a variable to be adjusted to agree with observed fractionation. Since no slip equates to 100% temperature glide, the label (100% glide) will be used to indicate no slip. Conversely, maximum slip equates to 0% temperature glide, so the label (0% glide) will indicate maximum slip.

Blend A Model Results

0% Temperature Glide Assumption Results

The dynamic heat pump model was run for a 7-pound charge of 21.1% R32/78.9% R134a (by weight) at DOE A* air side conditions. This charge composition and mass is consistent with Task 4 experimental test run #1 (see Table 4.2 and data shown). Maximum slip was specified (0% glide) for each component. A tenth of a second integration time step was also specified as the model was unstable for longer time steps and too slow and no more accurate for shorter steps. At time zero, the gas phase composition was calculated with the REFPROP subroutine to be 32% R32 and the liquid phase to be 20% R32 (Fig. 3.4, R32 concentration by component as a function of time). The sump, with 2.2 pounds of oil, was calculated (with the oil solubility subroutine developed in Task 1) to have absorbed refrigerant that was 28% R32.

After the first time step, compressor flow causes the more volatile R32 to preferentially boil out of the accumulator, raising the compressor, condenser, and expansion valve R32 concentrations. Liquid initially in the evaporator is quickly pulled to the accumulator. As time continues, most of the refrigerant is pumped to the condenser (see Fig. 3.5 for refrigerant location by component). This introduces much of the R134a to the condenser and lowers the relative R32 mass fraction in the condenser to about 24%. Notice in Fig. 3.1, that the gas phase compressor discharge composition, condenser overall composition with a quality near zero, and the liquid phase composition leaving the condenser to the expansion valve, are all nearly equal in mass concentration under the 0% temperature glide assumption. The accumulator in this model run has very little R32 concentration, but retains a significant mass of liquid refrigerant due to selection of fixed expansion orifice size for this operating condition. Both these results are confirmed by Task 4 testing. Heat exchanger pressures (Fig. 3.6) show good agreement with test data for the evaporator, accumulator and condenser. Predicted temperature values (Fig. 3.7) are also close to measured values except for more subcooling being predicted than achieved. This could be corrected in the model by calibrating the subcooling volume or heat transfer coefficient. Except for a brief high concentration of R32 in the system at startup, the model does not predict any unusual system operation with Blend A. System capacity was calculated to be down 9% relative to operation with R22. However, this capacity loss could be the result of less than ideal charging or orifice size selection.

100% Temperature Glide Assumption

Next the model was run with no slip or 100% temperature glide assumption to compare with the 0% glide results. Initial conditions were the same, but the model results show that R32 concentrations quickly converge to the filling percentage for all components (Fig. 3.8). This result was not consistent with test results. Figures 3.9-3.11 show less refrigerant in the accumulator and poorer pressure, but similar temperature agreement with test data. Cooling capacity was found to be similar for either slip assumption; however, efficiency was higher for the no slip assumption, since the required head rise was smaller.

* Nominally DOE A conditions are 95 Fdb/75 Fwb outdoor and 80 Gdb/67 Fwb indoor conditions (see Ref. 17)

The model was also run at the DOE E* rating condition. A 7 pound charge was specified at a filling composition of 25.6% R32 (shown in Task 4 as run # 3). The orifice for the heating condition is considerably smaller than for the cooling condition (.052 in. vs. .070 in.), which resulted in the accumulator running dry. Under these conditions, the compressor exit composition is nearly equal to the filling charge for either slip assumption (Figs. 3.12 and 3.13, R32 concentration by component). For the 0 temperature glide assumption, the charge in the evaporator and accumulator is 15.5% R32, and the refrigerant in the sump contains 24% R32. For the 100% temperature glide assumption, the evaporator and accumulator charge is 25.6% R32, while the refrigerant in the sump is 22.7% R32. In both cases, there is relatively little charge in these three components (Figs. 3.14 and 3.15, refrigerant location), which results in the condenser charge being close to the filling charge. Evaporator and accumulator pressures agree well with test data, but the condenser pressure is considerably lower than test data for a 7 pound charge (Figs. 3.16 and 3.17). The condenser pressure is closer to measured test data for a 5.4 pound charge. Apparently overcharging the system reduces the saturated heat transfer area and results in higher saturation temperatures and pressures. Interestingly, the condenser exit temperatures do not vary all that significantly, suggesting that there is more subcooling when there is excessive charge (Figs. 3.18 and 3.19). The model can be calibrated by adjusting either the saturated heat transfer coefficient or the fraction of heat exchanger containing subcooled refrigerant.

Fractionation Effects on System Performance

From the above two cases, it can be stated that fractionation does exist in systems charged with zeotropic blends, but the effects on system performance are minimal. When substituting zeotropic blends for refrigerants like R22, re-optimization of the charge and expansion devices is required. Liquid refrigerant in the accumulator appears to have the greatest effect on bulk fractionation during operation for two reasons. For one, it acts as a storage device for the less volatile refrigerant. Thus, its effect on system performance depends on the quantity of refrigerant it contains. This quantity is a function of operating conditions, refrigerant charge, and expansion valve operation in relation to the compressor performance. The most significant fractionation takes place when the system is off and at low temperature. Under these circumstances, the gas phase composition approaches 40% R32, a potentially flammable mixture (Ref. 18) with 60% R134a.

Evaluation of Fractionation Effects During System Leaks

When a system leaks at idle, the gas phase leak is rich in R32. Thus, the system charge contains less R32 and system performance becomes more like a R134a system. Recharging the system with a blend containing 25% R32 will not bring it back to its original composition. During system operation, the gas phase in all components is only slightly different from the filling charge. This is also true for the majority of liquid charge in the condenser. Consequently, system leaks during operation will not change the overall composition greatly.

* Nominally DOEE conditions are 47 Fdb/43 Fwb outdoor and 70 Fb/60 Fwb indoor conditions (see Ref. 17)

Model Modification for System Leaks

The computer model can be modified to estimate the effect of a leak on composition. The simplest method is to divert the expansion valve flow out of the system. Since the liquid refrigerant charge is in the colder component when the system is off (typically the evaporator), the condenser contains only gas. Turning on the compressor in the model results in gas phase refrigerant being pumped to the condenser and then overboard through the expansion valve. System pressures depend on the leak rate, which could be adjusted by varying the speed of the compressor.

Model Results

Gas phase leaks are shown in Figs. 3.20 and 3.21 for DOE A and E (see Ref. 17) operating conditions, respectively. The initial charge was set at 2 kilograms (4.4 pounds) of a 25% R32/R134a blend in both cases. A one kilogram charge of sump oil was also specified. The change in R32 mass fraction for the remaining refrigerant is shown as a function of remaining system charge. Good agreement was obtained between the model and Task 4 testing (see Table 4.1).

Finally, the model was next run for a DOE A (Ref. 17) condition with 5.8 pounds of charge containing 19.2% R32 by weight. This duplicated test run 1B in Table 4.2, which was a gas phase leak of 1.2 pounds of refrigerant from an initial 7 pound charge at 21.1% R32. For this case, both the 0% temperature glide and the 100% temperature glide assumptions under predict the measured. compressor discharge R32 composition (Figs. 3.22 and 3.23). However, the 0% temperature glide assumption is closer to the measured value. Heat exchanger pressure and temperature agreement are both better for the 0% temperature assumption (Figs. 3.24 and 3.27).

R407C Evaluation

Evaluation of Fractionation Effects within System Components

Refrigerant 407C, a blend of R32, R125, and R134a, has found wider acceptance than the blend of R32 and R134a previously tested (Blend A). Consequently, an evaluation of 407C was appended to this contract. Some changes to the model were required. The addition of a R125 component requires the addition of appropriate calls for this refrigerant and an oil model for a four component mixture (three refrigerants plus oil). The development of the oil model is discussed in Task 1 of the report. Additional instrumentation was also added to the test apparatus, with the goal of quantifying the nature of fractionation within the indoor coil. Pressure, temperature, and refrigerant sampling ports were added to the end turns of one circuit of the indoor coil to measure temperature glide and composition shifting in this component.

Model Results

The model results for DOE A operating condition will be discussed first. The model was run for a 6.4 pound charge of 20.45% R32, 25.22% R125, and 54.33% R134a since this was measured from the charging cylinder labeled R407C. This composition is not exactly R407C specification, and one must suspect either the gas chromatography measurements or the ability to maintain a consistent blend of R407C. However, the GC was calibrated several times during the

test and its measurements are considered to be accurate. The 6.4 pound charge corresponds to the ARTI 10 system test (shown in the next section - Test Results), where charge was set to achieve 10 degrees of superheat at the compressor inlet in the test facility. Model results are shown for the zero temperature glide assumption in Figs. 3.28-3.32. One observed advantage of R407C over Blend A is the lower R32 concentration ramp ups that are predicted at startup. The ratio of R32 to R125 remains fairly constant. This fact tends to prevent R32 from reaching a flammable ratio. During stable cooling operation, the circulating charge composition (expansion valve and compressor discharge) is somewhat higher in R32 and R125 than the filling composition (22% vs. 20.45% for R32). This is due to preferential storage of R134a in the evaporator, accumulator, and oil sump. However, the mass in those components is small, so the effect is also small. Test data shows no such change in composition, but they also show no temperature glide. Pressure and temperature agreement is excellent for both condenser and evaporator under the zero temperature glide assumption. Results for the 100% temperature glide analysis (Figs. 3.33-3.37) show a similar overall level of agreement (slightly better composition agreement, slightly worse temperature agreement). One conclusion could be that R407C is not very sensitive to fractionation assumptions.

Refrigerant sampling in Task 4, from within the evaporator, does little to clarify the fractionation mode. If the refrigerant sample results are assumed to be two phase, then the sampling results are consistent with the measured constant temperature in the two phase region (49.5 degrees). Figure 3.1 shows the model predicted liquid and vapor concentrations in the evaporator and condenser at DOE A pressures for the 407C blend tested and the 0% glide assumption. Notice that the liquid R32 concentration in the evaporator stays constant at about 12%, but the two phase region extends to the 20.5% R32 gas concentration. Now, if one assumes single phase sampling, then the liquid phase results appear to support the 100% temperature glide assumption (Fig. 3.2), however no such temperature glide is measured.

Model results for the DOE E heating condition and zero temperature glide assumption (Figs. 3.38-3.42) are very close to test data for refrigerant composition and temperatures. Condenser pressure is the one area of significant difference. Condenser pressure and saturation temperature were found to be highly dependent on system charge during the test portion of the Task 4. The explanation being that more charge in the condenser reduces the two phase region, which in turn increases the saturation temperature. All the temperatures measured in the condenser were below the saturation temperature, which suggests that the instrumented circuit was nearly flooded. The charge was set to achieve 10 degrees of superheat in the evaporator. It may be that the orifice is undersized for this refrigerant, and a high condenser pressure was required to achieve the compressor flow requirements to produce 10 degrees of superheat. The model divides the condenser volume into subcooled, saturated, and superheated regions, but it includes the gas line between compressor and indoor coil as condenser volume. Since the gas line volume is nearly as great as the indoor coil volume, the model tends to underestimate the subcooled region in the heating mode. As with the cooling analysis, model results for heating performance with 100% temperature glide look similar to those for the zero glide assumption (Figs. 3.43-3.47).

The refrigerant sampling results from the condenser indicate 20.5% R32, which is near the filling charge percentage. Since all the sampling appears to be in the subcooled region, neither temperature glide assumption is confirmed.

Evaluation of Fractionation Effects During System Leaks

During the Blend A evaluation, experimental and model efforts focused on system performance with partial charge. During the 407C evaluation, charge was kept constant by refilling after a leak. This latter approach represents the long term operating impact for zeotropic blends.

The effects of fractionation have been assumed to depend on when the leak occurs, during system operation or when the system is off. During operation, the circulating charge is close to or identical to the filling composition, so any leak should be of the filling composition. This is confirmed by both the model and test results. When the system is refilled, performance should be essentially identical. If the leak occurs when the system is idle, the gas phase will have a higher concentration of R32 and R125. If the leak is a gas leak, then the system composition will change significantly, and refilling can not correct the situation. These results were confirmed during the experimental portion of the Task 4, but the change in composition for the system off case was minor as were the changes in performance.

Model Development

As with the Blend A analysis, the system off leak was simulated by specifying the expansion valve flow to leave the system. Gas phase refrigerant was moved to the condenser with compressor flow, while the evaporator temperature was kept constant. All liquid refrigerant was in the evaporator.

Model Results

Both experimental results and model predictions are shown in Fig. 3.48 for a 47 degree evaporator. The system initially has 7.45 pounds of refrigerant. After 1.81 pounds of refrigerant gas are drawn from the experimental test system, the remaining refrigerant has a 19.45% R32 and 24.57% R125 composition. The model predictions were 17.44% R32 and 23.43% R125. Experimental results are only 37% of model predicted composition change for R32 and 42% of the model predicted change for R125. The conclusion is that either two phase refrigerant was removed during the experimental leak test, or that the local pressure at the leak sight was low enough for gas phase R134a leakage. Still, both the experimental and model results show how composition shifting can occur due to system leaks.

Overall Summary and Conclusions from Model Effort

- The lumped parameter approach provides a fairly accurate representation of the physical system performance. Model results can be made to closely agree with test results, when proper calibration and operating assumptions are made.
- In general, the 0% temperature glide assumption appeared to more closely match measured system performance. One important consequence of this for Blend A is the potential for flammable R32 concentrations, when the system is idle at low temperatures

and even more so during startup. Also, significant liquid in the accumulator will change the circulating charge composition and system performance.

- R407C appears to be much less sensitive to fractionation. However, the system refrigerant composition may change with successive recharging if only gas phase refrigerant leaks out.
- No extremes in temperature or pressure result from fractionation within the system.
- Oil in the system absorbs some refrigerant and contributes to fractionation in that it preferentially stores R134a. But, the oil solubility effect on performance is small.

References

17. ARI Standard 210/240 Standards for Unitary Air-Conditioning and Air Source Pump Equipment (1989).

18. Flammability and Reactivity of Select HFCs and Mixtures. ASHRAE Journal, December 1993, pp. 40-46.

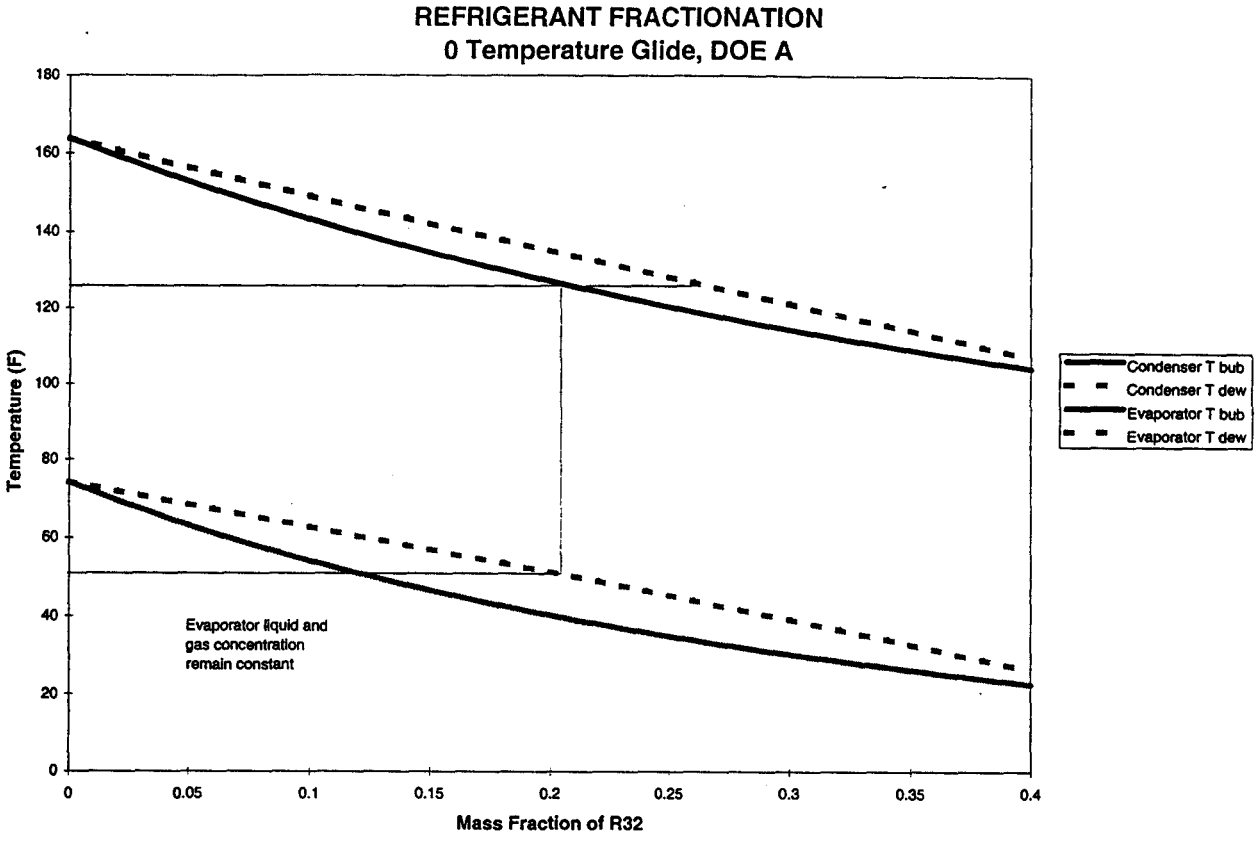

Fig 3.1 Refrigerant Fractionation 0 Temperature Glide, DOE A

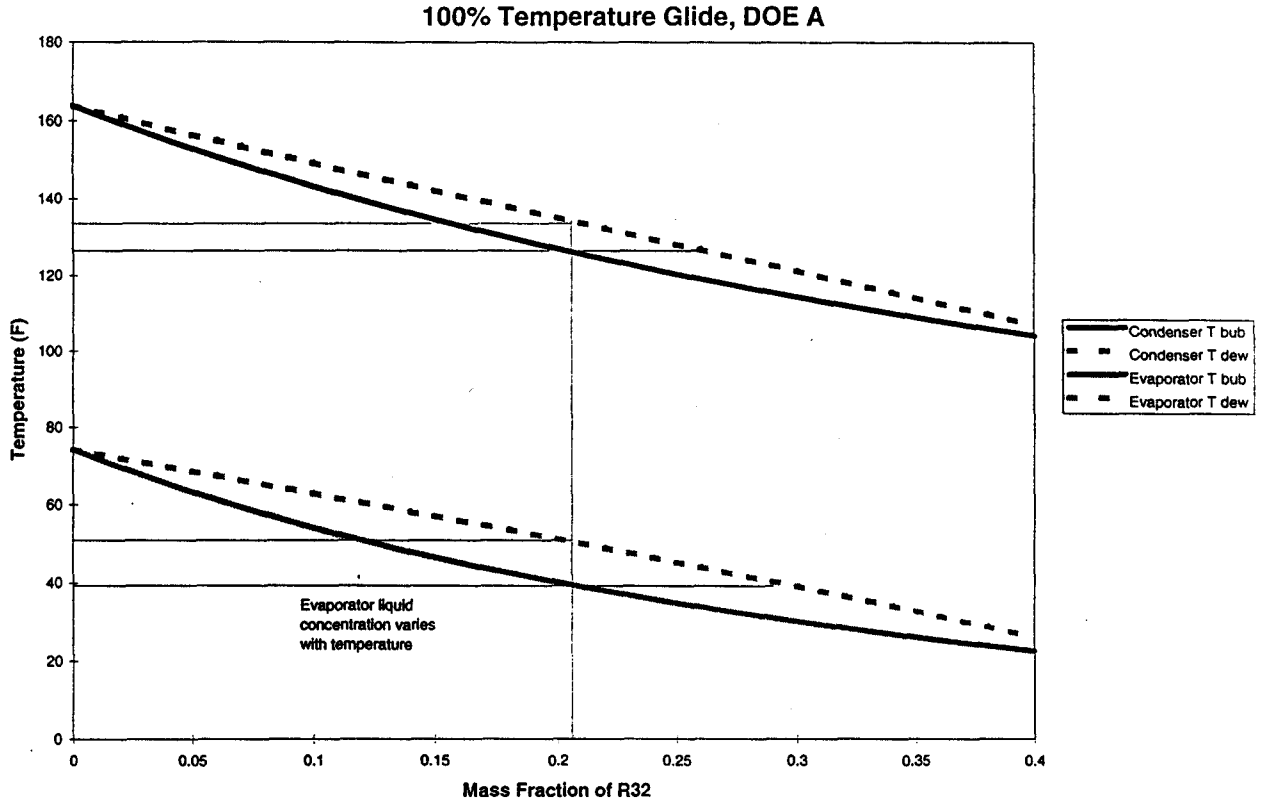

Fig 3.2 Refrigerant Fractionation 100% Temperature Glide, DOE A

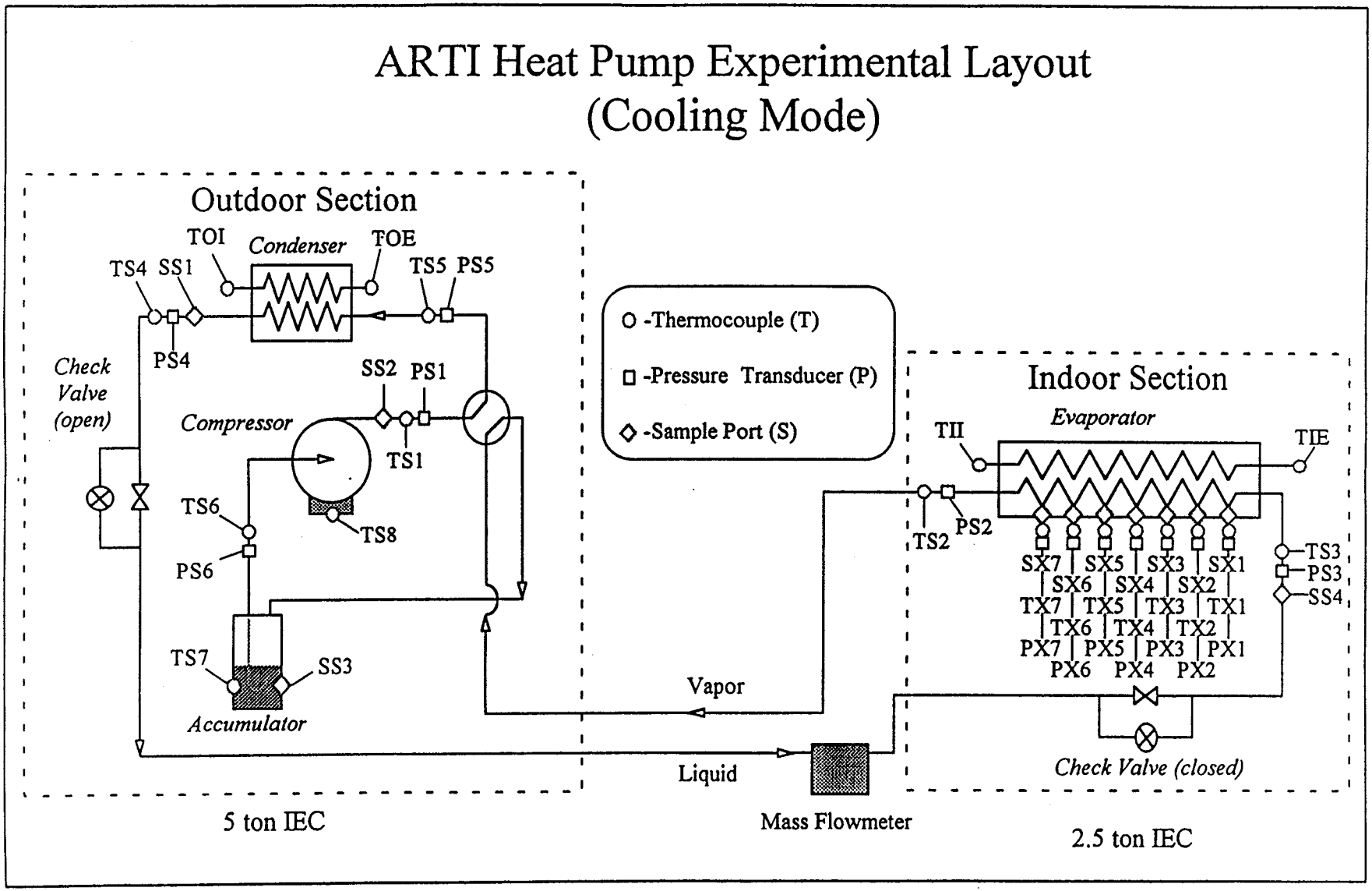

Fig. 3.3 ARTI Heat Pump Experimental Layout (Cooling Mode)

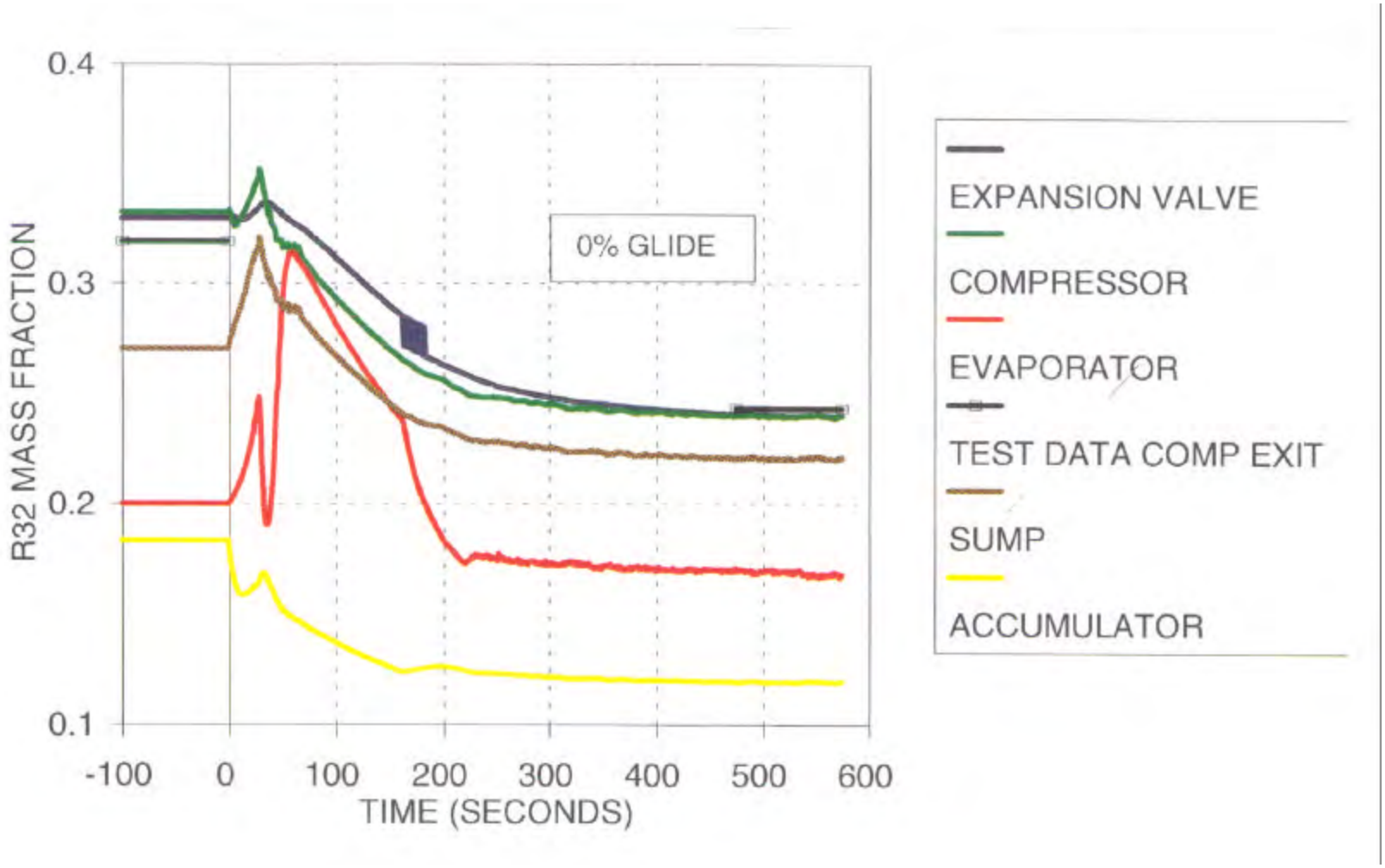

Fig. 3.4 R32 Concentration by Component - DOE A, 7.0 LB Refrigerant @ 21.1% R32

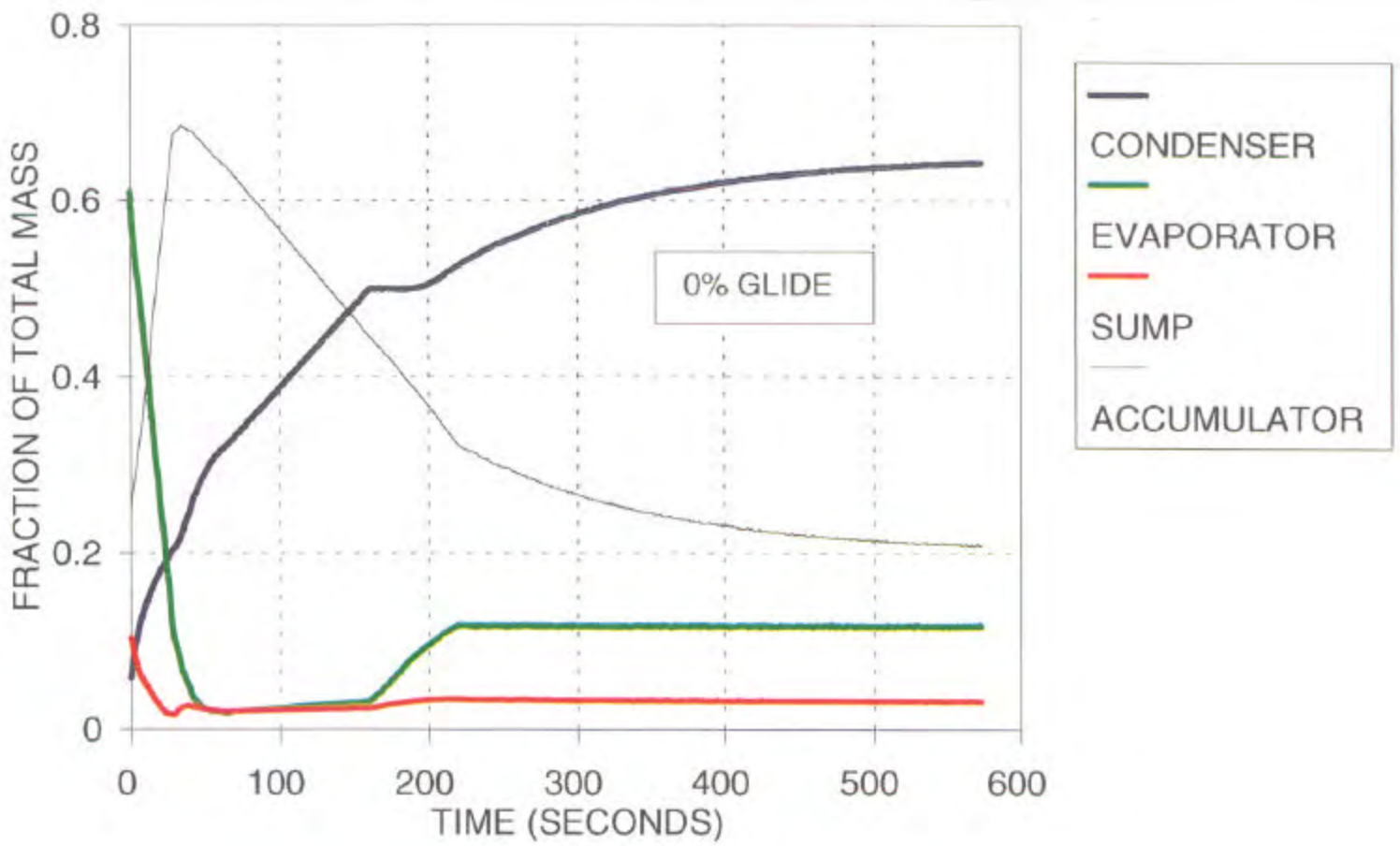

Fig. 3.5 Refrigerant Location - DOE A, 7.0 LB Refrigerant @ 21.1% R32

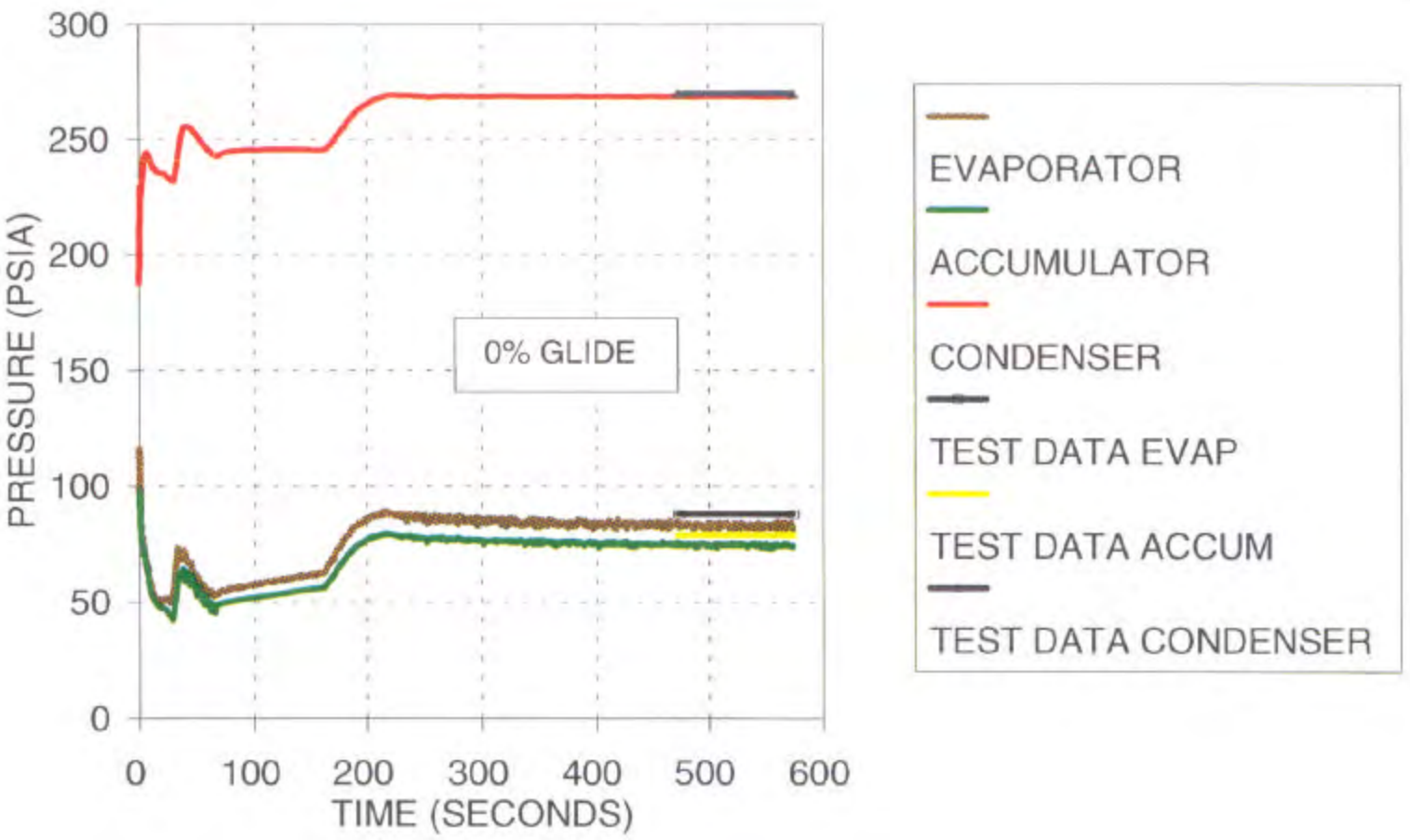

Fig. 3.6 Heat Exchanger Pressure - DOE A, 7.0 LB Refrigerant @ 21.1% R32

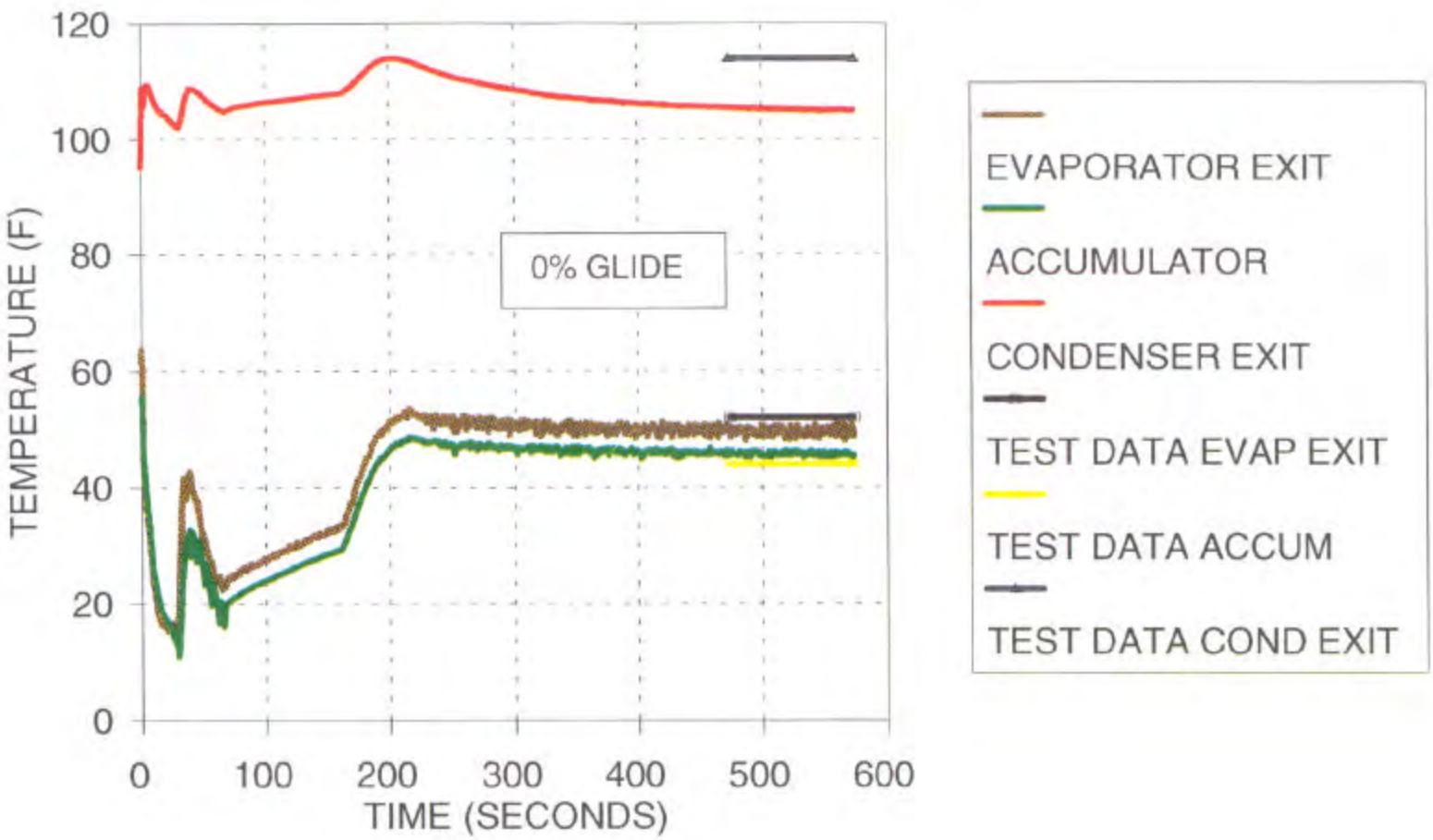

Fig. 3.7 Heat Exchanger Performance - DOE A, 7.0 LB Refrigerant @ 21.1% R32

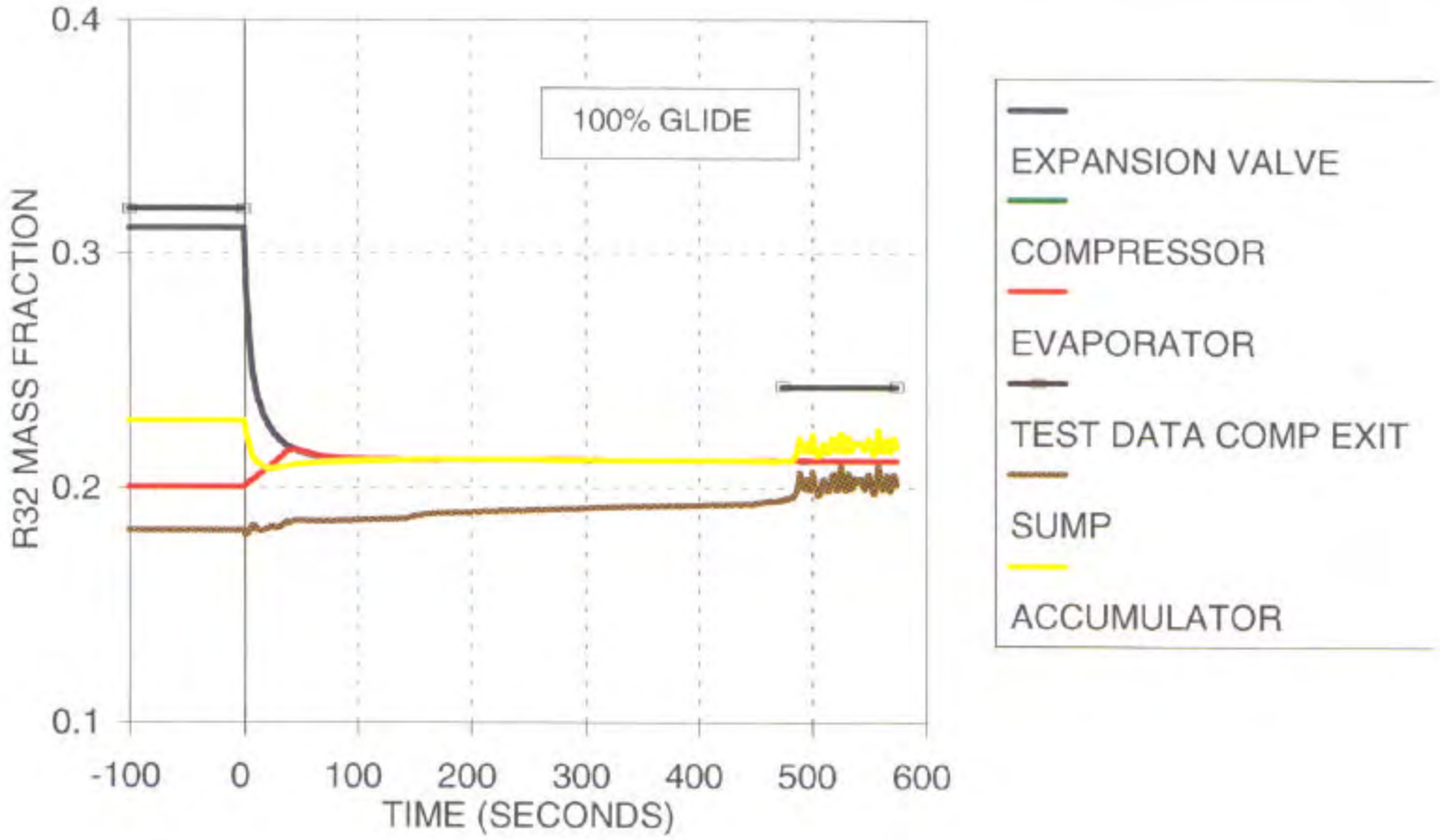

Fig. 3.8 R32 Concentration by Component - DOE A, 7.0 LB Refrigerant @ 21.1% R32

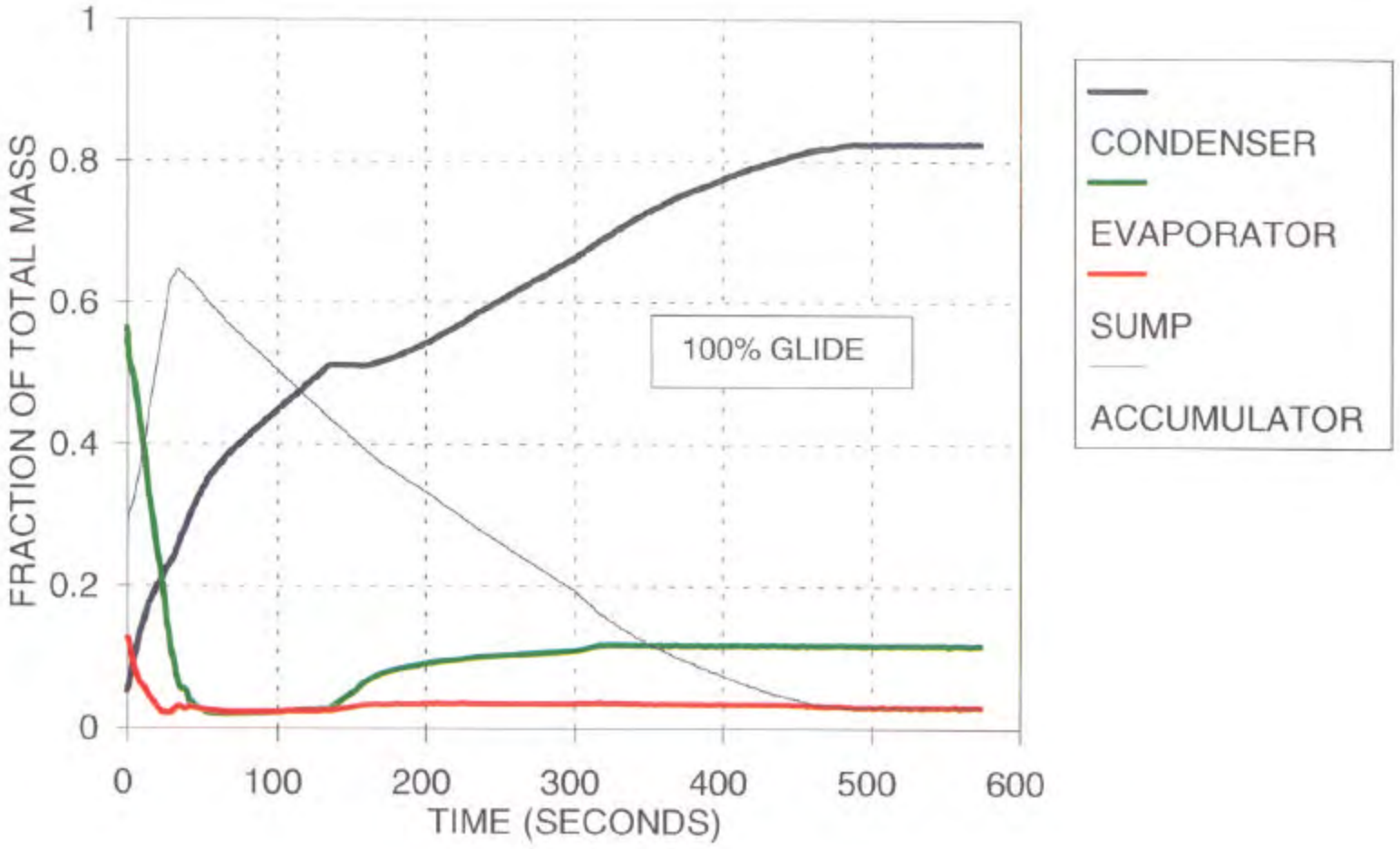

Fig. 3.9 Refrigerant Location - DOE A, 7.0 LB Refrigerant @ 21.1% R32

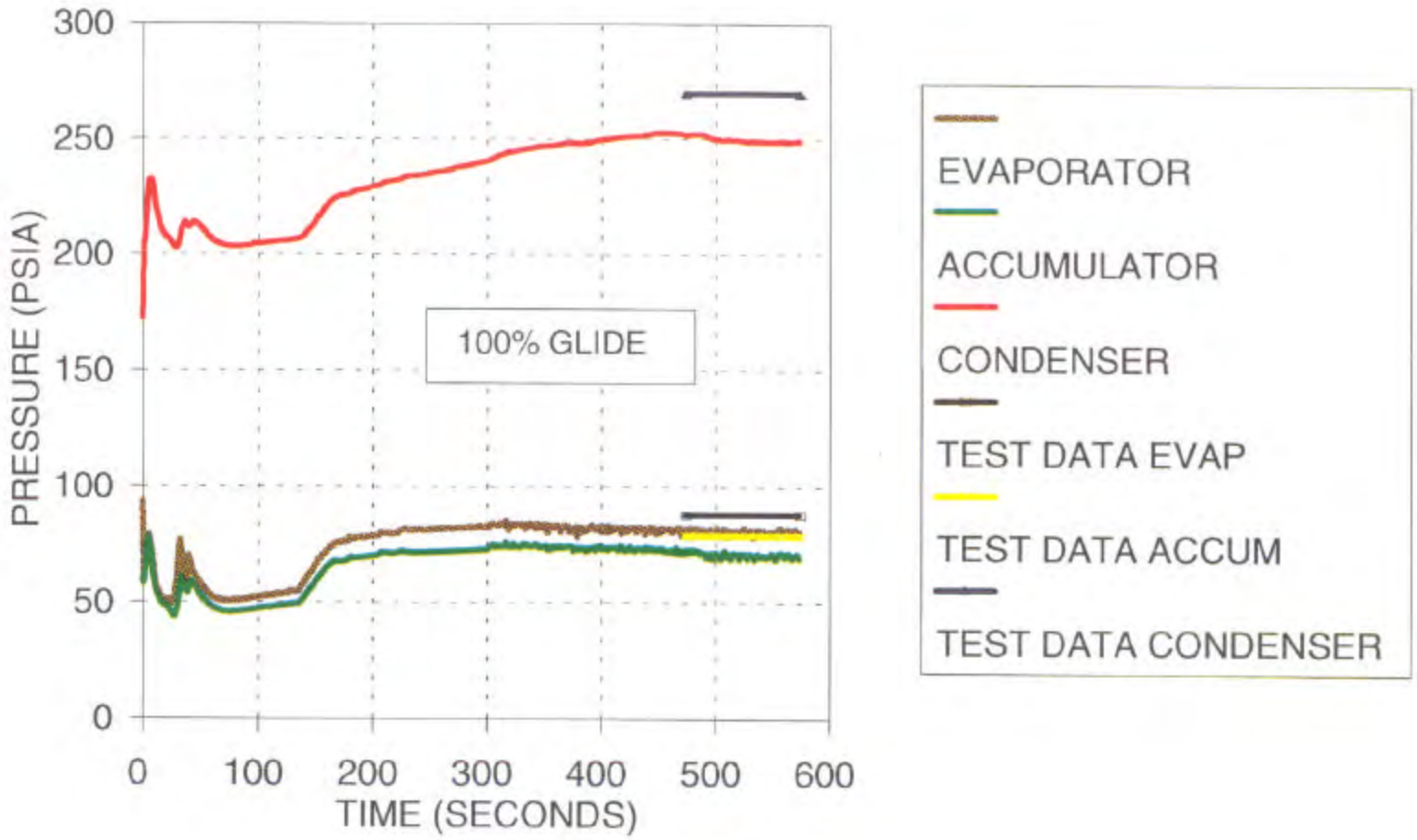

Fig. 3.10 Heat Exchanger Pressure - DOE A, 7.0 LB Refrigerant @ 21.1% R32

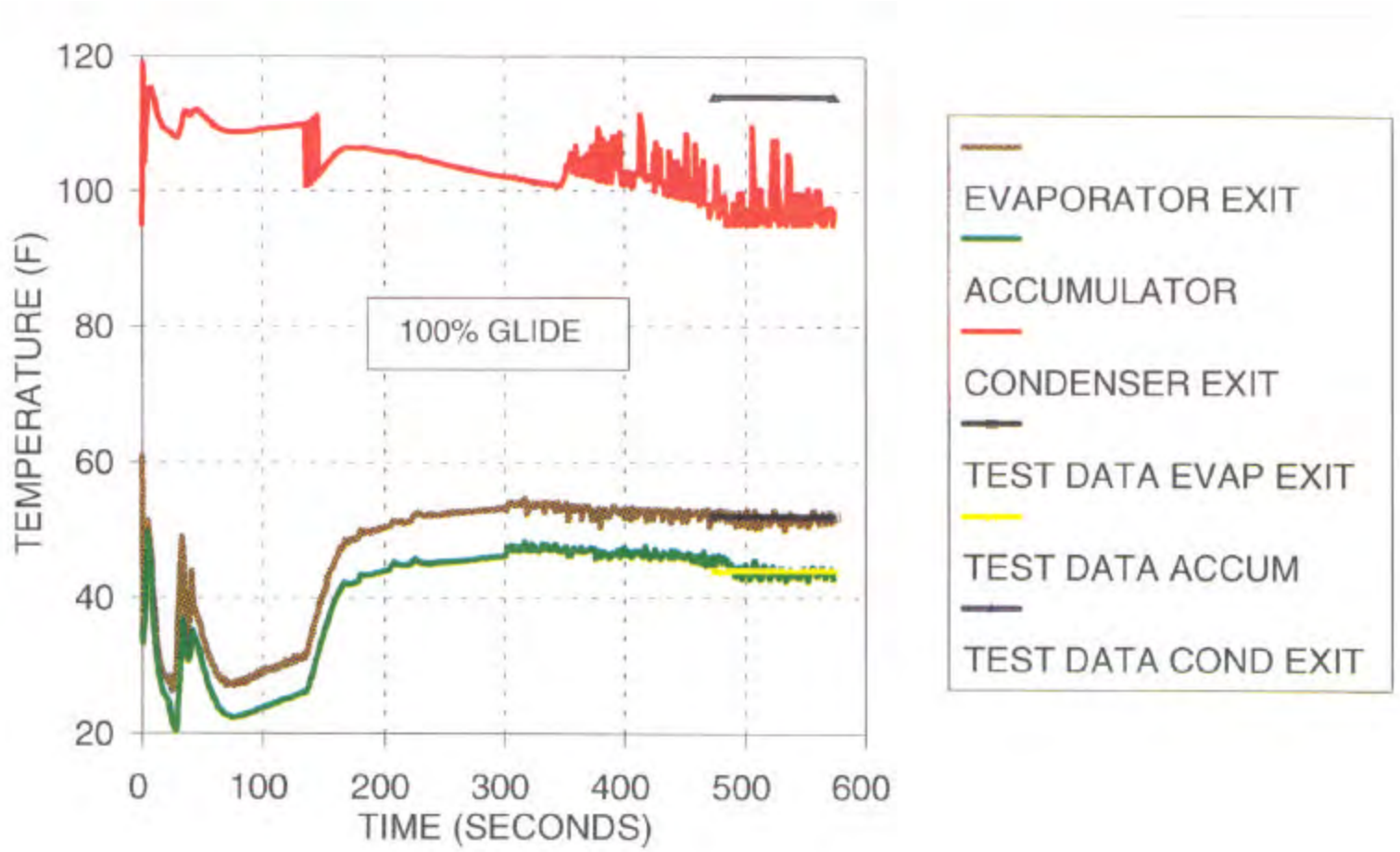

Fig. 3.11 Heat Exchanger Performance - DOE A, 7.0 LB Refrigerant @ 21.1% R32

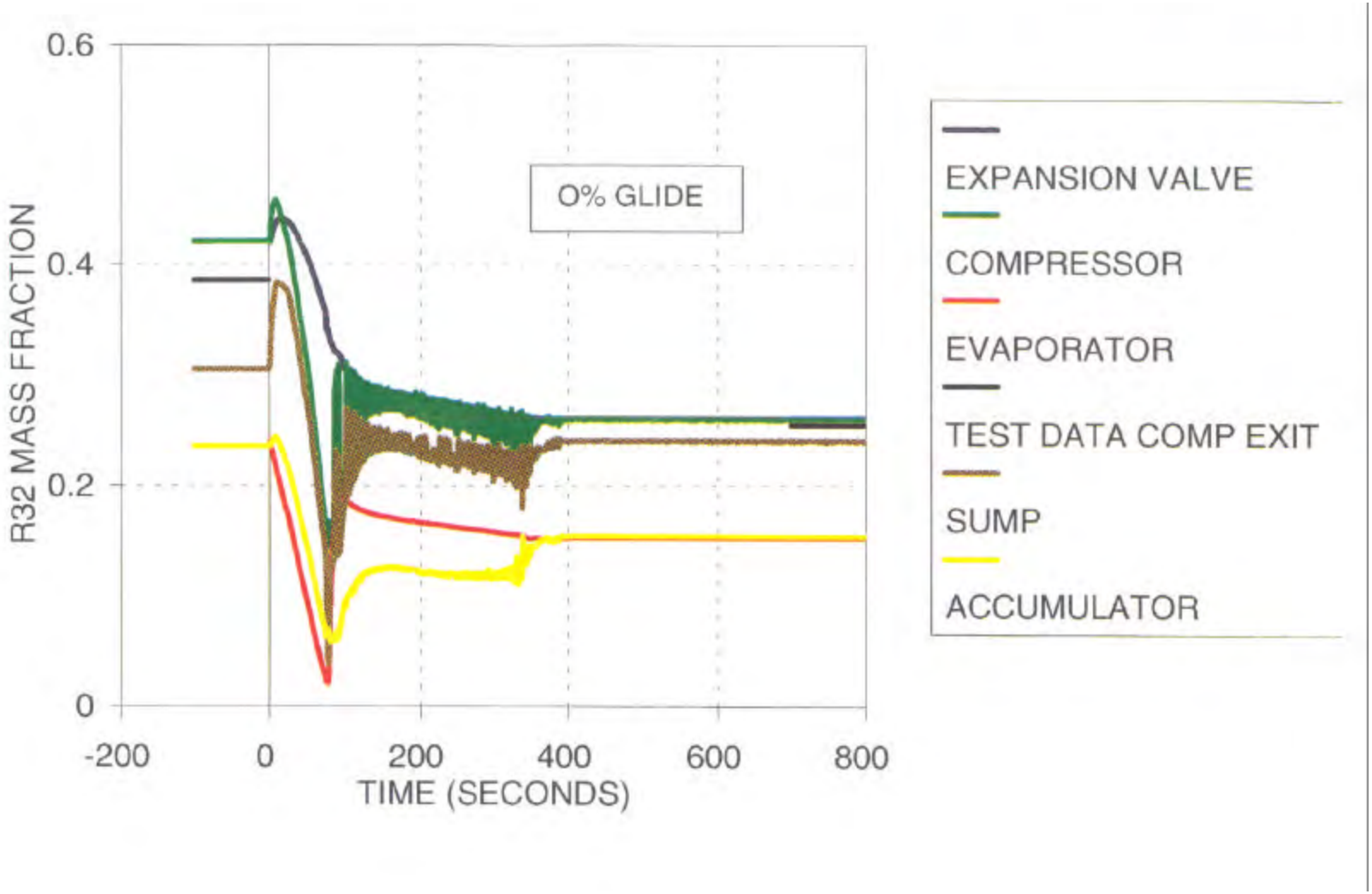

Fig. 3.12 R32 Concentration by Component - DOE E, 7.0 LB Refrigerant @ 25.6% R32

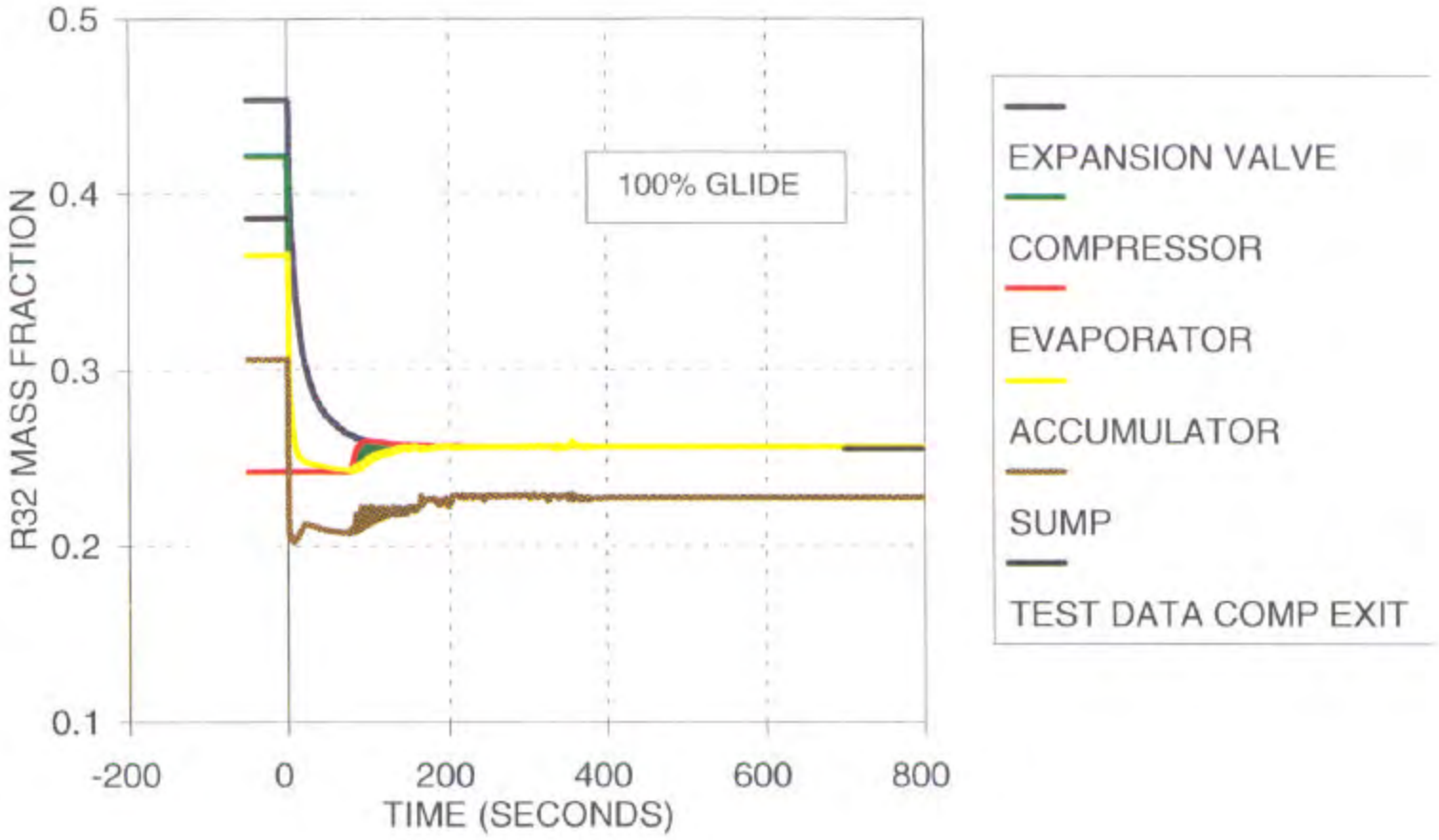

Fig. 3.13 R32 Concentration by Component - DOE E, 7.0 LB Refrigerant @ 25.6% R32

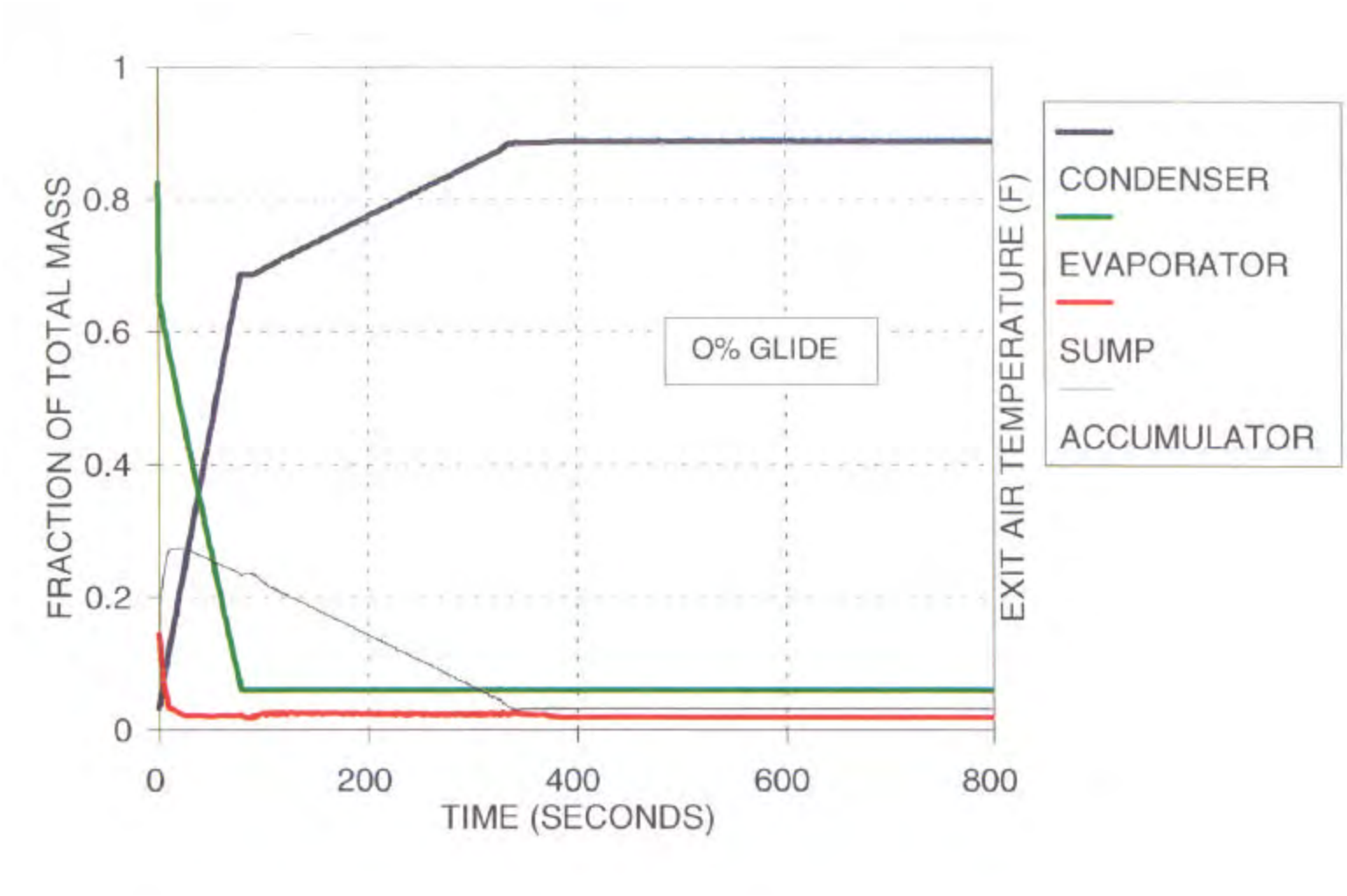

Fig. 3.14 Refrigerant Location - DOE E, 7.0 LB Refrigerant @ 25.6% R32

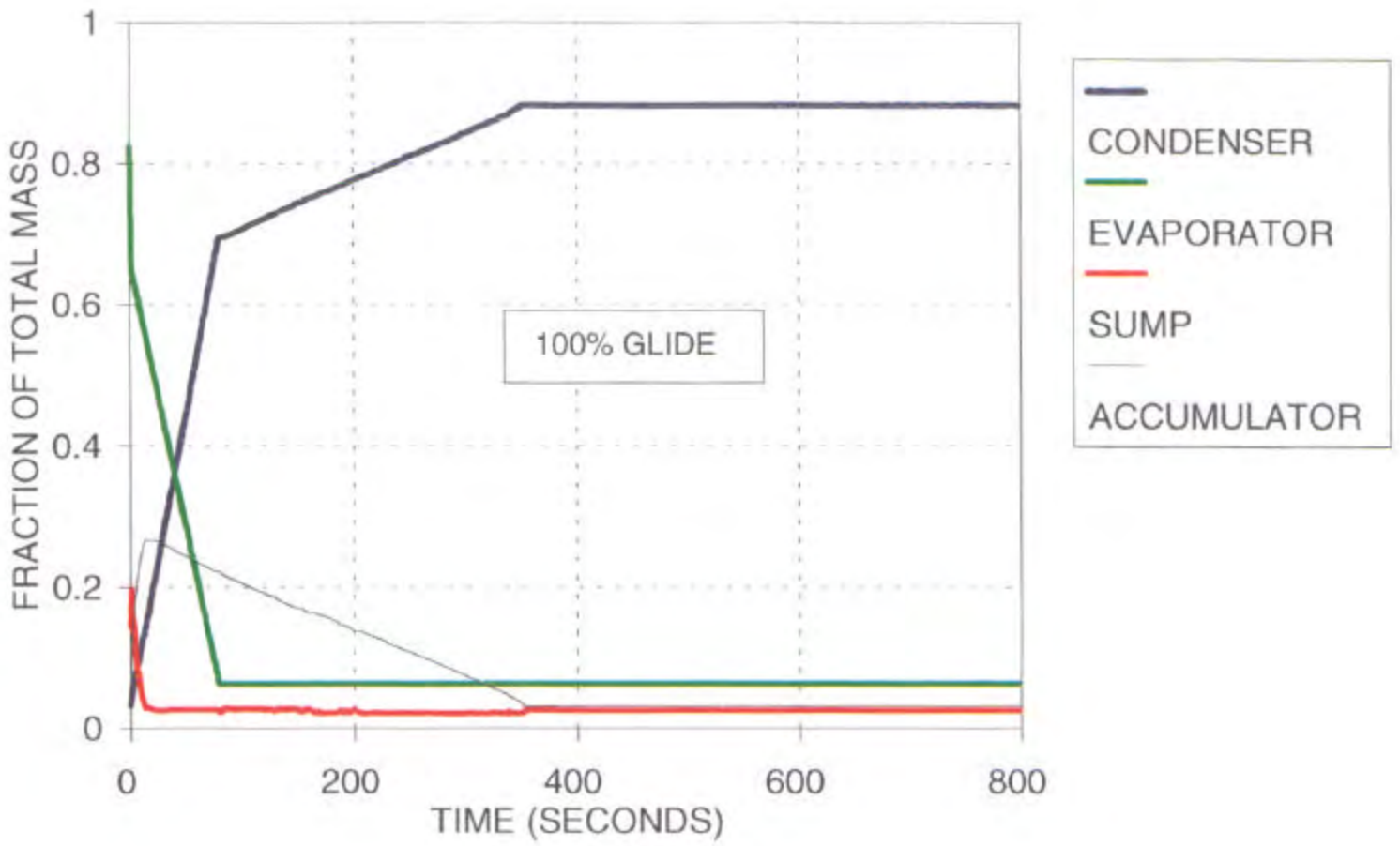

Fig. 3.15 Refrigerant Location - DOE E, 7.0 LB Refrigerant @ 25.6% R32

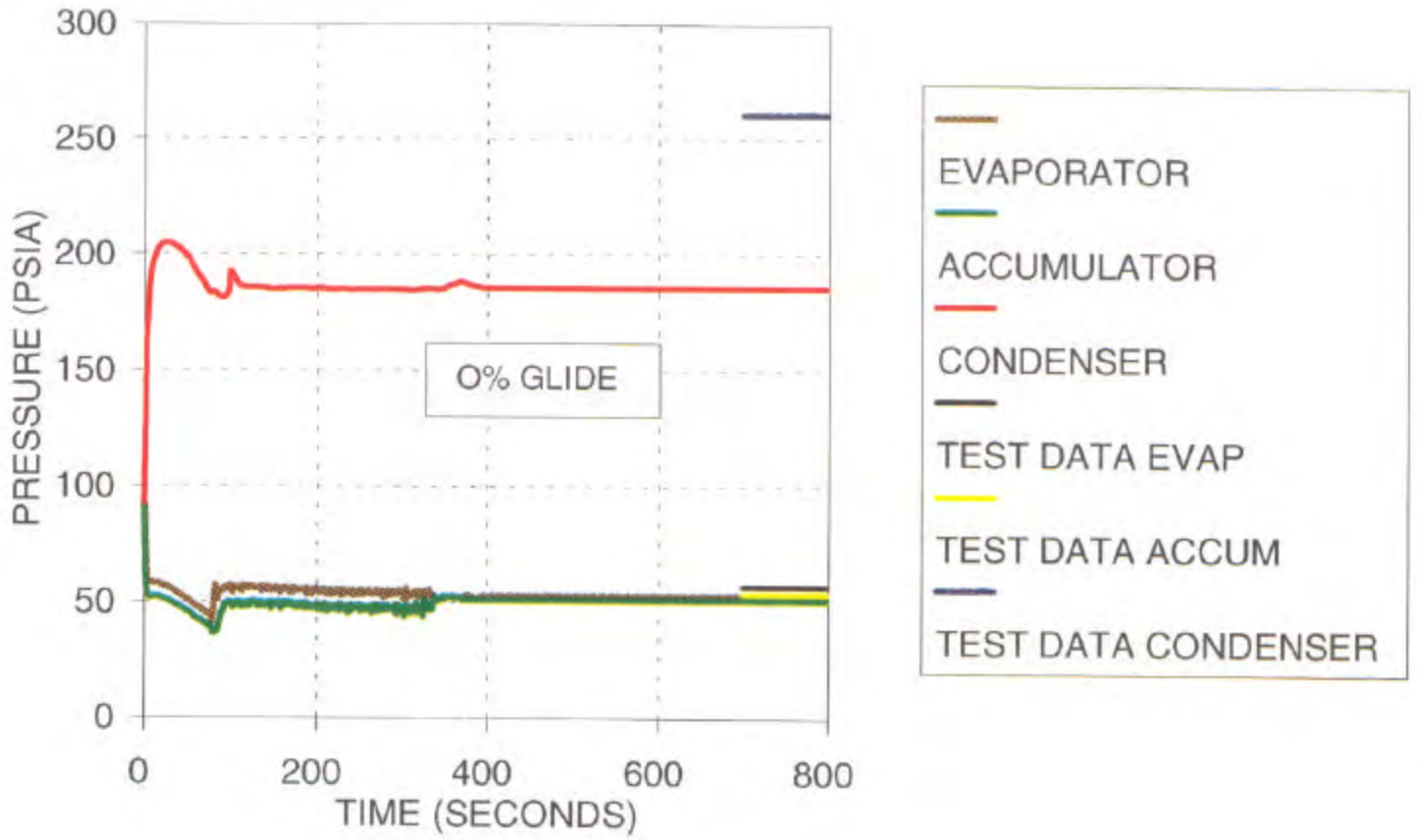

Fig. 3.16 Heat Exchanger Pressure - DOE E, 7.0 LB Refrigerant @ 25.6% R32

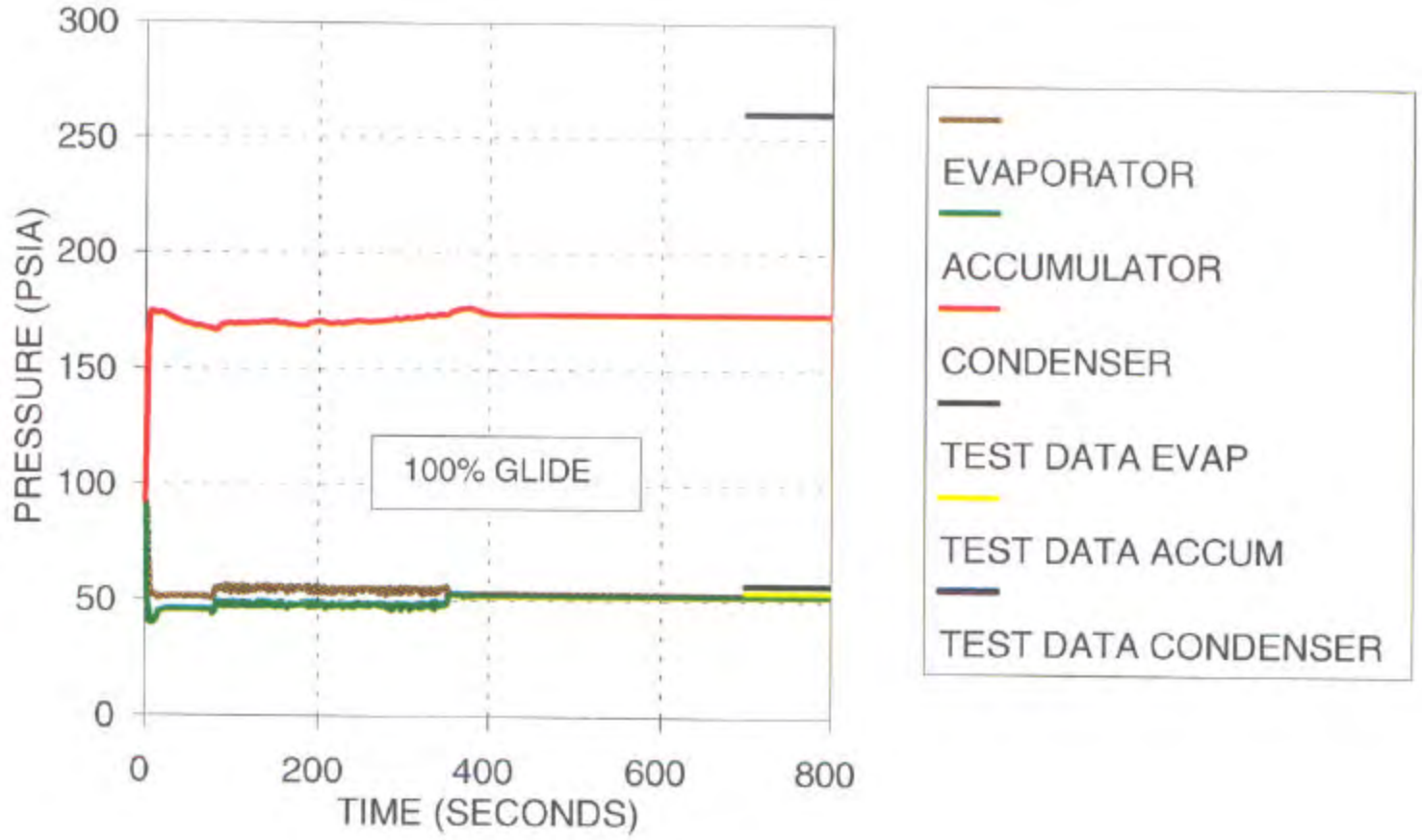

Fig. 3.17 Heat Exchanger Pressure - DOE E, 7.0 LB Refrigerant @ 25.6% R32

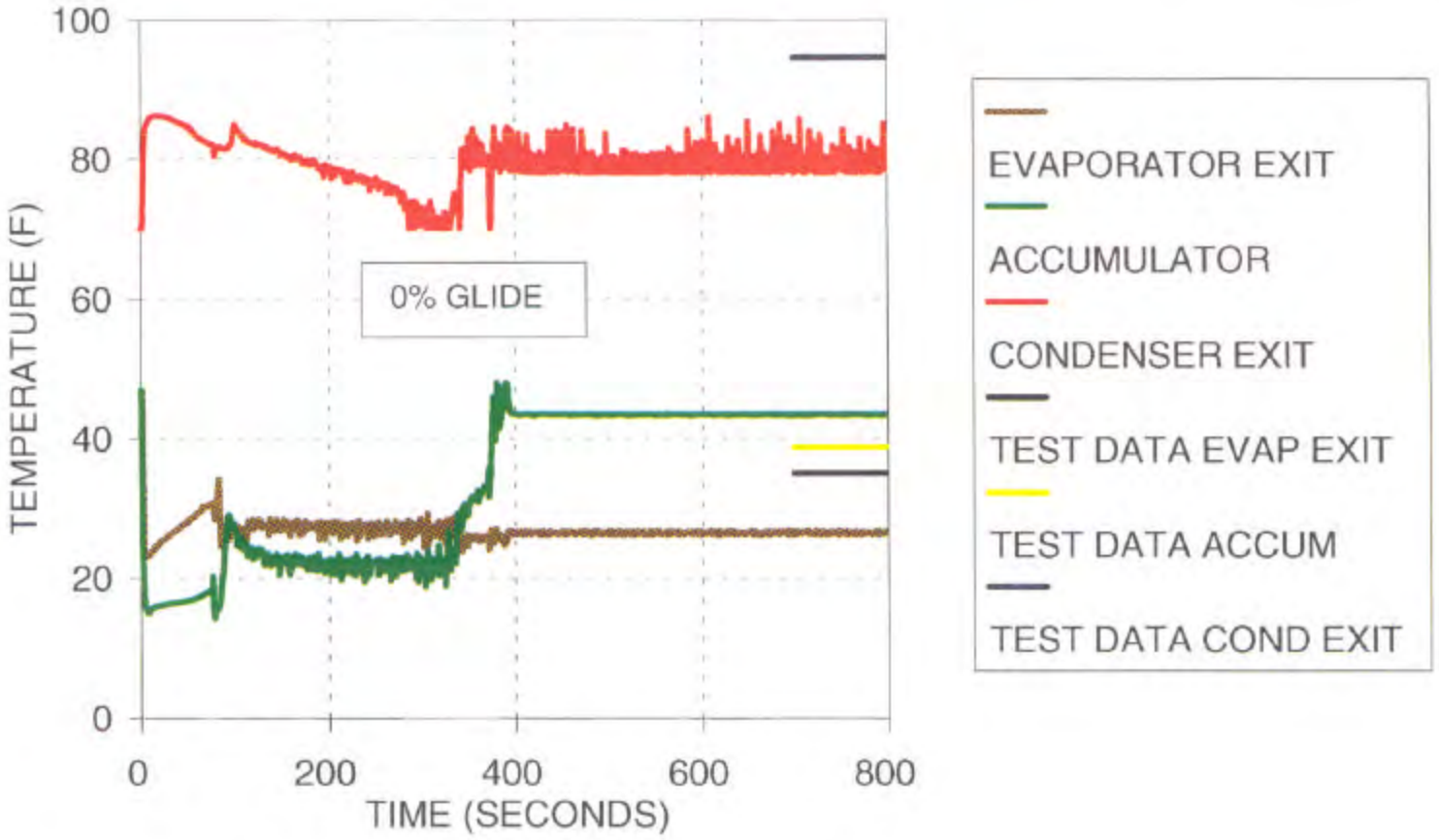

Fig. 3.18 Heat Exchanger Performance - DOE E, 7.0 LB Refrigerant @ 25.6% R32

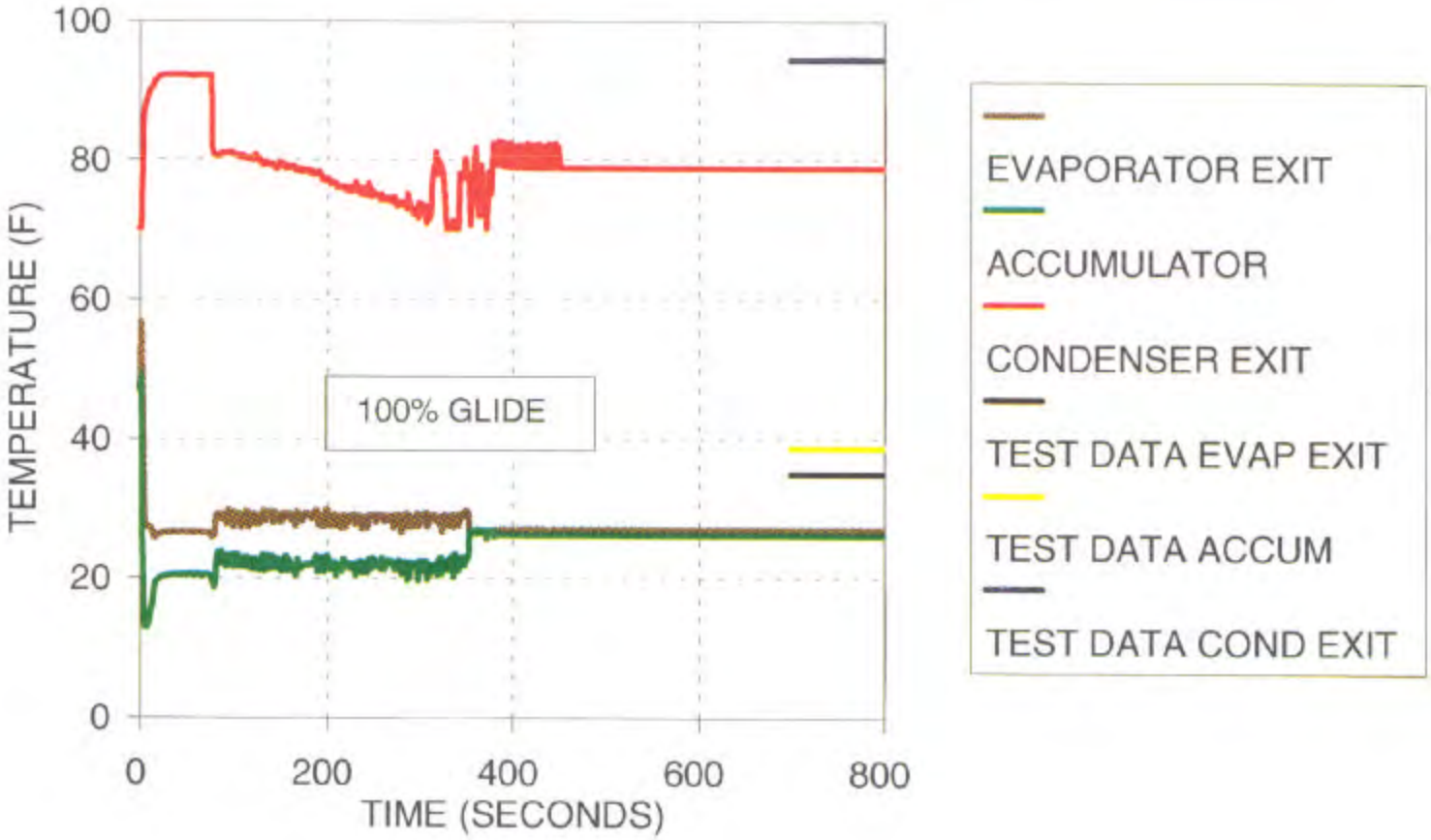

Fig. 3.19 Heat Exchanger Performance - DOE E, 7.0 LB Refrigerant @ 25.6% R32

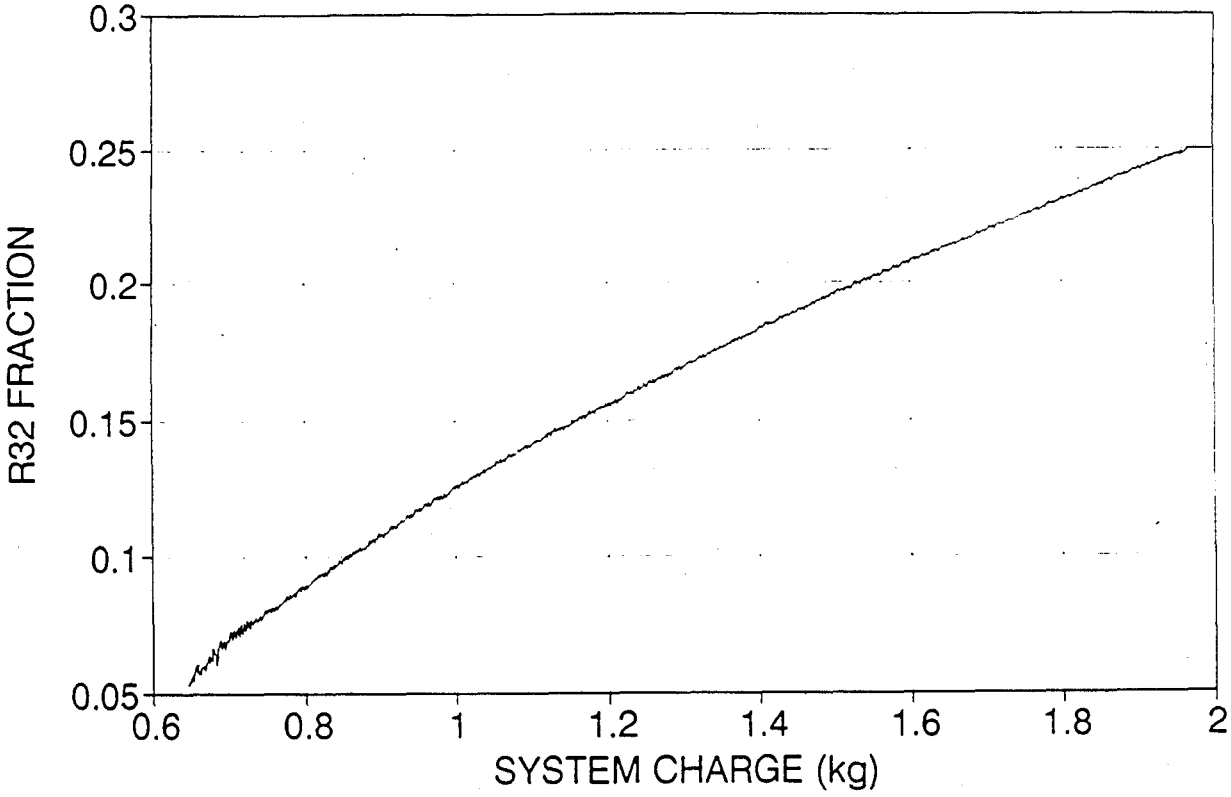

Fig. 3.20 Slow System Leak 2.5 Ton HP/DOE A/(25/75) Initial Charge

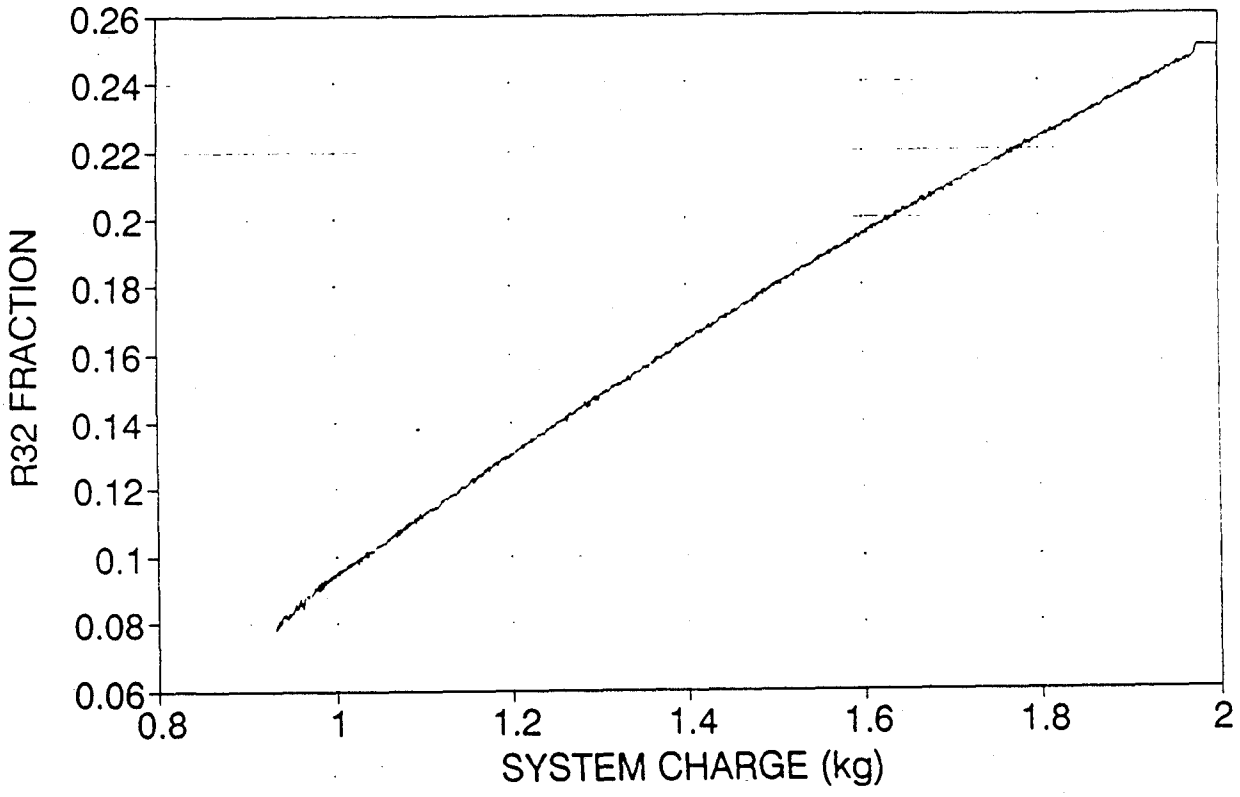

Fig. 3.21 Slow System Leak 2.5 Ton HP/DOE E/(25/75) Initial Charge

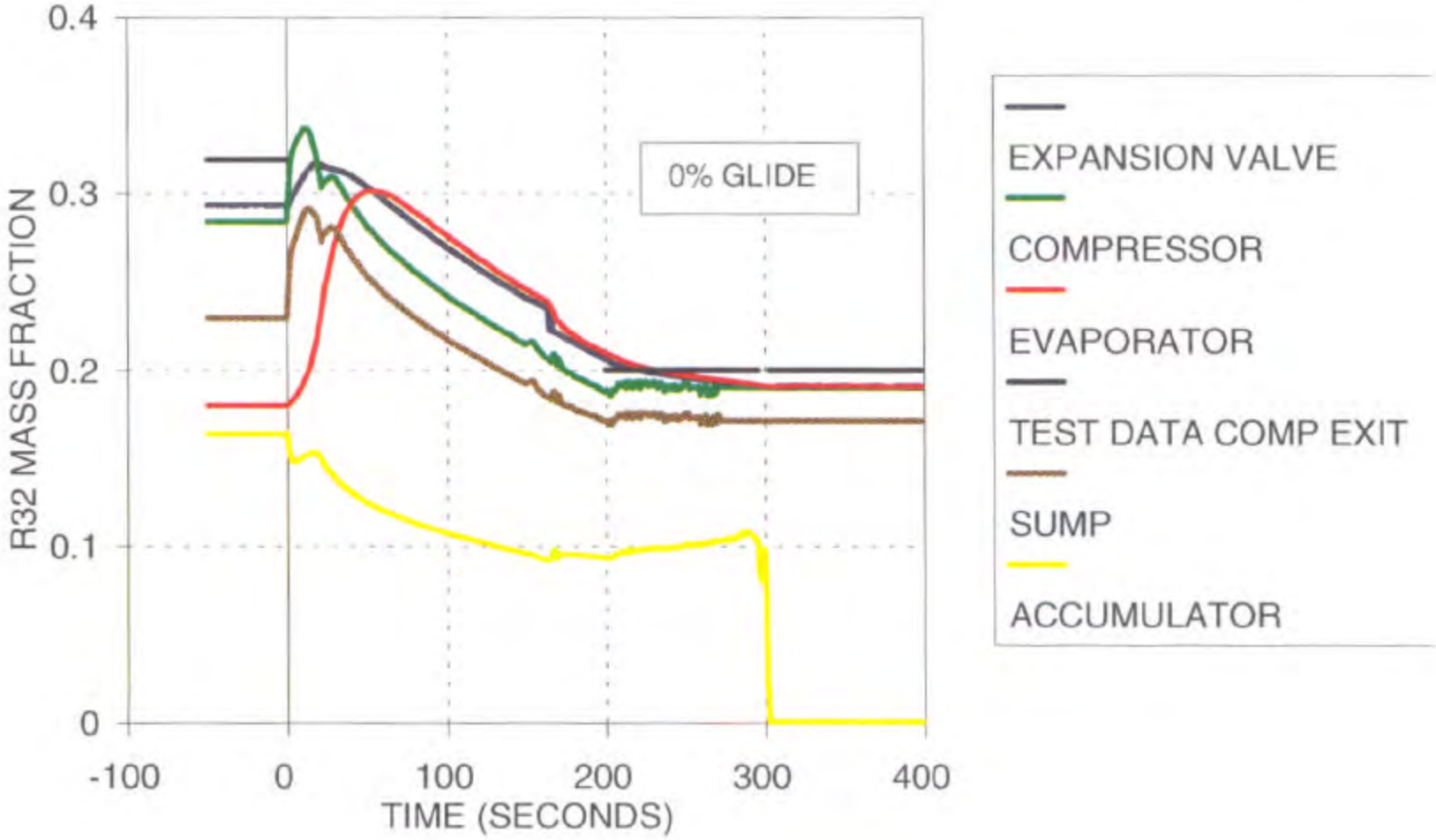

Fig. 3.22 R32 Concentration by Component - DOE A, 5.8 LB Refrigerant @ 19.2% R32

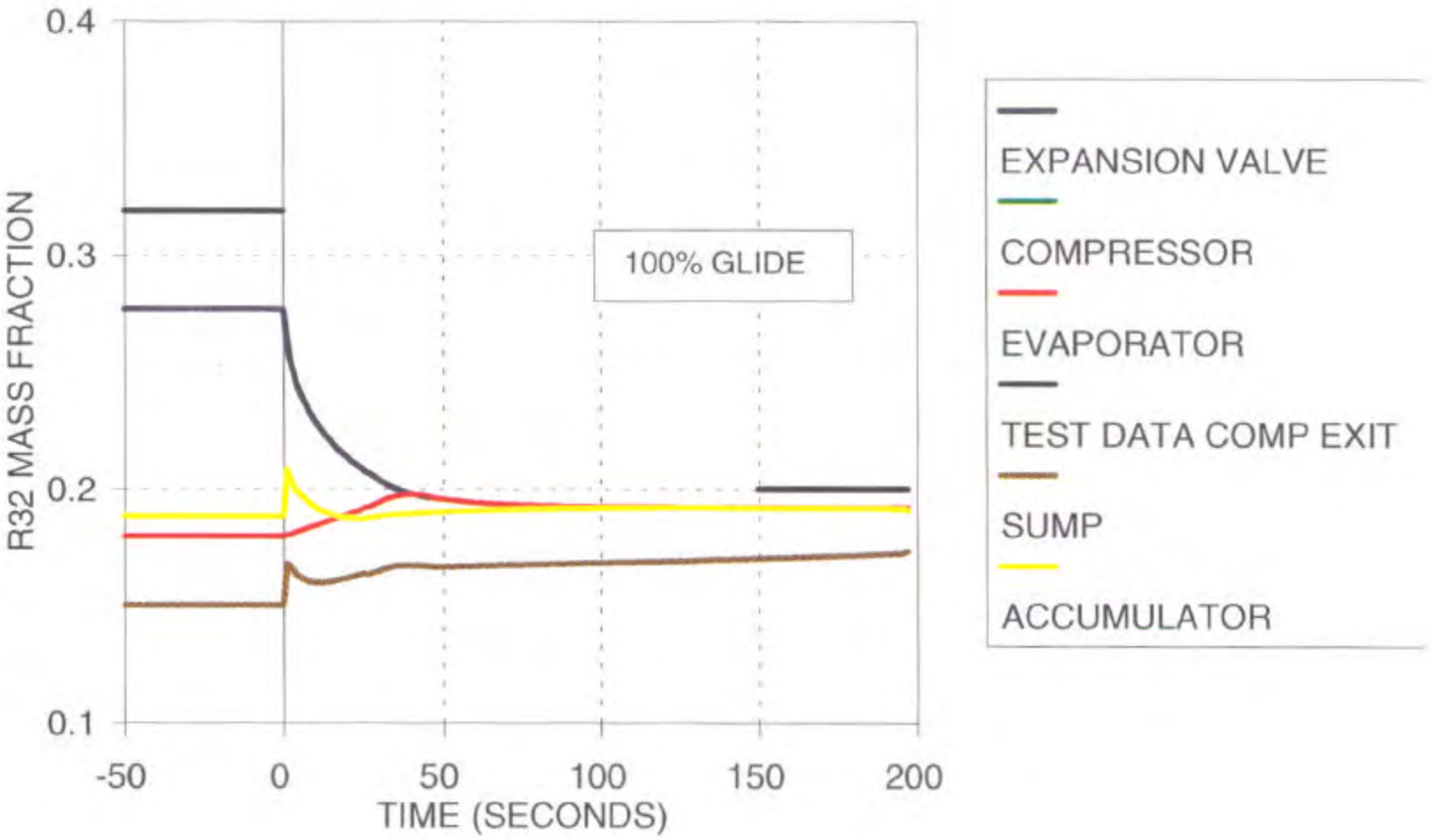

Fig. 3.23 R32 Concentration by Component - DOE A, 5.8 LB Refrigerant @ 19.2% R32

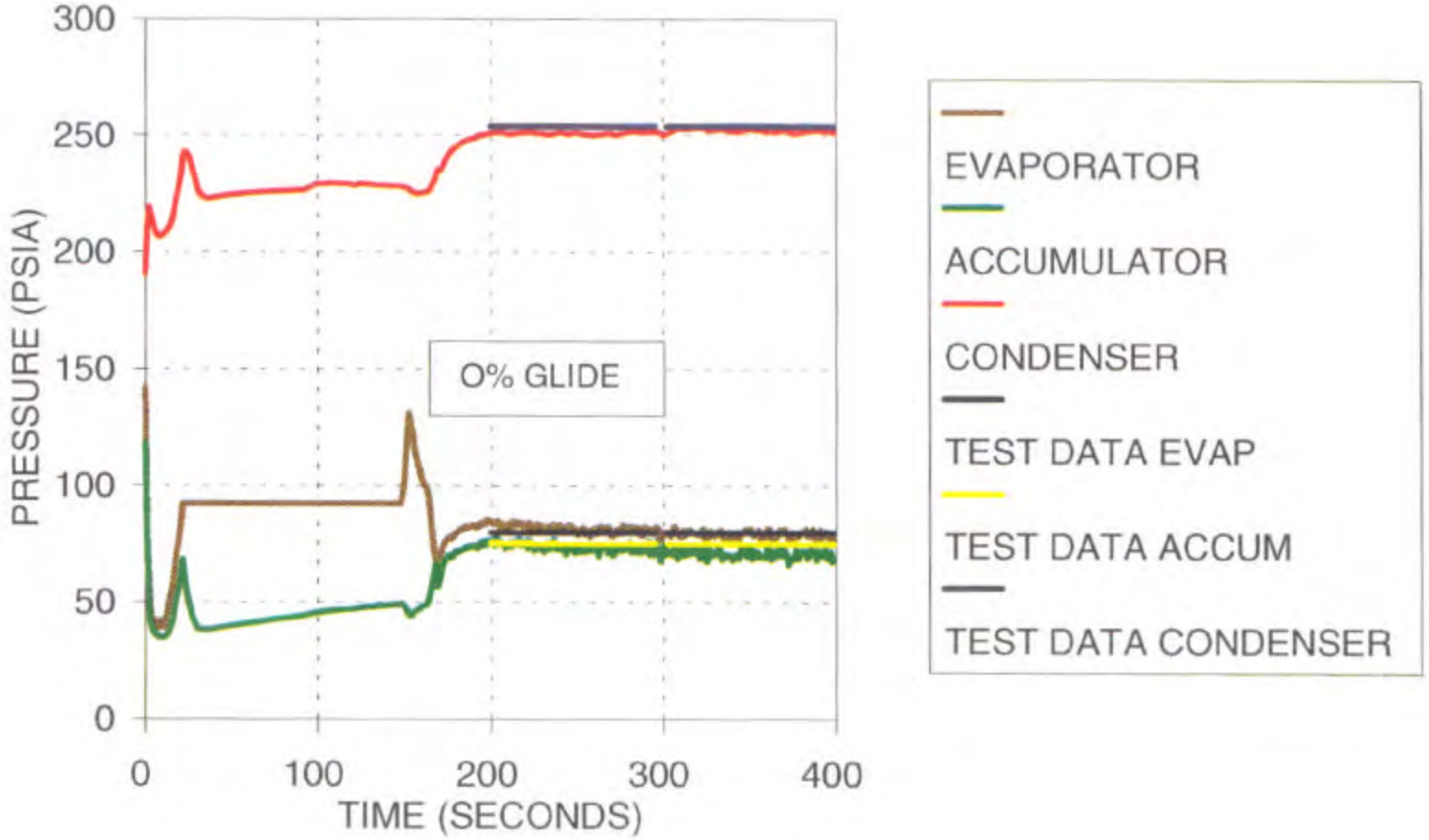

Fig. 3.24 Heat Exchanger Pressure - DOE A, 5.8 LB Refrigerant @ 19.2% R32

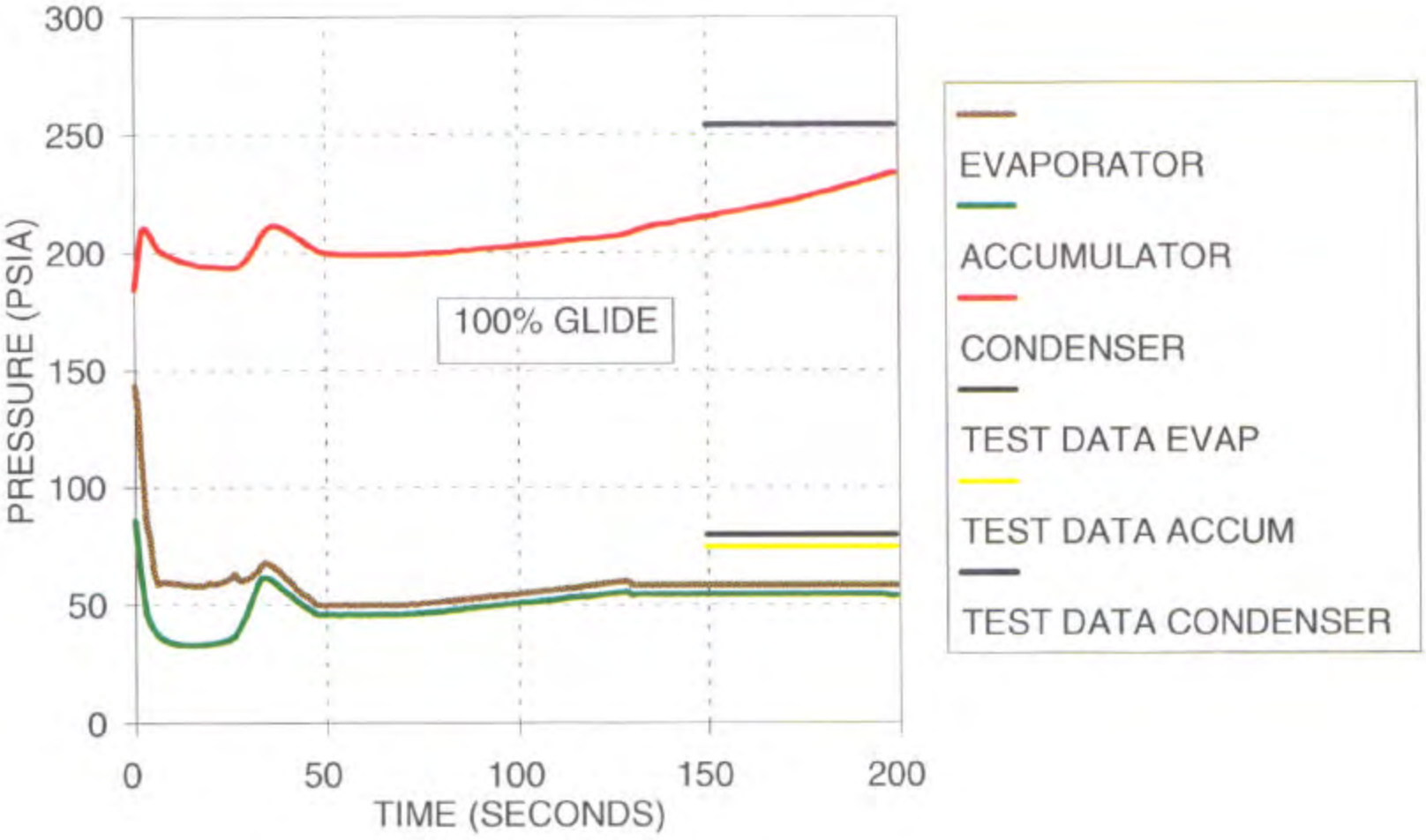

Fig. 3.25 Heat Exchanger Pressure - DOE A, 5.8 LB Refrigerant @ 19.2% R32

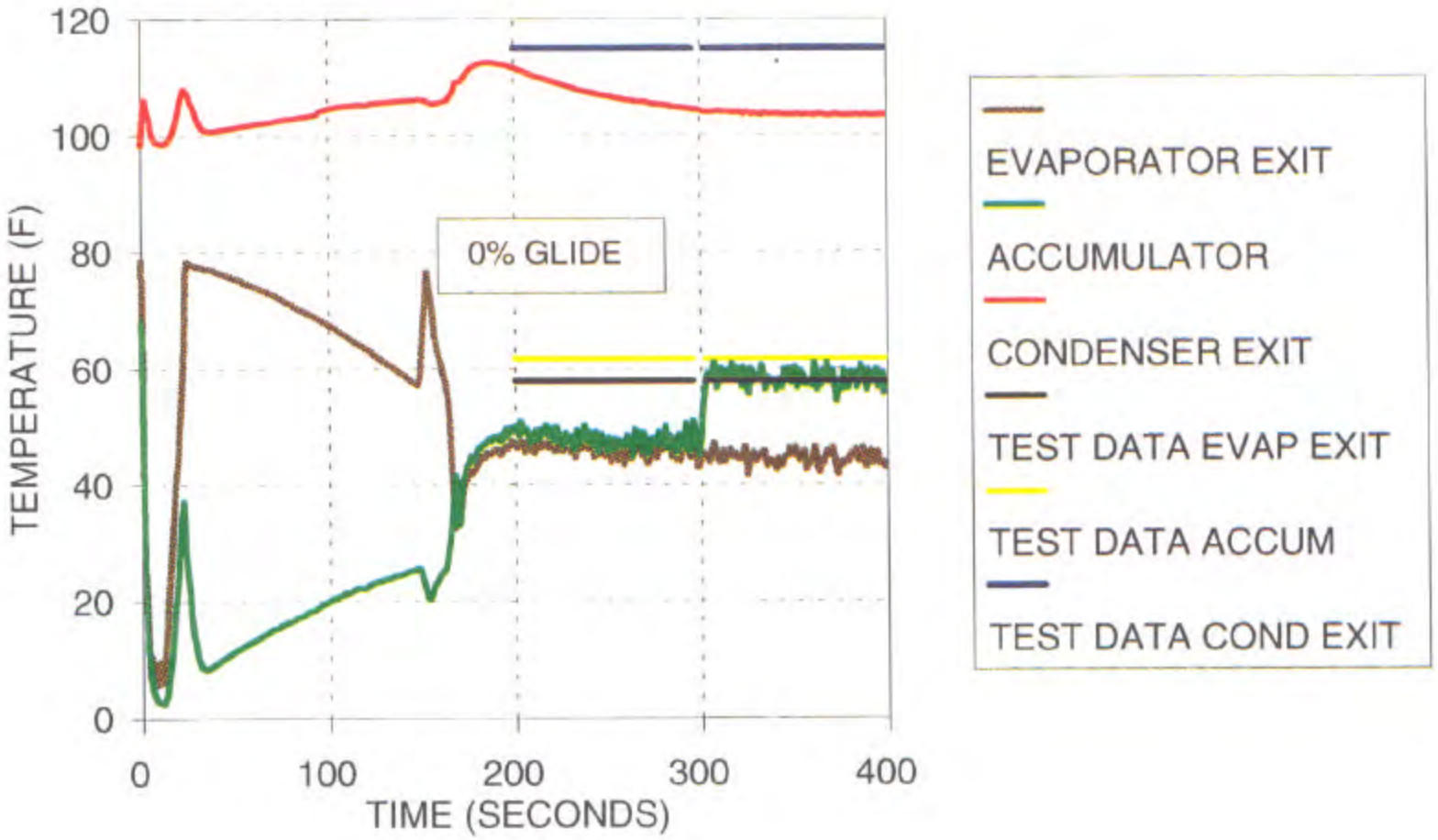

Fig. 3.26 Heat Exchanger Performance - DOE A, 5.8 LB Refrigerant @ 19.2% R32

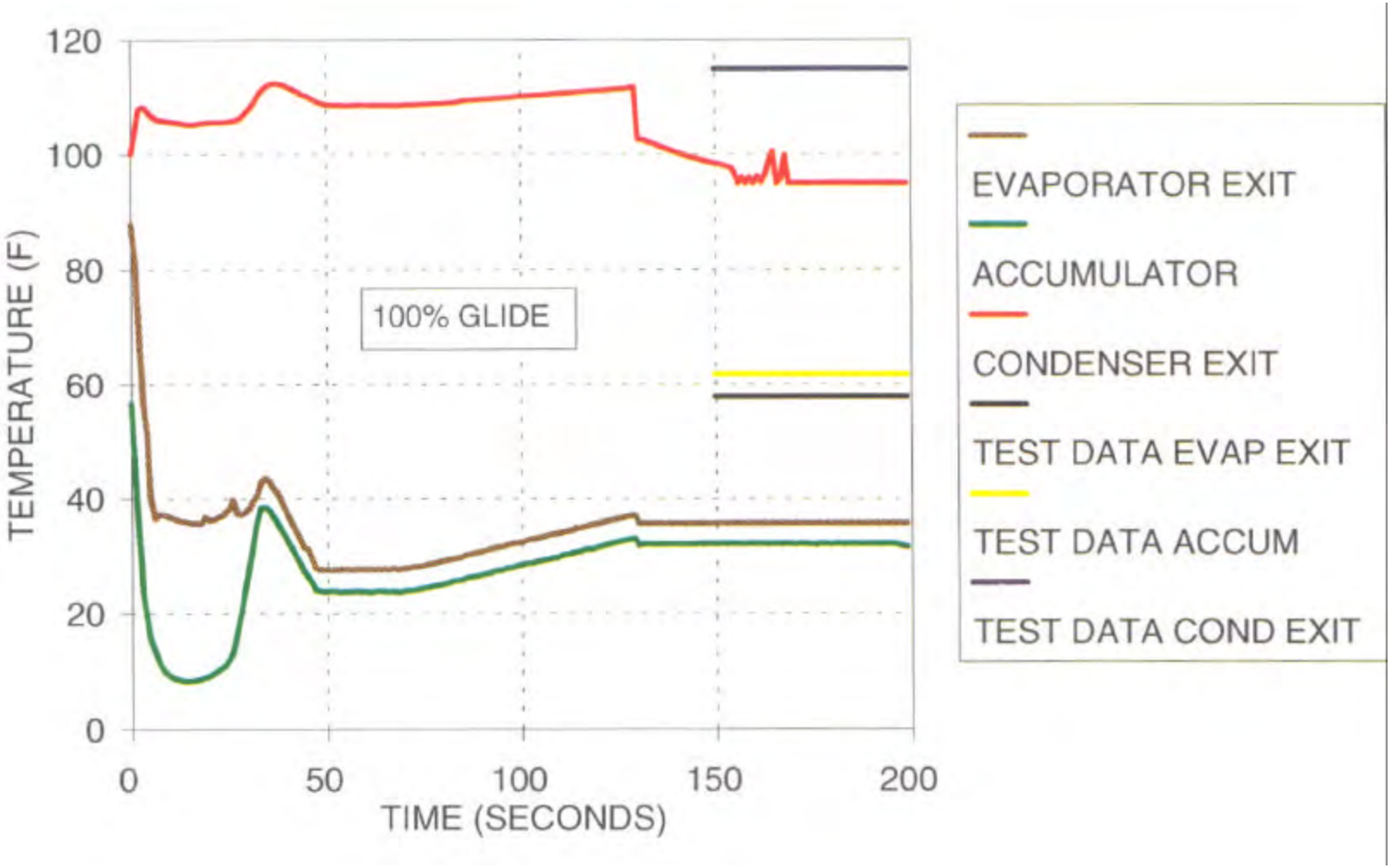

Fig. 3.27 Heat Exchanger Performance - DOE A, 5.8 LB Refrigerant @ 19.2% R32

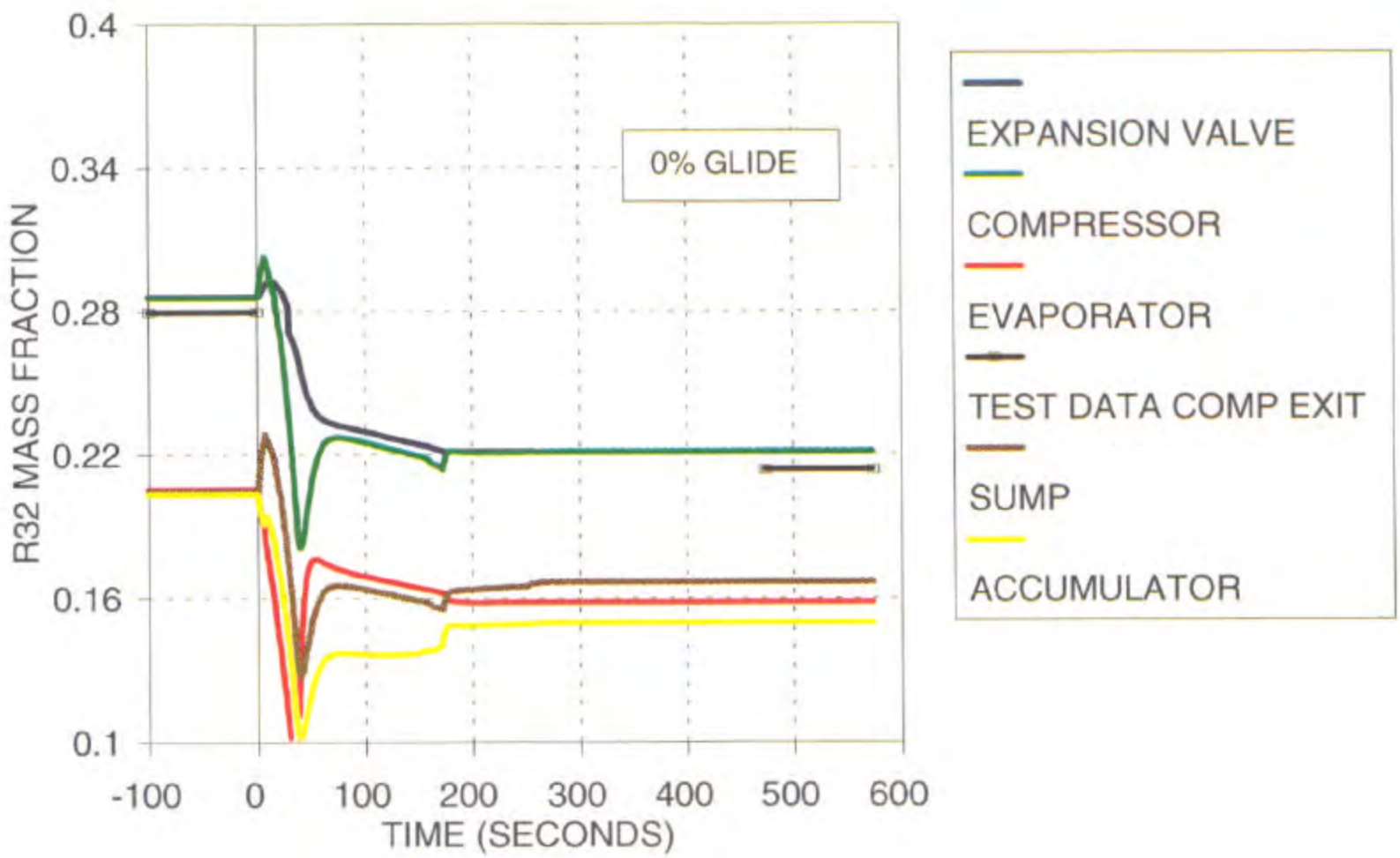

Fig. 3.28 R32 Concentration by Component - DOE A, 6.4 LB Refrigerant 407C

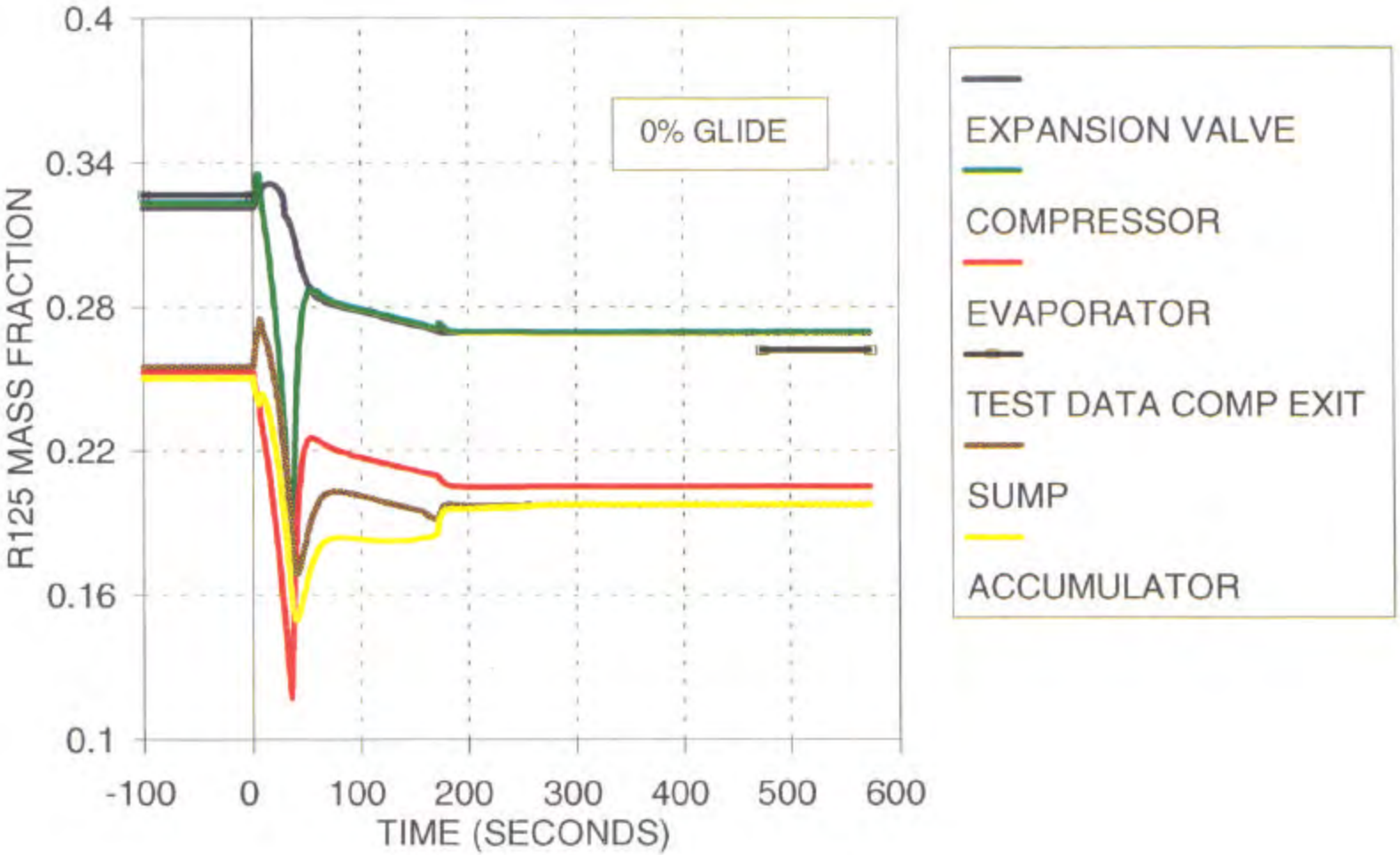

Fig. 3.29 R32 Concentration by Component - DOE A, 6.4 LB Refrigerant 407C

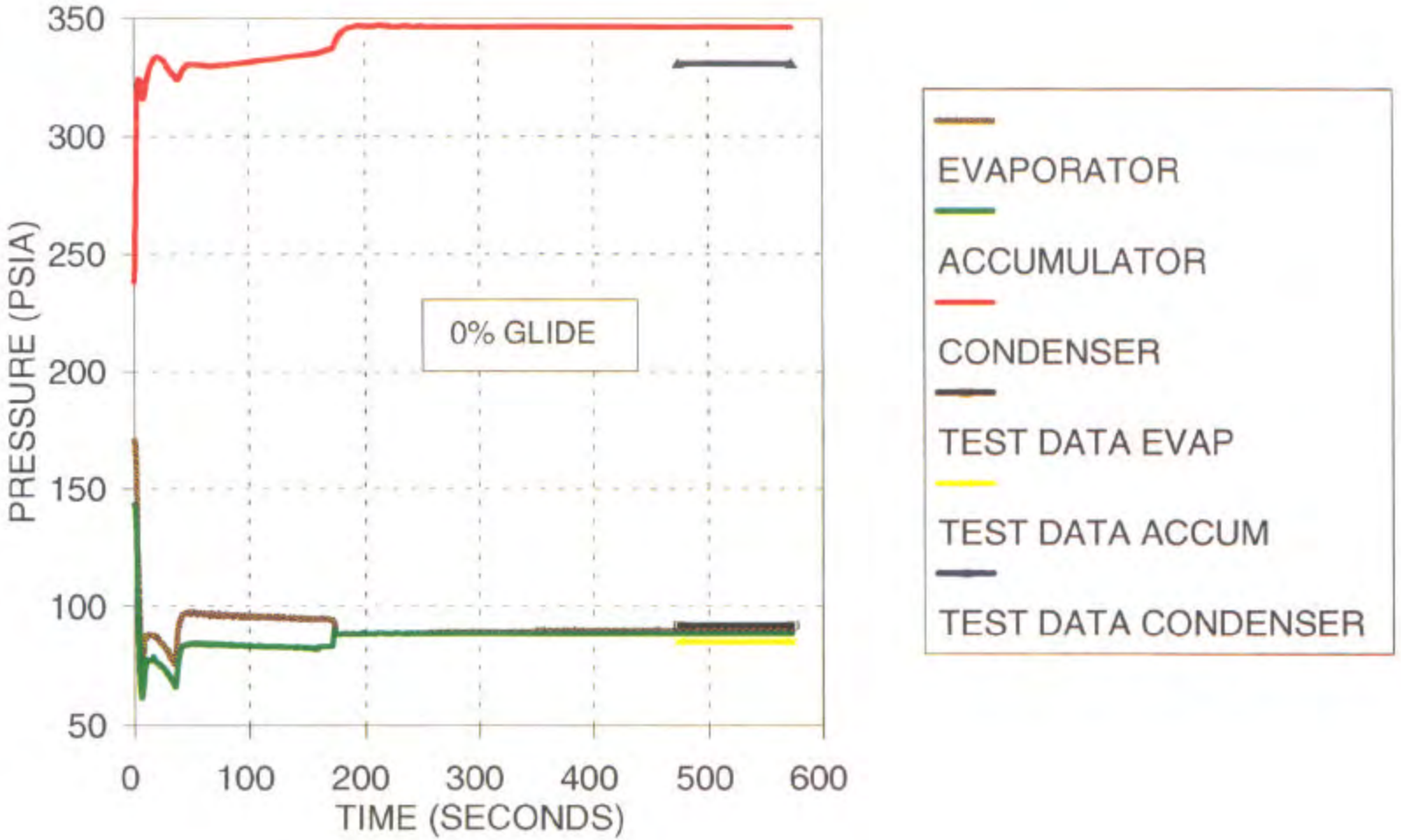

Fig. 3.30 Heat Exchanger Pressure - DOE A, 6.4 LB Refrigerant 407C

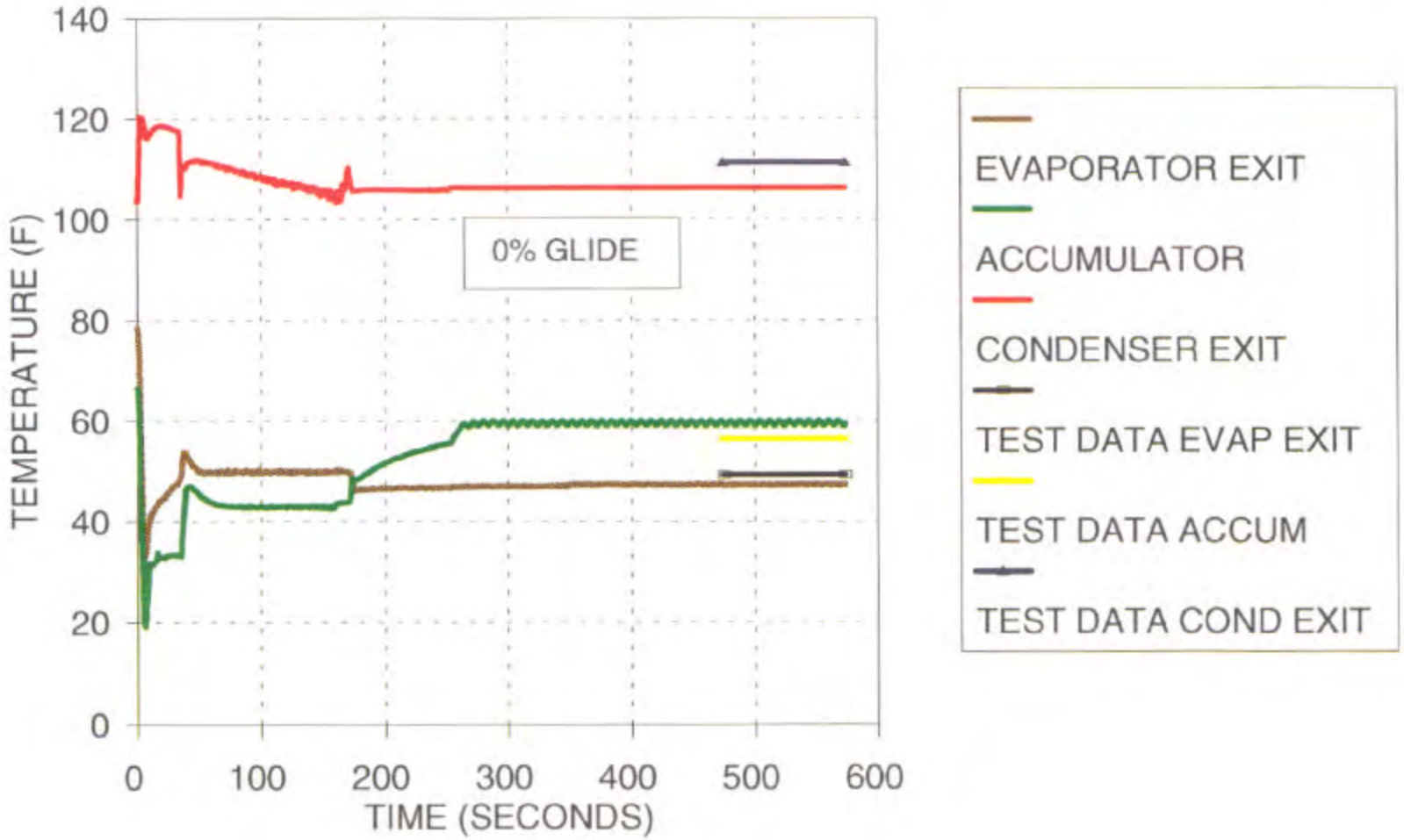

Fig. 3.31 Heat Exchanger Performance - DOE A, 6.4 LB Refrigerant 407C

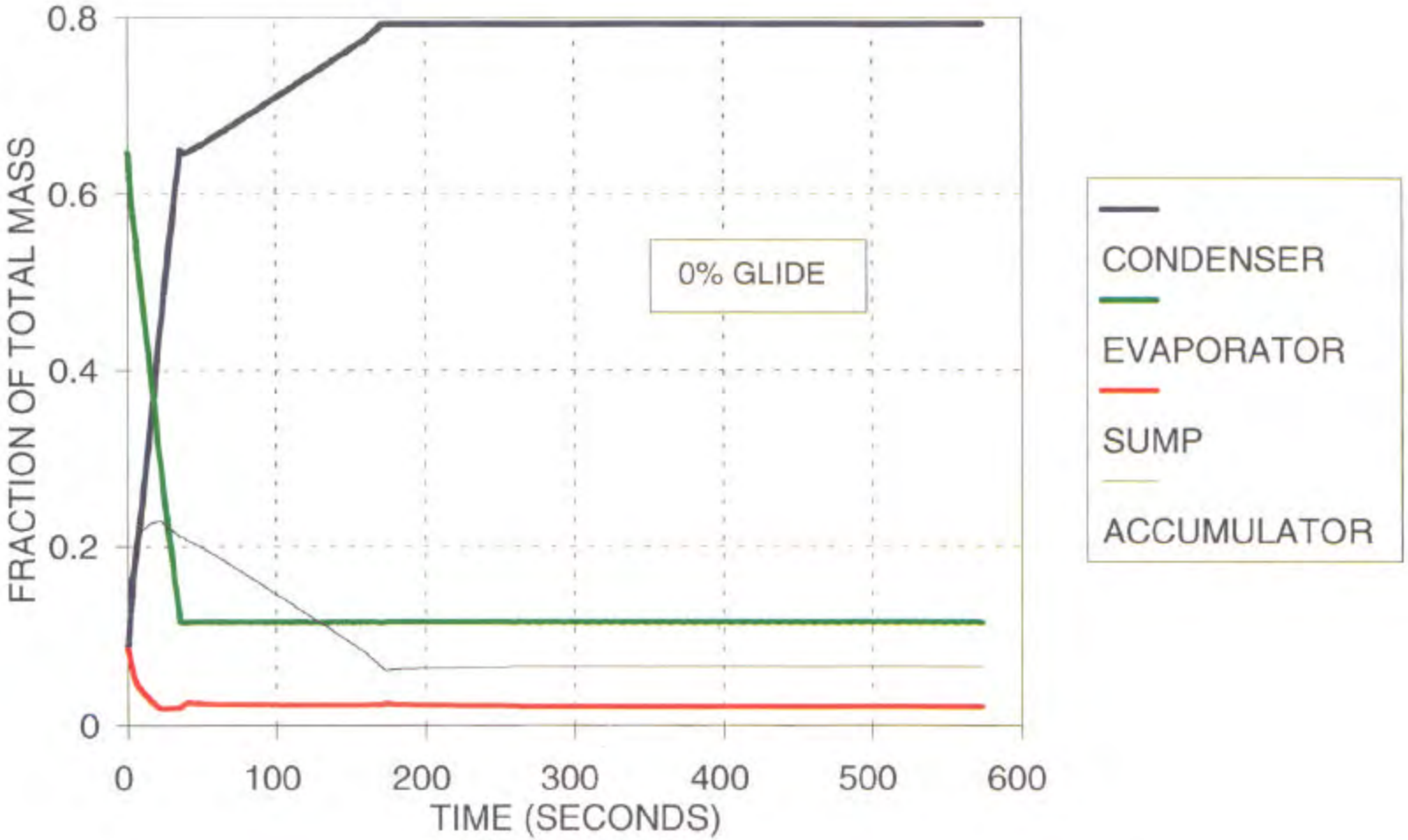

Fig. 3.32 Refrigerant Location - DOE A, 6.4 LB Refrigerant 407C

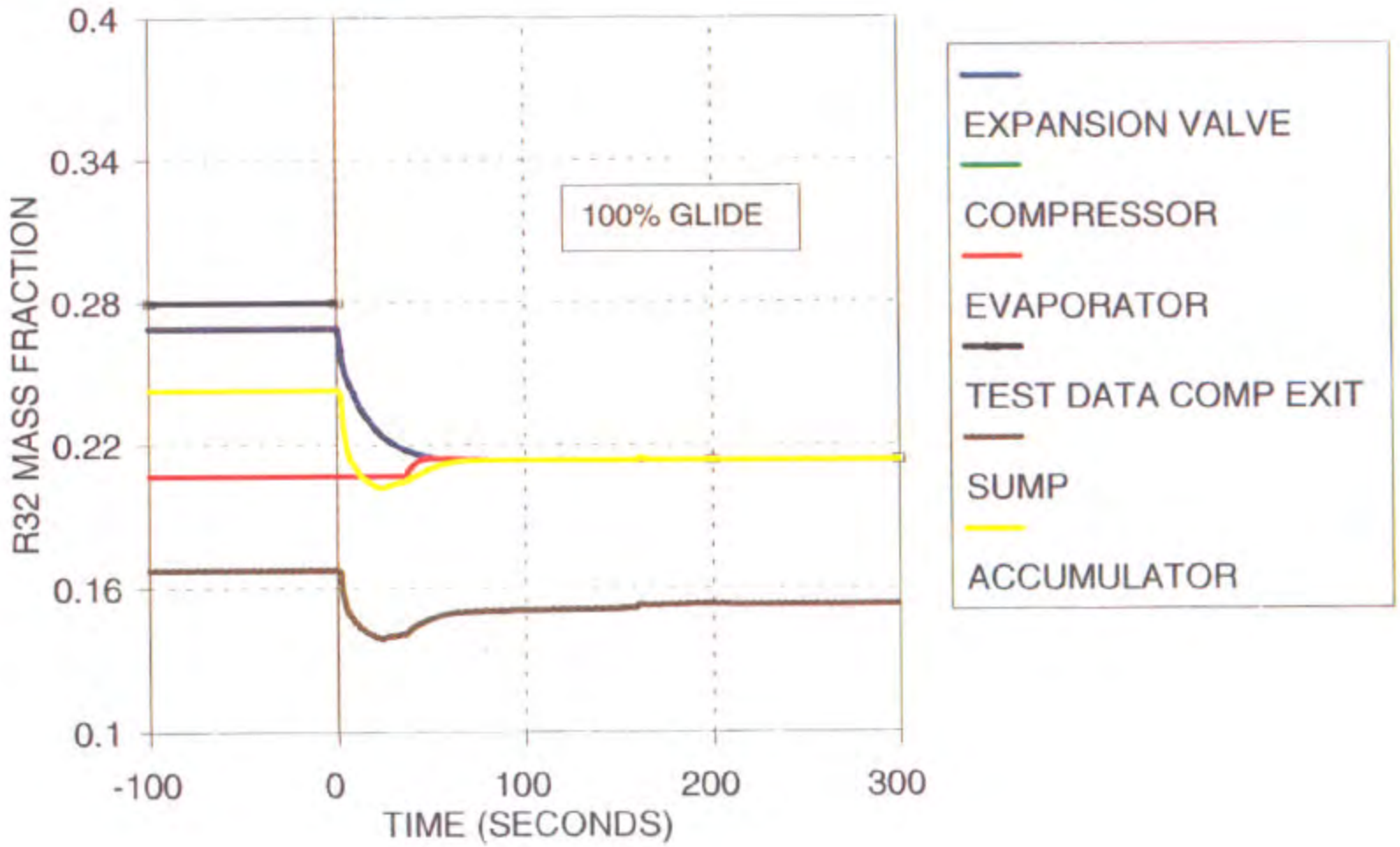

Fig. 3.33 R32 Concentration by Component - DOE A, 6.4 LB Refrigerant 407C

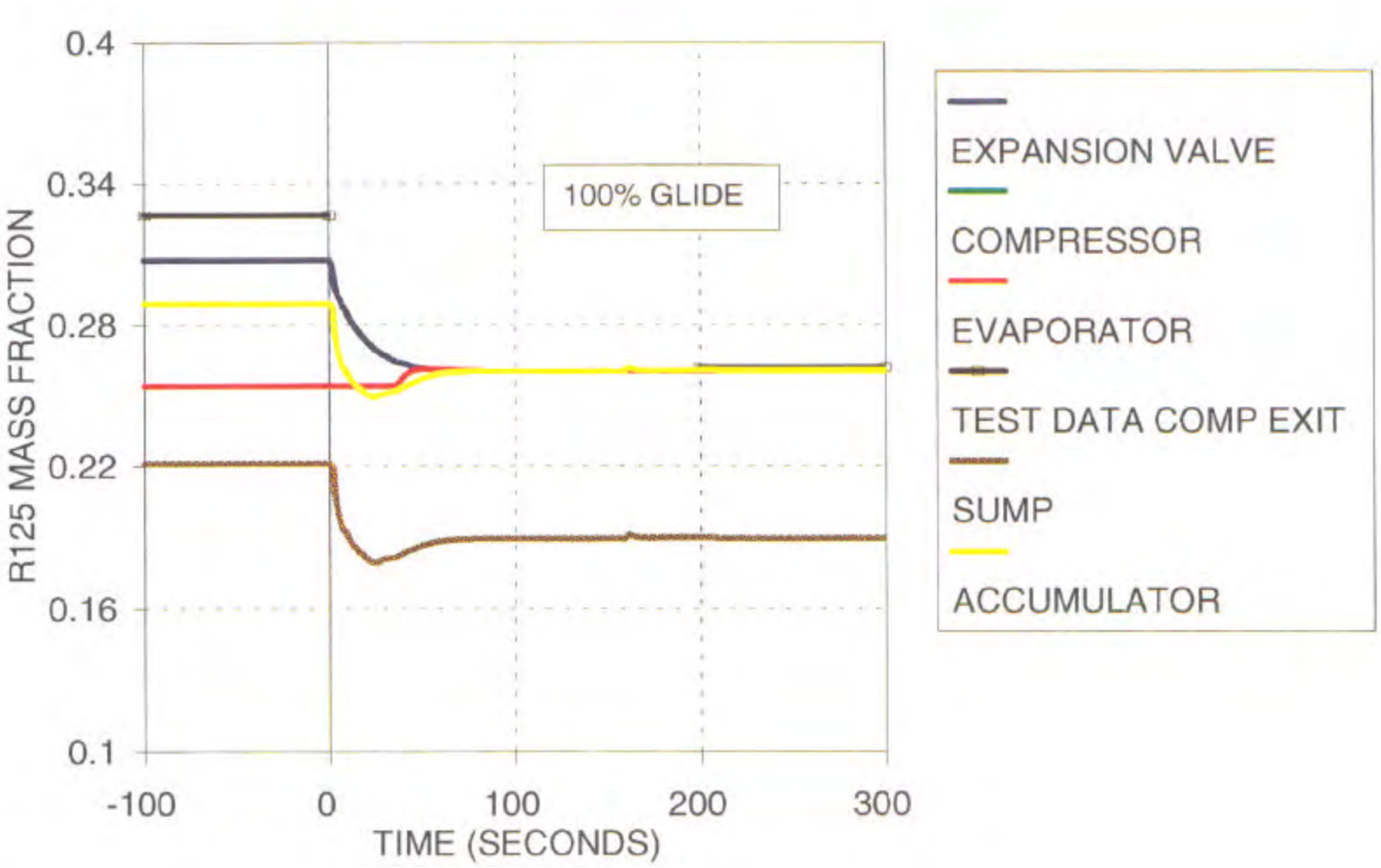

Fig. 3.34 R129 Concentration by Component - DOE A, 6.4 LB Refrigerant 407C

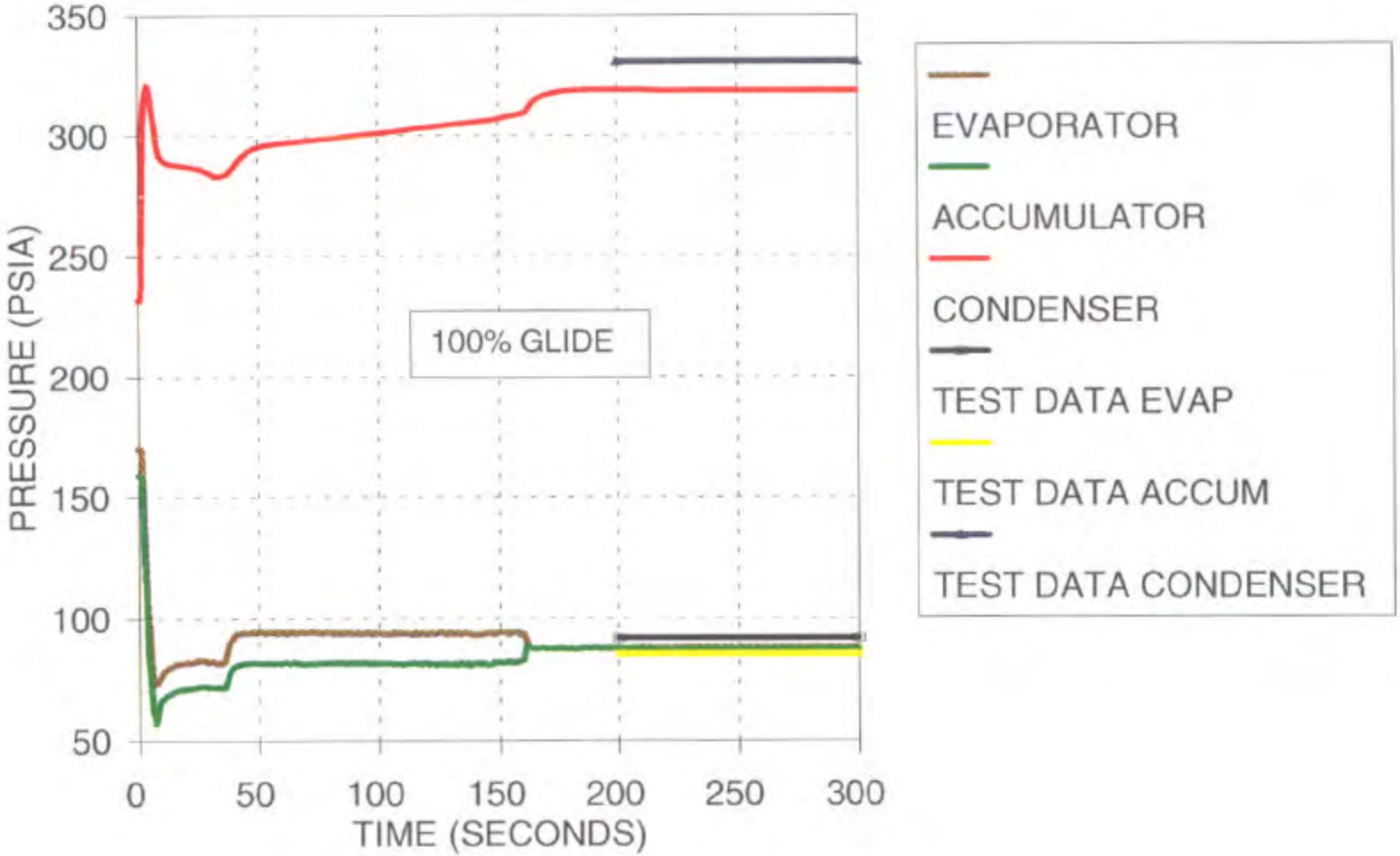

Fig. 3.35 Heat Exchanger Pressure - DOE A, 6.4 LB Refrigerant 407C

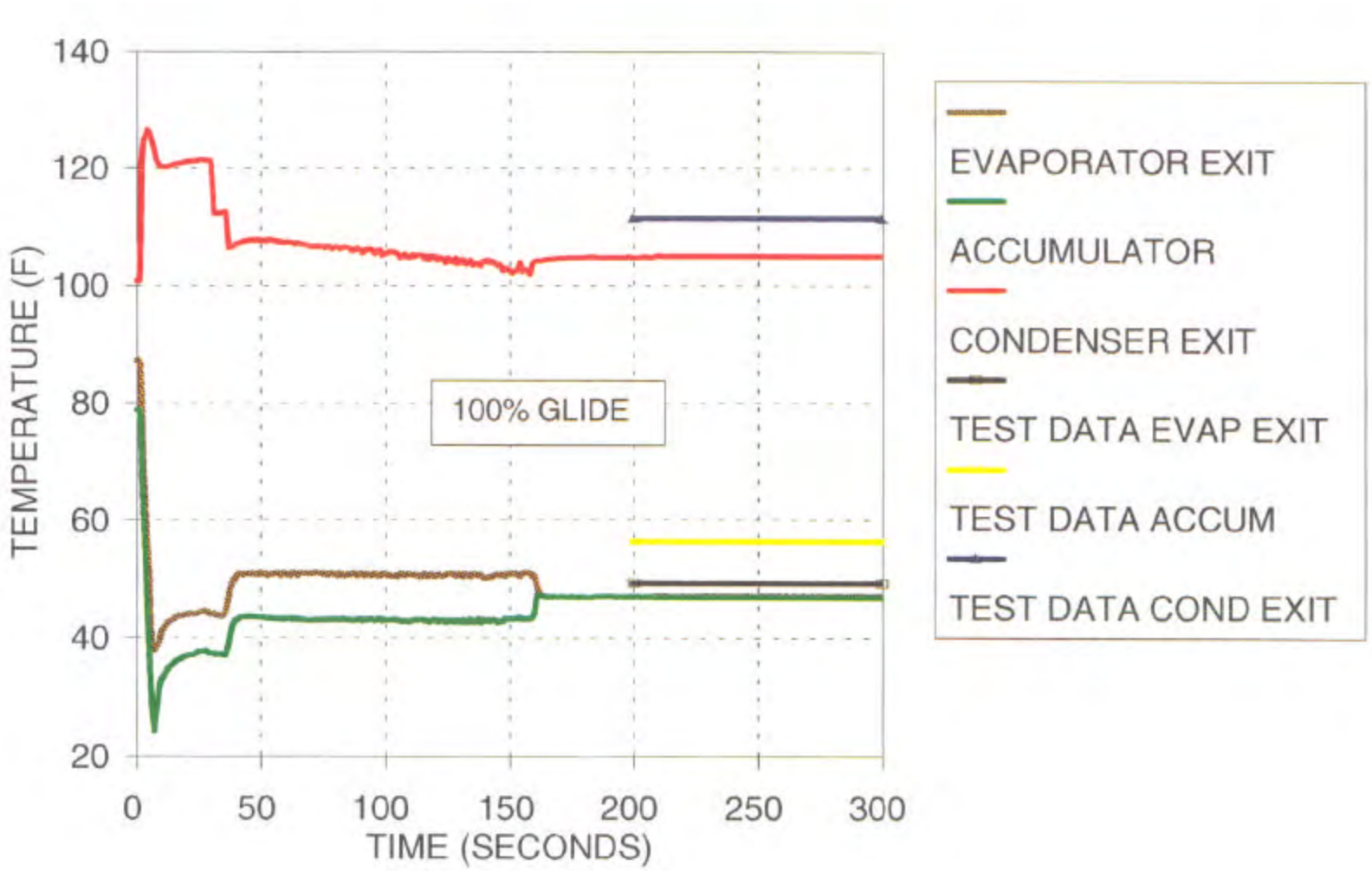

Fig. 3.36 Heat Exchanger Performance - DOE A, 6.4 LB Refrigerant 407C

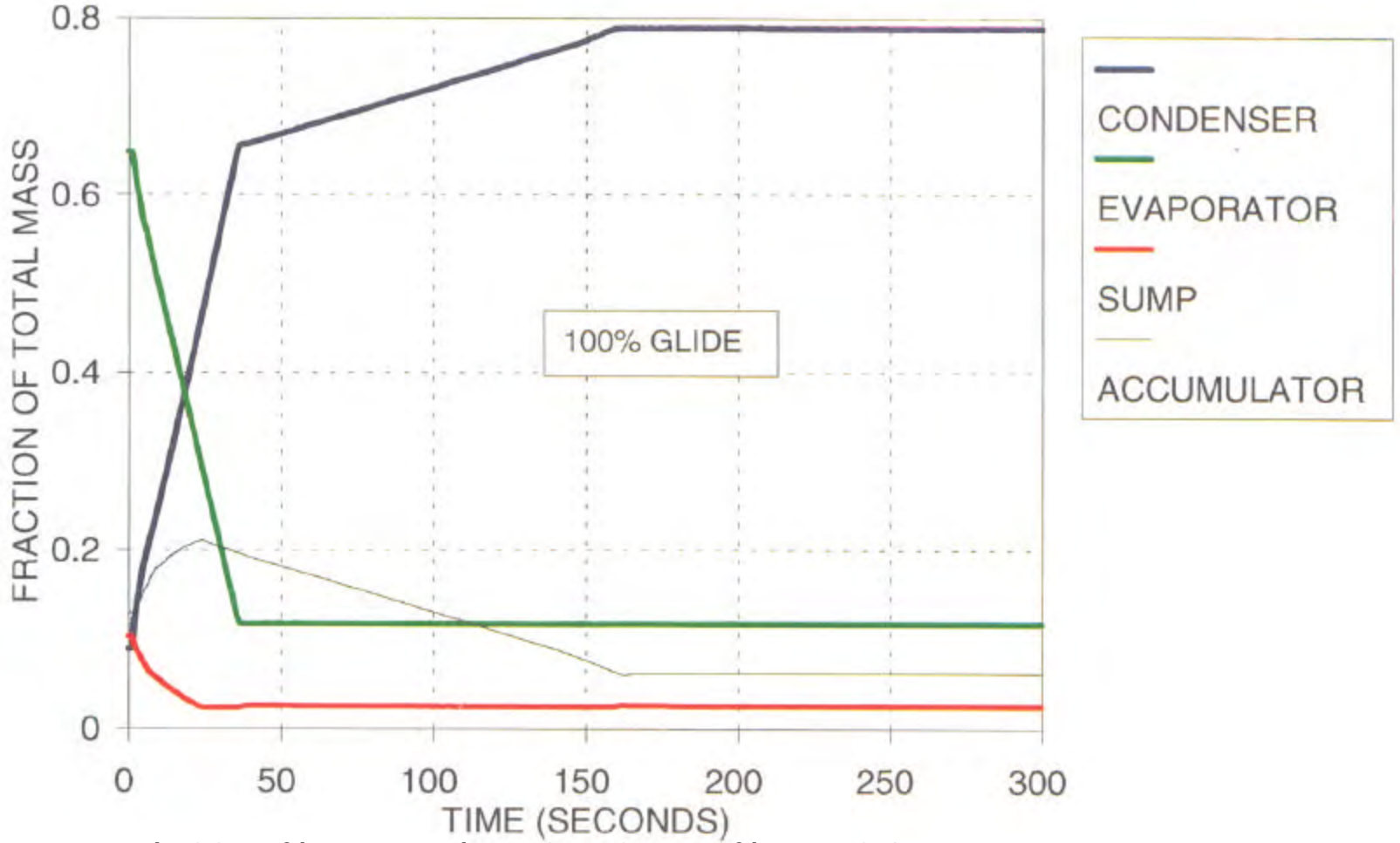

Fig. 3.37 Refrigerant Location - DOE A, 6.4 LB Refrigerant 407C

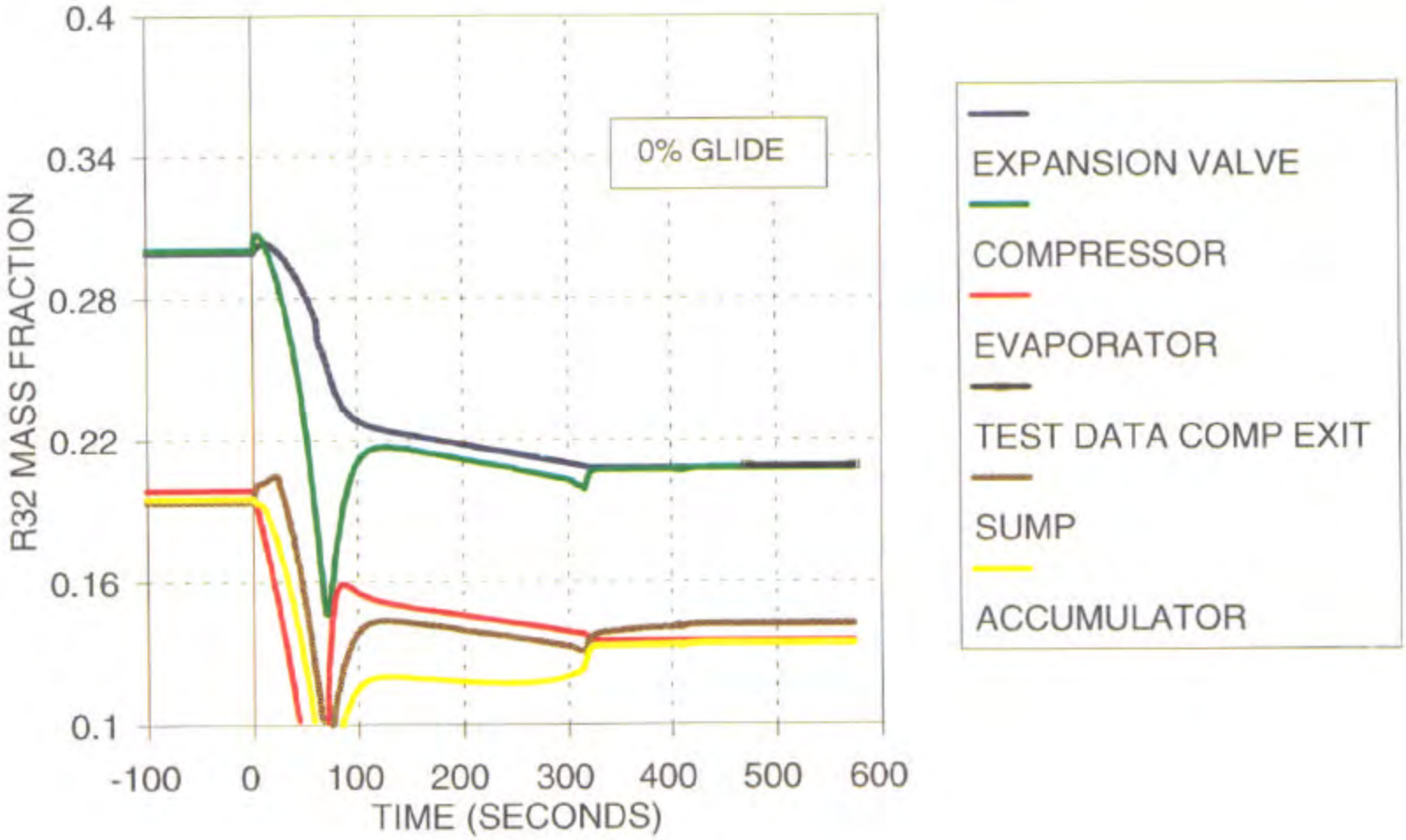

Fig. 3.38 R32 Concentration by Component - DOE E, 7.47 LB Refrigerant 407C

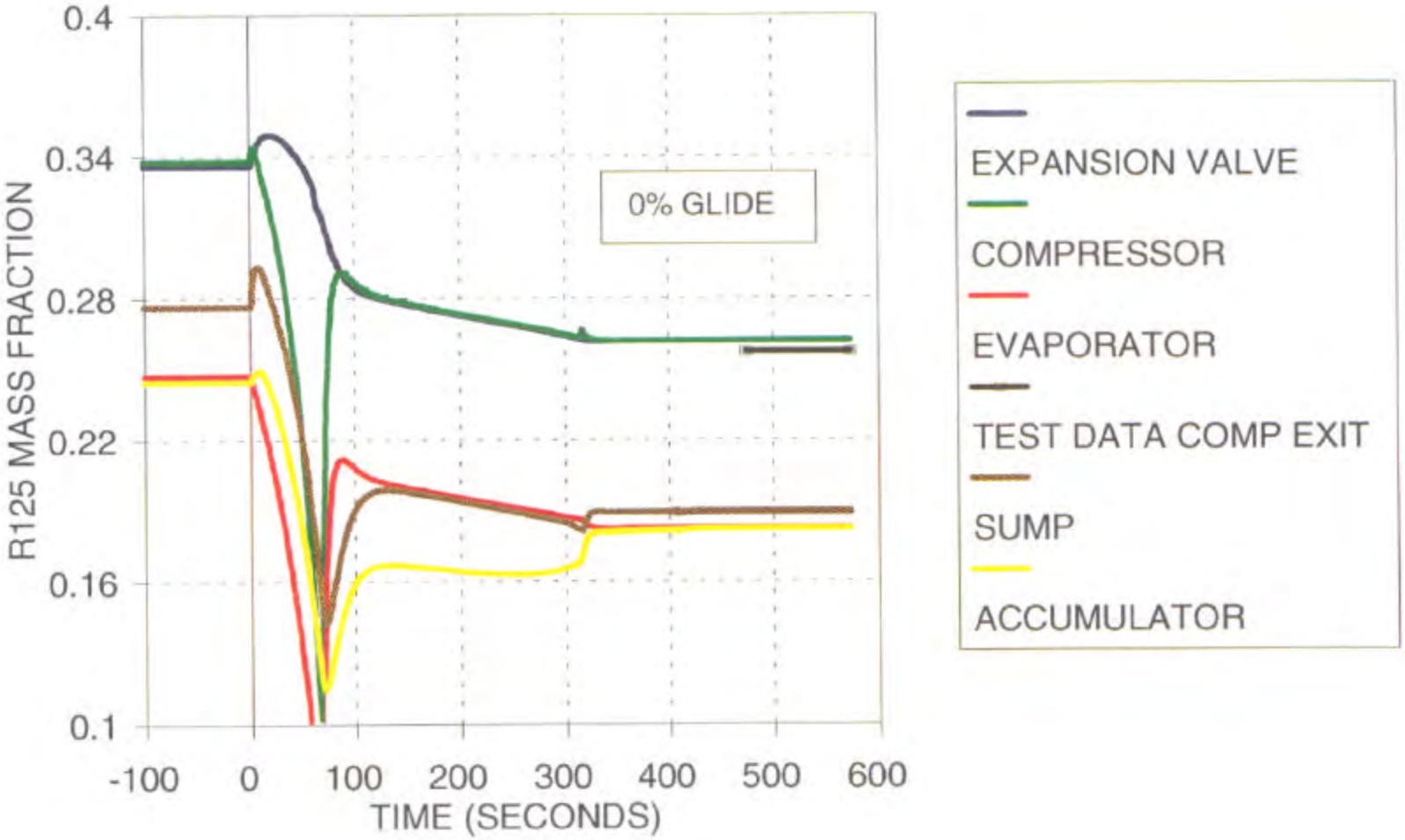

Fig. 3.39 R32 Concentration by Component - DOE E, 7.47 LB Refrigerant 407C

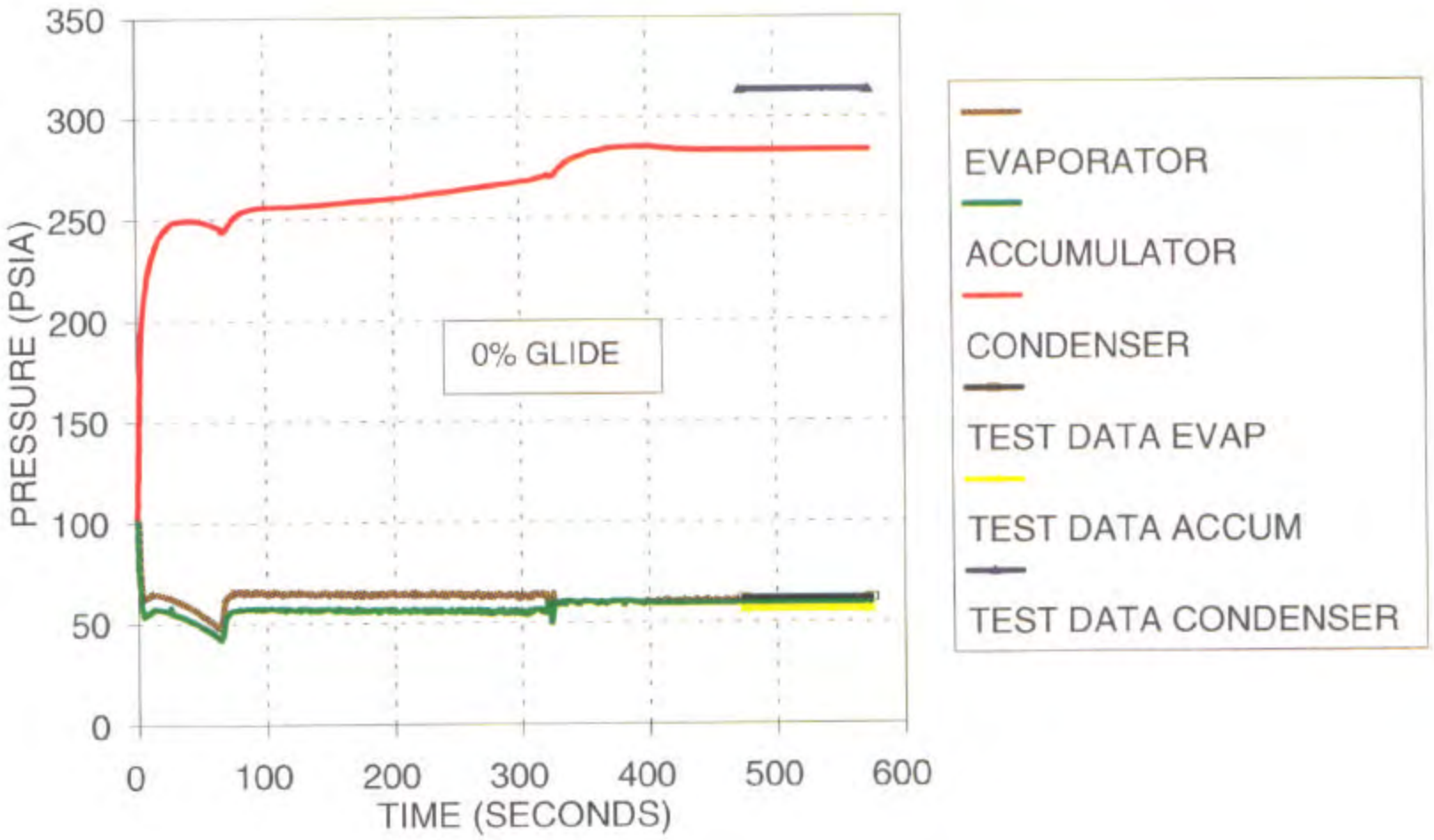

Fig. 3.40 Heat Exchanger Pressure - DOE E, 7.47 LB Refrigerant 407C

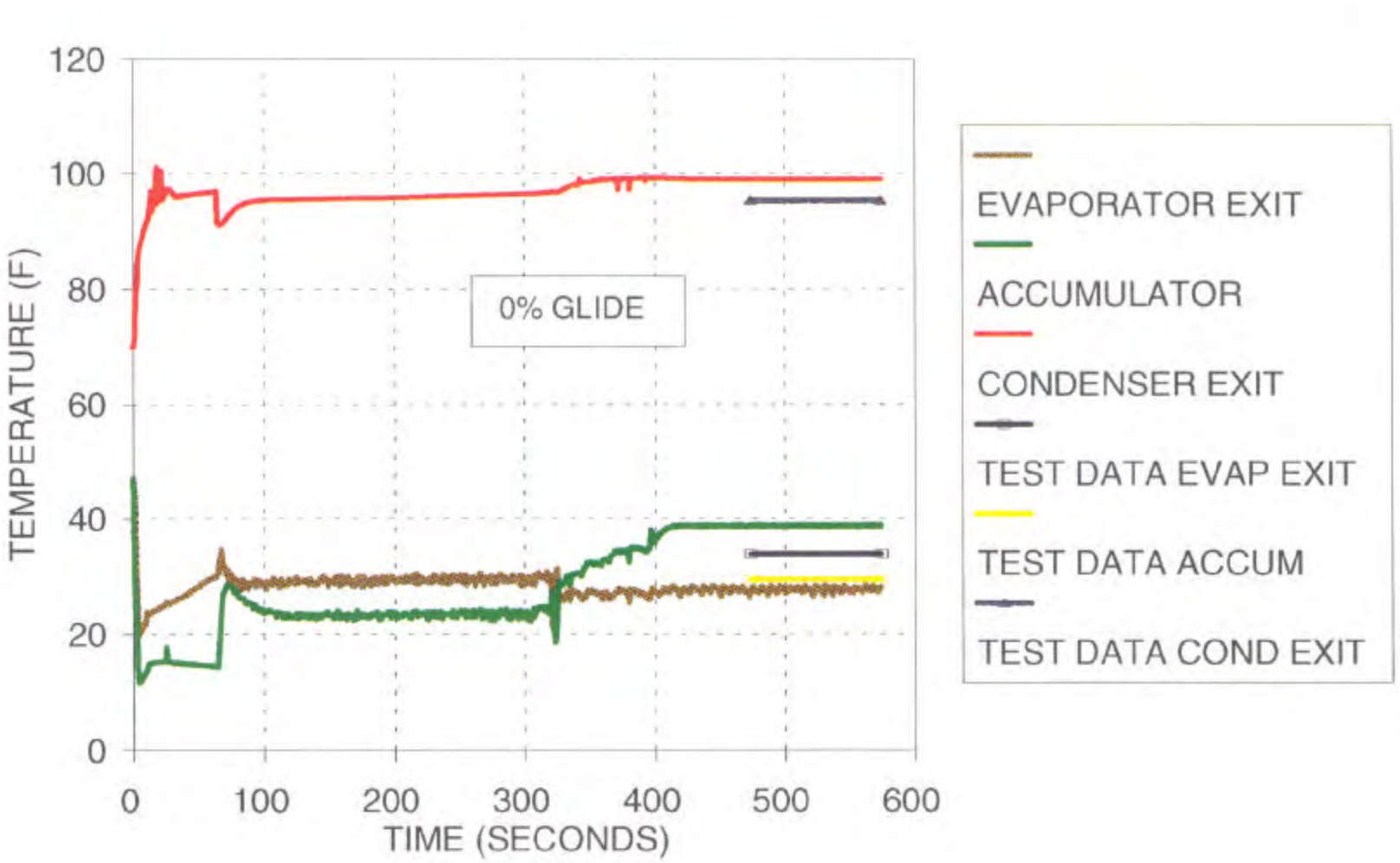

Fig. 3.41 Heat Exchanger Performance - DOE E, 7.47 LB Refrigerant 407C

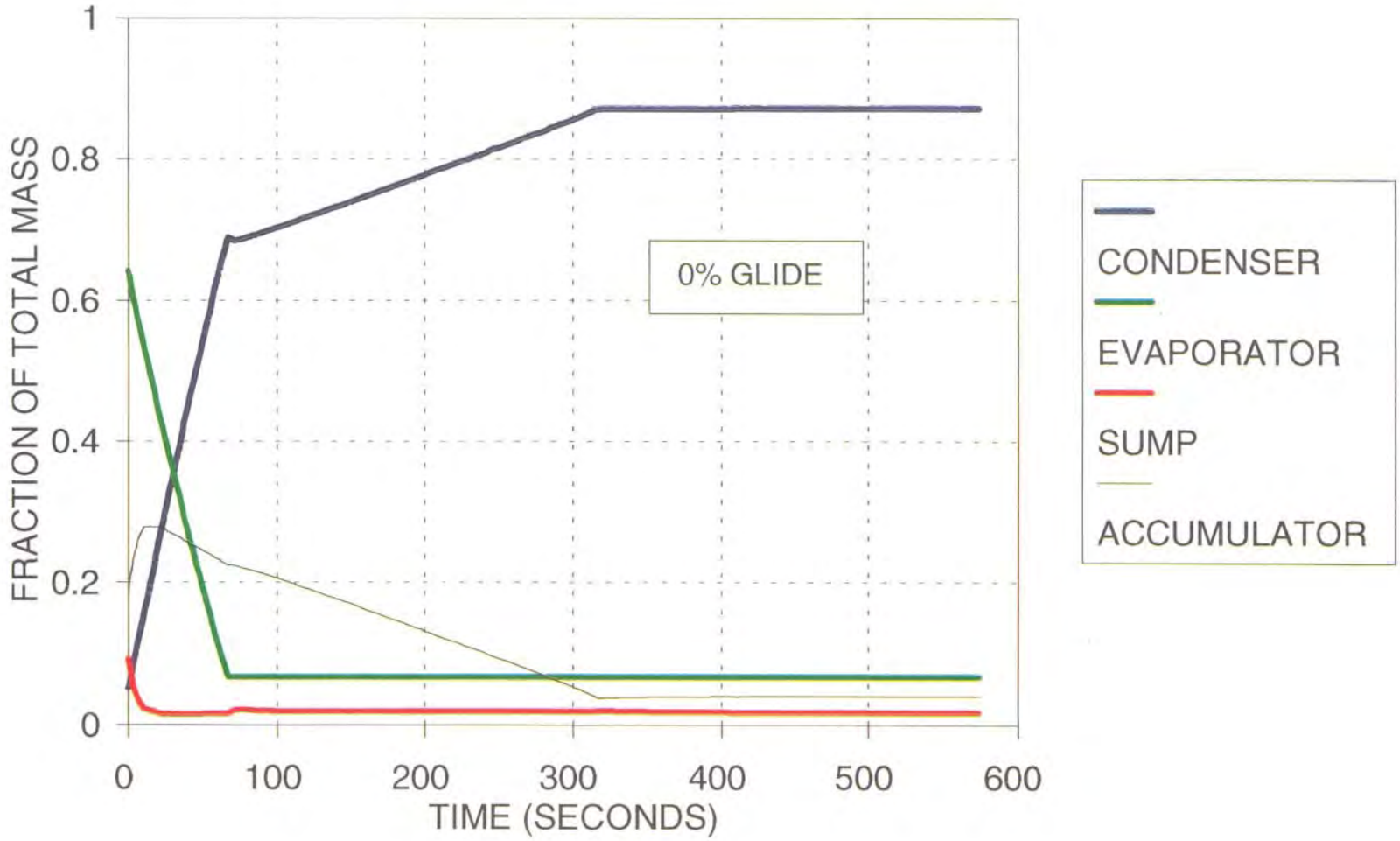

Fig. 3.42 Refrigerant Location - DOE E, 7.47 LB Refrigerant 407C

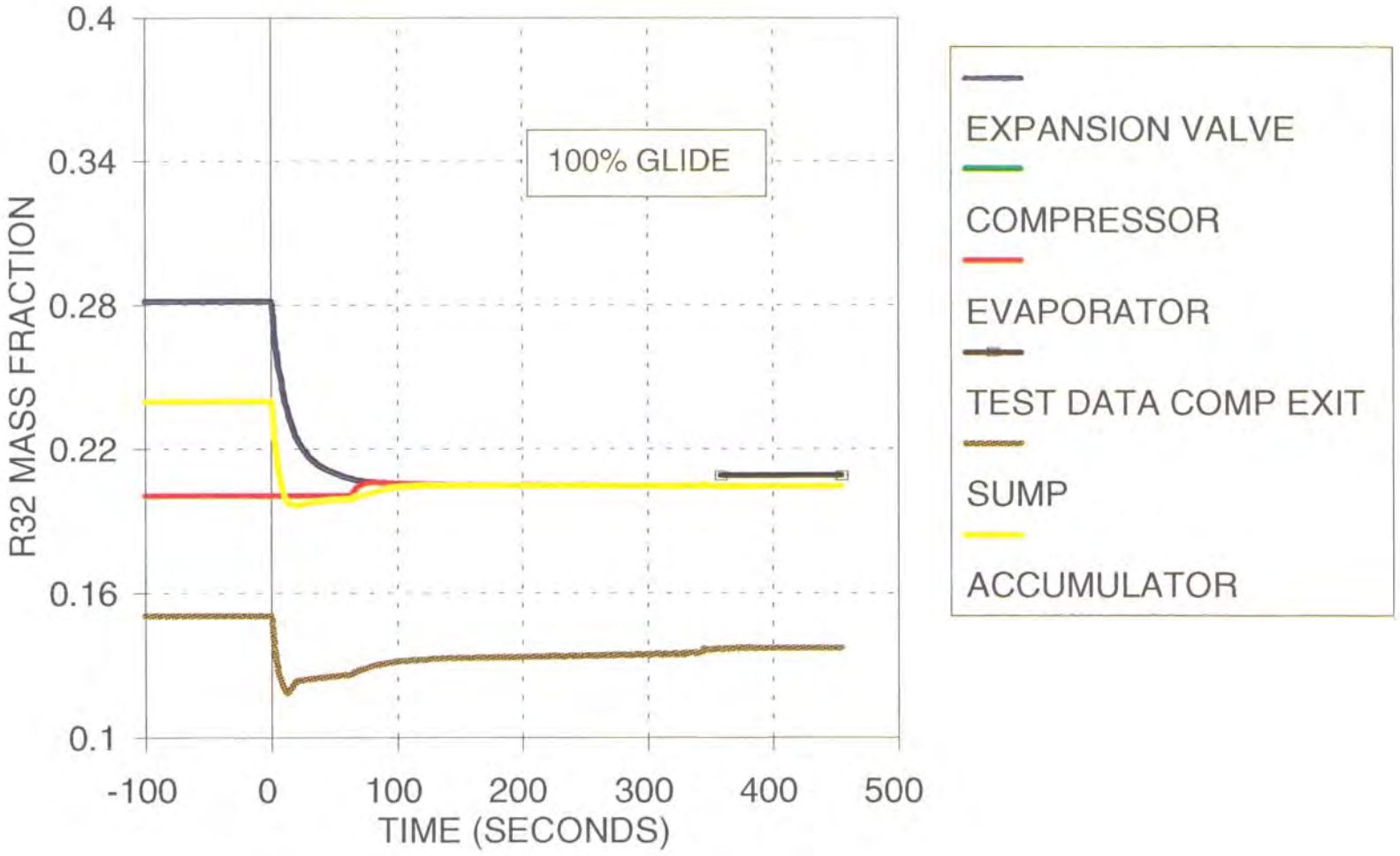

Fig. 3.43 R32 Concentration by Component - DOE E, 7.47 LB Refrigerant 407C

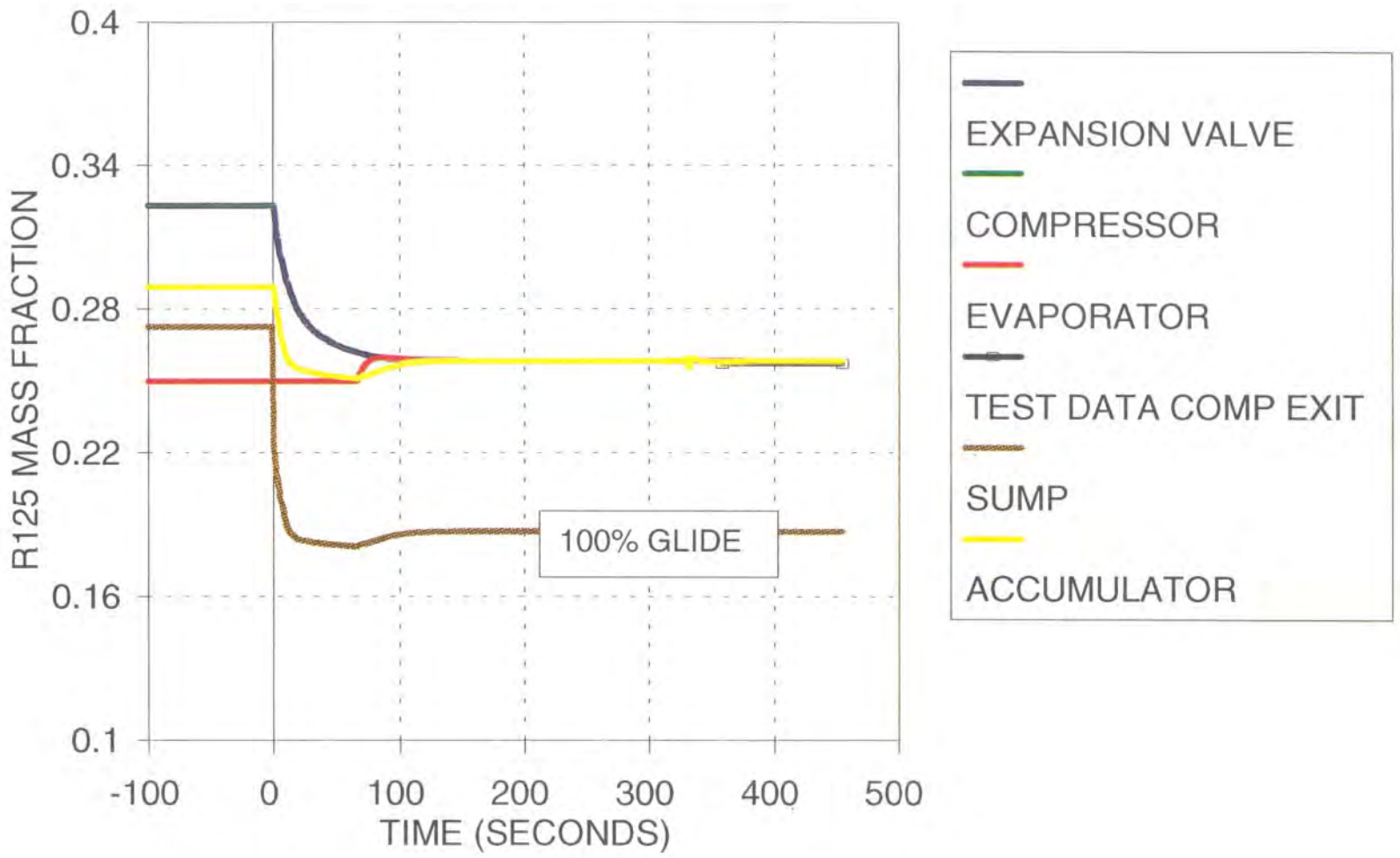

Fig. 3.44 R125 Concentration by Component - DOE E, 7.47 LB Refrigerant 407C

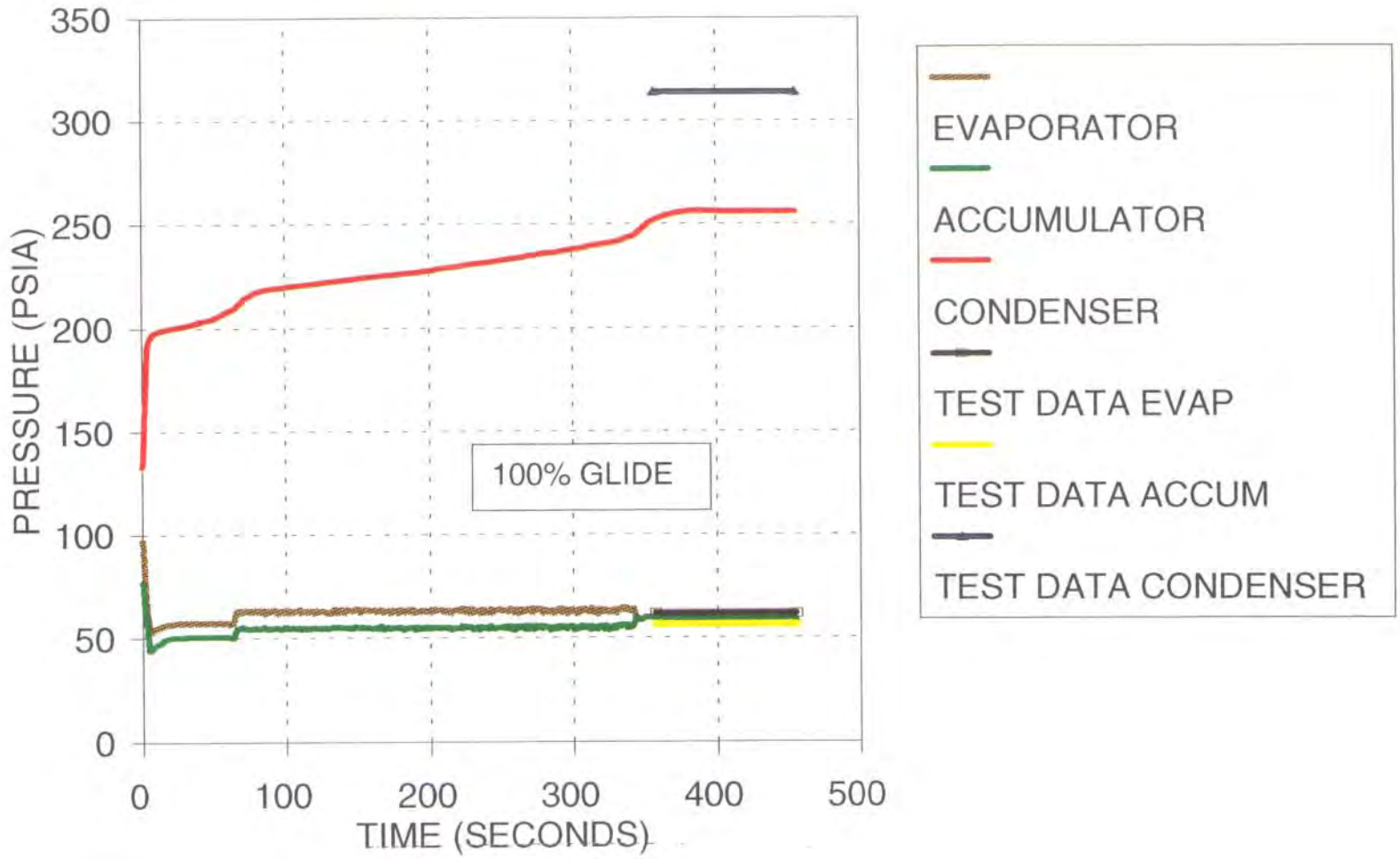

Fig. 3.45 Heat Exchanger Pressure - DOE E, 7.47 LB Refrigerant 407C

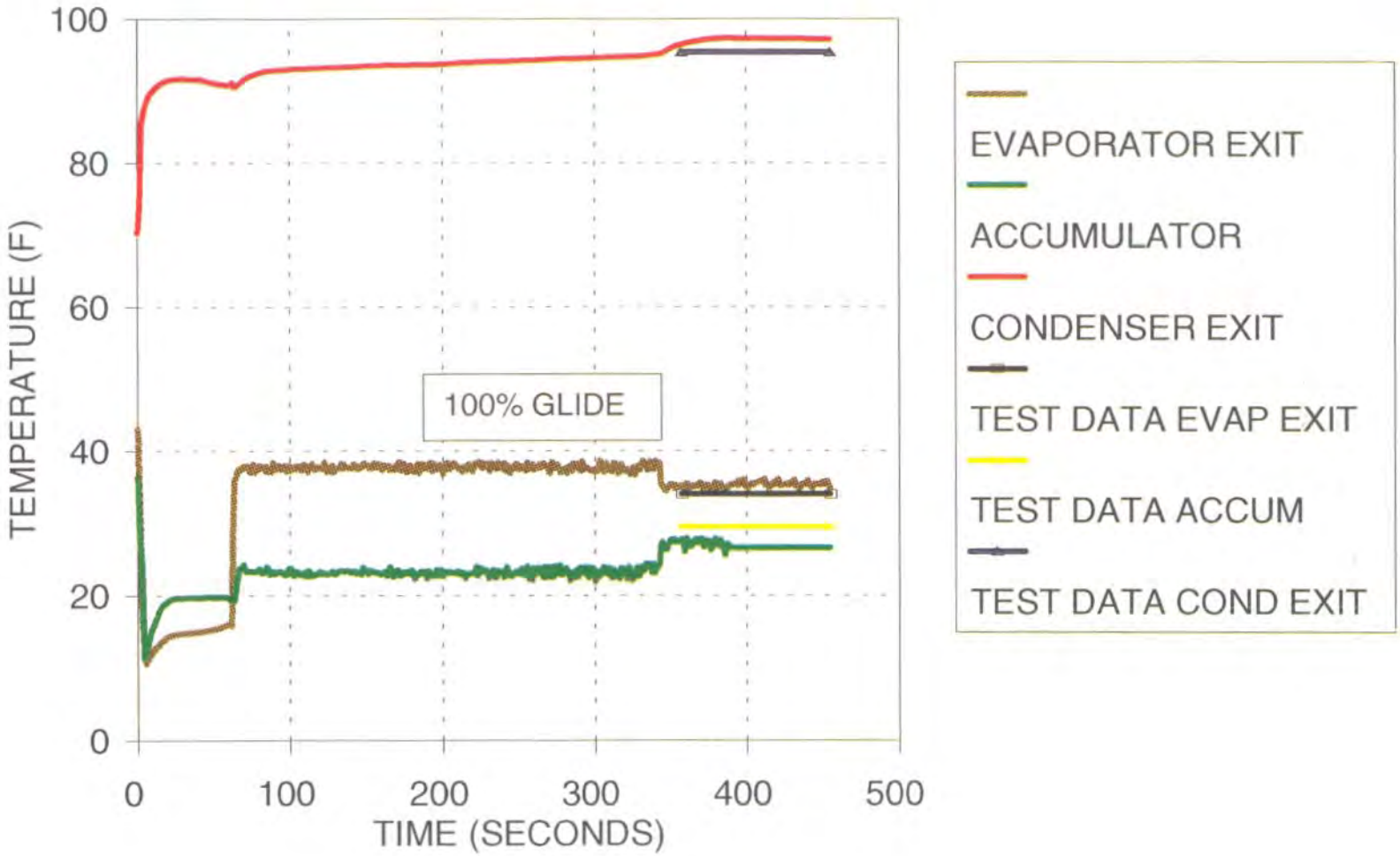

Fig. 3.46 Heat Exchanger Performance - DOE E, 7.47 LB Refrigerant 407C

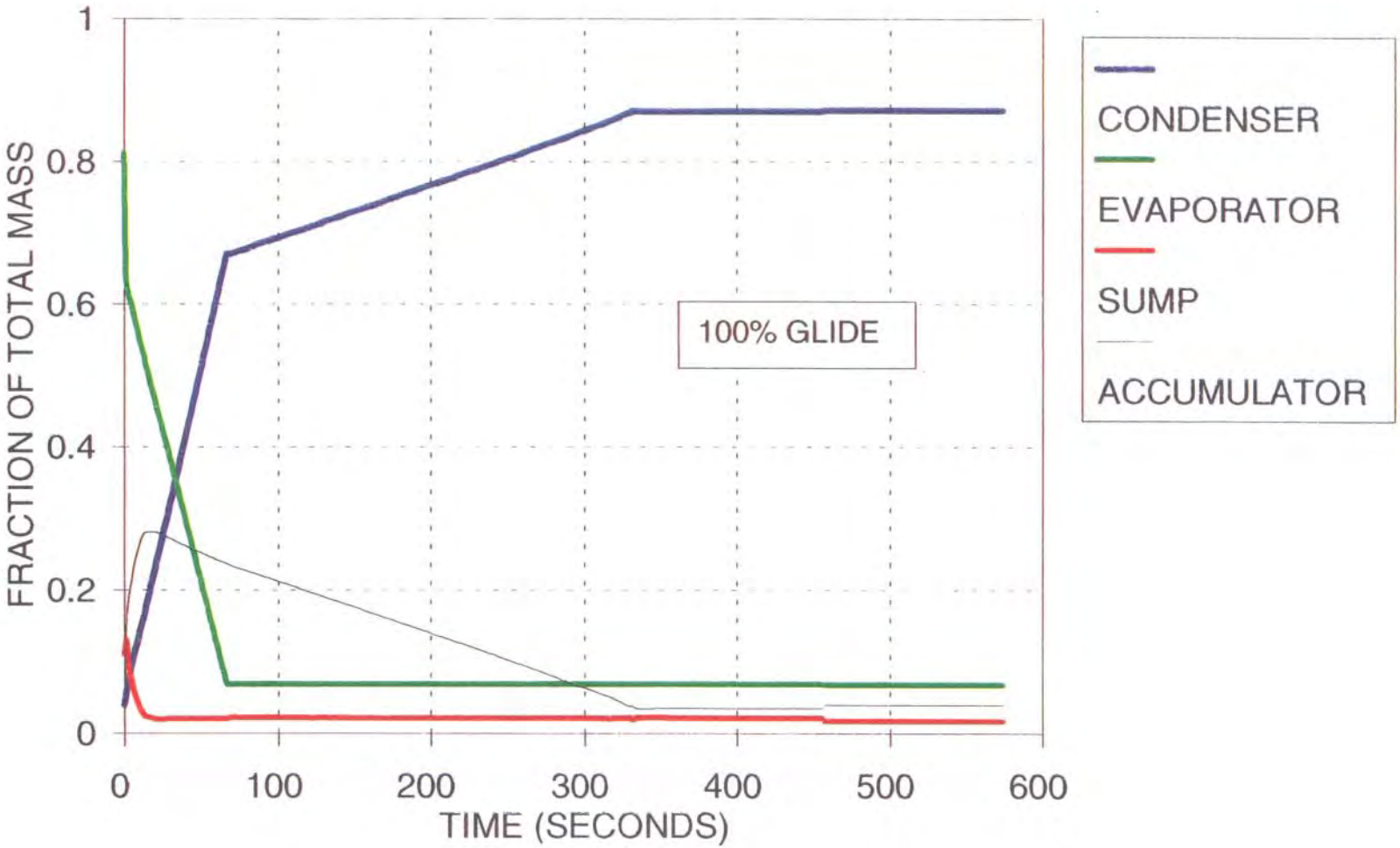

Fig. 3.47 Refrigerant Location - DOE E, 7.47 LB Refrigerant 407C

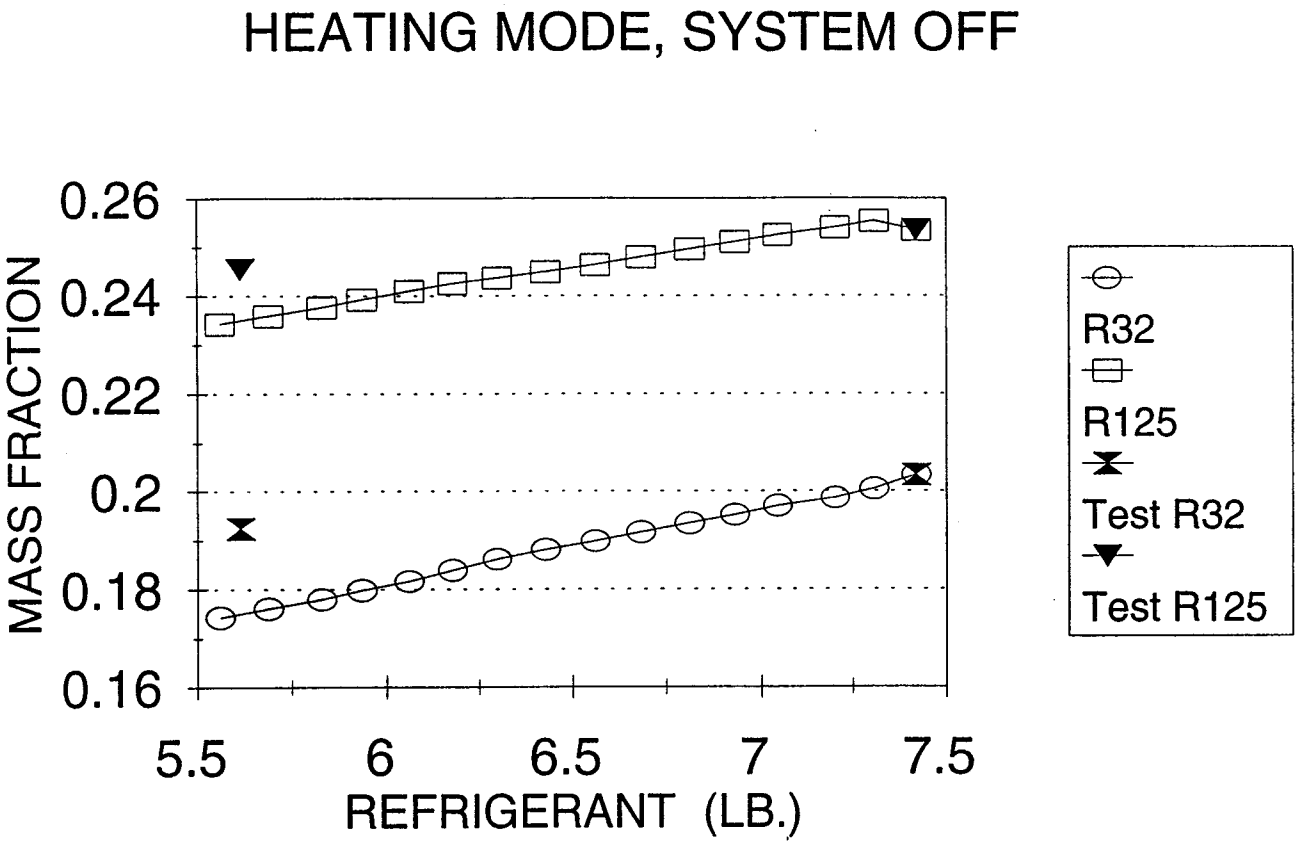

Fig. 3.48 Refrigerant Concentration During Leak - Heating Mode, System Off

(This page intentionally left blank)

TASK 4 - EXPERIMENTAL EVALUATION OF FRACTIONATION EFFECTS IN SYSTEM AND COMPONENTS DURING OPERATION AND AFTER SYSTEM LEAKS

Background

The objective of this task was to experimentally determine the fractionation behavior of two nonazeotropic refrigerant blends, before and after system leaks in a split system heat pump, and determine any performance, operational, or service concerns. The results of these tests were used to confirm the analytical model described in Task 3.

When leaks occur in HVAC systems, the charge is topped off with the same refrigerant as was originally filled. For a system with a nonazeotropic refrigerant blend, leaks in the system may cause the original composition to shift, resulting in changes in system performance and capacity. Furthermore, when the charge is topped off, the composition may not return to the original filling charge. The basic questions are to what degree does this occur, and what are the effects of the composition shift on the performance and safety of the system.

For Blend A, the system was run and data was taken at three different charge levels during each test. Three environmental conditions were run (1 cooling and 2 heating), and two different leaking scenarios were investigated (system on and system off leak).

In the second phase of the program (R407C), modifications were made to the test facility to obtain more detailed information concerning the composition shift occurring in the indoor coil, during heating and cooling operation. The system was fully charged, leaked, and recharged a total of three times, during the course of each test. Two environmental conditions were run, and two different types of leaks were performed (described in the test plan).

Experimental Facilities

To verify the dynamic fractionation model, a representative 2.5 ton heat pump with a scroll compressor was instrumented and was run at normal rating conditions for heating and cooling. The indoor and outdoor units of the heat pump were placed into separate Indoor Environmental Chambers (IECs), which provided precise temperature, humidity, and airflow conditions for simulation of various operative conditions. During the course of each test, transient pressure and temperature data were taken, as well as steady state and some transient composition data.

Indoor Environmental Chambers (IECs)

The experimental facility included two IECs, a nominal 2.5 ton capacity and a nominal 5 ton capacity system. The IECs can provide exact control of supply temperature from 47°F to 150°F, relative humidity from ambient to 100%, and airflow up to 3000 cfm. The supply air side of the indoor unit of the heat pump was connected directly to the 2.5 ton IEC. In contrast, the outdoor unit was placed in a large chamber which was connected to the 5 ton IEC. This is shown schematically in Fig. 4.1.

Pressure and Temperature Data Acquisition

Blend A

Eight thermocouples and six pressure transducers were installed in the system to provide an accurate determination of refrigerant state throughout the cycle. Type J thermocouples were selected for their good low temperature response. Figures 4.2 (cooling mode) and 4.3 (heating mode) show the instrumentation locations, as installed in the system for the Blend A tests.

R407C

Figures 4.4 (cooling mode) and 4.5 (heating mode) show the instrumentation locations, as installed in the system for the R407C tests. One entire circuit of the indoor coil was instrumented at the return bends (7 total) with thermocouples and pressure transducers for the R407C tests. Figure 4.6 shows the instrumentation locations on the indoor coil. The R407C tests also included two air-side thermocouples at the entrance and exit of each test section. The thermocouple and pressure transducer data were sampled once per second by a dedicated PC (PC2 on Figure 4.1). Labtech Notebook, a commercially available software package, was used to display and record the data.

The R407C tests also included a number of other data samples. The flow through the liquid line was measured by a S025 Micromotion flow meter and recorded every 5 seconds. A Valhalla Scientific model 2300 power meter was used to record power into both the indoor and outdoor units. Capacity was estimated by determining the temperature difference through each coil, as the flowrates are known and set by the IECs. The power meter was used to determine efficiency.

A highly accurate scale was used to determine the amount of refrigerant charged into the system. The scale, an A&D model EP-60KA, has a resolution of 0.005 lbs. The charge weight was determined by weighing the refrigerant cylinder before and after charging.

Refrigerant Composition Measurement and Data Acquisition

Refrigerant was sampled from four locations in the system to determine the steady state composition at various conditions. The indoor unit also had seven additional sampling ports in the R407C tests, located at the return bends of one circuit. In addition, during the course of the tests, refrigerant was removed from various parts of the system to simulate different leak scenarios. Finally, one (for Blend A tests) or two (for R407C tests) gas cylinders with known compositions were also periodically sampled to confirm the consistency of the results.

Sampling Locations and Procedure

The refrigerant composition sampling locations are shown in Figs. 4.2-4.5. The basic sampling concept is simple: a small diameter, long capillary tube is connected directly to the refrigerant system at one end, and a 'Tee' at the other. One side of the 'Tee' is directed through a bubbler, and the other fed through a series of filters to the Gas Chromatograph (GC). The refrigerant enters the capillary tube, and gradually expands to near atmospheric pressure as it flows through the tube. This ensures that the sample entering the GC is fully vaporized.

Each of the sampling ports was actually arranged somewhat differently, depending on the conditions expected during testing. Sample ports 1 and 4 were connected to a 27 foot long section of 0.01 in. diameter line. These lines were attached to shutoff valves to trap any liquid in this section while the lines were not being sampled. Another 20 foot long section of 0.02 in. diameter line followed the first section and was attached to a six position selector valve. After the selector valve, a two foot section of 0.04 in. diameter line led to the T in the line. One end of the T was connected to a bubbler, to both ensure that gas was flowing through the line and to determine the flowrate of the gas. The other end of the T passed through an oil filter and a particulate filter, before entering the GC. These two sample ports had the longest length because liquid was expected and at least one port was to be exposed to a high pressure, while the system was operating. Sample port 2 was connected to a 27 foot section of 0.01 in. line, which fed directly to the selector valve. High pressure was expected here, but no liquid. Sample port 4 was connected to a 10 foot section of 0.01in. line connected directly to the selector valve. This port was always exposed to the low pressure side of the system, with the possibility of liquid being present. The known sample was connected to a 27 foot section of 0.01 in. line attached to the selector valve. The long length here was to minimize the flowrate in order to increase the total number of samples possible. Each of the seven sampling ports in the indoor coil return bends were connected to a 27 foot section of 0.01 in. line, attached to a selector valve.

The GC was used to measure the peak location and area for each component in the sample. The actual procedure used to obtain the peak areas was the same for each set of data points. First, each of the standard (known composition) bottles were sampled. The selector valve was switched to the standard bottle position, and vapor was drawn through the capillary tubes for approximately 30 seconds. At this point, the GC was started on its programmed sampling routine. The vacuum pump in the GC operated for 20 seconds, to clear the capillary lines of any residual blend from previous runs. Then, the columns on the GC were exposed to the blend for 15 milliseconds. About one minute was required for the columns to separate the components, display the results, and save them. The vacuum pump was then operated again, and the procedure was repeated again. A total of five (four for R407C) sample runs were taken in this manner for each sampling location. When the data was analyzed, the first of the runs was always discarded, and the remaining runs were averaged, in order to obtain the average peak areas for each location. After the standard sample was taken, the selector valve was switched to the number one port location. Since liquid was expected at this location, an intermediate shut off valve was located in the capillary line. This valve was opened, and the blend from the outdoor unit began to flow through the lines. After waiting 30 seconds for the capillaries to be purged, the GC was again started on its programmed sampling routine, as described above. After sampling, the shut off valve was closed, and the selector valve was turned to the port two location (compressor discharge). After half a minute, the GC was again started. This procedure was repeated for the number three (accumulator) port. The number four (indoor unit) port was sampled in the same way as the number one valve. After the four system ports were sampled, each of the seven heat exchanger ports were sampled in order, using the same procedure. Next, the standard bottles were again sampled. The entire sampling procedure for one set of data points took approximately twenty minutes for the Blend A tests, and one hour for the R407C tests.

GC Calibration Techniques

The averaged peak area data were used to determine refrigerant mass composition, using two different methods. The first method used a calibration curve of the area count for a number of known samples versus the known sample composition. The second method used a calibration curve of the ratio of area counts versus the known sample composition. The second method was deemed more reliable after a number of preliminary tests.

Test Plan

Test Plan for Blend A

The test plan developed for Blend A examined three different environmental conditions, using two different leak scenarios. Tests were run in cooling mode at DOE-A, and heating mode at DOE-E and low temperature (same as DOE-E, except 40°F outdoor temperature). System on and system off leaks were performed.

The Blend A test plan is shown in Table 4.1 below. The system was run at 7 lbs of charge (nominally designated as 100% charge), approximately 75% of full charge, and approximately 50% of full charge for each test. The 100% charge level was the same amount of charge that the system required, with R22 as the refrigerant. This test plan required six full blend charges. No recharges were conducted for these tests. The oil was not changed between runs. When the system reached steady state for each condition, four samples (two liquid, one vapor, and one unknown) were taken and analyzed in the GC. The last two tests were designated low temperature tests, as the intent was to run the outdoor IEC to the lowest possible delivery temperature. This temperature only turned out to be about 7 degrees below the DOE-E tests. A detailed explanation of the procedures used in each test is presented in Appendix B.

Before the system was tested, the old refrigerant and oil was removed from the system. The oil was replaced with a POE compatible with the blend: Castrol SW-68. In order to ensure the removal of all of the old oil, the oil sump was drained, refilled with SW-68, and run with R134a. This procedure was repeated three times.

Test	Description
1	Cooling Mode (DOE-A) test with system-off leaks
2	Cooling Mode (DOE-A) test with system-on leaks
3	Heating Mode (DOE-E) test with system-off leaks
4	Heating Mode (DOE-E) test with system-on leaks
5	Heating Mode (low temp) test with system-off leaks
6	Heating Mode (low temp) test with system-on leaks

Table 4.1 Test Plan for Blend A

Test Plan for R407C

The test plan for R407C, shown in Table 4.2 below, examined two different environmental conditions (DOE-A and DOE-E), using two different leak scenarios (system on and system off). The plan for this set of tests was somewhat different than that of the Blend A tests. The system was charged to a steady state level of approximately 10 degrees of suction superheat, as measured by TS6 and PS6 (see Figure 4.4). Next, about 25% of the charge was leaked, and the system was topped off to 10 degrees of suction superheat. This was repeated three times for each test. The original test plan required four full blend charges, and twelve top offs. The oil was not changed between runs. When the system reached steady state for each condition, eleven samples (four system & seven heat exchanger) were taken and analyzed in the GC. A detailed explanation of the procedures used in each test is presented in Appendix B2.

After the results from the first four tests were reviewed, it was determined that an inordinate amount of frost had accumulated on the outdoor coil during the DOE-E heating cases (tests 2 and 4) while the system was at low charge, affecting both the performance of the system, and the amount of charge required. To address these concerns, both heating condition cases were re-run, with a defrost cycle initiated prior to any data being taken.

Test	Description
1	Cooling Mode (DOE-A) test with system-on leaks
2	Heating Mode (DOE-E) test with system-on leaks
3	Cooling Mode (DOE-A) test with system-off leaks
4	Heating Mode (DOE-E) test with system-off leaks
5	Heating Mode (DOE-E) test with system-on leaks
6*	Heating Mode (DOE-E) test with system-off leaks
* repeat tests of 2 and 4 due to frosting concerns	

Table 4.2 Test Plan for R407C

Test Results

The raw data collected consisted of pressure and temperature data as a function of time, with additional information (flowrate and power) for R407C. In addition, refrigerant composition data was taken at steady state conditions. The raw plots of all the data are shown in Appendix B1 (Blend A) and Appendix B2 (R407C). On the plots, the shaded areas represent the time during which composition data was taken. They also represent the times during which the pressures and temperatures were taken and averaged to determine steady state values. The steady state data including composition data is presented on summary sheets for each test in Appendix B1 (Blend A) and Appendix B2 (R407C). The results for each of the blends are presented below.

Test Results for Blend A

Typical test plots of temperature and pressure with time for the Blend A tests are shown in Figs. 4.7 and 4.8. These plots are for test 3, which is a heating mode test where the leak

occurs when the system is off. The label on each of the shaded lines indicates the data file name for that set of steady state data, corresponding to the data sheet for test 3. As is normally expected in a system, the compressor discharge and sump temperatures increase, as the mass flow through the system is reduced, lowering the amount of cooling to the compressor. The system pressures drop radically with charge reduction, as shown in Fig. 4.8. Data sheets for the rest of the tests can be found in Appendix B1.

One of the primary concerns when dealing with a nonazeotropic refrigerant blend is whether the blend composition, which is used to charge the system, will be the same as the one circulating in the system when in operation. This is a concern, as a different composition could have different system operating pressures, capacities, and efficiencies. This blend separation, or fractionation, will occur in the system whenever there is a potential for liquid accumulation, or pooling. This happens most noticeably in an overcharged situation, when the accumulator has liquid in it. The liquid is relatively stagnant, and will tend to contain a higher fraction of the low pressure component of the charge, leading to a reduction in the fraction of the low pressure component in the circulating charge. Depending on the geometry of the specific equipment used, pooling of liquid can also occur in other areas of the system, such as the condenser, where the majority of the charge typically resides. To a much lesser degree this can also occur in the evaporator.

When the system operates at a lower charge, the potential for pooling is reduced, as the accumulator is typically dry at this condition. Pooling can still occur in other parts of the system, and the effect of this pooling may be greater now as the mass flow through the system is now lower. The amount of composition shifting caused by pooling of liquid in the heat exchangers will vary depending on the specific geometry of the equipment. For the units used in this study, the potential for pooling in the heat exchangers was deemed to be moderately low.

Table 4.3 shows a summary of the Blend A tests. The charging composition is the overall mass fraction of R32 in the system; the remainder is R134a. This data was obtained by sampling the four ports in the system after charging and obtaining liquid and vapor R32 mass fractions, while the system was off. Knowing the liquid and vapor compositions, the total mass of the charge, and the total internal volume of the system, the overall charge composition was calculated. Charge compositions after discharges were found by sampling the discharged sample and determining how much of each component was removed, and thus determining the remaining charge. The circulating charge composition is the mass fraction of R32, while the system was on. This value is an average of the ports, which show the circulating charge. Port 2, the compressor discharge port, usually gives the most reliable indication of the circulating charge. When the accumulator is dry, port 3 should also show the same composition. Ports 1 and 4 depend on the mode being run. In the cooling mode, port 4 is in a capillary line between the expansion valve and the entrance of one of the evaporator circuits. In this case, the sample is in a partially expanded two-phase state. In the heating mode, subcooled liquid is expected in this location. Port 1 in the cooling mode occurs at the exit of the condenser, where liquid is normally expected. Unfortunately, this port was positioned in such a way that vapor or two phase samples (which do not indicate the true circulating charge at this point) were generally taken throughout

the Blend A tests. For this reason, the samples from this port are not plotted in the next three Figs. 4.9-4.11.

	Charging Compos. (%R32)	Circulating Compos. (%R32)	Charge Compos. after Discharge #1 (%R32)	Circulating Compos. after Discharge #1 (%R32)	Charge Compos. after Discharge #2 (%R32)	Circulating Compos. after Discharge #2 (%R32)	Charge Fractionation?
Run #1	21.1	24.4	19.2	19.8	16.8	16.7	YNN
Run #2	20.5	23.8	20.1	20.7	20.1	20.6	YNN
Run #3	25.6	25.5	25.4	25.4	22.1	21.2	NNN
Run #4	24.2	24.0	24.1	23.9	24.2	23.8	NNN
Run #5	23.5	24.7	21.0	21.6	18.1	18.4	YNN
Run #6	23.4	24.1	22.9	23.2	22.6	23.1	NNN

Table 4.3 Summary of Blend A Tests

The circulating charge composition is compared to the total charge composition. System charge fractionation is assumed, when the circulating charge composition is more than 1% different then the total charge composition. The table shows that the only place where major differences in the charging and circulating compositions occur is when the accumulator has liquid in it, which will have a much lower R32 content than the circulating charge, as is shown in Fig. 4.9.

Cooling Mode Results

Figure 4.9 shows the R32 mass fraction at the four sampling locations and the overall R32 mass fraction as a function of amount of charge for two different leaking scenarios in the cooling mode at DOE-A conditions. 100% charge, as described previously, is defined as 7 pounds of charge, which was the correct amount of charge for R22. The results indicate that at this level with Blend A, the accumulator (port 3) has liquid in it, since the mass fraction of R32 is much lower in this location. Since a lower percentage of R32 (as compared the overall charge composition) is stored in the accumulator, the amount left to circulate is higher, leading to the higher R32 fraction circulating than charged. As the charge in the system is leaked, the accumulator dries, and the circulating charge is very close to the same as the overall charge.

In test 1, the leaking occurs when the system is off and from the vapor side, and therefore a higher fraction of R32 (again as compared to the overall charge composition) will be leaked out. As a result, the overall R32 mass fraction in the system is expected to decrease as the amount of charge in the system decreases. This is shown very clearly in Fig. 4.9 and in Table 4.3. The overall charge R32 fraction drops from 21% to about 17% over the course of the test. As a side note, vapor leak is very close to being flammable for the first leak (in excess of 30% R32). For the second test, the leak occurs while the system is on, from a two phase port located between the expansion valve and the evaporator inlet. The composition of the leak in this case is

very close to the circulating charge, and therefore very little change in the overall charge composition is expected. This is again demonstrated in the test results shown in Figure 4.9 and Table 4.3. In this case, the composition stays constant at around 20% R32. For both of these tests, port #4 is located in the capillary line between the expansion valve and the evaporator inlet, where a pure vapor, pure liquid, or two phase sample could have been taken, depending on exact flow conditions in the capillary line. For this reason, the results from this port are not indicative of the circulating composition.

Heating Mode Results

For the remainder of the tests, a different charging cylinder was used, which had a composition much closer to the nominal 25% R32 composition expected in Blend A. The remainder of the tests were also heating mode tests. For the DOE-E cases, the 7 lbs used to charge the typically yielded a 10 degrees of suction superheat condition, which indicated that the accumulator should be dry. This means that the overall charge should always be close to the circulating charge. Figure 4.10 shows the results of the heating mode tests run at DOE-E conditions. Both of the DOE-E test results indicate good agreement between the circulating and overall charge.

The first leak performed in the heating mode (test 3) actually caused some liquid to be discharged during the course of the leak, resulting in a leaked composition close to the overall composition. The result of this was to reduce the impact of the leak on the overall charge composition for the first leak. The rest of the leak testing was performed normally. For the second leak in test 3, the composition was much closer to the vapor side composition, resulting in a reduction of the R32 mass fraction in the system. For the system on leaks, little change in the overall composition was expected, and little was found in the tests. The overall composition was measured to be constant at about 24% for these tests, as shown in Fig. 4.10 and Table 4.3.

Low Temperature Heating Mode Results

The intent with the low temperature tests (tests 5 and 6) was to see what effect temperature would have on the composition shift due to leaking. Unfortunately, the IECs could not be operated stably below 40°F, and so were operated at about 40°F as compared to 47°F for the DOE-E tests (tests 3 and 4). The results for these tests are very close to those of the DOE-E tests, with the exception that the first leak in the system off tests was performed properly in this case. The results of these tests are presented in Fig. 4.11. For these lower temperature tests, the ideal amount of charge (for 10 degrees of suction superheat) is lower than the DOE-E tests. Consequentially, the 7 lbs charged actually yields zero superheat and some liquid in the accumulator. The liquid level inside the accumulator is lower than the sampling port, which is located about a quarter the distance from the bottom of the accumulator, and so the sample taken from this port still indicates the circulating composition. The effect of this is to again raise the R32 fraction of the circulating composition from the overall composition. This is shown in Fig. 4.11 and Table 4.3. As mentioned earlier, the system off leaks were performed properly for this set of tests, and thus the fraction of R32 in the circulating and overall charge consistently drops over the course of the system off leak (from 24% to 18% R32). For the system on leaks, the mass fraction of R32 once again stays relatively constant at about 23%.

One of the interesting results from the Task 3 transient model is that it predicts a rise in the R32 concentration at startup. This is due to the higher pressure component (R32) concentration being higher in the vapor phase, where the compressor starts drawing from at startup. As the vapor on the suction side is depleted, liquid boils and releases vapor, again at a greater concentration of the higher pressure component. Figure 4.12 shows this actually occurring. This figure shows the three startups in test 5. Each startup shows an initial 'spike' in the R32 concentration before it settles down to the circulating composition. Another interesting observation is that all three startups have a flammable composition in the vapor phase before startup, although the R32 composition does drop with leaks. A final observation for this figure is that when the charge is extremely low, the circulating composition no longer stays constant, but cycles as mass moves through the system.

Test Results for R407C

Typical test plots of temperature and pressure with time for the R407C tests are shown in Figs. 4.13 and 4.14. These plots are for test 3, which is a cooling mode test where the leak occurs when the system is off. The label on each of the shaded lines indicates the data file name for that set of steady state data, corresponding to the data sheet for test 3. For these tests, the system was charged to 10 degrees of suction superheat, leaked 25% of the full charge, and refilled to 10 degrees of suction superheat. This was repeated three times. Using this procedure, the effect of successive recharges can be seen in the system parameters. Looking at just the pressure and temperature data presented in Figs. 4.13 and 4.14, it is clear that the pressures in the system become lower with successive recharges, since the blend is losing more of the high pressure components with each leak. For the R407C tests, a great deal more data was taken and will be discussed in detail later in this section. Data sheets containing all of the data taken for all of the tests can be found in Appendix B2.

For this set of tests, the data gathering was somewhat more complex, since three refrigerant components were now present. However, as was predicted in the analytical phases and as will be shown for this phase, the blend of R32, R125, and R134a can actually be thought of as a binary blend of: (1) a high pressure component (R32/R125), and (2) R134a. This is because the blend of R32 and R125 behaves much like an azeotrope over its entire composition range.

The method for determining the overall composition for the R407C tests was also somewhat different than the Blend A tests. Since the system was filled to a constant superheat level, the system was in operation while filling, and thus taking a sample at ambient system-off conditions was not possible. The charging cylinder was sampled before the tests in order to determine the composition coming from the liquid side, as this is where the system would be charged from. In the last two tests, the charging cylinder was actually sampled (from the liquid side) before and after each charge or recharge. The results of these two samples were averaged in order to obtain the actual composition for each charge. The same sampling of the leak cylinders was performed as in the Blend A tests, and the same mass balance was performed to calculate the overall composition as in the Blend A tests.

The sampling port locations for the R407C tests remained the same as in the Blend A tests. However, the port 1 geometry was modified to give a more accurate representation of the flow composition for these tests. Port 1 still indicated a two phase sample for the heating mode tests, as did port 4 for the cooling mode tests.

Since the system was filled to a superheated condition, minimal liquid was normally expected in the accumulator for this set of tests. For this reason, the degree of separation between the circulating charge and the overall charge was expected to be less (for the full charge condition) as compared to the Blend A tests. Liquid can exist in the accumulator, and can affect the circulating composition, even at a superheated vapor condition because the liquid composition typically has a lower fraction of high pressure components than the vapor. Taken to an extreme, pure R134a can exist in the accumulator as a liquid with R407C circulating with 20 degrees of suction superheat.

Table 4.4 shows a summary of the results from the six tests. Only the R32 composition is shown here because, as mentioned previously, the R125 concentration closely follows the R32 concentration trends. The table shows that, in general, the circulating composition stays very close to the overall composition for most of the tests.

	(% R32)	Test 1	Test 2	Test 3	Test 4	Test 5	Test 6
Full charge	Circulating	21.4†	21.0	21.7†	21.0	20.8	20.6
	Overall	20.4	20.4	20.4	20.4	20.4	20.3
After leak #1	Circulating	20.8	21.0	20.1	20.2	*	*
	Overall	20.5	20.5	19.7	19.6	20.4	19.2
After refill #1	Circulating	21.2	21.6†	20.7	21.7†	20.8	19.5
	Overall	20.5	20.5	19.9	19.8	20.4	19.5
After leak #2	Circulating	20.9	20.8	19.3	16.7	*	*
	Overall	20.6	20.5	19.1	16.7	20.5	18.5
After refill #2	Circulating	21.3	21.1	20.1	18.1	20.4	19.1
	Overall	20.6	20.5	19.5	17.8	20.5	19.0
After leak #3	Circulating	20.7	20.6	18.5	15.5	*	*
	Overall	20.7	20.2	18.0	15.9	20.5	18.9
After refill #3	Circulating	21.1	21.5†	19.5	17.3	20.6	19.5
	Overall	20.6	20.2	18.7	17.3	20.4	19.5

* Data not taken
† Indicates fractionation

Table 4.4 Summary of R407C Tests (R32 Composition Only)

Test 1 (Cooling Mode - System on Leaks) Results

The system composition data for test 1 is shown in Fig. 4.15. The figure shows that the circulating composition does vary, by a small degree, from the circulating composition, while the system is at full charge. When the system is operating at the reduced charge level, the degree of separation is much less. Port 4 is located in the two phase portion of the line, as indicated earlier, and does not represent the circulating composition. The composition trends for R125, shown on

the right side of the figure, tend to follow those of the R32, shown on the left. Over the course of the three leaks and recharges, the system composition varied only by 0.2% R32; essentially not at all. This is because the leaks occurred when the system was operating, and both the leak composition and recharging composition were very close to the circulating composition.

Figure 4.16 shows the composition data taken inside the evaporator for test 1. To understand this data, refer back to Figs. 3.1, 3.2, and 4.6, which show the arrangement of the sampling ports in the heat exchanger and the saturation diagram for a nonazeotropic refrigerant blend. The refrigerant enters the heat exchanger at port 1 in a two phase state. The sampling port, however, is physically at the end of the return bend of the line. Liquid will tend to flow around the outer edges of the bend due to inertia. Therefore, when there is a significant liquid flow (when the quality is low and the liquid flowrate is high), the sample taken will tend to be liquid. This explains the low concentration of R32 and R125, as compared to the circulating composition. The R32 and R125 concentrations continue to drop as the blend travels through the circuit, as these components will tend to boil first. The point in the heat exchanger at which the sample is no longer totally liquid, will vary with charge. At port 4, the sample starts to be less then totally liquid for some cases. When the refrigerant has reached port 5, the sample is now vapor. The remaining liquid refrigerant no longer moves at sufficient speed to flow around the outer edges of the bend. The vapor sample, at this point, indicates a slightly higher concentration of the higher pressure components than the circulating charge, since there is still some liquid refrigerant present, which will have a low concentration of the high pressure components (see Figs. 3.1 and 3.2). When the system is at the reduced charge condition, several things happen. First, the liquid will tend to evaporate faster inside the heat exchanger, and the suction superheat will tend to be higher. Also, the liquid flowrate will be less. Figure 4.16 shows the sampled composition being liquid for only the first port in the heat exchanger. The rest of the ports are vapor, which is not surprising since the system pressure and temperature data indicates 50 degrees of suction superheat at this point. Figure 4.17 shows the evaporator temperature profile at the seven sampling ports, with the saturated liquid and vapor lines superimposed. The two charts on the left side show the test 1 results. This data tends to confirm the observations made above. When looking at the data from inside the heat exchanger, one must realize that this data represents only one of the four operational circuits inside the indoor coil. The other circuits may have more or less heat transfer, and thus show different results. The overall heat exchanger exit temperature may therefore not be the same as the circuit exit temperature

Figure 4.18 shows the system capacities and efficiencies as a function of time for test 1. Both the cooling and heating performance factors are shown, even though this was a cooling mode test. The heating mode results are simply an analysis of the condenser (outdoor unit) performance. This figure shows that the system performance did not change over the course of the three recharges. Of course, when the system is at the reduced charge level, both the capacity and efficiency are reduced, as expected.

Test 2 (Heating Mode - System on Leaks) Results

Test 2 is a heating mode test at DOE-E conditions, again with a system on leak. Since the leaks are performed with the system on, it is expected that the circulating and overall compositions will not vary much over the course of the three leaks and recharges. The system

composition results are shown in Fig. 4.19. Port 1 in this case is a two-phase port and so is not shown. The results show a very small variation in the composition levels (0.5%). The results also show a larger degree of separation between the circulating and overall compositions than the first test, with the degree of separation becoming slightly larger as the tests continued. What happened for this test 2 and for test 4 is that the outdoor coil was never intentionally defrosted over the course of the leaks and recharges. The one defrost cycle which did occur was before the second leak. The buildup of frost on the outdoor unit effectively led to a reduction in the heat transfer area, as the airflow was reduced and eventually entirely blocked. When the system was recharged, less and less refrigerant was required to achieve 10 degrees of suction superheat. Also, after the recharge was performed, the superheat continued to drop as more frost built up, and eventually the accumulator began to fill with liquid. Once this began, it was expected that the circulating and overall compositions would start to diverge, as seen in Fig. 4.19.

The composition results measured inside the condenser are shown in Fig. 4.20. For the heating mode, vapor from the compressor discharge enters the coil from port 7 and flows to port 1, where it exits as a subcooled liquid. The majority of the refrigerant in the system tends to be in the condenser, so it is no surprise that the refrigerant has totally condensed by the time it reaches port 5. Port 1 indicates a vapor sample, possibly with liquid in the line for some of the charges. Port 2 indicates a liquid sample with vapor in the line. The R32 and R125 compositions are low here in comparison to the overall composition because the vapor phase contains higher mass fractions of these two components.

Figure 4.21 shows the performance results for test 2. As indicated earlier, this test had no defrost cycles intentionally initiated, and so the severe performance degradation shown in this figure is due to the frost buildup on the outdoor coil. The frost tended to build up much more quickly at the reduced charge levels because the evaporating pressures and temperatures are lower at reduced charge levels. The effect of the frost can be seen in the difference between the performance before and after the defrost cycles before the second leak was performed, which shows almost a 50% rise in capacity.

Test 3 (Cooling Mode - System off Leaks) Results

Test 3 was a cooling mode test at DOE-A conditions with system off leaks. The system leaks were withdrawn from the vapor side, which had a higher concentration of the high pressure components of the blend (R32 and R125) than the overall concentration. It was expected that the overall high pressure component compositions would decrease over successive leaks and recharges. The composition results for test 3 are presented in Fig. 4.22, and shows that the overall and circulating high pressure component compositions drop by about 2% each. The differences between the circulating and overall charge compositions is about 1% or less for the full charge conditions. This difference could be accounted for by the possibility of liquid being present in the accumulator, as the superheat is low. The reduced charge compositions show a very close match between the circulating and overall compositions. Port 4 in this test is again a two-phase sample port, and has likely pulled in a liquid sample.

The compositions measured inside the evaporator for test 3 are shown in Fig. 4.23. The explanation for these results is very similar to that of the test 1 results. The major difference in

test 3 is that the system high pressure component compositions are continually dropping. Figure 4.17 also shows the heat exchanger temperature profile for this test. It shows that the liquid tends to evaporate faster for this test than test 1. From this, the compositions in Fig. 4.23 should also change to vapor earlier in the heat exchanger.

The system performance levels for test 3 are shown in Fig. 4.24. They show that the system capacities and efficiencies remain relatively constant over the three recharges, even though the composition of the circulating blend has shifted to a slightly lower pressure. This result indicates that even if the system does leak from the vapor side and is refilled several times with the original blend composition, there will be little impact on the performance.

Test 4 (Heating Mode - System off Leaks) Results

Test 4 consisted of a heating mode test at DOE-E conditions with system off leaks. Once again the vapor leaked was expected to have a higher fraction of the high pressure components, leading to a reduction in these components in the circulating and overall compositions for successive refills. The system was again not intentionally defrosted over the course of the recharges. One defrost cycle did occur after the second leak. Figure 4.25 shows the system composition results for test 4. Port 1 is again a two-phase port in the heating mode, and so is not shown on this figure. The figure shows several interesting results. First, the system R32 and R125 compositions are clearly dropping as a result of leaks. The overall drop is about 3% for each high pressure component. Secondly, the figure shows that the accumulator has liquid in it after the first refill. The accumulator port (#3) shows a lower fraction of both high pressure components, and both the compressor discharge (vapor) and the condenser exit (liquid) show higher concentrations of the high pressure components relative to the overall composition. At the reduced charge levels, the circulating and overall compositions are again very close to each other.

Heat exchanger component compositions for test 4 are presented in Fig. 4.26. In general, the graphs on this figure can be looked at the same way as the test 2 results. One major difference from the test 2 results is that the circulating composition after the first refill actually is higher in the high pressure components than the original charge. This is because, as previously mentioned, the system had liquid in the accumulator at this condition, leading to a reduction in the relative amount of circulating R134a. The next two refills show successively lower concentrations of the high pressure components, as expected. The second item of note is that port 2 seems to show a spike in both the R32 and R125 concentrations, which goes away after the second refill. An explanation of this may be that a vapor bubble somehow became trapped at this port.

System capacity and efficiency are shown as a function of time on Fig. 4.27. The figure shows that, as in the test 2 results, the performance drops off significantly over time, again because of frost on the evaporator. The defrost cycle, performed after the second leak, increased the performance levels briefly. The effect of frost formation can be seen very clearly in the way the performance drops off when the system is at full charge. Because of the severe frosting effects in both this test and test 2, these tests were redone.

Tests 5 and 6 (Heating Mode - System on & off Leaks) Results

For the last two tests, a defrost cycle was performed before each set of data was taken. No composition data was taken when the system was at reduced charge levels in order to minimize the effects of frosting, which occurs much faster at the reduced charge levels. In addition, in order to more accurately track the overall composition, a sample of the liquid side of the charging cylinder was taken before and after each charge and recharge. The two samples were averaged to find the exact filling composition. Also, since port 1 is a two-phase sample for both of these heating tests, it is not plotted in the results.

Test 5 was a heating mode test at DOE-E conditions with system on leaks. As the leaked composition should be close to the overall composition, no major change in the overall composition was expected for this set of tests. The system and heat exchanger compositions for test 5 are shown in Fig. 4.28. The system and overall compositions do not change significantly over the course of the three leaks and recharges. The circulating charge composition also remains very close to the overall charge composition over the course of the test. The heat exchanger compositions show very similar results as test 2. The system performance for this test is presented in Fig. 4.29. It shows that both the capacity and efficiency remain relatively constant, with a slight drop-off in capacity because of the beginnings of frosting at the later recharges, throughout the test.

For test 6, a heating mode system off leak test was performed at DOE-E conditions. The system and overall high pressure component compositions were again expected to drop during the course of this test, as in tests 3 and 4. Figure 4.30 shows the system and heat exchanger compositions for test 6. In general, it shows the circulating and overall R32 and R125 compositions dropping over a number of recharges. The last system leak introduced a liquid sample into the leak, which led to the increase in the R32 and R125 concentrations for the last recharge. The system and overall compositions are again very close to each other, as in test 5. The heat exchanger results also behave very similarly to the test 5 results, with the major difference being that the circulating high pressure component compositions drop over successive recharges. Figure 4.31 shows the system capacity and efficiency as a function of time for test 6. This shows that although the system performance does drop off, the effects are relatively minor (4% reduction in capacity, with some reduction due to frosting). The efficiency actually very slightly (2%) improves with the lower pressure blend.

Summary

A total of six tests were conducted with Blend A, and six more with R407C. Two cooling mode tests and four heating mode tests were performed for each blend. System leaks were performed while the system was on and off. The Blend A tests leaked the system down to 50% of the original charge. The R407C tests consisted of a series of three leaks to 75% original charge and three refills.

The Blend A tests showed significant composition shifting (up to 5% reduction R32 composition) when leaked from the vapor side when the system was off. Very little composition shifting was observed when the leak occurred while the system was in operation. The results also indicated little difference between the circulating and overall blend composition unless the

accumulator contained liquid. A sharp increase in the R32 composition was noted as occurring briefly after startup, before it dropped to the circulating composition level.

The R407C tests confirmed many of the observations made during the Blend A tests. Again, the composition was observed to vary, although not as significantly, as refrigerant was removed from the vapor side while the system was off. Refilling of the system with blend of the original composition caused the overall blend to move closer to the original composition. After three vapor side system off leaks, the overall composition of both R32 and R125 decreased a maximum of about 3%. The impact of this blend shift on the system capacity and efficiency was small. Little change in the blend composition was observed when the leak occurred while the system was operating. In addition, if the system was refilled with blend of the same composition, it essentially retains the original blend composition, with no resulting changes in performance.

Conclusions

Several important conclusions can be made from the experience gained from the experimental tests. These conclusions can be generalized to other systems and blends.

- Fractionation (a difference between the circulating and charged blend composition) of a nonazeotropic blend in a system will only occur when there is potential for significant liquid holdup or storage.
- The degree of fractionation will depend on both the amount of liquid stored and the thermodynamic properties (such as temperature glide) of the refrigerant blend.
- Leaks can alter the composition of the refrigerant blend and are most significant when they occur from the vapor side while the system is off.
- When leaks occur while the system is on, very little composition shifting will occur.
- Recharging the system after a leak with a blend of the original composition will bring the blend closer to the original system composition.
- Changes in the system blend composition will result in changes in system performance.

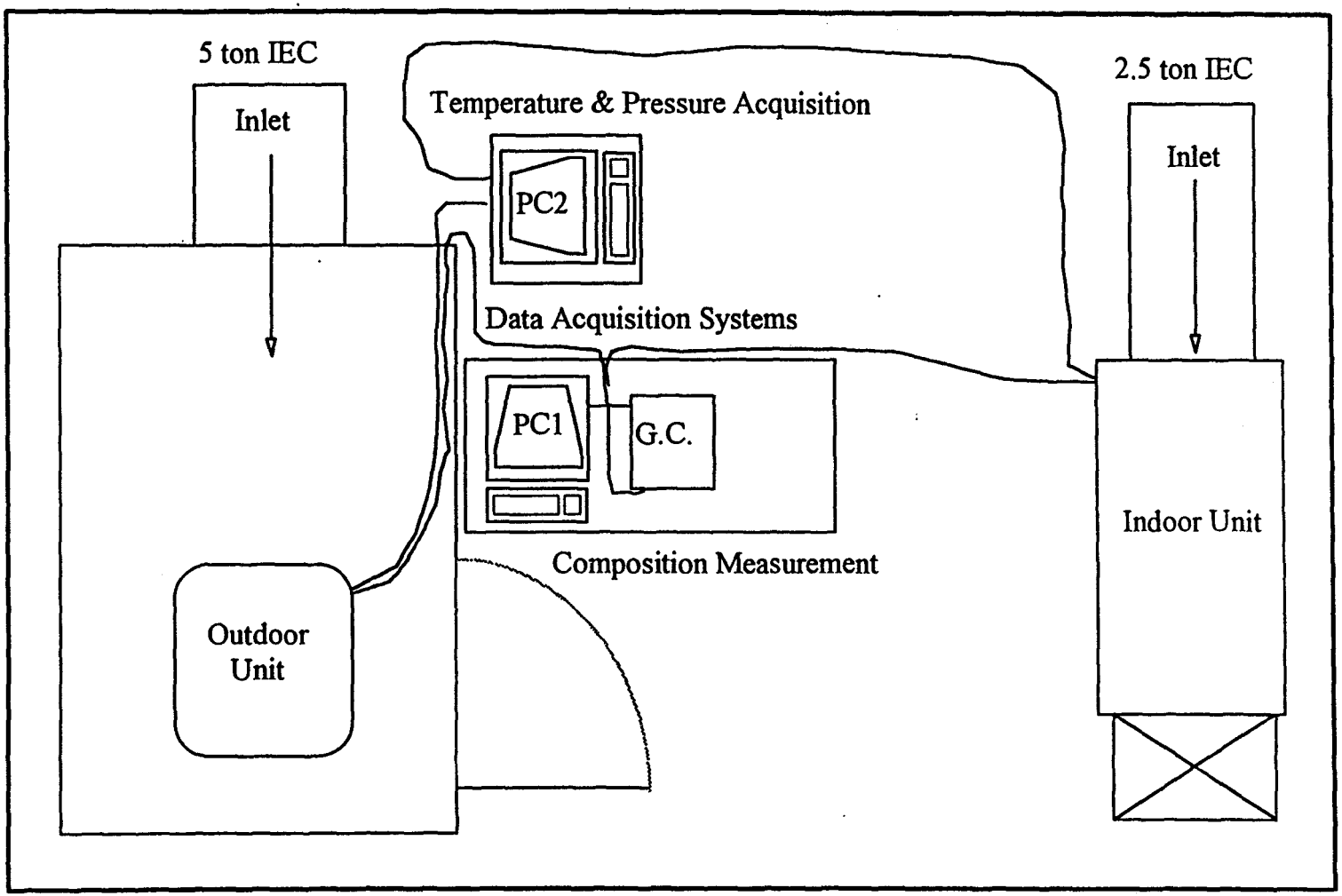

Fig 4.1 Lab Arrangement for Blend A and R407C Fractionation Tests

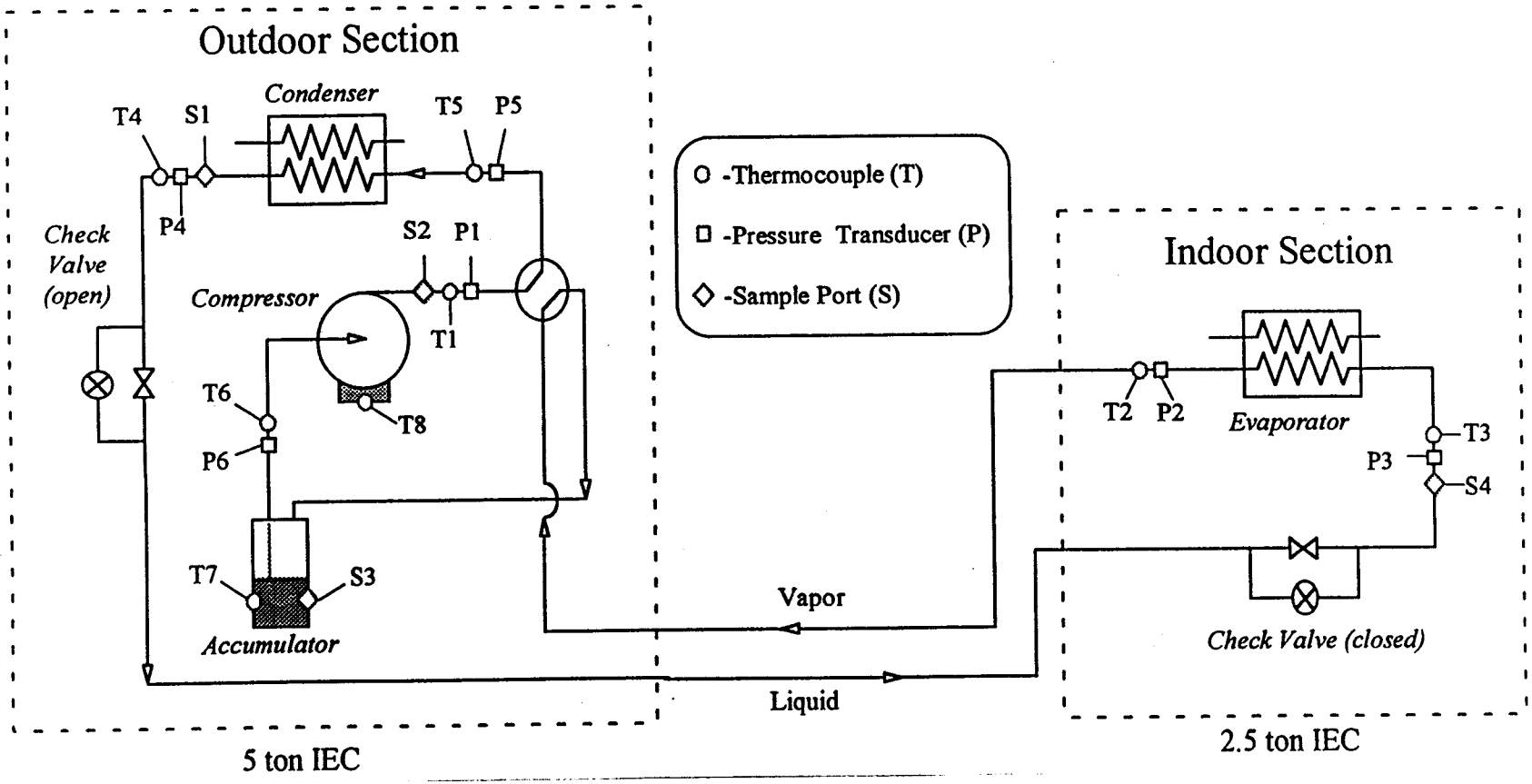

Fig 4.2 ARTI Heat Pump Experimental Layout for Blend A Tests (Cooling Mode)

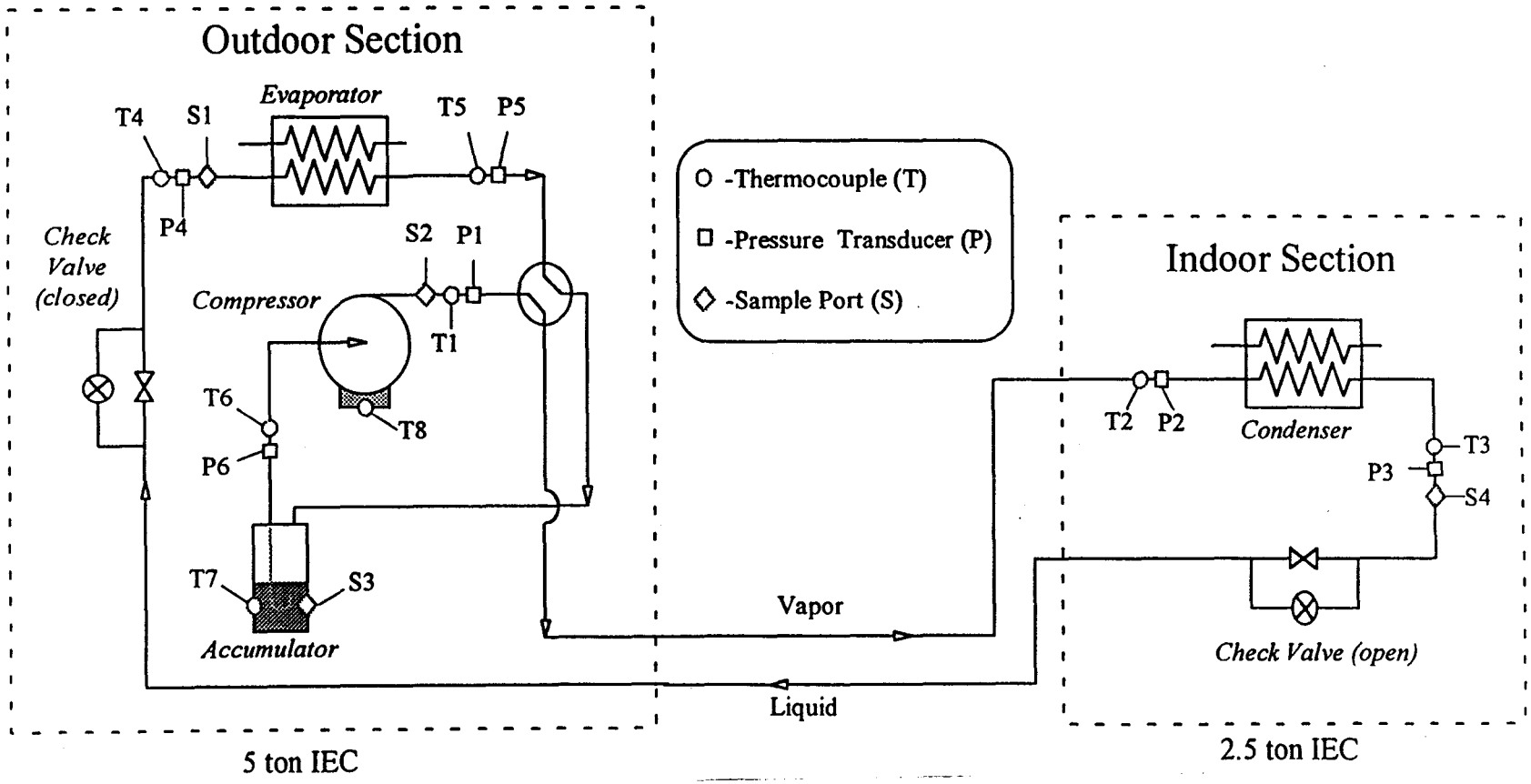

Fig. 4.3 ARTI Heat Pump Experimental Layout for Blend A Tests (Heating Mode)

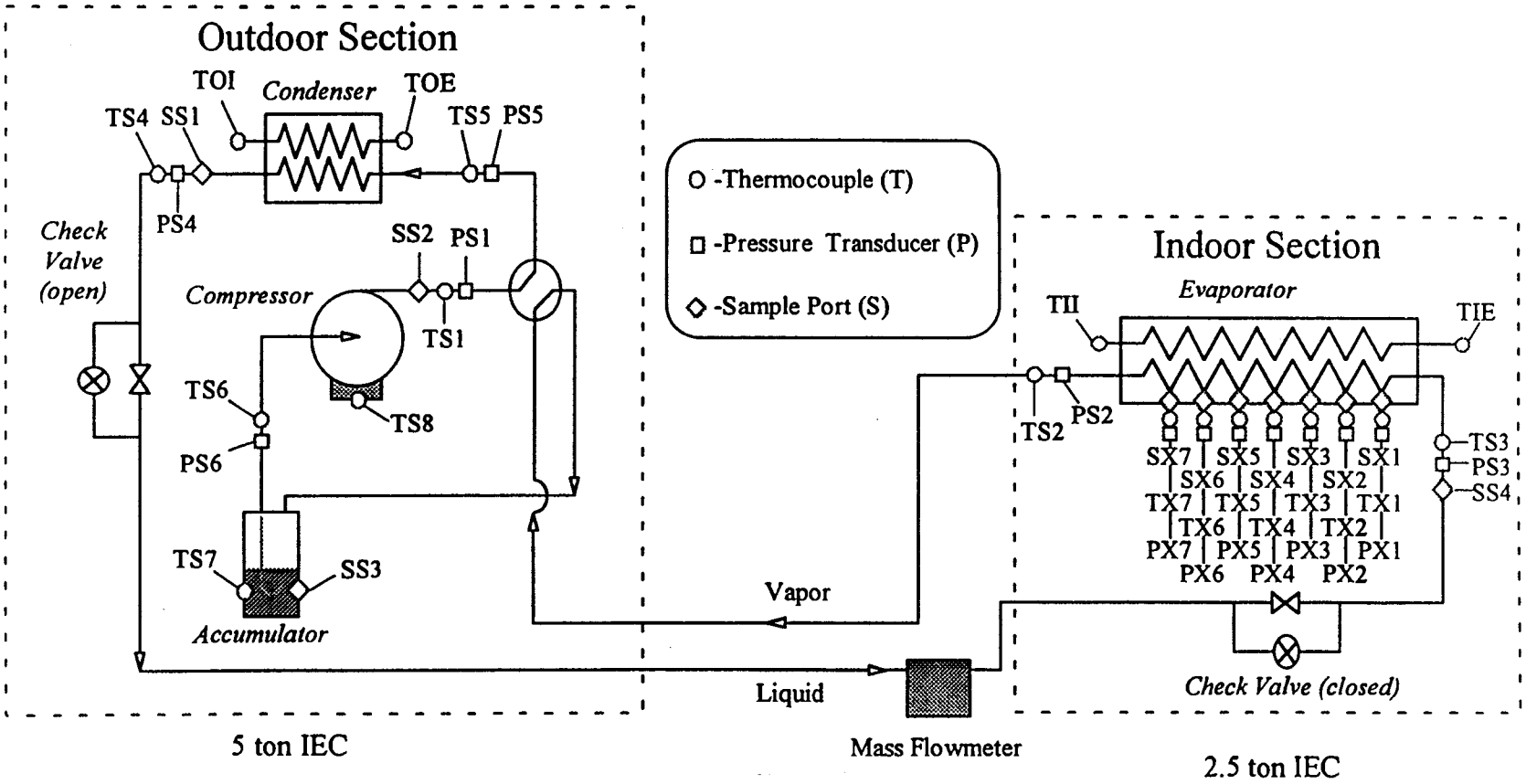

Fig. 4.4 ARTI Heat Pump Experimental Layout for R407C Tests (Cooling Mode)

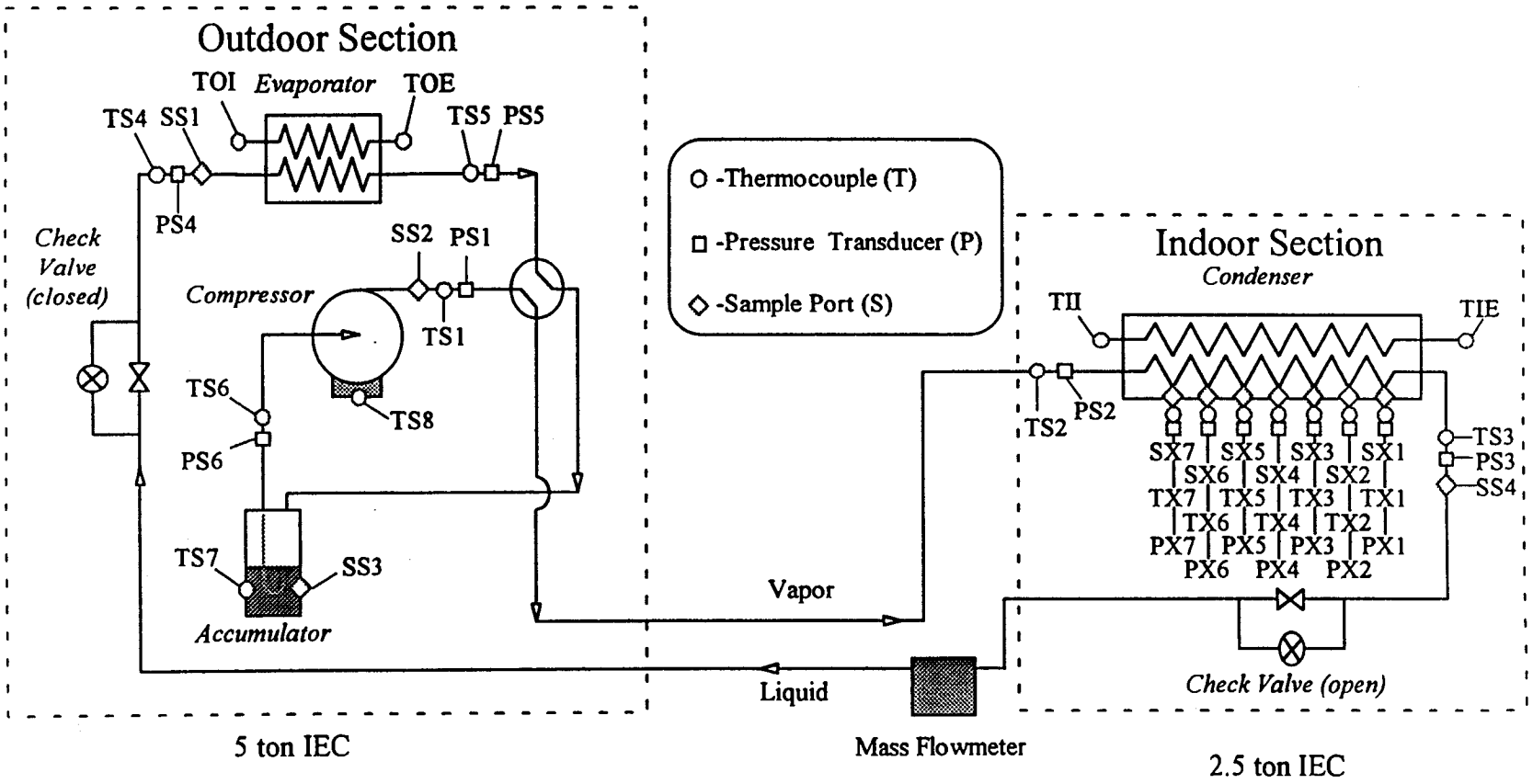

Fig. 4.5 ARTI Heat Pump Experimental Layout for R407C Tests (Heating Mode)

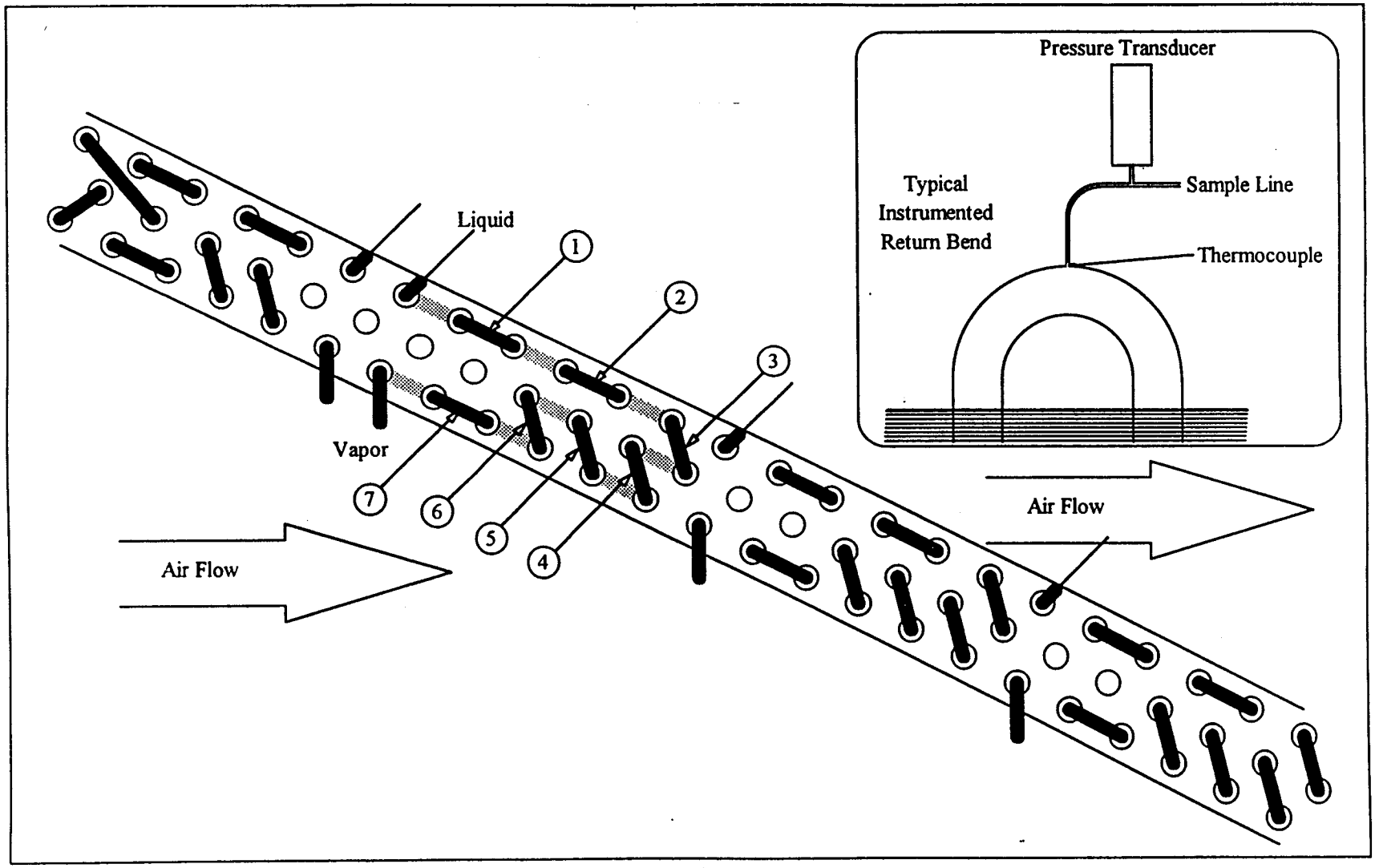

Fig. 4.6 Indoor Unit Heat Exchanger Instrumentation Layout

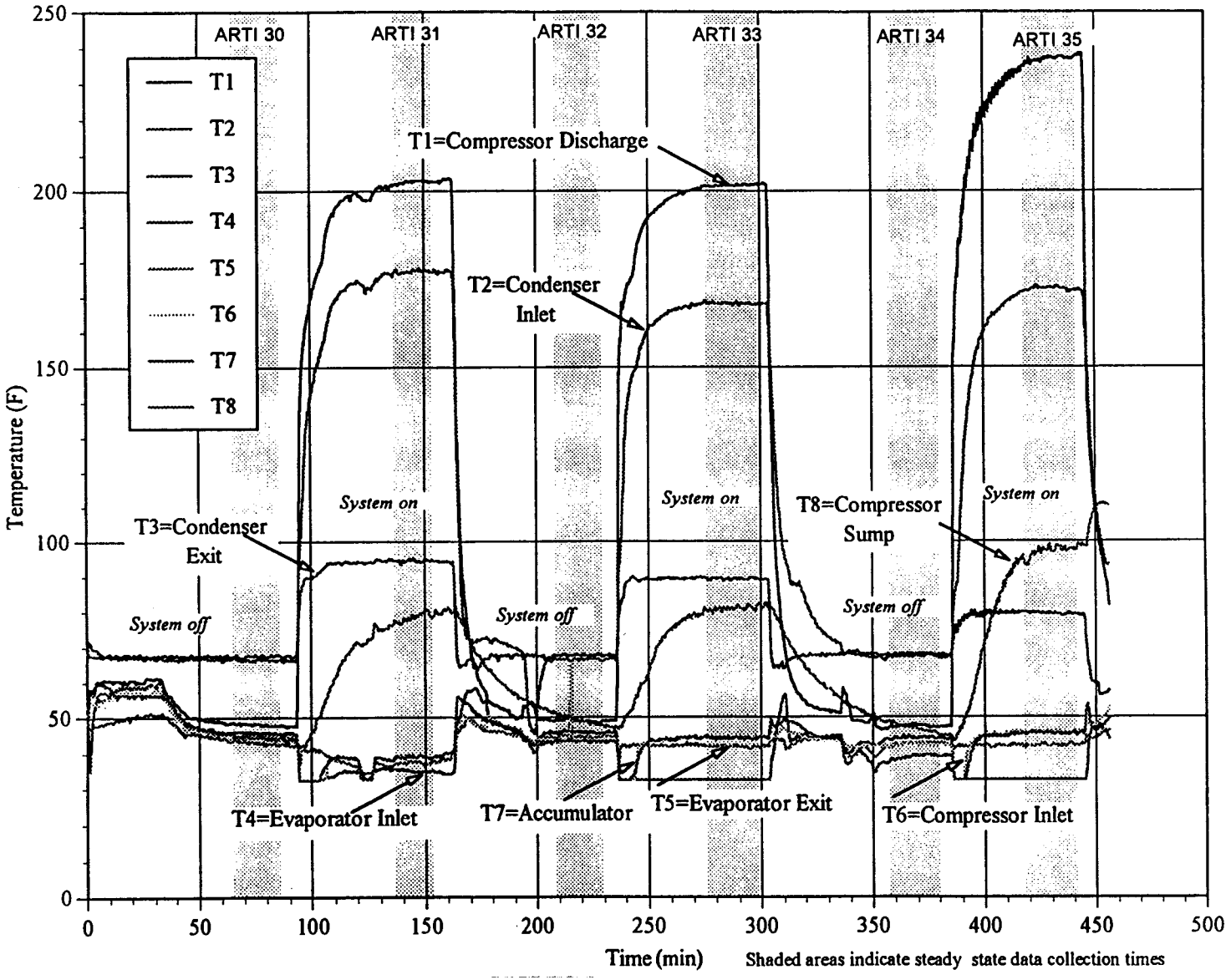

Fig. 4.7 Blend A Heat Pump Test #3 - Smoothed Temperature Data

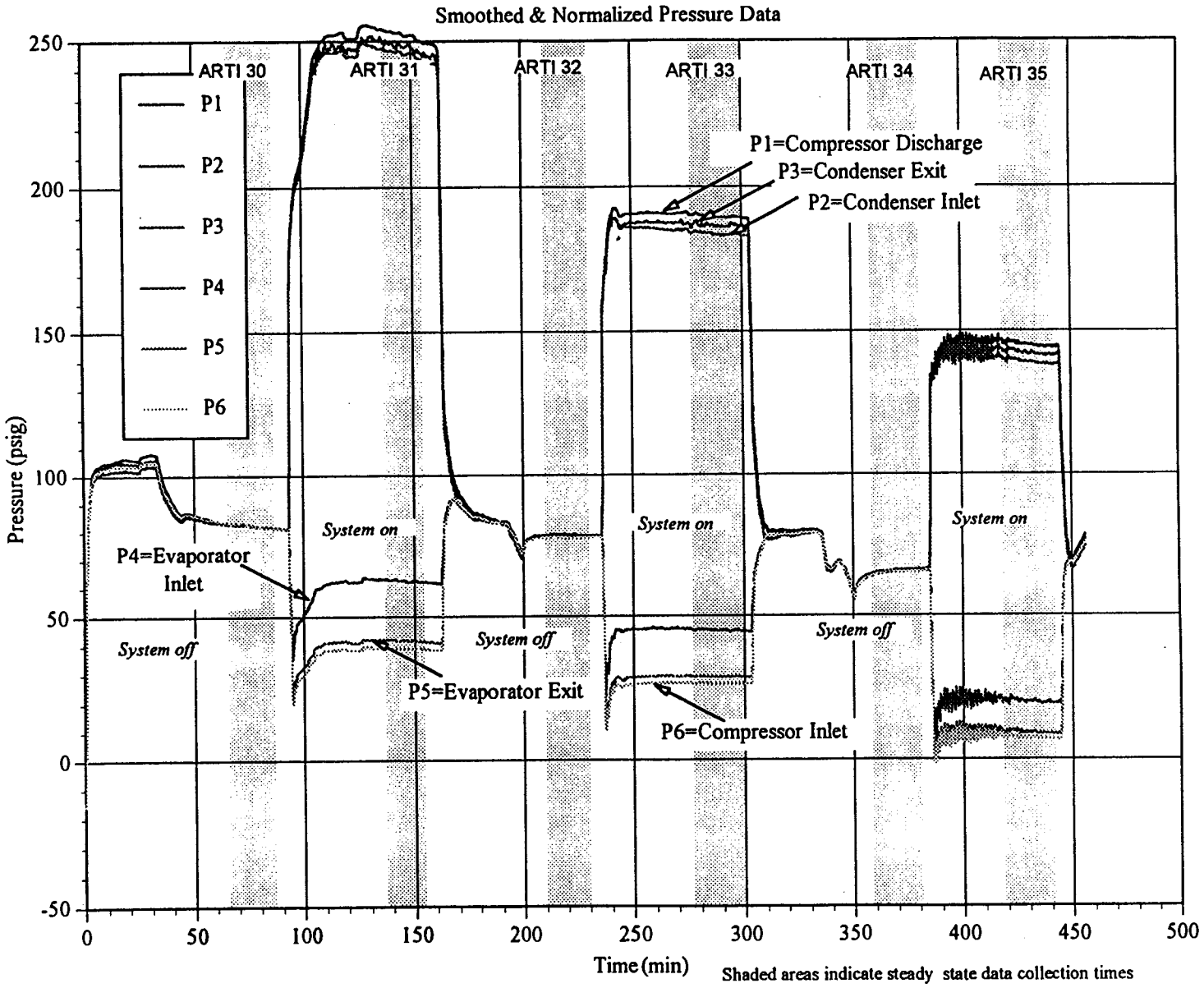

Fig. 4.8 Blend A Heat Pump Test #3 - Smoothed and Normalized Pressure Data

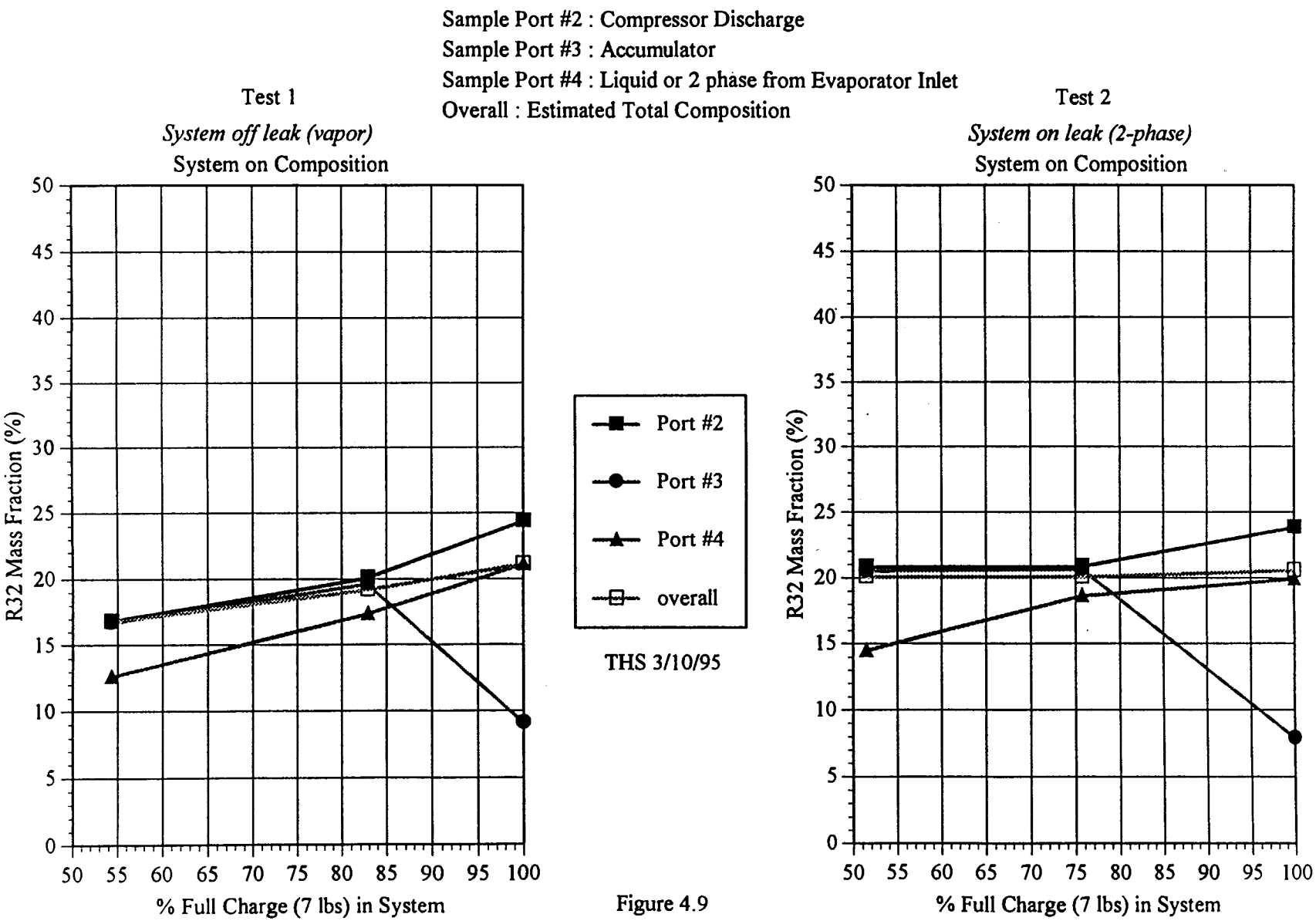

Fig. 4.9 System Fractionation in Blend A DOE-A Tests

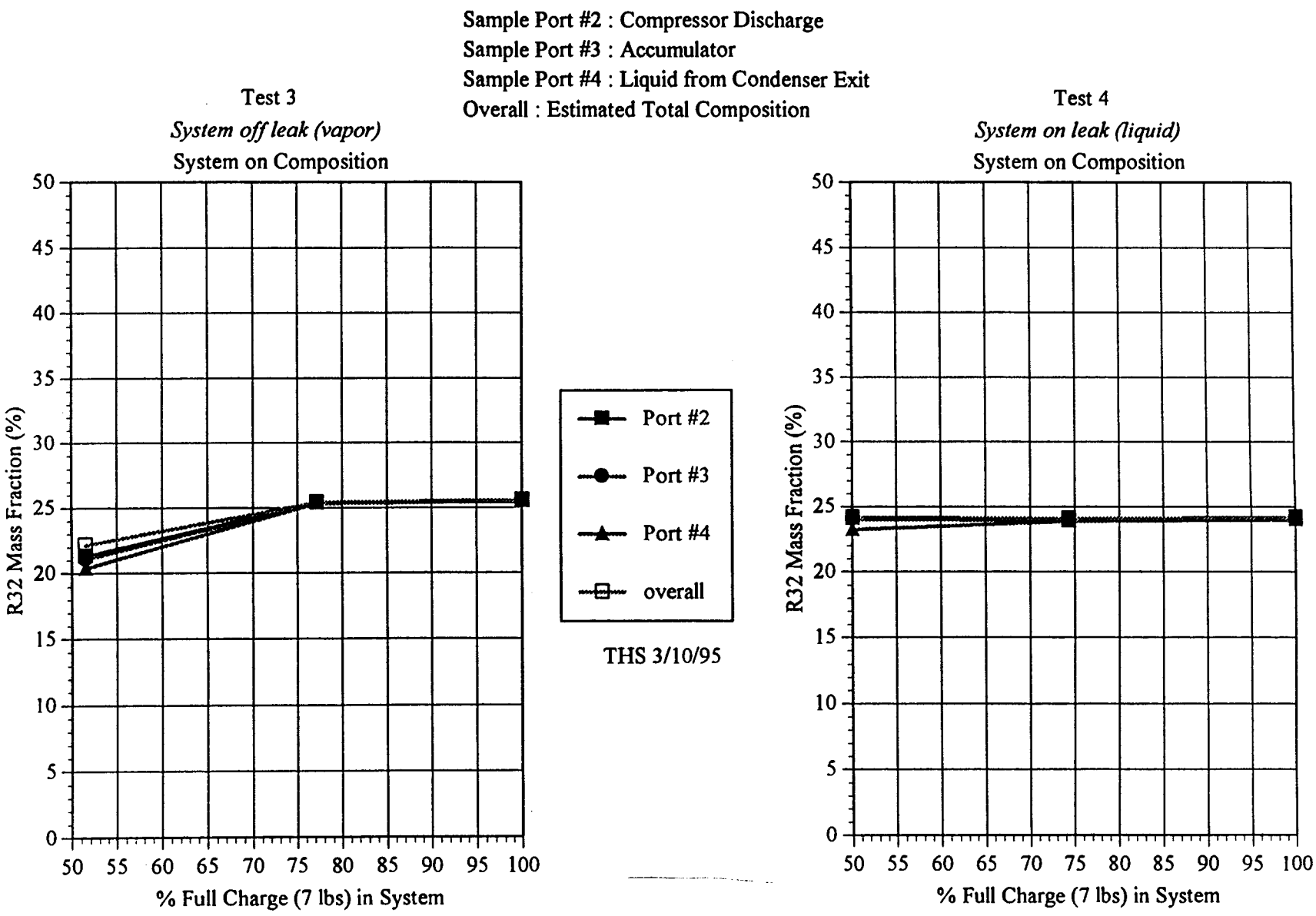

Fig. 4.10 System Fractionation in Blend A DOE-E Tests

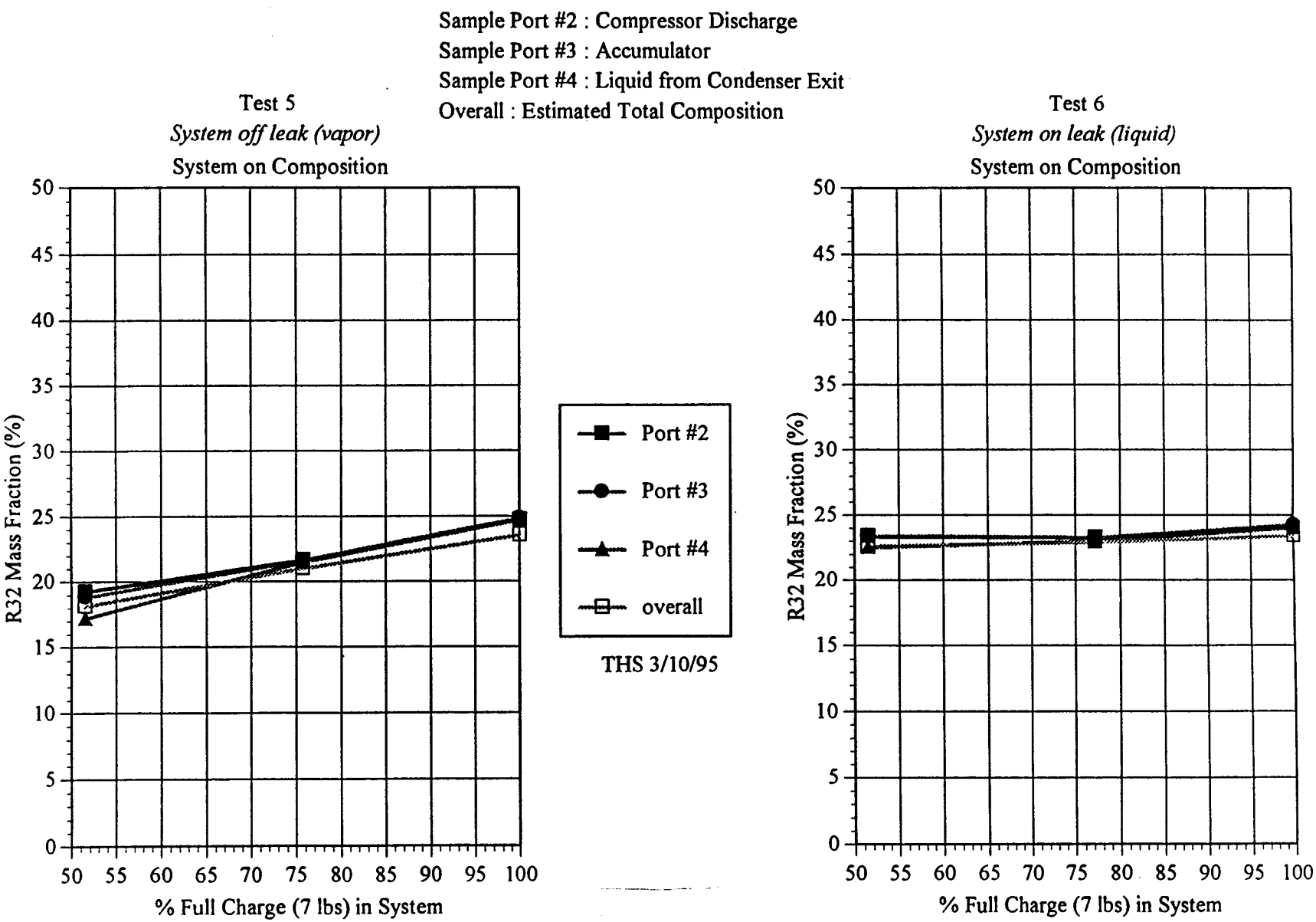

Fig. 4.11 System Fractionation in Blend A Low Temp Tests

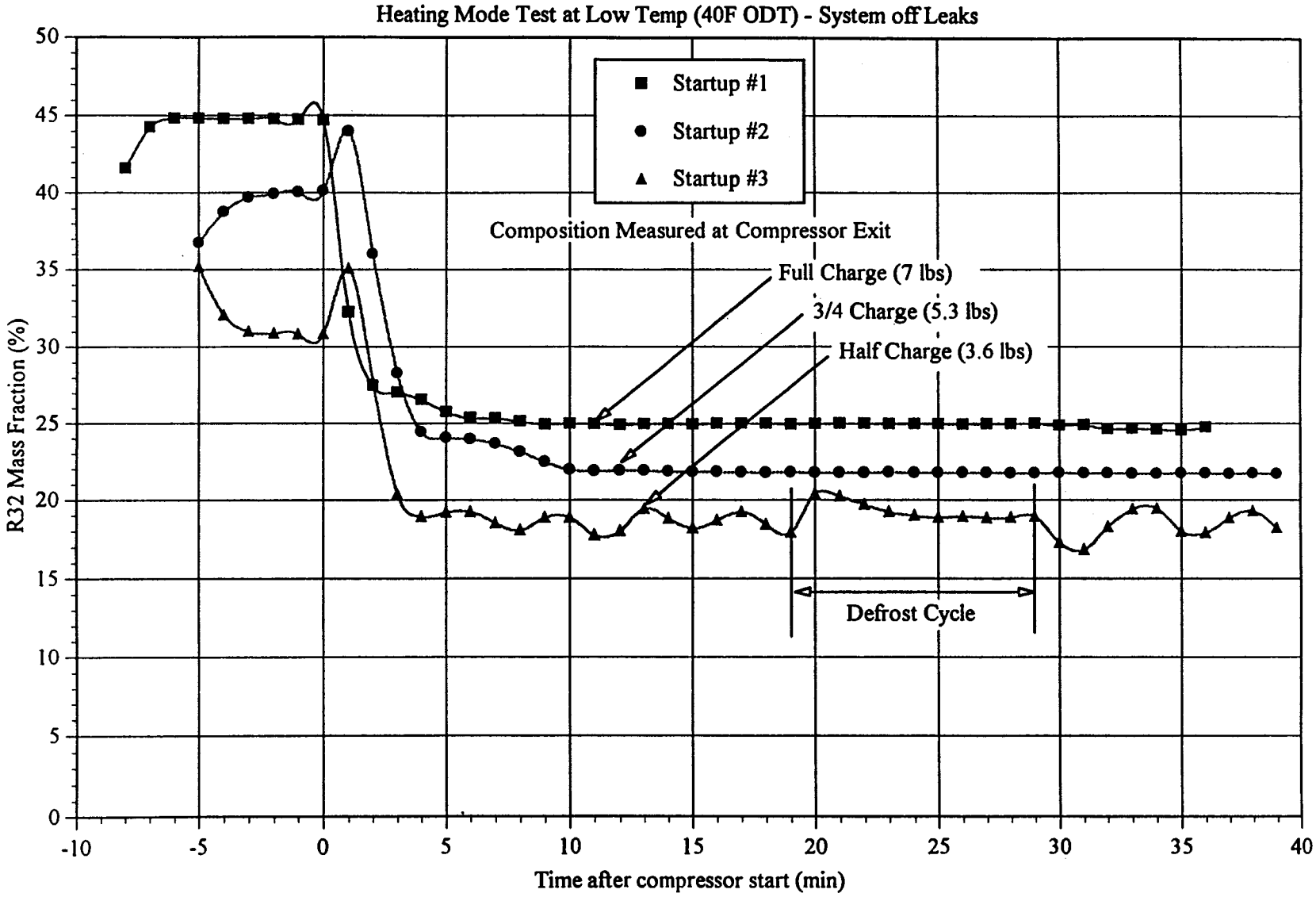

Fig. 4.12 Blend A Transient Composition Study: Run #5

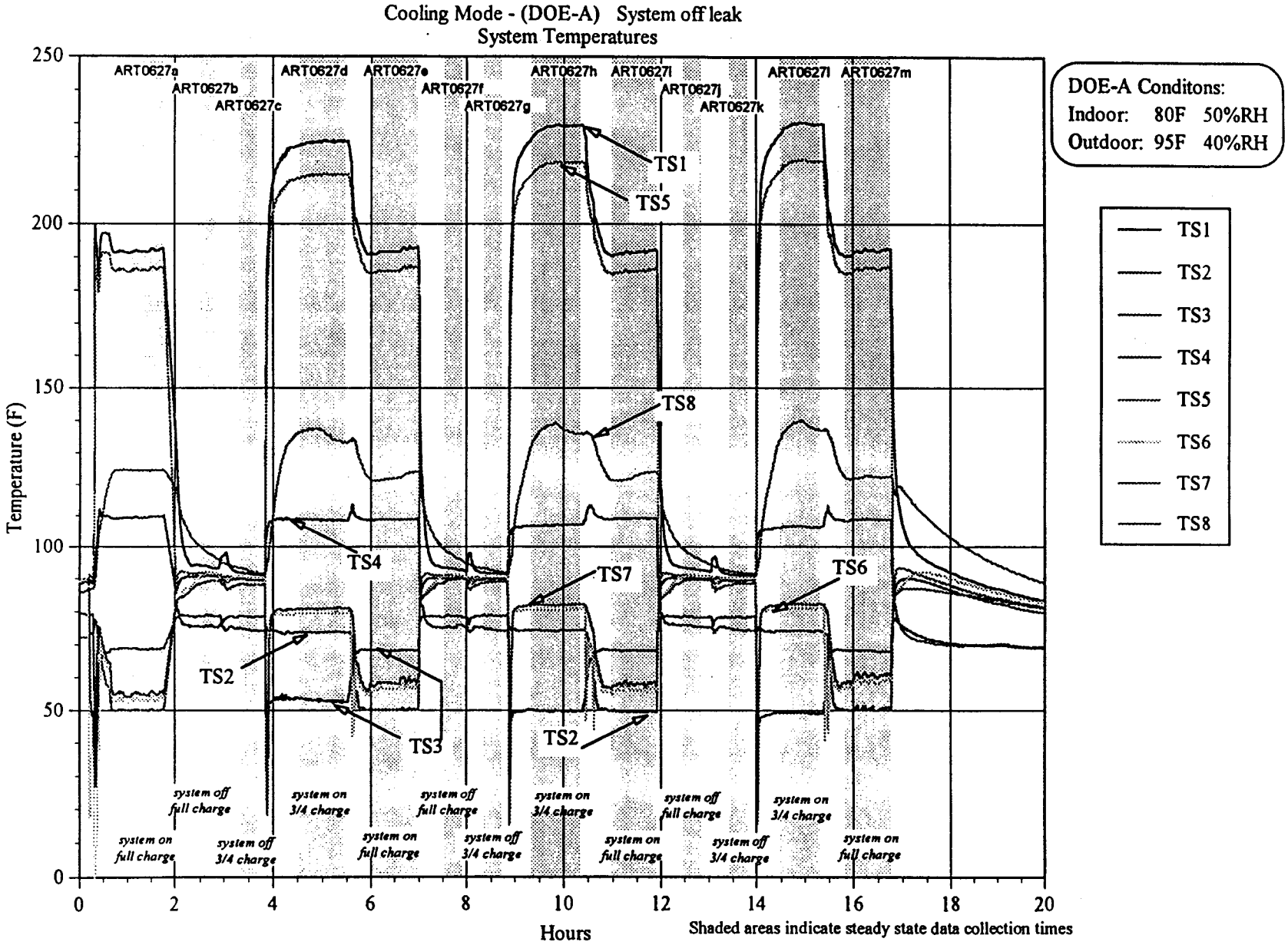

Fig. 4.13 R407C Heat Pump Test #3 Cooling Mode - (DOE-A) System Off Leak System Temperatures

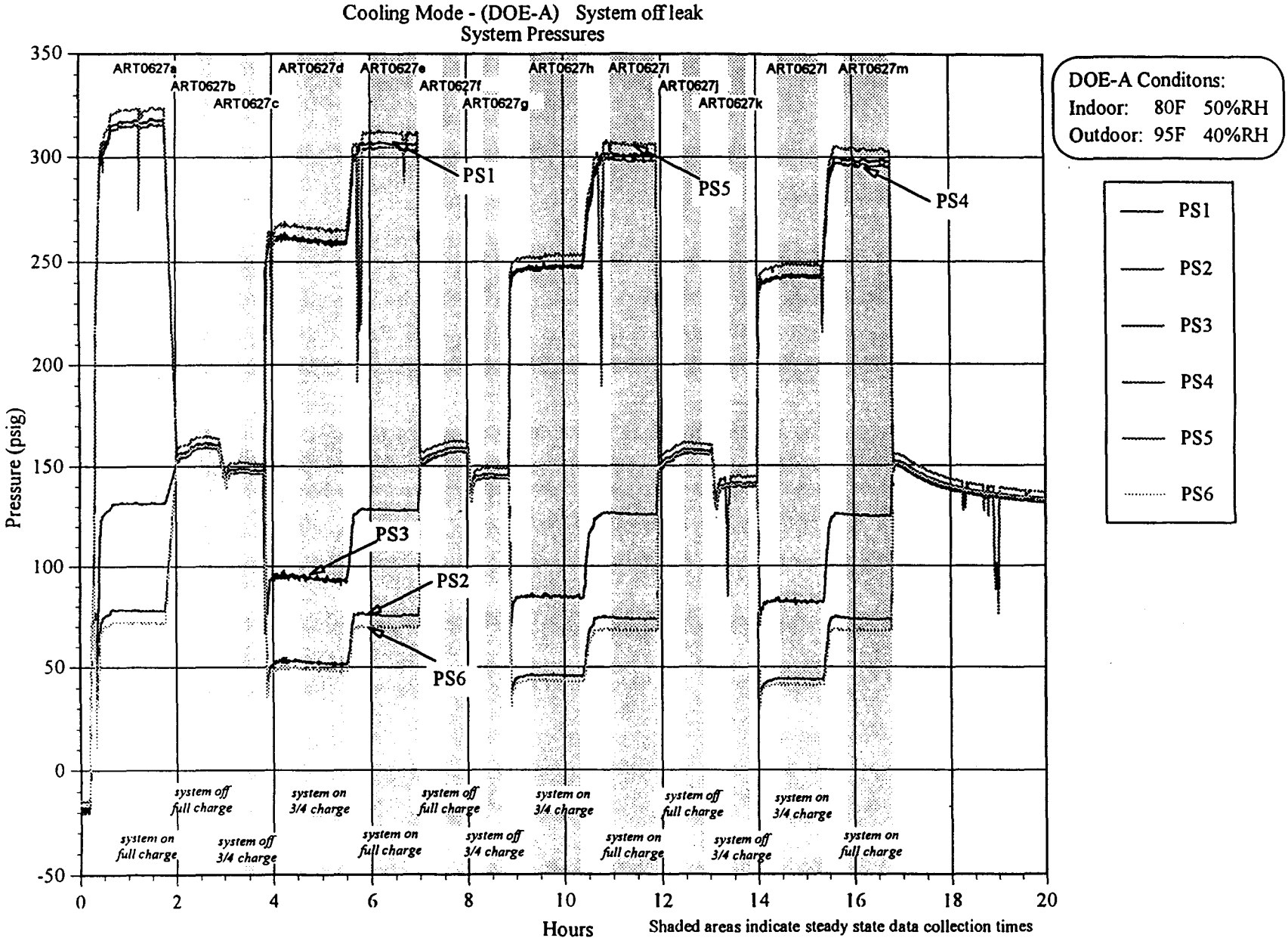

Fig. 4.14 R407C Heat Pump Test #3 Cooling Mode - (DOE-A) System Off Leak System Pressures

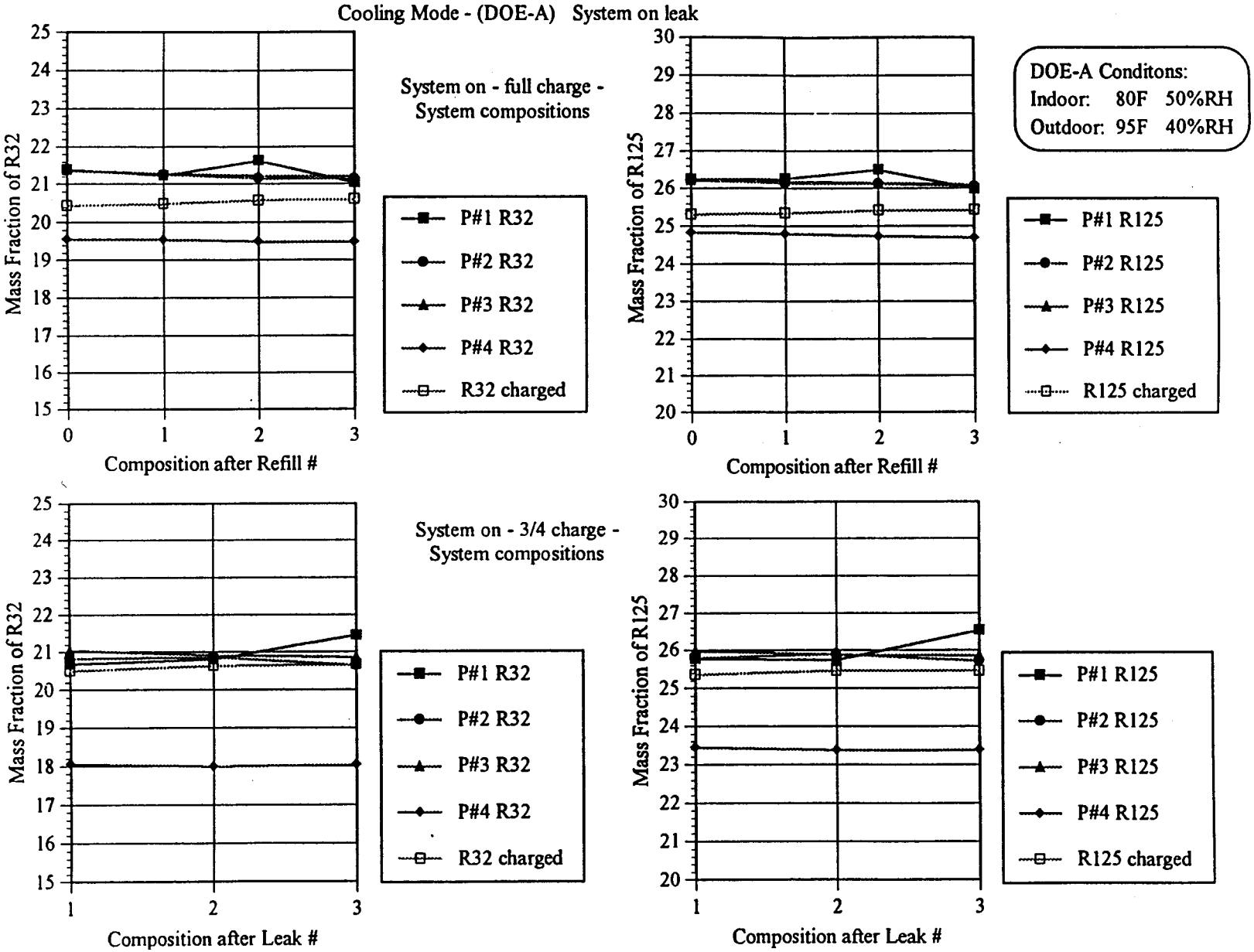

Fig. 4.15 System Fractionation in R407C Test 1

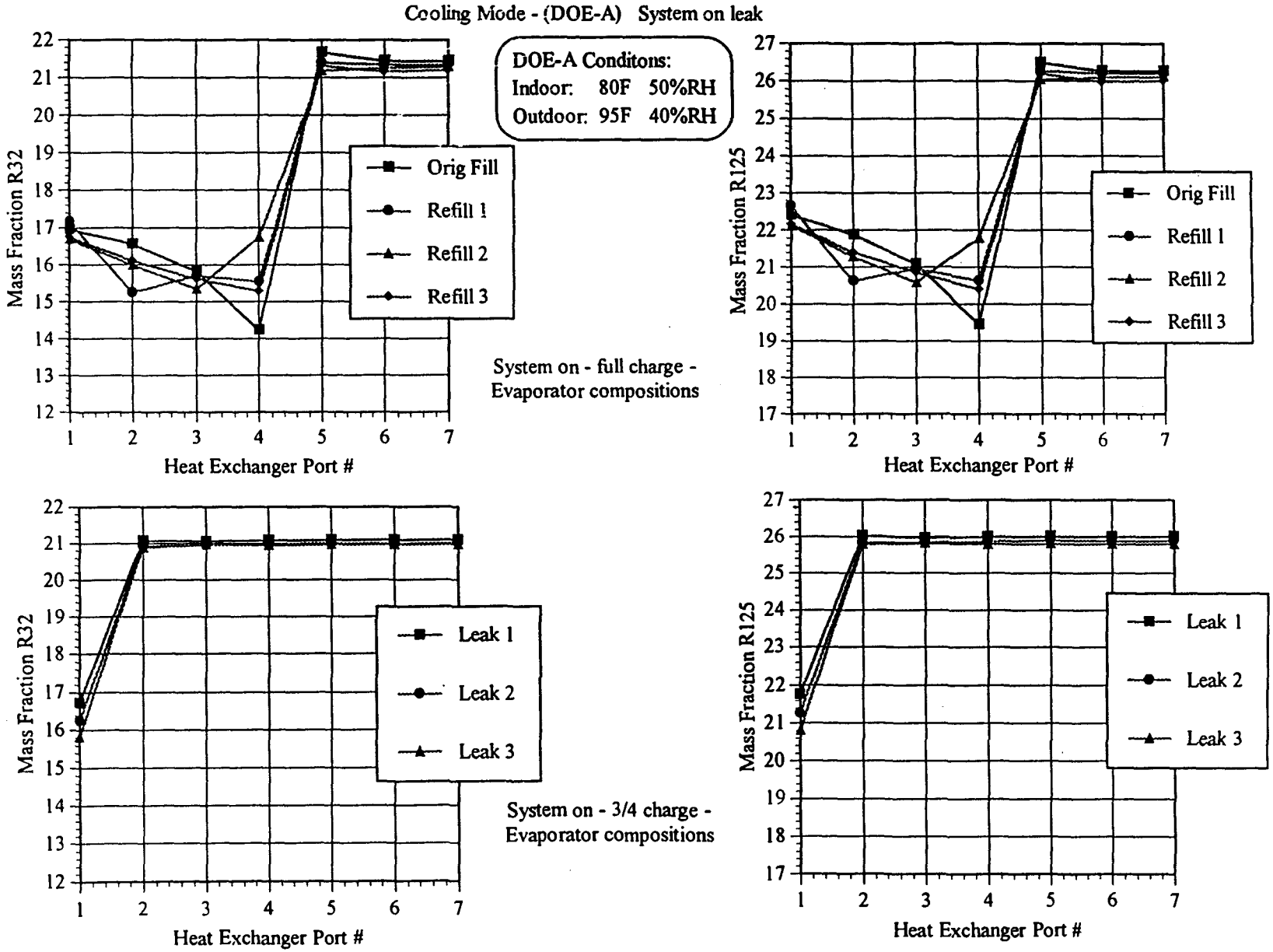

Fig. 4.16 Component Fractionation in R407C Test 1

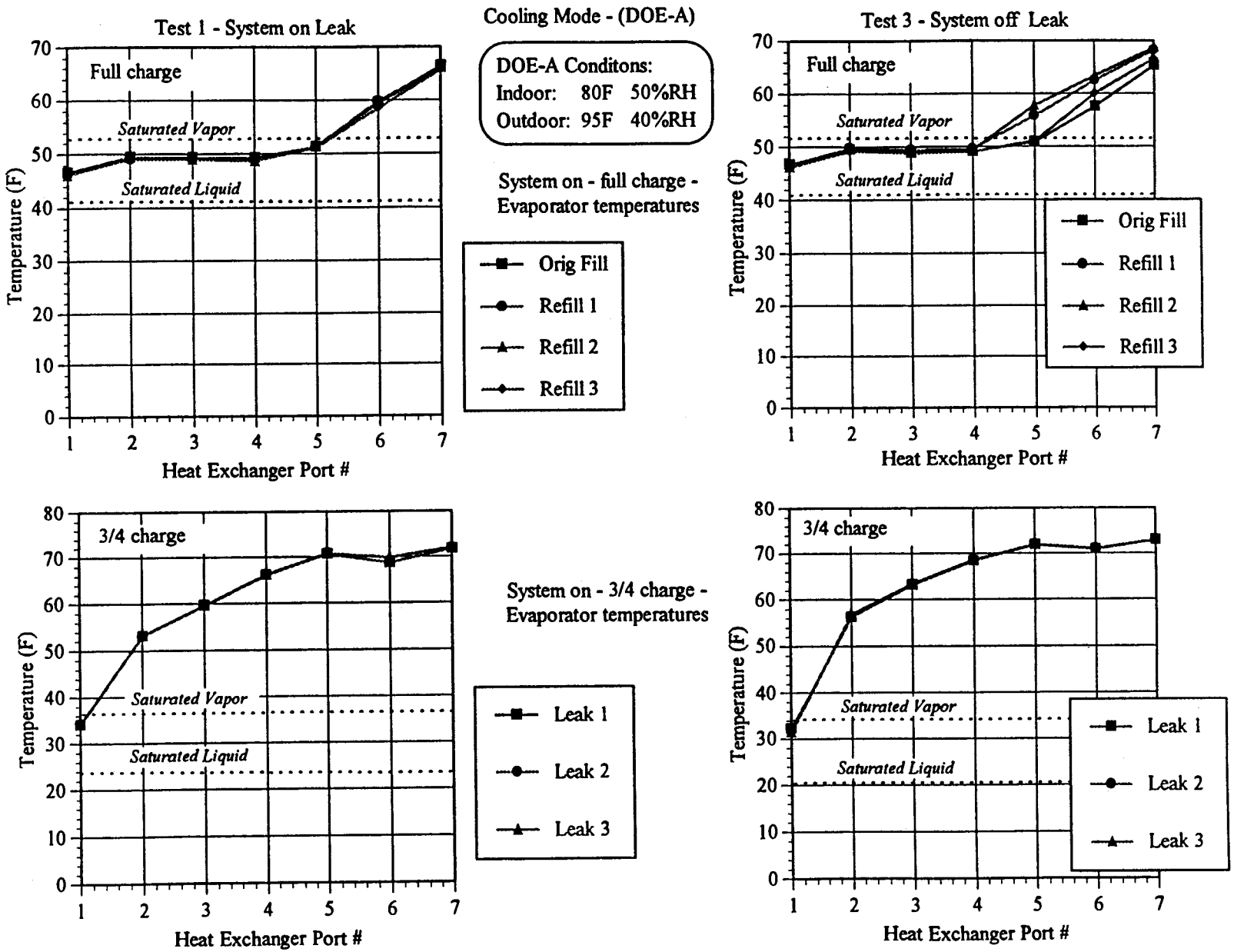

Fig. 4.17 Component Temperatures in R407C Tests 1 and 3

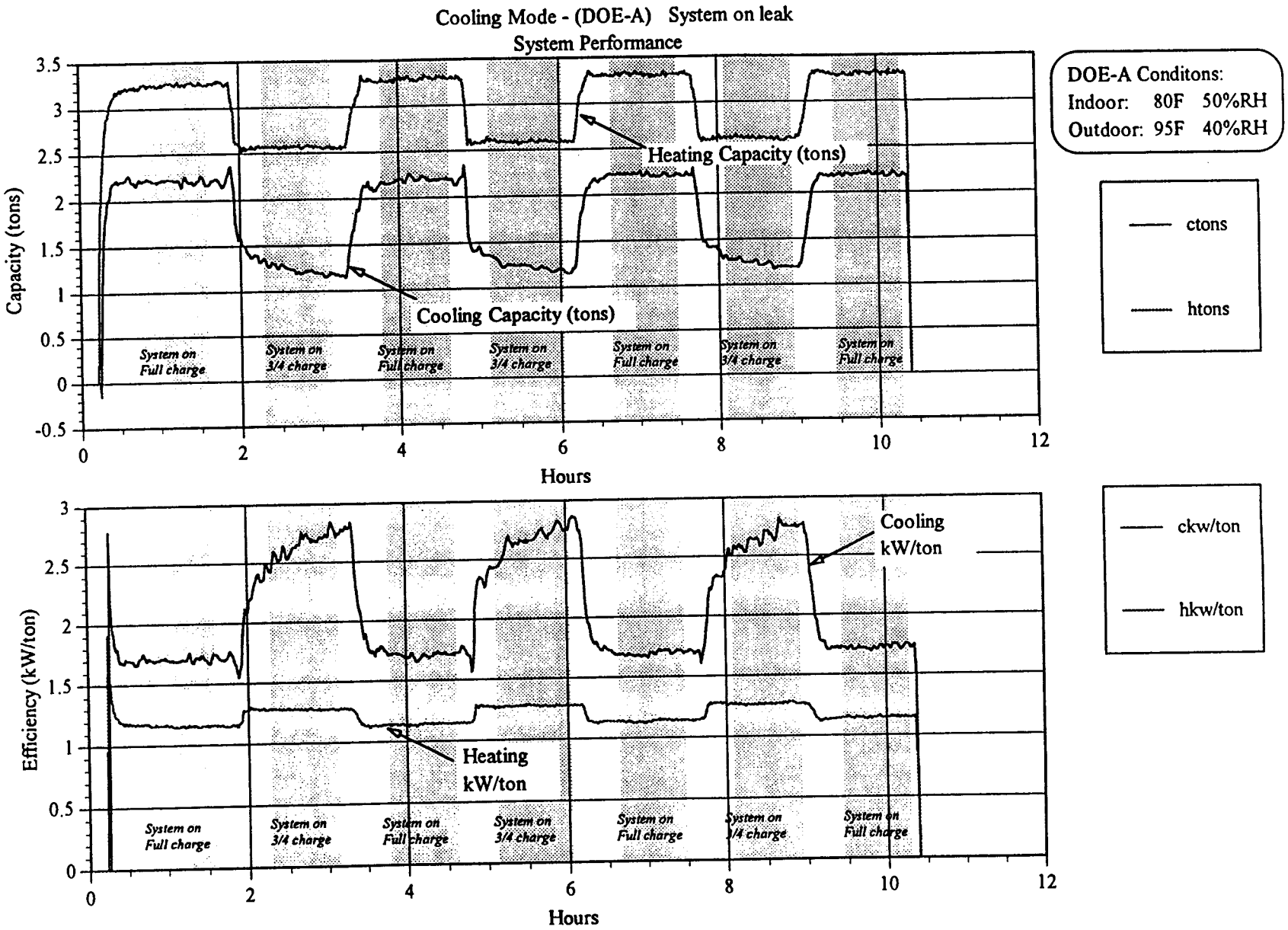

Fig. 4.18 R407C Heat Pump Test #1 Cooling Mode - (DOE-A) System On Leak System Performance

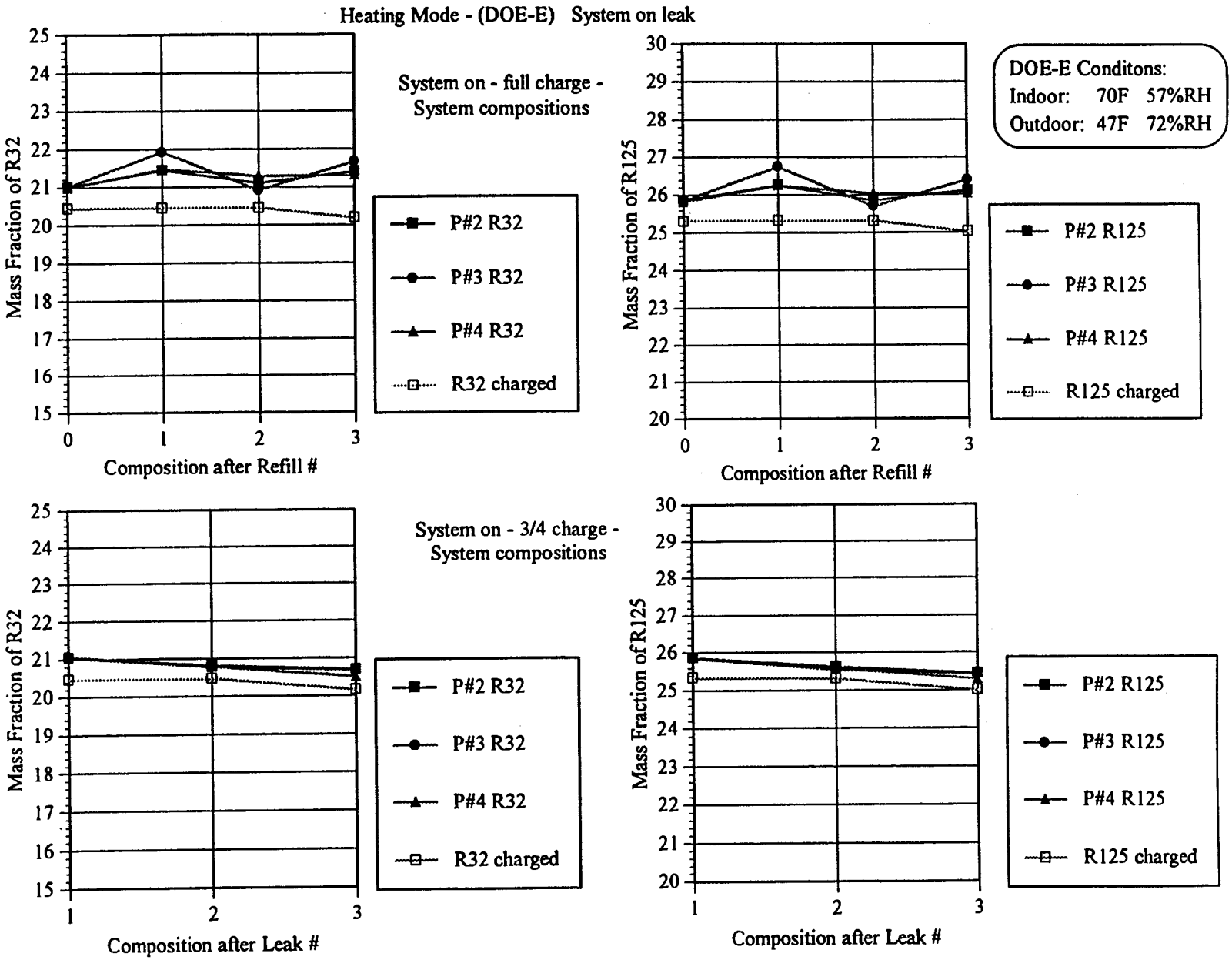

Fig. 4.19 System Fractionation in R407C Test 2

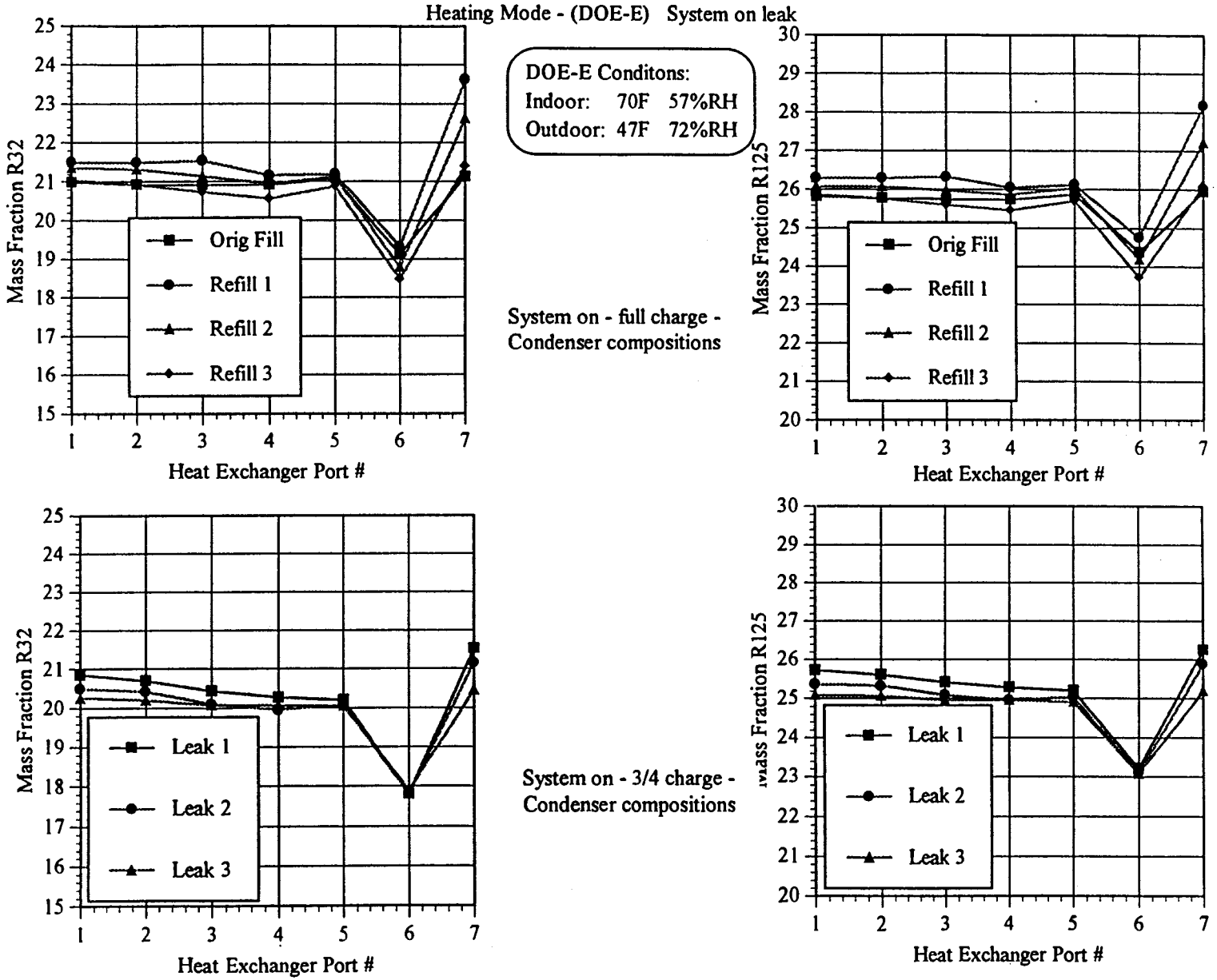

Fig. 4.20 Component Fractionation in R407C Test 2

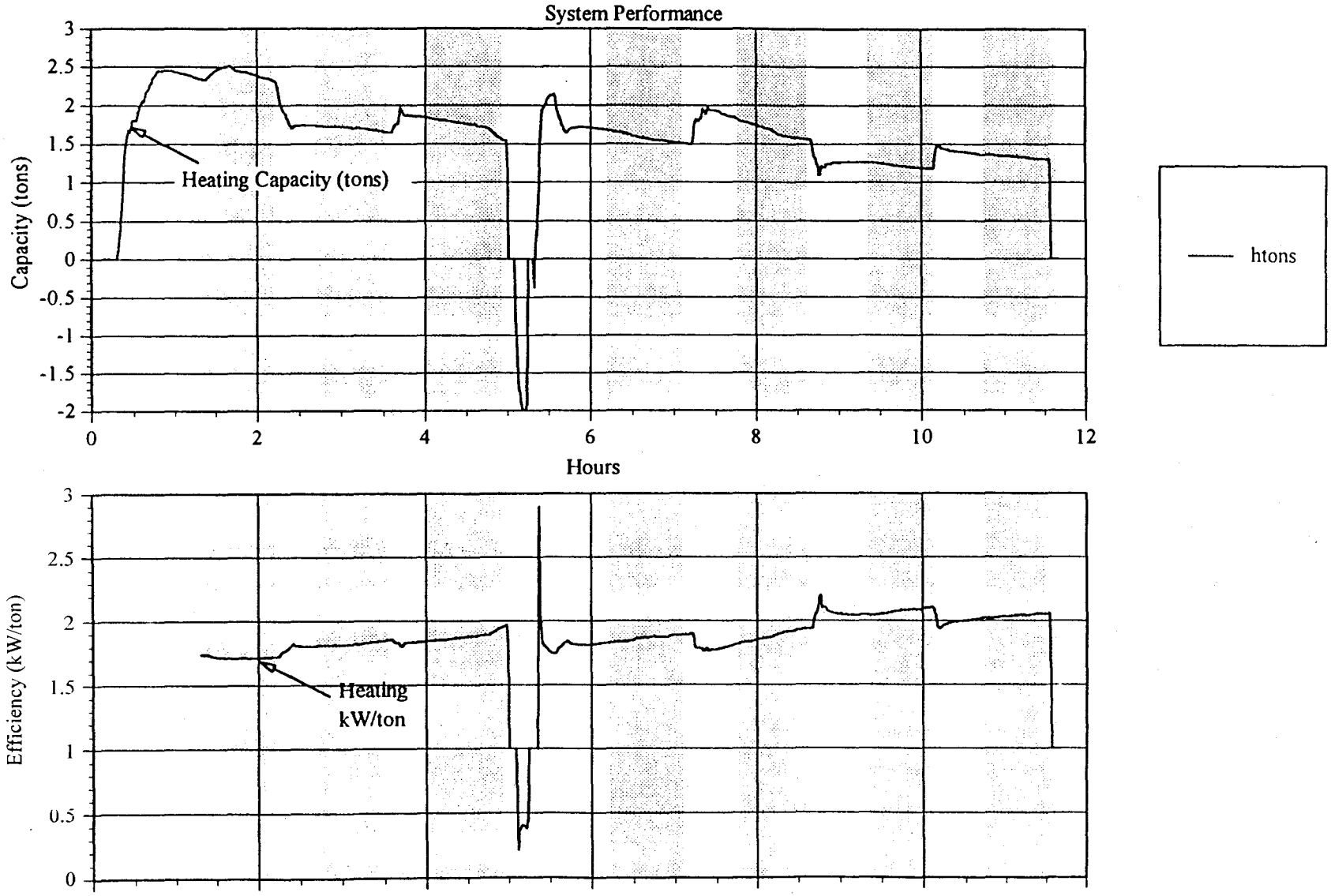

Fig. 4.21 System Performance

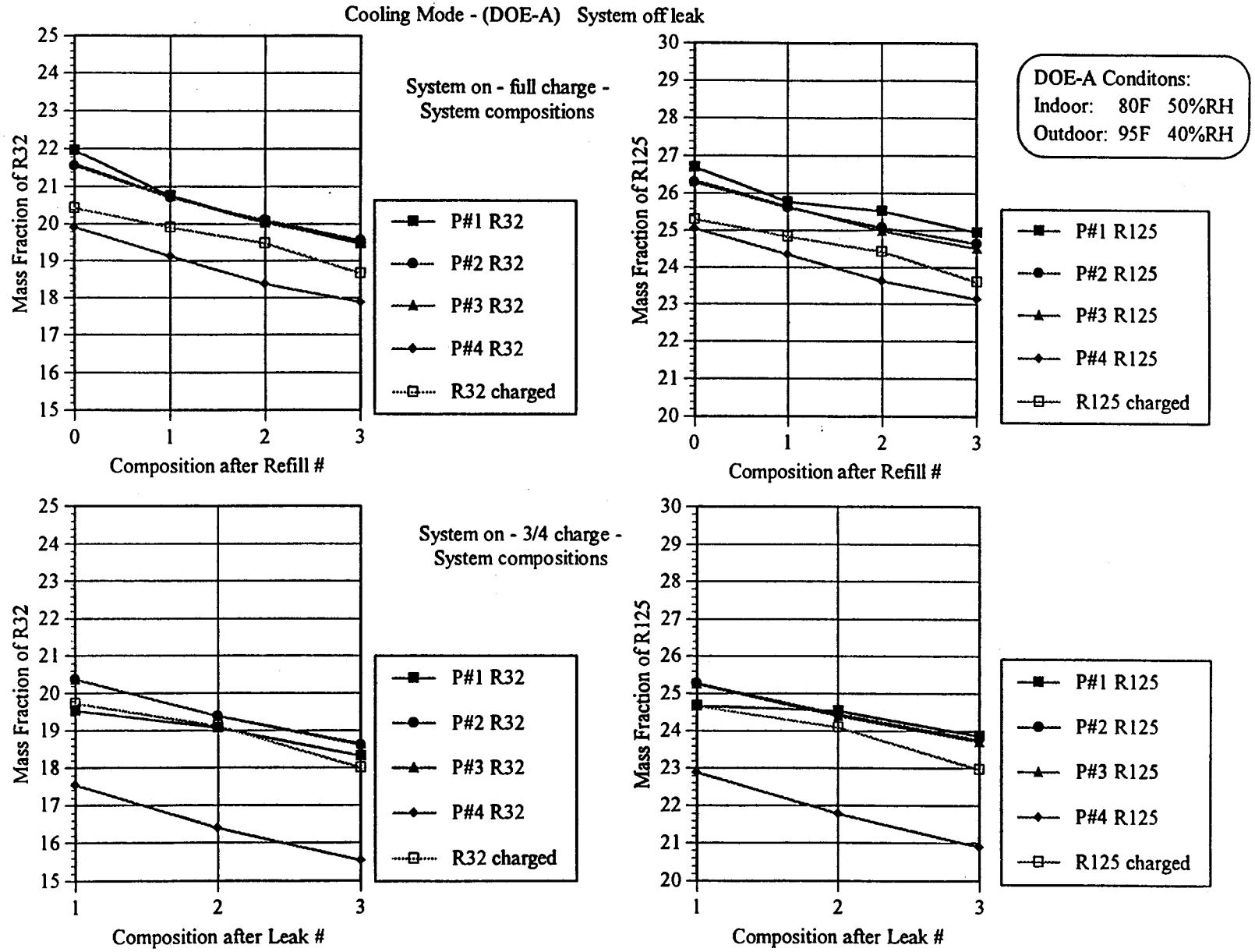

Fig. 4.22 System Fractionation in R407C Test 3

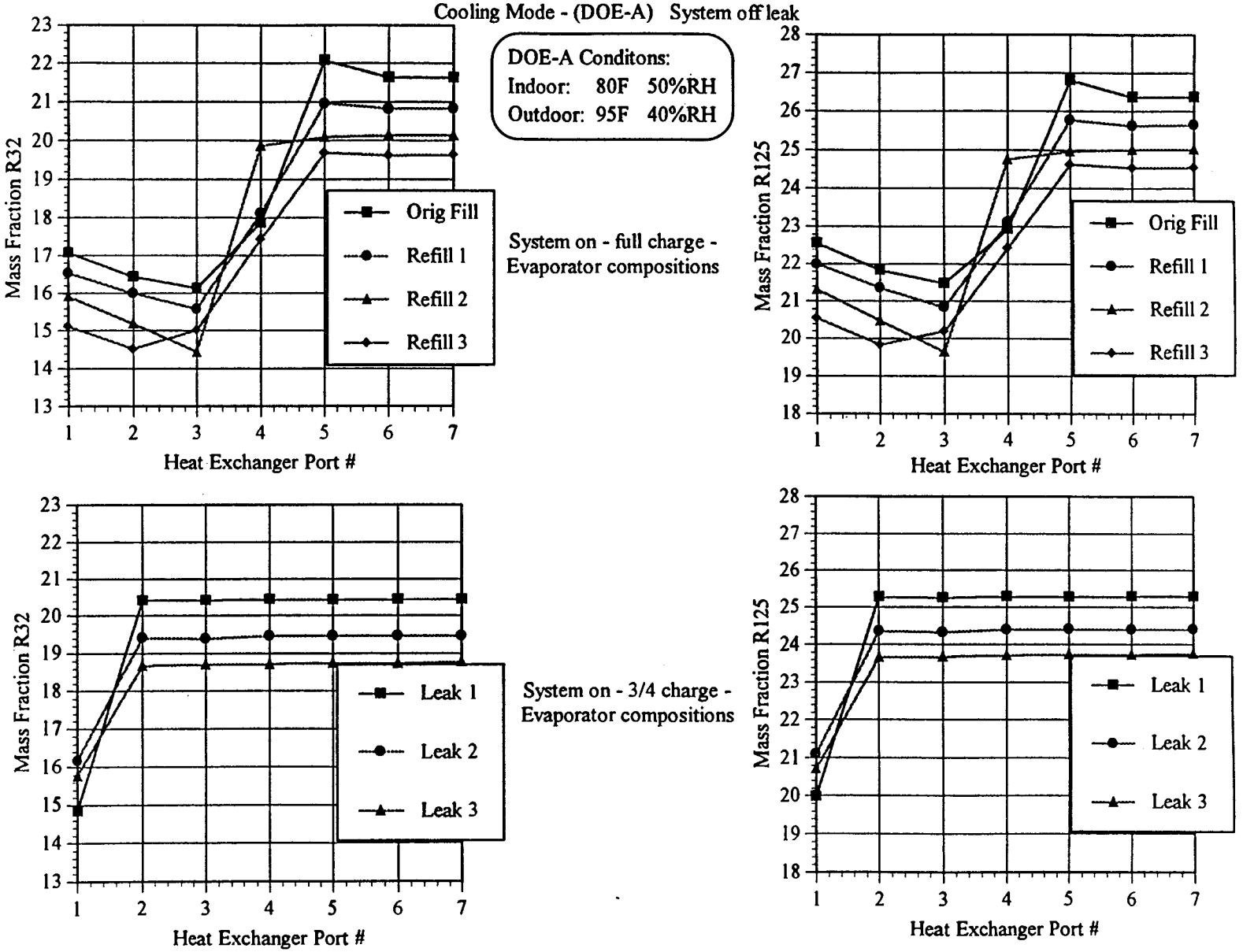

Fig. 4.23 Component Fractionation in R407C Test 3

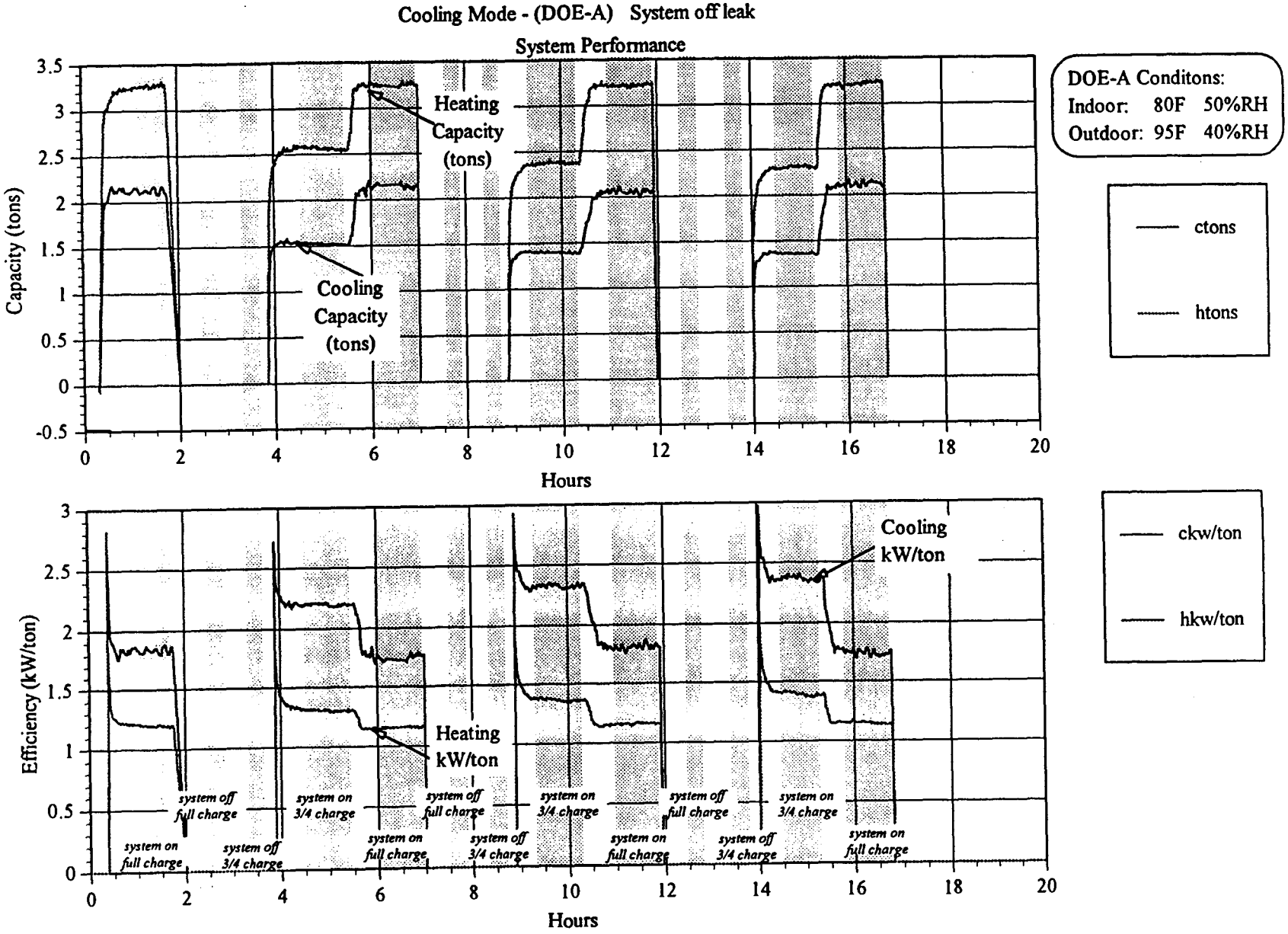

Fig. 4.24 R407C Heat Pump Test #3

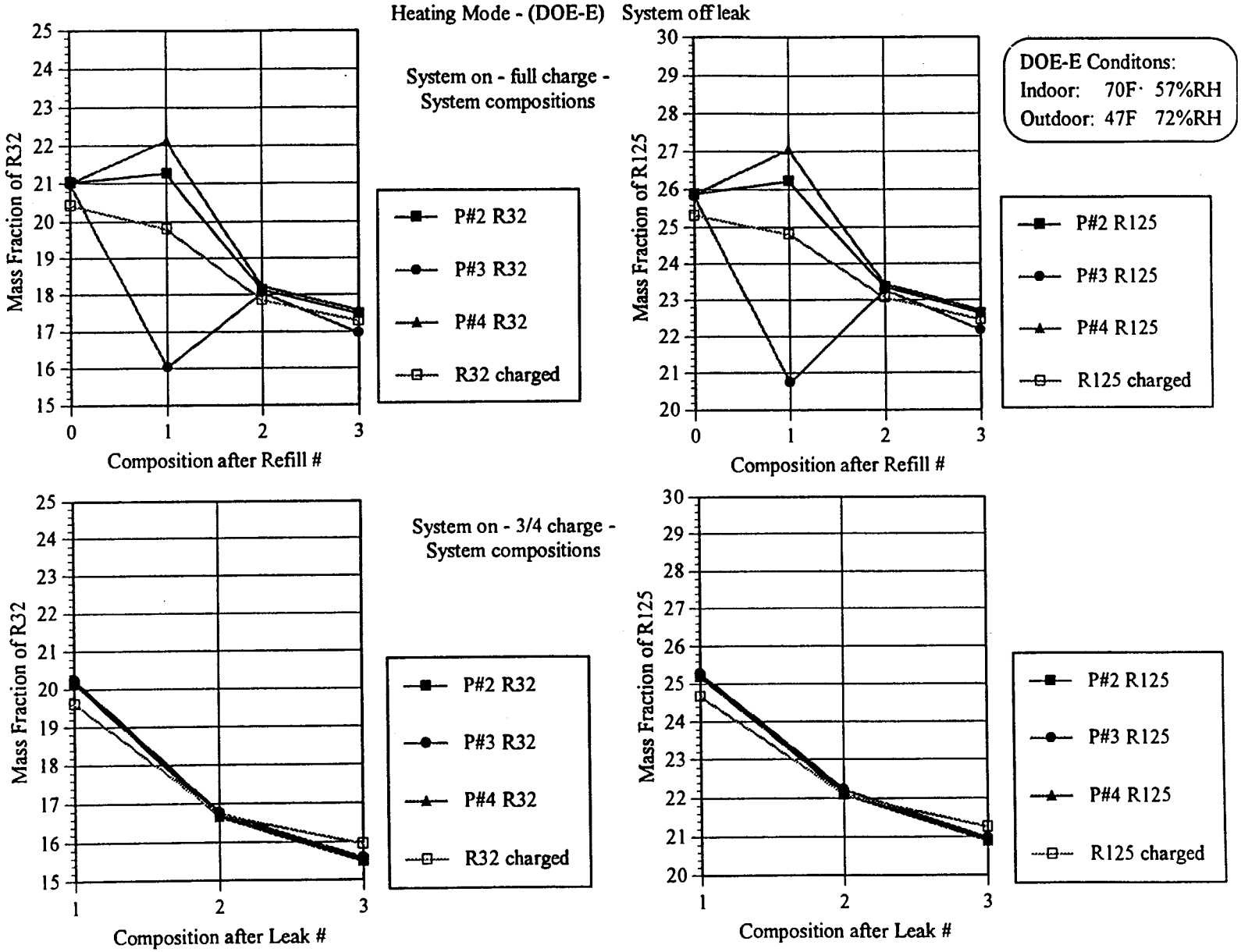

Fig. 4.25 System Fractionation in R407C Test 4

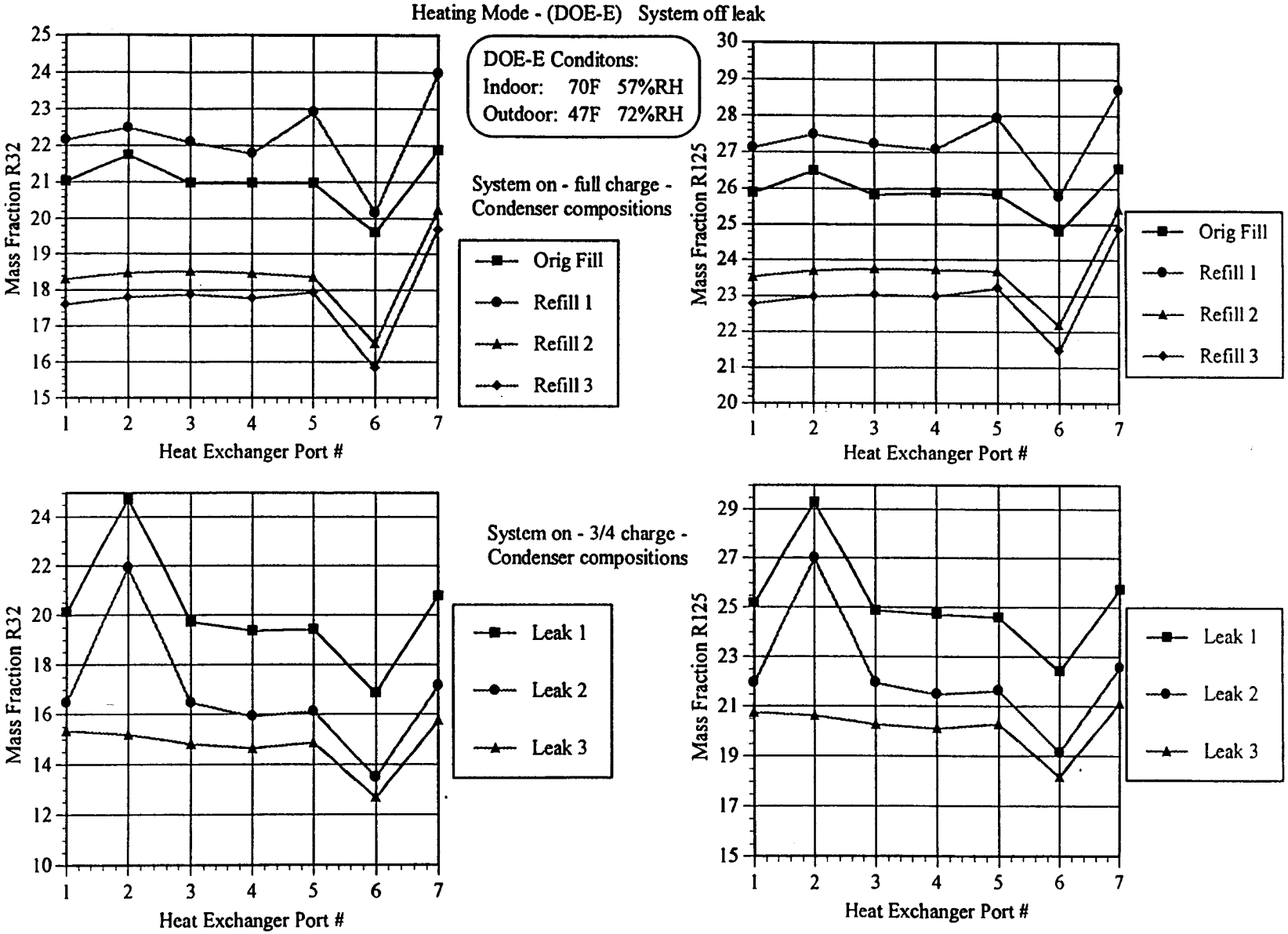

Fig. 4.26 Component Fractionation in R407C Test 4

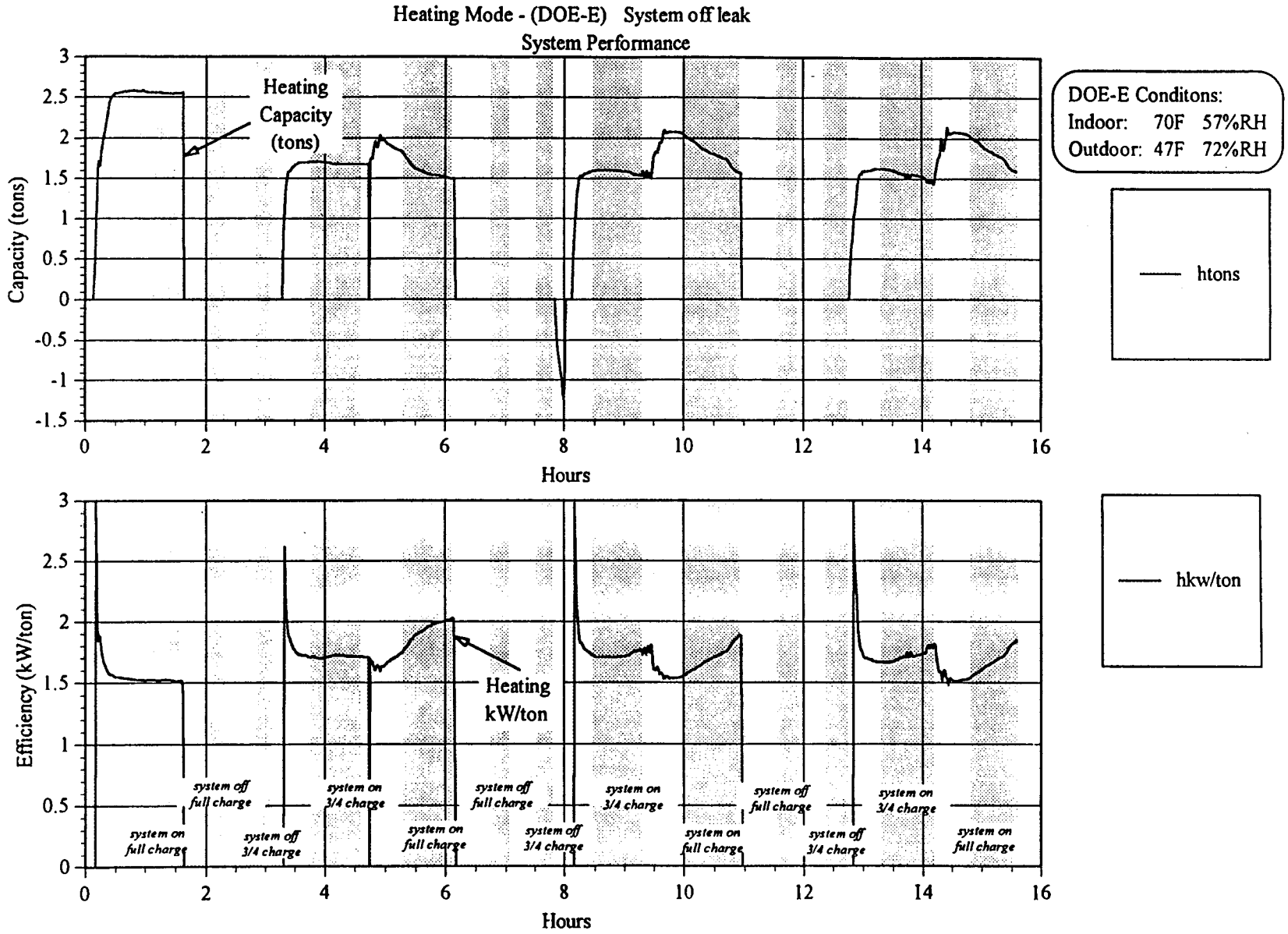

Fig. 4.27 R407C Heat Pump Test #4

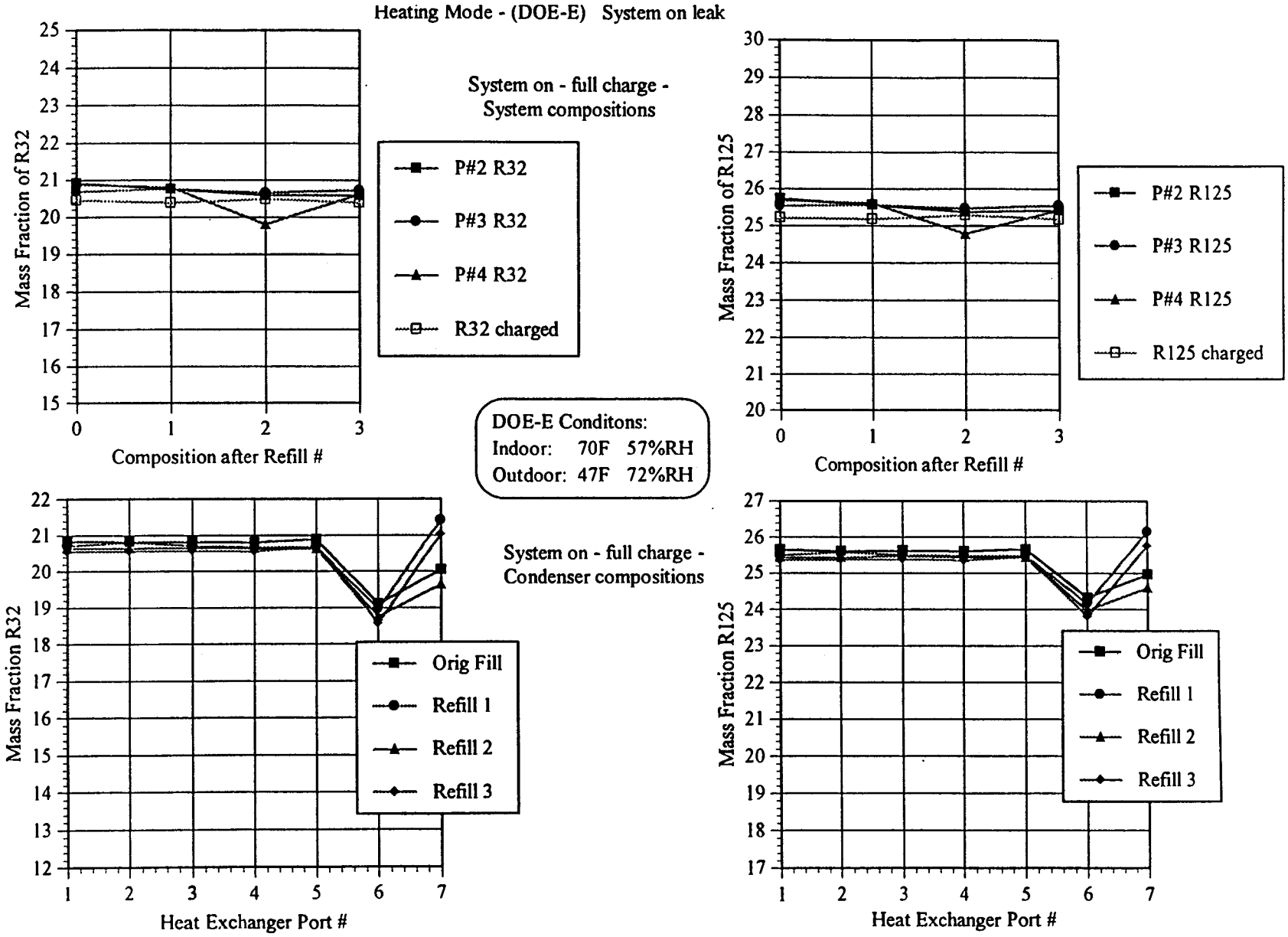

Fig. 4.28 System and Component Fractionation in R407C Test #5

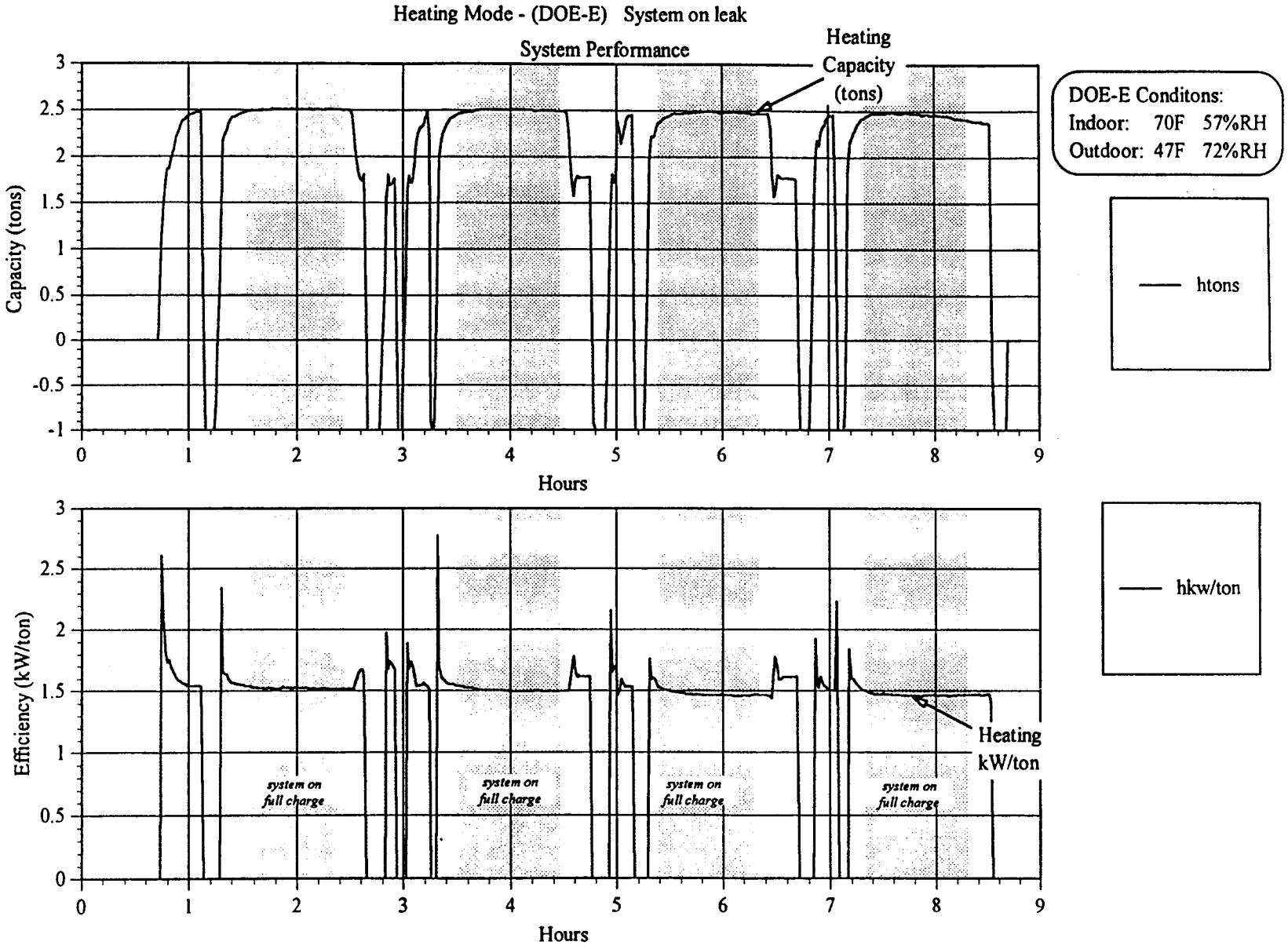

Fig. 4.29 R407C Heat Pump Test #5

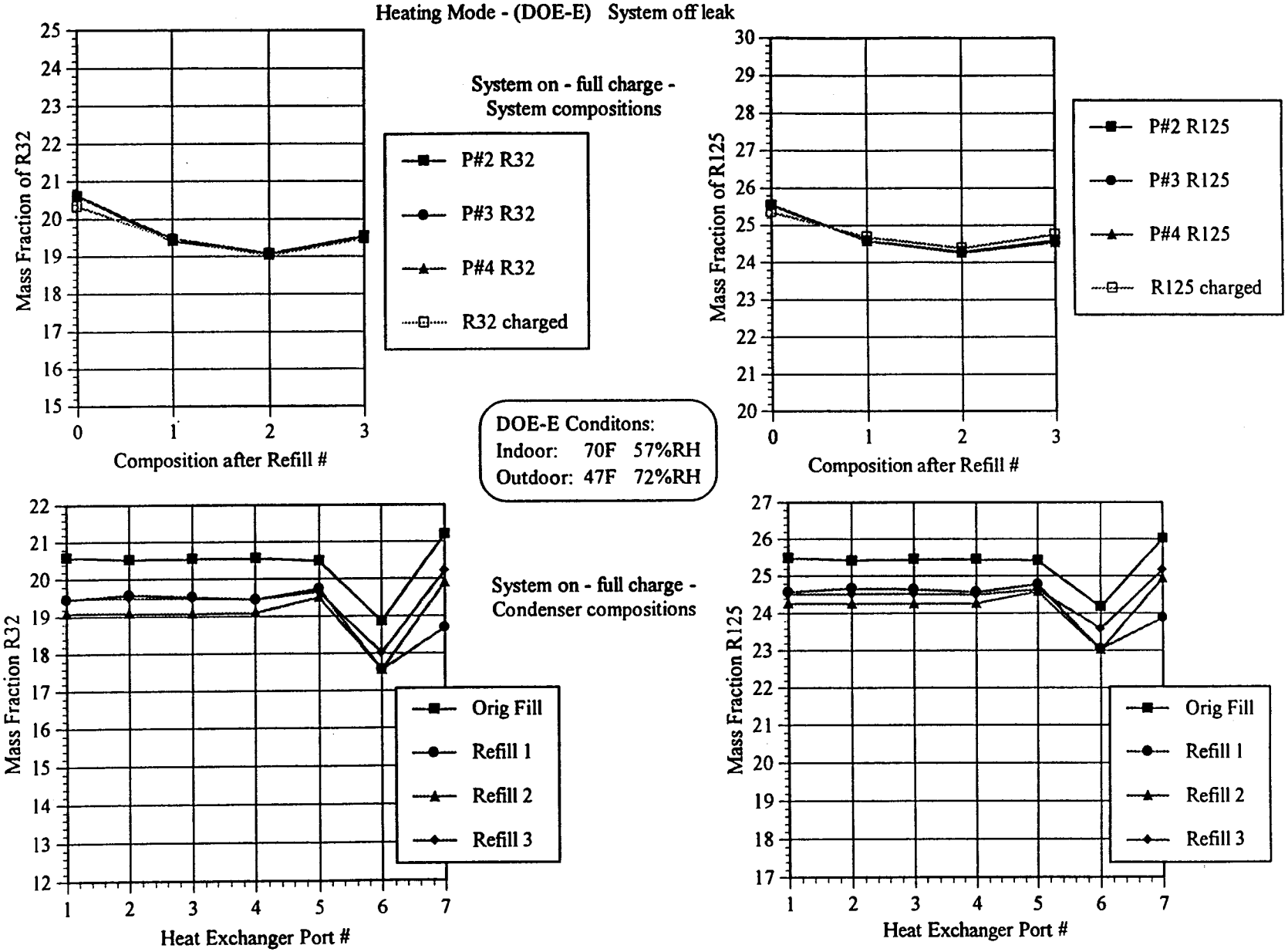

Fig. 4.30 System and Component Fractionation in R407C Test #6

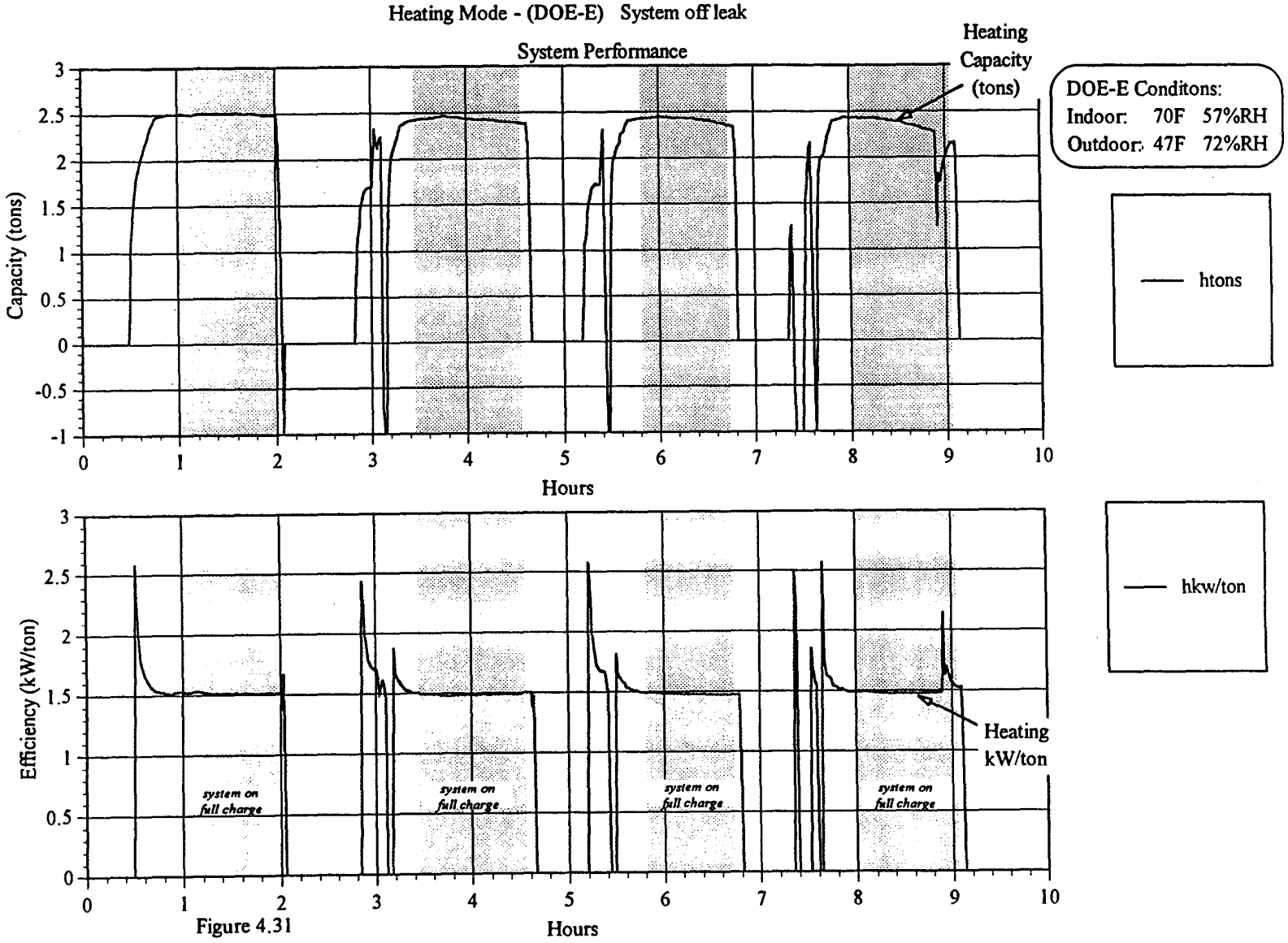

Figure 4.31

Fig. 4.31 R407C Heat Pump Test #6

APPENDIX A - NISC MODEL DETAILED DATA

In this Appendix, additional details used to develop the refrigerant blend/lubricant NISC model are provided along with the forms of the Wohl [3]-suffix equations used to predict the solubility and fractionation results. The derived form of the Wohl [3]-suffix equations for ternary mixtures becomes:

$$\ln \gamma_1 = z_2^2 [A_{12} + 2z_1 (\frac{q_1}{q_2} A_{21} - A_{12})] + z_3^2 [A_{13} + 2z_1 (\frac{q_1}{q_3} A_{31} - A_{13})] \qquad \text{(I)}$$

$$+ z_2 z_3 [\frac{1}{2} (\frac{q_1}{q_2} A_{21} + A_{12} + \frac{q_1}{q_3} A_{31} + A_{13} - \frac{q_1}{q_2} A_{23} - \frac{q_1}{q_3} A_{32})$$

$$+ z_1 (\frac{q_1}{q_2} A_{21} - A_{12} + \frac{q_1}{q_3} A_{31} - A_{13}) + (z_2 - z_3)(\frac{q_1}{q_2} A_{23} - \frac{q_1}{q_3} A_{32}) - (1 - 2z_1) C^*_{123}]$$

The expression for γ_2 and γ_3 can be obtained from Eq. (I) by cyclic permutation of subscripts. All of the required A_{ij} can be evaluated from the binary pair data. C*, which contains only 3-body collision probabilities, is taken as zero.

The derived form of the Wohl [3]-suffix equations for component 1 in a quaternary mixture becomes:

$$\ln \gamma_1 = z_2^2 [A_{12} + 2z_1 (\frac{q_1}{q_2} A_{21} - A_{12})] + z_3^2 [A_{13} + 2z_1 (\frac{q_1}{q_3} A_{31} - A_{13})] + z_4^2 [A_{14} + 2z_1 (\frac{q_1}{q_4} A_{41} - A_{14})]$$

$$+ z_2 z_3 [\frac{1}{2} (\frac{q_1}{q_2} A_{21} + A_{12} + \frac{q_1}{q_3} A_{31} + A_{13} - \frac{q_1}{q_2} A_{23} - \frac{q_1}{q_3} A_{32})$$

$$+ z_1 (\frac{q_1}{q_2} A_{21} - A_{12} + \frac{q_1}{q_3} A_{31} - A_{13}) + (z_2 - z_3)(\frac{q_1}{q_2} A_{23} - \frac{q_1}{q_3} A_{32}) - (1 - 2z_1) C^*_{123}] \qquad \text{(II)}$$

$$+ z_2 z_4 [\frac{1}{2} (\frac{q_1}{q_2} A_{21} + A_{12} + \frac{q_1}{q_4} A_{41} + A_{14} - \frac{q_1}{q_2} A_{24} - \frac{q_1}{q_4} A_{42})$$

$$+ z_1 (\frac{q_1}{q_2} A_{21} - A_{12} + \frac{q_1}{q_4} A_{41} - A_{14}) + (z_2 - z_4)(\frac{q_1}{q_2} A_{24} - \frac{q_1}{q_4} A_{42}) - (1 - 2z_1) C^*_{124}]$$

$$+ z_3 z_4 [\frac{1}{2} (\frac{q_1}{q_3} A_{31} + A_{13} + \frac{q_1}{q_4} A_{41} + A_{14} - \frac{q_1}{q_3} A_{34} - \frac{q_1}{q_4} A_{43})$$

$$+ z_1 (\frac{q_1}{q_3} A_{31} - A_{13} + \frac{q_1}{q_4} A_{41} - A_{14}) + (z_3 - z_4)(\frac{q_1}{q_3} A_{34} - \frac{q_1}{q_4} A_{43}) - (1 - 2z_1) C^*_{134}]$$

$$+ 2 z_2 z_3 z_4 C^*_{234}$$

For a quaternary mixture (3 refrigerants plus 1 lubricant), 18 binary parameters plus 4 ternary parameters are required. All of the required A_{ij} can be evaluated from the binary pair

data alone. The C*'s, which contain only non-identical 3-body collision terms, are initially taken as zero. These can be adjusted for a better overall description by analysis of ternary VLE data.

Appendix B.1 - Blend A

Test Data, Figures and Tables

APPENDIX B.1
BLEND A - TEST RESULTS AND DATA DETAILS

In this Appendix, the actual data from the Blend A tests are presented for those interested in additional details. Also included for easier reference are the Test Plan for Blend A (Table 4.1) and Summary of Blend A Test levels (Table 4.3) already presented and discussed in the Task 4 material.

The test data is shown in table form for #2 through 6 test sequences. Each test is broken into further intervals identified as ARTI 20, 21, 22, 23, 24, and 25, for example. Along with each test sequence is an identification of system status, refrigerant charge, temp, etc. The traces for the pressure and temperature data are provided in accompanying figures for each test. The shaded areas on the figures show the time increment corresponding to each ARTI test designated. Hence in Fig. B.1.1a, ARTI 21 test data is centered around 31.50 min, while ARTI 22 test data is centered around 108.75 min, etc.

Test	Description
1	Cooling Mode (DOE-A) test with system-off leaks
2	Cooling Mode (DOE-A) test with system-on leaks
3	Heating Mode (DOE-E) test with system-off leaks
4	Heating Mode (DOE-E) test with system-on leaks
5	Heating Mode (low temp) test with system-off leaks
6	Heating Mode (low temp) test with system-on leaks

Table 4.1 Test Plan for Blend A

	Charging Compos. (% R32)	Circulating Compos. (% R32)	Charge Compos. after Discharge #1 (% R32)	Circulating Compos. after Discharge #1 (% R32)	Charge Compos. after Discharge #2 (% R32)	Circulating Compos. after Discharge #2 (% R32)	Charge Fractionation?
Run #1	21.1	24.4	19.2	19.8	16.8	16.7	YNN
Run #2	20.5	23.8	20.1	20.7	20.1	20.6	YNN
Run #3	25.6	25.5	25.4	25.4	22.1	21.2	NNN
Run #4	24.2	24.0	24.1	23.9	24.2	23.8	NNN
Run #5	23.5	24.7	21.0	21.6	18.1	18.4	YNN
Run #6	23.4	24.1	22.9	23.2	22.6	23.1	NNN

Table 4.3 Summary of Blend A Tests

ARTI Lab Arrangement

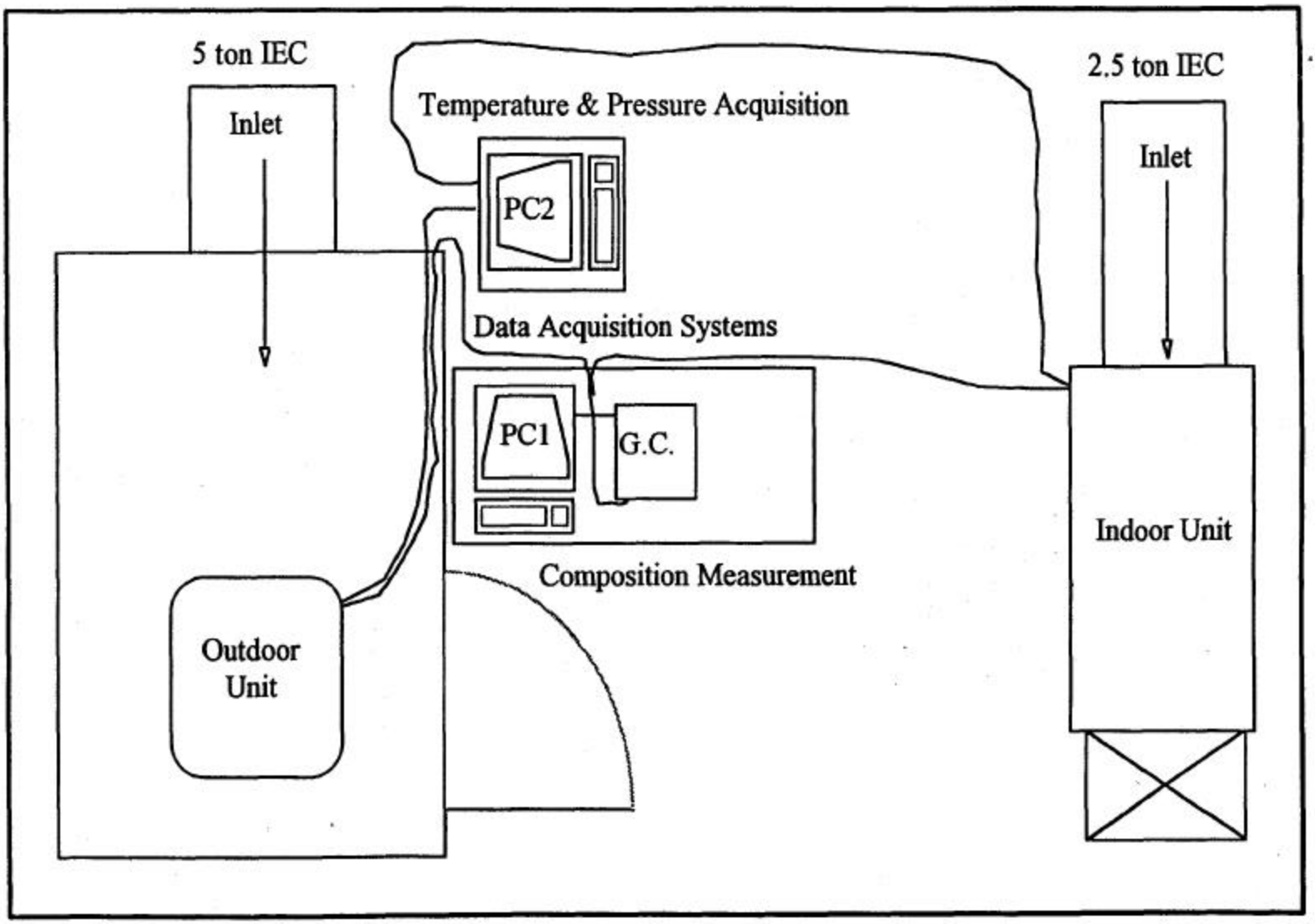

Table B.1-1. Blend A - Test Data - #2 Test Sequence

Summary of ARTI Test Run #2: Cooling Mode operation at DOE-A with 2-Phase Leak

THS 2/2/95

charge weight (lbs)= 7

- nonstandard averaging
- data suspect (two phases detected)

	Standard	Port #1	Port #2	Port #3	Port #4	Standard	Notes:
ARTI 20	34.96	18.12	18.62	18.46	27.14	35.02	System at 70 F; IECs off
ARTI 21	35.02	32.42	20.47	5.48	32.29	34.92	System off; IECs on
ARTI 22	34.92	34.80	23.79	7.85	19.89	34.54	System on; IECs on
ARTI 23	34.54	32.62	20.83	20.62	18.63	34.50	1.7 lbs removed; System on; IECs on
ARTI 24	34.50	31.72	20.80	20.49	14.48	34.34	1.7 lbs removed; System on; IECs on
ARTI 25	35.24	27.93	29.49	29.15	24.53	35.21	System at 70 F; IECs off

charge composition	
startup	20.5
after d#1	20.1
after d#2	20.1

Sample Port #1 : Liquid from Condenser Exit
Sample Port #2 : Compressor Discharge
Sample Port #3 : Accumulator
Sample Port #4 : Liquid or 2 phase from Evaporator Inlet

Discharge	wt (lbs)	Liquid %	Vapor %	Total %
#1	1.70	10.57	23.86	22.02
#2	1.70	9.29	21.79	19.98

Averaged Values from Data Acquisition System:

	Tstart	Tfinish	T1	T2	T3	T4	T5	T6	T7	T8
ARTI 20	0.00	0.00	0.00	0.00	0.00	0.00	0.00	0.00	0.00	0.00
ARTI 21	17.75	45.25	87.99	73.59	76.70	81.78	84.53	83.97	82.55	82.36
ARTI 22	94.25	123.25	170.76	50.93	67.49	112.57	160.01	43.05	44.82	112.15
ARTI 23	149.25	178.75	183.67	52.68	67.25	112.91	172.44	52.88	51.36	119.01
ARTI 24	212.25	240.75	231.86	72.97	48.86	105.69	210.65	78.71	78.76	137.13
ARTI 25	0.00	0.00	0.00	0.00	0.00	0.00	0.00	0.00	0.00	0.00

	P1	P2	P3	P4	P5	P6	Time(min)
ARTI 20	0.00	0.00	0.00	0.00	0.00	0.00	0.00
ARTI 21	138.59	134.24	134.93	129.90	133.51	133.47	31.50
ARTI 22	275.13	71.81	119.55	253.62	264.52	63.46	108.75
ARTI 23	263.52	67.53	113.40	241.98	252.83	60.69	164.00
ARTI 24	229.30	41.01	75.40	210.52	219.47	37.79	226.50
ARTI 25	0.00	0.00	0.00	0.00	0.00	0.00	0.00

T in deg F
P in psig

Fig. B.1.1a Blend A Heat Pump Test #2 Sequence

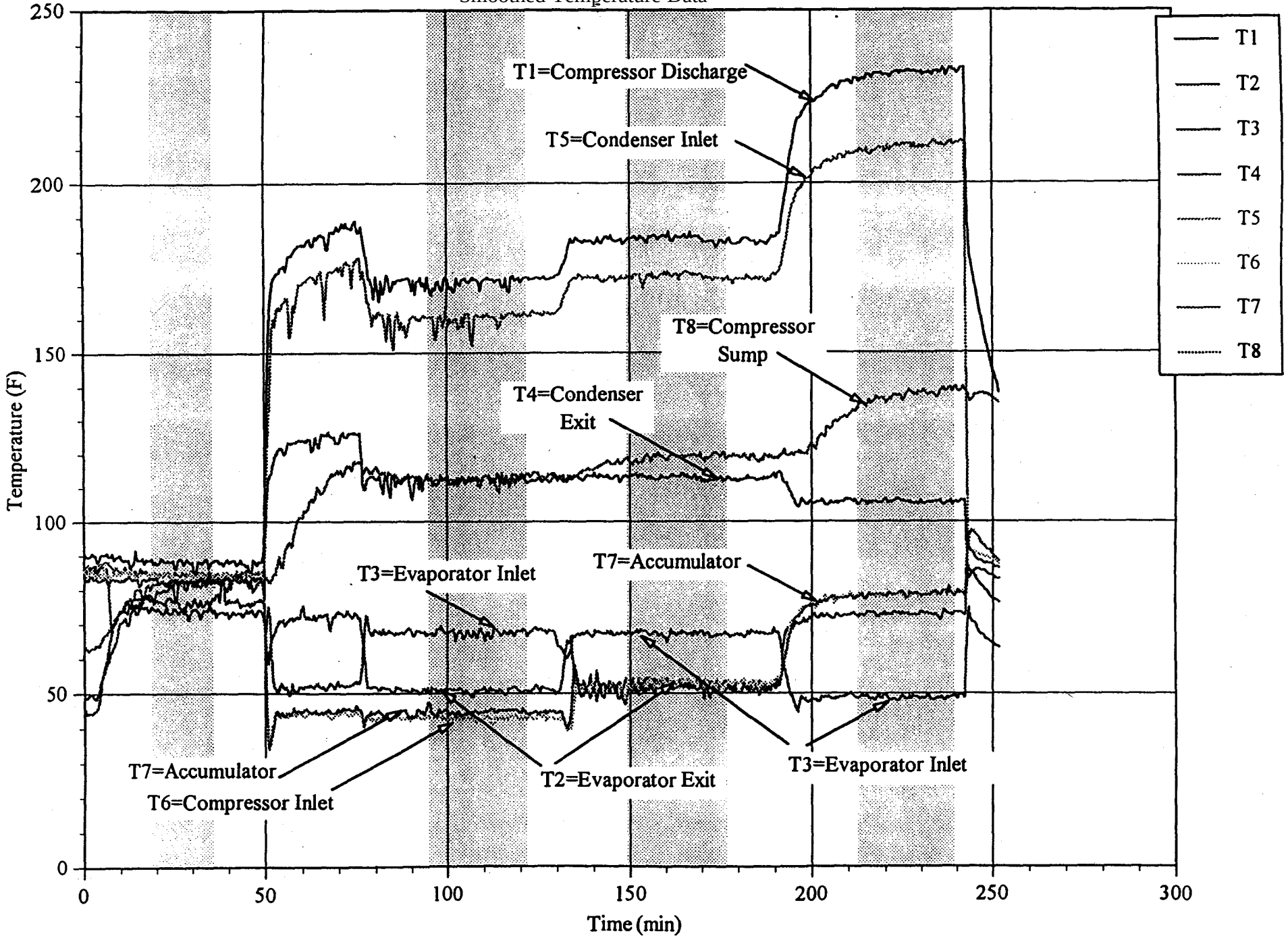

Fig. B.1.1b Blend A Heat Pump Test #2 Sequence

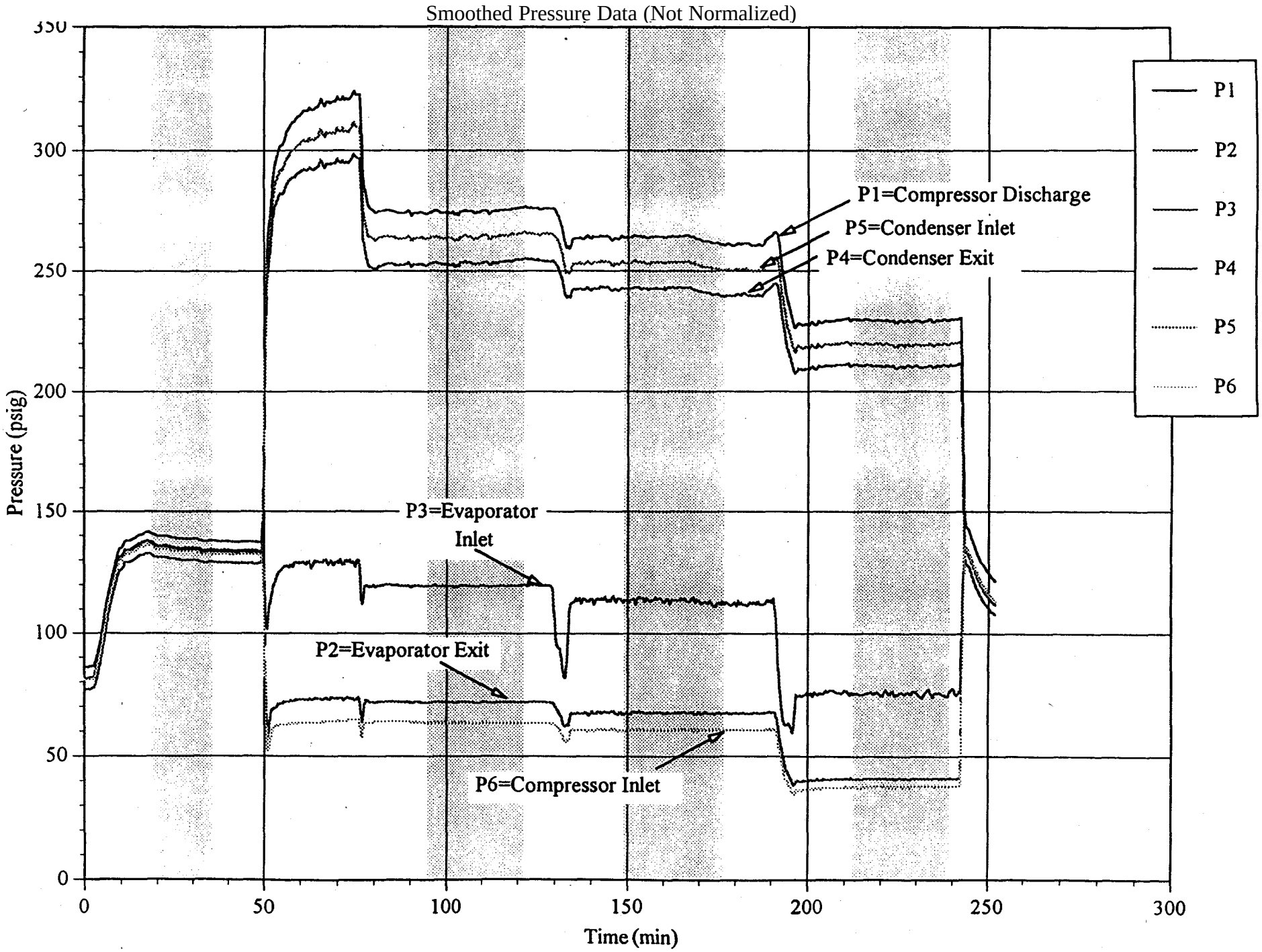

Table B.1-2. Blend A - Test Data - #3 Test Sequence

Summary of ARTI Test Run #3: Heating Mode operation at DOE-E with Slow leak

THS 2/7/95 charge weight (lbs) 7

- nonstandard averaging
- data suspect (two phases detected)

	Standard	Port #1	Port #2	Port #3	Port #4	Standard	Notes:
ARTI 30	35.20	44.30	25.28	23.32	38.68	35.21	System off; IECs on
ARTI 31	35.21	22.77	25.49	25.49	25.46	35.18	System on; IECs on
ARTI 32	35.18	22.54	23.71	40.45	30.17	35.18	1.6 lbs removed; System off; IECs on
ARTI 33	35.18	40.34	25.37	25.38	25.31	35.17	System on; IECs on
ARTI 34	35.17	29.58	35.98	36.70	27.98	35.17	1.8 lbs removed; System off; IECs on
ARTI 35	35.17	31.05	21.26	21.01	20.34	35.16	System on; IECs on
ARTI 36	35.13	25.05	28.53	28.44	24.81	35.20	System at 70 F; IECs off

charge composition	
startup	25.6
after d#1	25.4
after d#2	22.1

Sample Port #1 : Liquid or 2 phase from Evaporator Inlet
Sample Port #2 : Compressor Discharge
Sample Port #3 : Accumulator
Sample Port #4 : Liquid from Condenser Exit

Discharge	wt (lbs)	Liquid %	Vapor %	Total %
#1	1.60	13.88	27.07	26.12
#2	1.80	18.83	34.39	31.98

Averaged Values from Data Acquasition System:

	Tstart	Tfinish	T1	T2	T3	T4	T5	T6	T7	T8
ARTI 30	64.25	86.75	48.17	66.36	67.41	45.85	44.92	43.92	44.54	43.09
ARTI 31	132.25	153.75	202.18	177.10	94.56	35.18	37.22	38.92	38.85	77.88
ARTI 32	208.25	228.75	49.07	66.41	67.56	45.79	44.54	44.74	43.26	49.35
ARTI 33	276.25	297.75	201.47	167.99	89.14	32.40	41.80	44.36	44.09	80.66
ARTI 34	358.25	380.75	47.47	67.14	67.78	44.15	42.53	42.26	38.88	46.76
ARTI 35	418.25	439.75	236.62	172.23	79.24	32.40	42.16	45.92	45.39	96.87
ARTI 36	0.00	0.00	0.00	0.00	0.00	0.00	0.00	0.00	0.00	0.00

	P1	P2	P3	P4	P5	P6	Time(min)
ARTI 30	82.43	82.38	82.37	82.34	82.37	82.42	75.50
ARTI 31	252.99	246.52	248.93	62.64	41.87	39.04	143.00
ARTI 32	78.07	78.82	78.88	78.23	77.80	77.84	218.50
ARTI 33	189.89	183.99	186.82	45.02	28.92	26.59	287.00
ARTI 34	65.14	65.48	65.50	65.07	64.87	65.11	369.50
ARTI 35	145.22	139.28	142.37	20.18	9.39	7.73	429.00
ARTI 36	0.00	0.00	0.00	0.00	0.00	0.00	0.00

T in deg F
P in psig

Fig. B.1.2a Blend A Heat Pump Test #3 Sequence

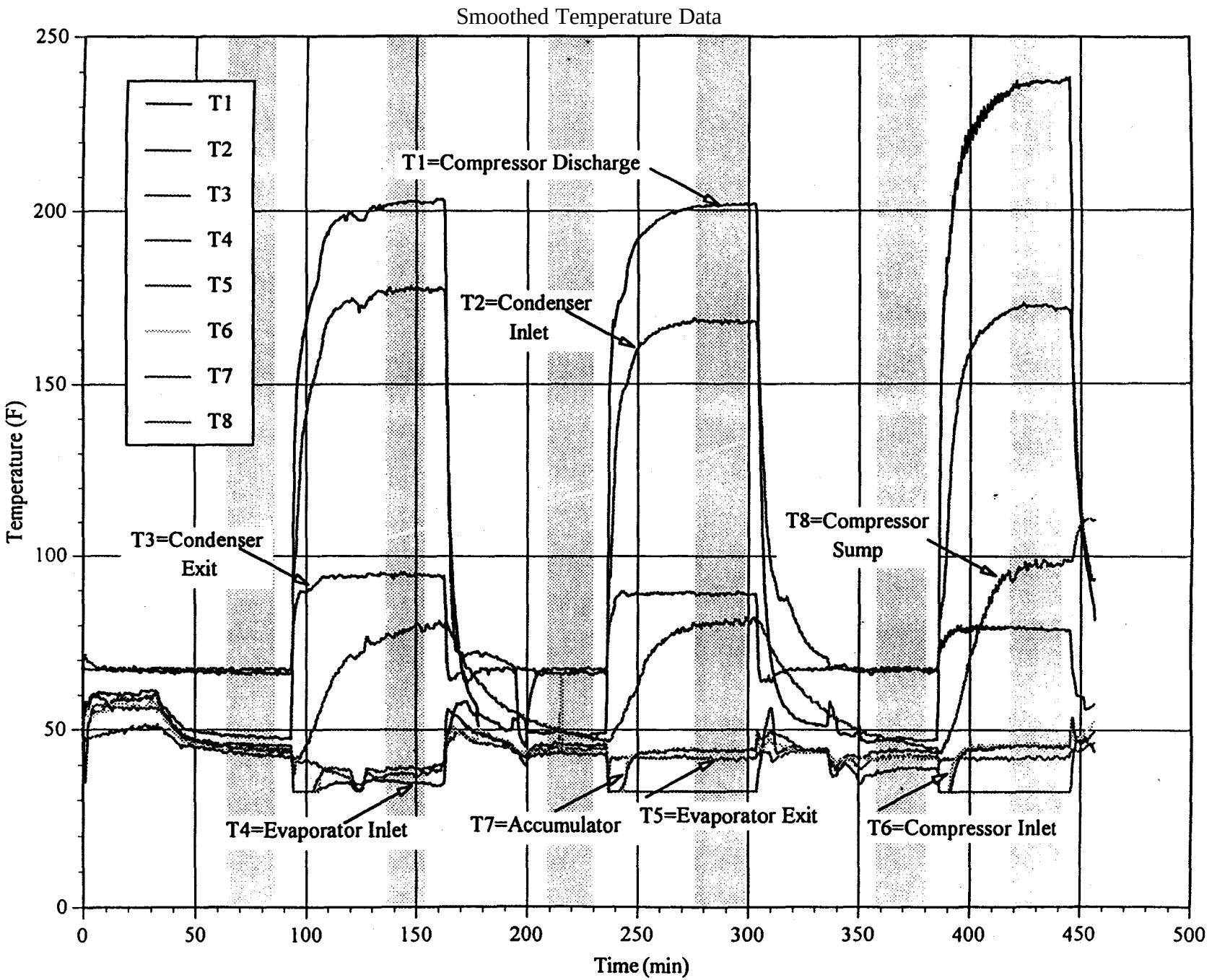

Fig. B.1.2b Blend A Heat Pump Test #3 Sequence

Smoothed & Normalized Pressure Data

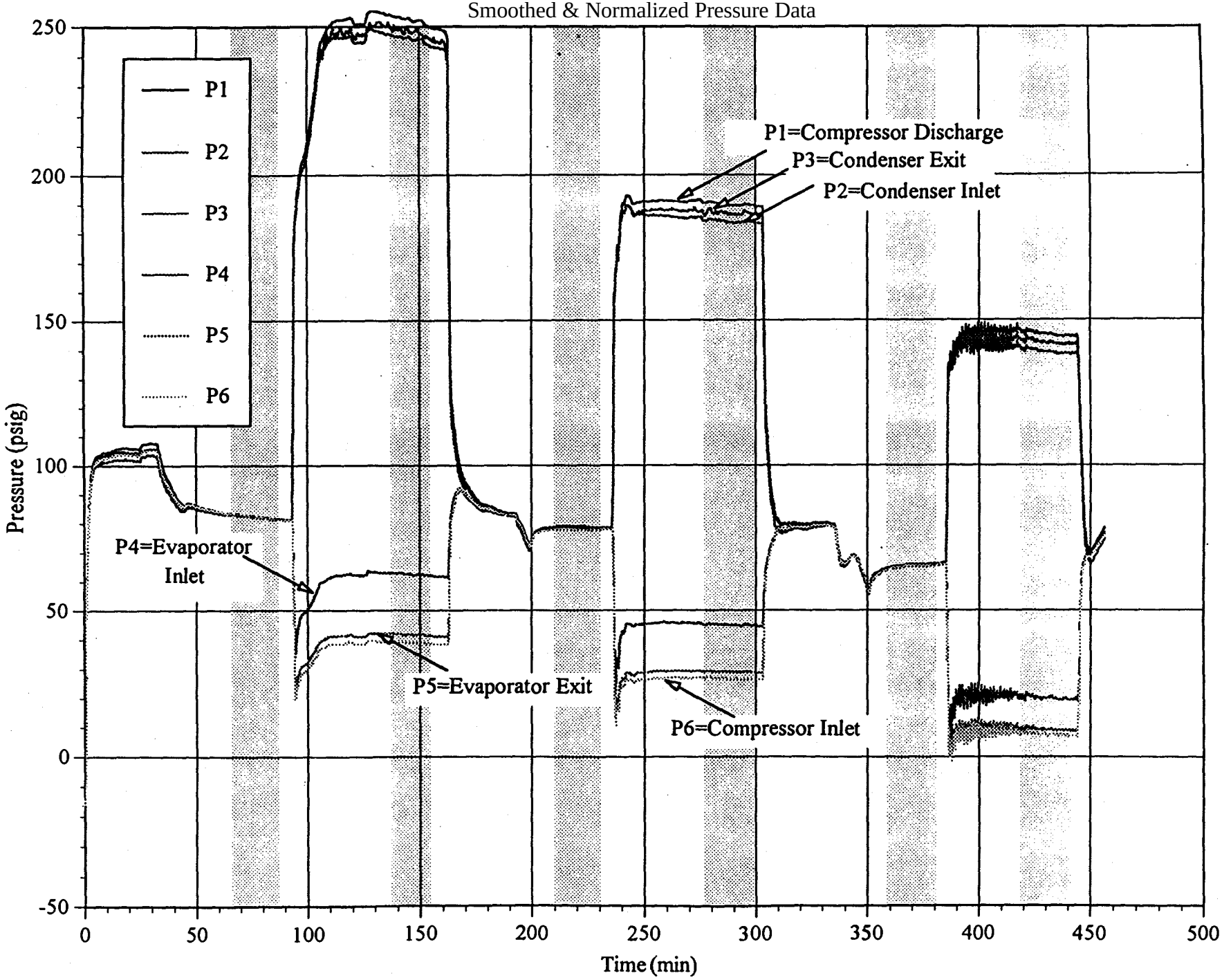

Table B.1-3. Blend A - Test Data - #4 Test Sequence

Summary of ARTI Test Run #4: Heating Mode operation at DOE-E with 2-Phase Leak

THS 2/14/95 charge weight (lbs) 7

- nonstandard averaging
- data suspect (two phases detected)

	Standard	Port #1	Port #2	Port #3	Port #4	Standard	Notes:
ARTI 40	35.23	18.88	36.99	18.40	32.33	35.20	System at 70 F; IECs off
ARTI 41	35.20	20.11	40.10	18.76	29.90	35.19	System off; IECs on
ARTI 42	35.19	23.52	24.06	24.05	23.96	35.17	System on; IECs on
ARTI 43	35.17	38.29	23.88	23.91	23.87	35.17	1.8 lbs removed; System on; IECs on
ARTI 44	35.17	36.62	24.06	24.02	23.21	35.18	1.7 lbs removed; System on; IECs on
ARTI 45	35.18	14.61	30.14	29.78	25.46	35.17	System at 70 F; IECs off

charge composition	
startup	24.2
after d#1	24.1
after d#2	24.2

Sample Port #1 : Liquid or 2 phase from Evaporator Inlet
Sample Port #2 : Compressor Discharge
Sample Port #3 : Accumulator
Sample Port #4 : Liquid from Condenser Exit

Discharge	wt (lbs)	Liquid %	Vapor %	Total %
#1	1.80	13.15	26.87	24.42
#2	1.70	12.59	25.61	23.88

Averaged Values from Data Acquasition System:

	Tstart	Tfinish	T1	T2	T3	T4	T5	T6	T7	T8
ARTI 40	5.75	31.25	58.74	62.30	61.18	56.78	56.34	54.63	53.74	51.96
ARTI 41	119.75	143.25	46.59	63.94	66.79	44.56	43.72	42.75	42.76	41.33
ARTI 42	189.75	209.25	201.39	175.37	95.92	34.83	38.10	39.83	40.04	70.54
ARTI 43	281.75	302.25	204.28	170.29	90.15	32.40	41.63	43.74	43.65	81.11
ARTI 44	327.75	351.25	244.80	172.05	78.50	32.40	43.40	47.25	46.80	99.13
ARTI 45	0.00	0.00	0.00	0.00	0.00	0.00	0.00	0.00	0.00	0.00

	P1	P2	P3	P4	P5	P6	Time(min)
ARTI 40	95.75	94.92	94.90	93.57	94.72	94.44	18.50
ARTI 41	77.11	77.65	77.65	78.52	77.91	77.81	131.50
ARTI 42	249.28	241.82	243.90	61.62	40.30	37.37	199.50
ARTI 43	189.65	182.50	185.47	44.35	27.78	25.48	292.00
ARTI 44	150.23	144.12	147.58	19.91	9.06	7.43	339.50
ARTI 45	0.00	0.00	0.00	0.00	0.00	0.00	0.00

T in deg F
P in psig

Fig. B.1.3a Blend A Heat Pump Test #4 Sequence
Smoothed Temperature Data

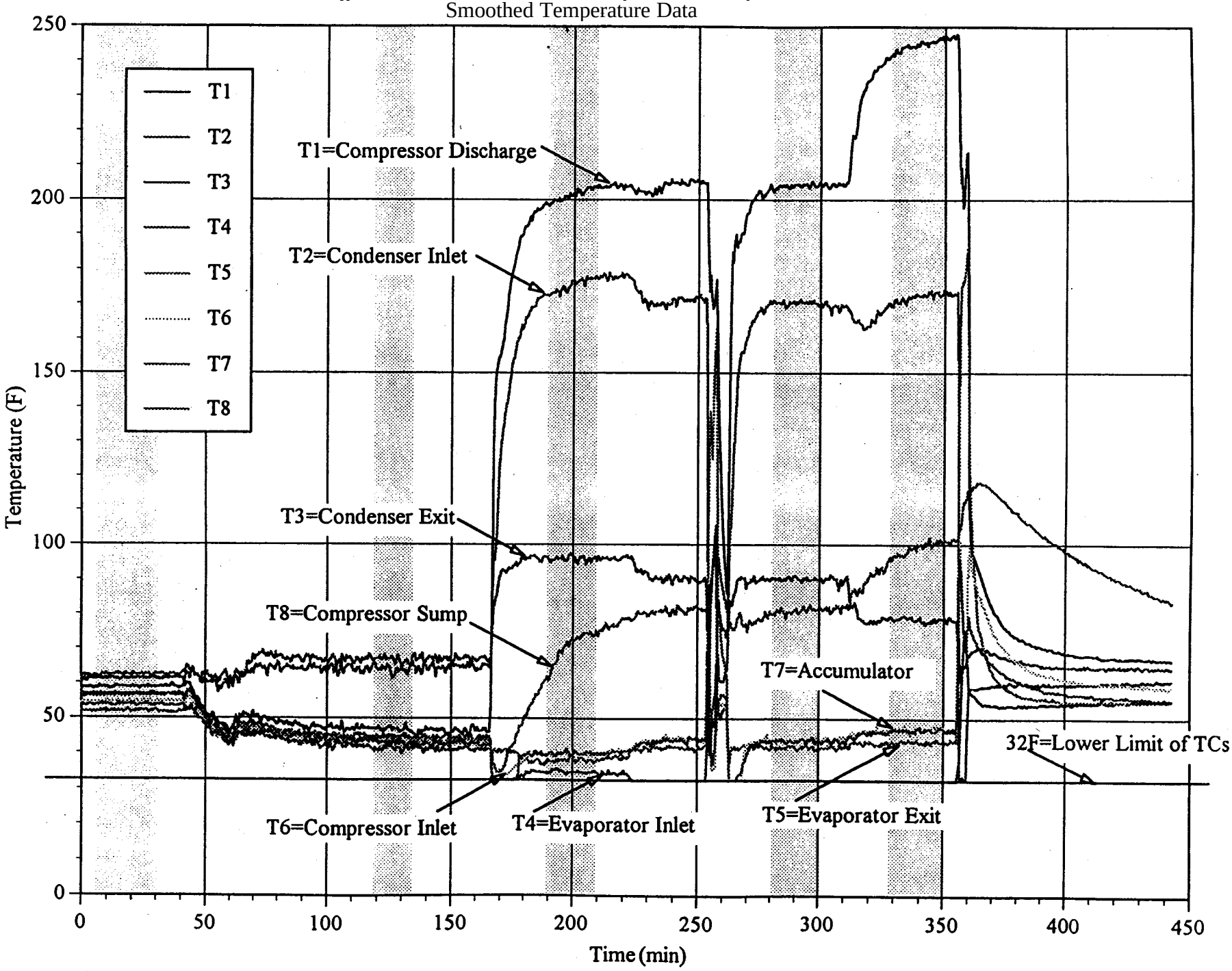

Fig. B.1.3b Blend A Heat Pump Test #4 Sequence

Smoothed & Normalized Pressure Data

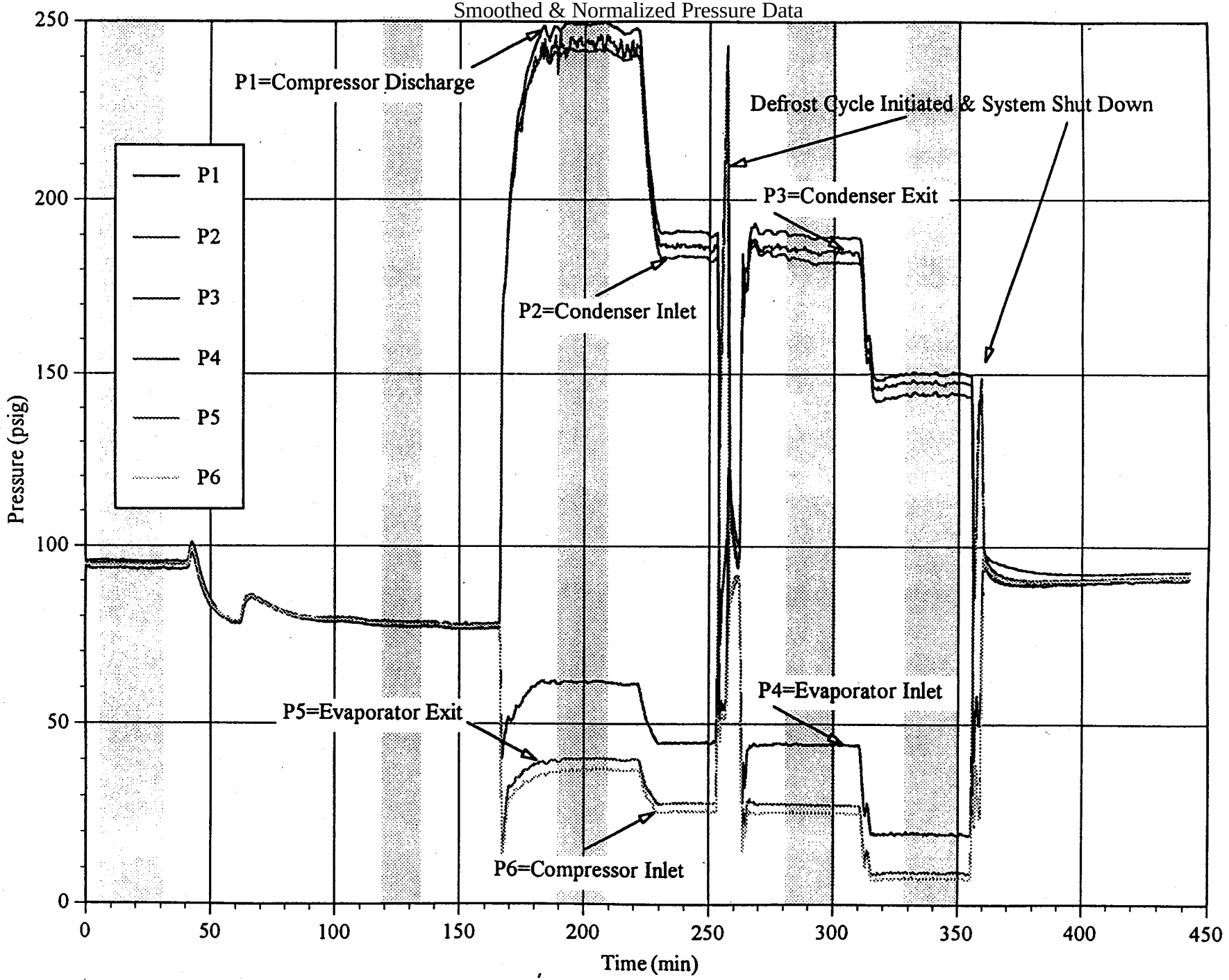

Table B.1-4. Blend A - Test Data - #5 Test Sequence

Summary of ARTI Test Run #5: Heating Mode operation at Low Temp with Slow leak

THS 2/22/95 charge weight (lbs) 7

- nonstandard averaging
- data suspect (two phases detected)

	Standard	Port #1	Port #2	Port #3	Port #4	Standard	Notes:
ARTI 50	35.17	21.22	37.07	20.49	38.44	35.22	System off; IECs on
ARTI 51	35.22	39.63	24.67	24.82	24.67	35.16	System on; IECs on
ARTI 52	35.16	30.57	36.79	21.76	31.46	35.17	1.7 lbs removed; System off; IECs on
ARTI 53	35.17	35.49	21.60	21.60	21.49	35.13	System on; IECs on
ARTI 54	35.13	25.15	32.89	29.70	24.49	35.14	1.7 lbs removed; System off; IECs on
ARTI 55	35.14	26.52	19.24	18.78	17.16	34.65	System on; IECs on
ARTI 56	35.17	10.84	22.44	23.22	18.97	35.19	System at 70 F; IECs off

charge composition	
startup	23.5
after d#1	21.0
after d#2	18.1

Sample Port #1 : Liquid or 2 phase from Evaporator Inlet
Sample Port #2 : Compressor Discharge
Sample Port #3 : Accumulator
Sample Port #4 : Liquid from Condenser Exit

Discharge	wt (lbs)	Liquid %	Vapor %	Total %
#1	1.70	17.40	33.05	31.35
#2	1.70	14.48	28.86	27.10

Averaged Values from Data Acquasition System:

	Tstart	Tfinish	T1	T2	T3	T4	T5	T6	T7	T8
ARTI 50	0.00	0.00	0.00	0.00	0.00	0.00	0.00	0.00	0.00	0.00
ARTI 51	120.25	141.75	176.67	150.17	90.65	26.38	19.12	15.85	16.94	61.01
ARTI 52	254.25	275.75	38.51	65.38	66.27	35.90	34.68	34.61	30.30	36.75
ARTI 53	353.25	372.75	189.46	158.93	89.06	20.73	33.08	36.17	36.10	73.26
ARTI 54	419.25	437.25	39.50	65.55	66.09	35.92	34.75	35.74	34.72	44.54
ARTI 55	507.25	525.25	225.53	158.86	76.68	-4.65	35.36	41.25	40.88	97.67
ARTI 56	0.00	0.00	0.00	0.00	0.00	0.00	0.00	0.00	0.00	0.00

	P1	P2	P3	P4	P5	P6	Time(min)
ARTI 50	0.00	0.00	0.00	0.00	0.00	0.00	0.00
ARTI 51	224.23	217.58	219.62	53.67	34.25	31.50	131.00
ARTI 52	59.08	58.46	58.46	58.89	58.71	58.79	265.00
ARTI 53	184.65	176.54	179.52	42.86	27.13	24.58	363.00
ARTI 54	54.70	53.96	54.11	54.31	54.29	54.23	428.25
ARTI 55	136.80	129.79	132.51	16.38	6.75	4.93	516.25
ARTI 56	0.00	0.00	0.00	0.00	0.00	0.00	0.00

T in deg F
P in psig

Fig. B.1.4a Blend A Heat Pump Test #5 Sequence

Smoothed Temperature Data

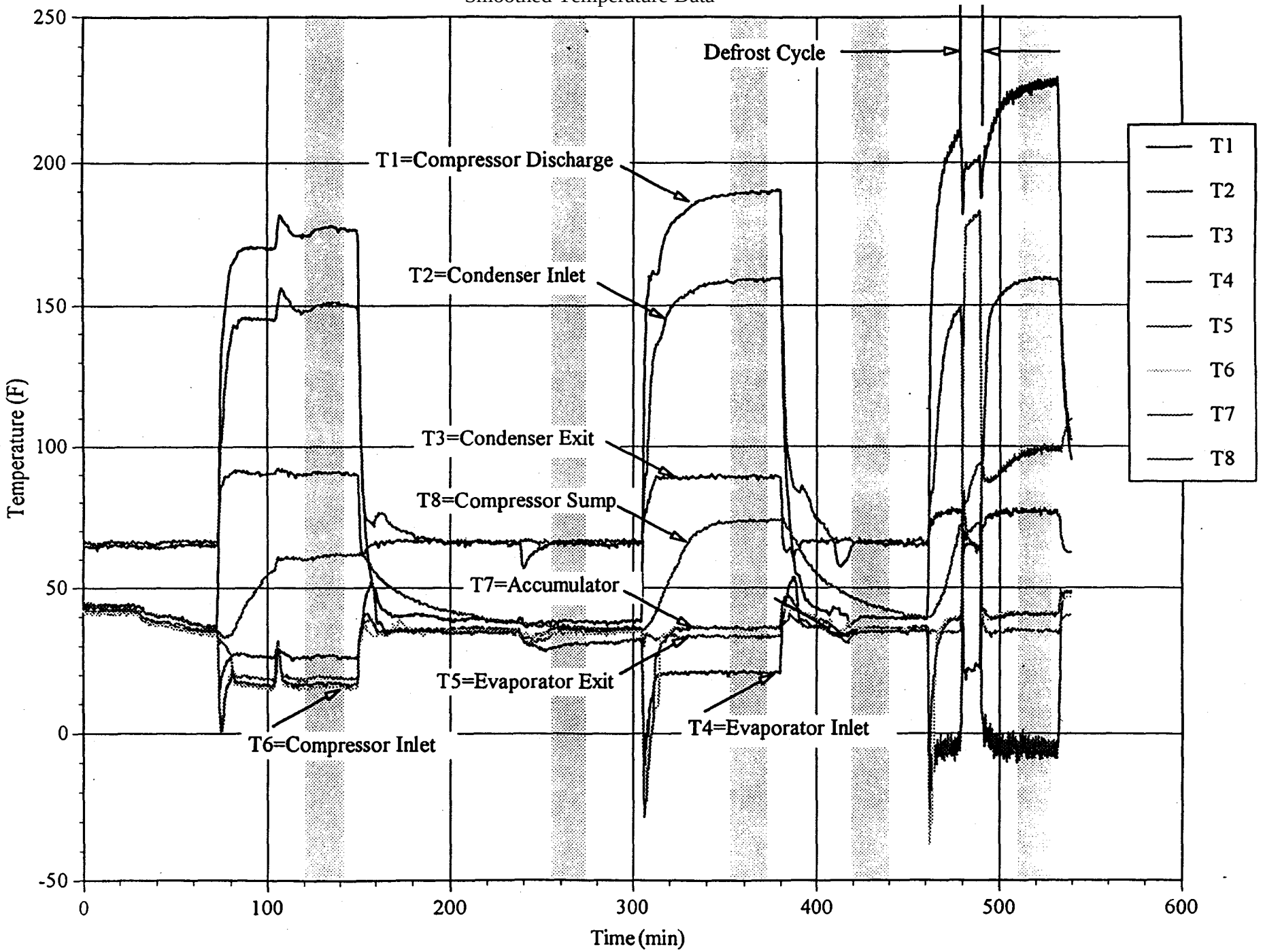

Fig. B.1.4b Blend A Heat Pump Test #5 Sequence

Smoothed & Normalized Pressure Data

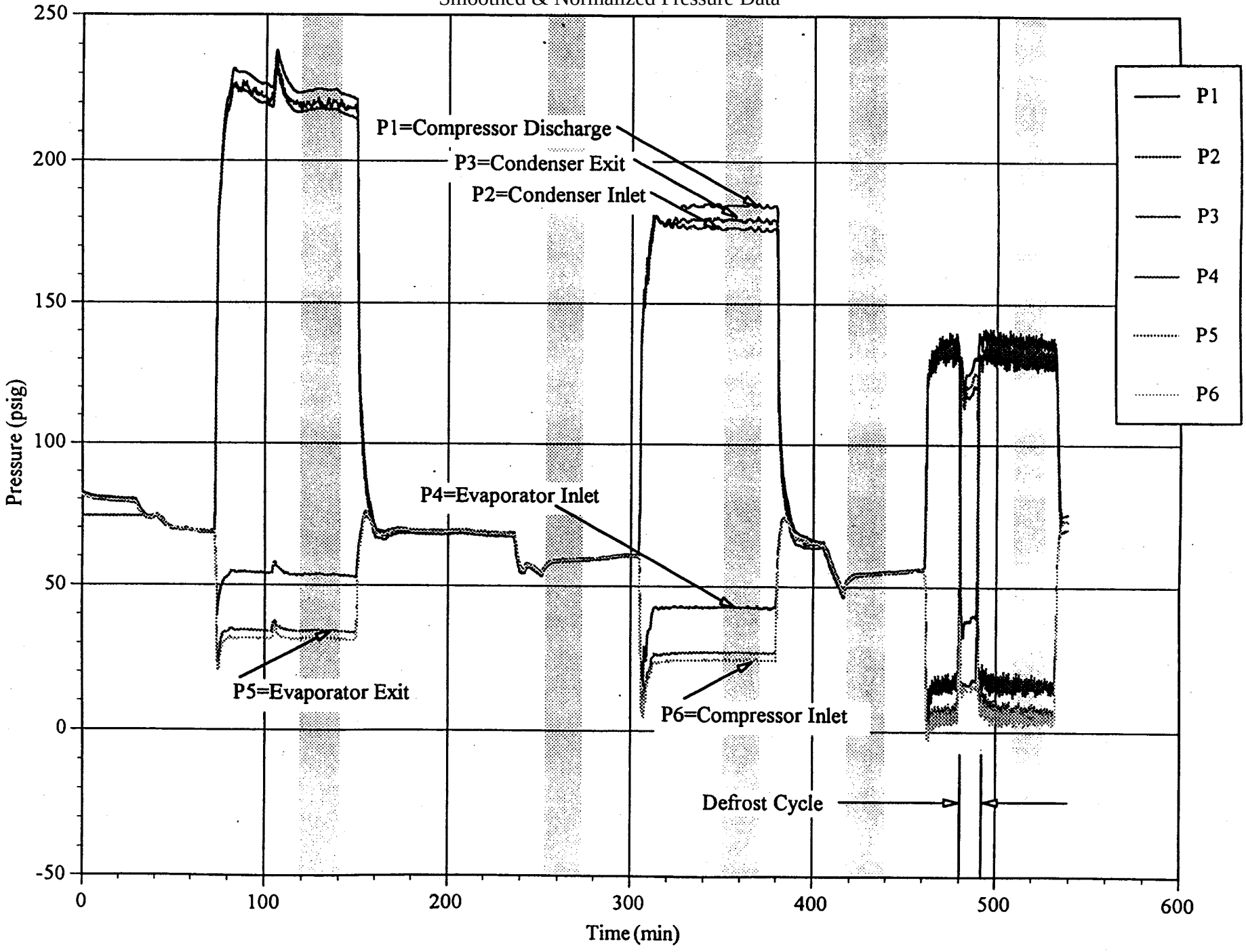

Fig. B.1.5a Blend A Heat Pump Test #6 Sequence

Smoothed Temperature Data

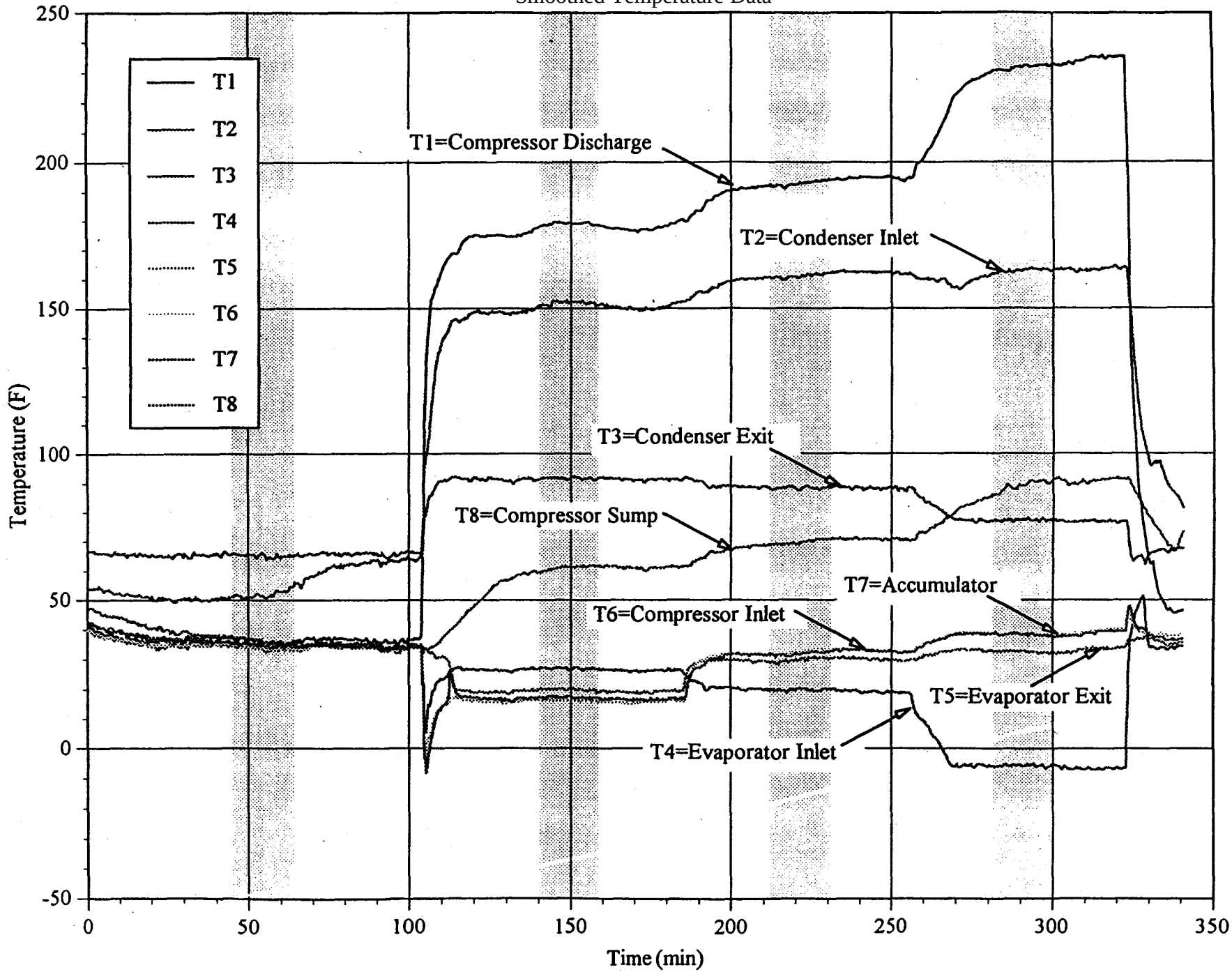

Fig. B.1.5b Blend A Heat Pump Test #6 Sequence

Smoothed & Normalized Pressure Data

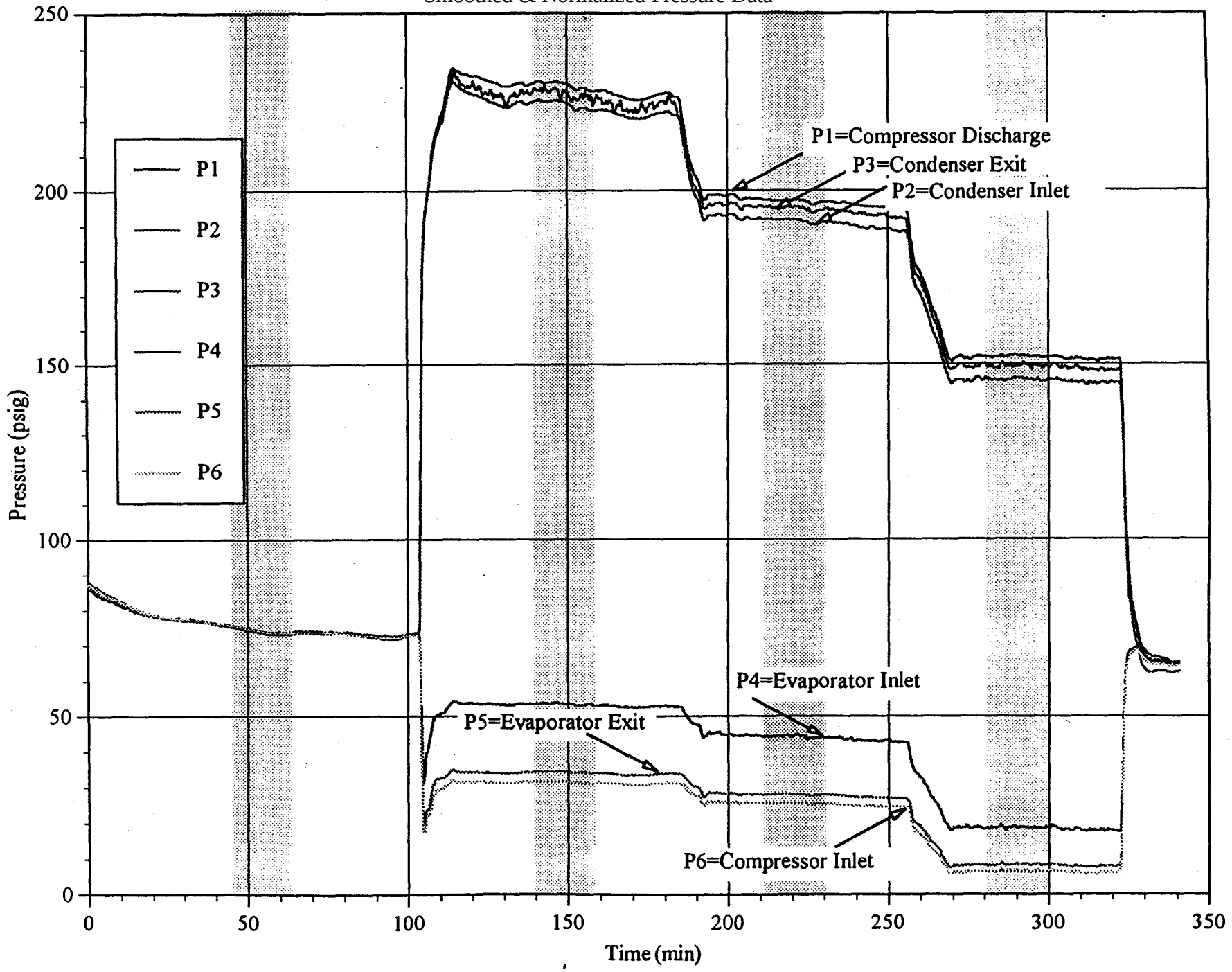

Table B.1-5. Blend A - Test Data - #6 Test Sequence

Summary of ARTI Test Run #6: Heating Mode operation at Low Temp with 2-Phase Leak

THS 2/24/95 charge weight (lbs) 7

- nonstandard averaging
- data suspect (two phases detected)

	Standard	Port #1	Port #2	Port #3	Port #4	Standard	Notes:
ARTI 60	35.17	23.88	39.91	19.04	38.30	35.28	System at 70 F; IECs off
ARTI 61	35.28	45.91	47.27	20.06	25.79	35.15	System off; IECs on
ARTI 62	35.15	30.34	23.97	24.25	24.01	35.09	System on; IECs on
ARTI 63	35.09	37.85	23.27	23.24	22.99	35.06	1.6 lbs removed; System on; IECs on
ARTI 64	35.06	35.59	23.35	23.41	22.52	35.04	1.8 lbs removed; System on; IECs on
ARTI 65	35.23	12.23	33.16	33.18	35.82	35.19	System at 70 F; IECs off

charge composition	
startup	23.4
after d#1	22.9
after d#2	22.6

Sample Port #1 : Liquid or 2 phase from Evaporator Inlet
Sample Port #2 : Compressor Discharge
Sample Port #3 : Accumulator
Sample Port #4 : Liquid from Condenser Exit

Discharge	wt (lbs)	Liquid %	Vapor %	Total %
#1	1.60	11.84	26.13	25.06
#2	1.80	11.69	26.20	23.57

Averaged Values from Data Acquasition System:

	Tstart	Tfinish	T1	T2	T3	T4	T5	T6	T7	T8
ARTI 60	0.00	0.00	0.00	0.00	0.00	0.00	0.00	0.00	0.00	0.00
ARTI 61	45.75	64.25	36.11	52.08	65.16	34.52	33.81	33.80	36.19	34.88
ARTI 62	140.75	159.25	178.96	151.85	91.67	27.01	19.89	16.35	17.24	61.11
ARTI 63	212.75	231.25	192.86	161.05	88.29	19.81	29.92	32.61	31.97	69.71
ARTI 64	281.75	300.25	231.67	162.75	77.11	-5.66	32.69	38.61	38.37	89.09
ARTI 65	0.00	0.00	0.00	0.00	0.00	0.00	0.00	0.00	0.00	0.00

Appendix B.2 - R407C

Test Data, Figures and Tables

APPENDIX B.2
R407C - TEST RESULTS AND DATA DETAILS

In this Appendix, the actual data from the Blend R407C tests are presented for those interested in additional details. Also included for easier reference are the Test Plan for Blend 407C (Table 4.2) and Summary of Blend 407C Test levels (Table 4.4) already presented and discussed in the Task 4 material.

The initial test data shows the fractionation effects measured in the seven locations in the heat exchanger.

The test data is shown in tables for #1 through 6 test sequences. Each test is broken into further intervals identified as ARTI 06200 to 06207, for example. Along with each test sequence is an identification of system status, refrigerant charge, temp, etc. The traces for the pressure and temperature data are provided in accompanying figures for each test. The shaded areas on the figures show the time increment corresponding to each ARTI test designated.

Figure B.1.2.14 also shows the heating capacity and kW/ton for the various tests. They show the effects of the different system leak scenario on system performance kW/ton and capacity.

Test	Description
1	Cooling Mode (DOE-A) test with system-on leaks
2	Heating Mode (DOE-E) test with system-on leaks
3	Cooling Mode (DOE-A) test with system-off leaks
4	Heating Mode (DOE-E) test with system-off leaks
5	Heating Mode (DOE-E) test with system-on leaks
6*	Heating Mode (DOE-E) test with system-off leaks
* repeat tests of 2 and 4 due to frosting concerns	

Table 4.2 Test Plan for R407C

	(% R32)	Test 1	Test 2	Test 3	Test 4	Test 5	Test 6
Full charge	Circulating	21.4†	21.0	21.7†	21.0	20.8	20.6
	Overall	20.4	20.4	20.4	20.4	20.4	20.3
After leak	Circulating	20.8	21.0	20.1	20.2	*	*
#1	Overall	20.5	20.5	19.7	19.6	20.4	19.2
After refill	Circulating	21.2	21.6†	20.7	21.7†	20.8	19.5
#1	Overall	20.5	20.5	19.9	19.8	20.4	19.5
After leak	Circulating	20.9	20.8	19.3	16.7	*	*
#2	Overall	20.6	20.5	19.1	16.7	20.5	18.5
After refill	Circulating	21.3	21.1	20.1	18.1	20.4	19.1
#2	Overall	20.6	20.5	19.5	17.8	20.5	19.0
After leak	Circulating	20.7	20.6	18.5	15.5	*	*
#3	Overall	20.7	20.2	18.0	15.9	20.5	18.9
After refill	Circulating	21.1	21.5†	19.5	17.3	20.6	19.5
#3	Overall	20.6	20.2	18.7	17.3	20.4	19.5

* Data not taken
† Indicates fractionation

Table 4.4 Summary of R407C Tests (R32 Composition Only)

Table B.2-1. R407C - Test Data - Sequence #1

ARTI Run 1 (DOE A - System on leak)

Data Summaries:	start	finish	avg	time(se	POWE	SCALE	FLOW	ctons	htons	ckw/ton	hkw/ton
ART06200	2691	5850	4270.5	4263	3767	-33	485	2.21	3.26	1.71	1.16
ART06201	8009	11259	9634	9633	3287	0	-81	1.24	2.57	2.65	1.28
ART06202	13264	16474	14869	14883	3748	-0	483	2.19	3.29	1.71	1.14
ART06203	18415	21603	20009	20013	3313	16	-73	1.24	2.60	2.67	1.28
ART06204	23528	26680	25104	25113	3761	1	482	2.22	3.31	1.70	1.14
ART06205	28691	31779	30235	30197	3301	17	-76	1.26	2.60	2.62	1.27
ART06206	33680	36840	35260	35226	3785	-2	486	2.20	3.30	1.72	1.15

	TIE1	TIE2	TII1	TII2	TOE1	TOE2	TOI1	TOI2
ART06200	57.2	56.2	78.5	78.9	107.0	108.6	92.2	93.3
ART06201	61.3	60.3	78.5	79.0	103.9	105.1	92.2	93.0
ART06202	57.4	56.2	78.4	79.0	107.4	108.9	92.3	93.5
ART06203	61.4	60.2	78.5	79.0	104.4	105.7	92.6	93.4
ART06204	57.3	56.3	78.6	79.1	107.7	109.2	92.5	93.7
ART06205	61.3	60.2	78.6	79.0	104.2	105.5	92.4	93.2
ART06206	57.4	56.4	78.6	79.0	107.9	109.4	92.8	94.0

	PS1	PS2	PS3	PS4	PS5	PS6
ART06200	316.2	76.6	129.7	314.0	319.7	70.8
ART06201	268.8	51.7	93.6	267.9	272.3	48.5
ART06202	316.6	76.1	130.3	314.5	320.1	70.2
ART06203	270.1	51.8	94.5	269.2	273.6	48.7
ART06204	317.0	75.9	130.4	314.9	320.4	70.1
ART06205	269.4	51.8	94.5	268.4	272.8	48.7
ART06206	318.9	76.3	131.2	316.7	322.2	70.3

	TS1	TS2	TS3	TS4	TS5	TS6	TS7	TS8
ART06200	195.5	50.1	68.8	111.5	189.9	56.5	58.4	127.0
ART06201	229.8	73.5	52.7	110.3	219.6	80.1	81.5	135.7
ART06202	195.3	49.8	68.9	111.3	189.5	56.0	57.7	124.8
ART06203	230.3	73.6	53.3	110.8	220.2	80.2	81.7	136.2
ART06204	195.8	49.7	68.9	111.6	189.9	55.9	57.6	125.0
ART06205	229.6	73.5	53.4	110.6	219.5	80.1	81.6	135.4
ART06206	194.5	49.8	69.3	111.6	188.8	54.2	55.9	124.7

	PX1	PX2	PX3	PX4	PX5	PX6	PX7
ART06200	78.0	77.5	77.7	77.4	77.5	77.0	77.1
ART06201	51.7	51.3	51.6	51.6	51.8	51.5	51.8
ART06202	77.6	77.0	77.3	76.9	77.0	76.6	76.7
ART06203	51.8	51.5	51.8	51.8	52.0	51.7	52.0
ART06204	77.4	76.9	77.1	76.7	76.8	76.4	76.5
ART06205	51.9	51.4	51.8	51.8	52.0	51.7	52.0
ART06206	77.8	77.2	77.5	77.1	77.2	76.8	76.8

	TX1	TX2	TX3	TX4	TX5	TX6	TX7
ART06200	46.6	49.4	49.3	49.2	51.3	59.5	66.4
ART06201	34.0	53.1	59.7	66.2	70.6	68.7	71.7
ART06202	46.1	49.0	48.9	48.8	51.4	59.7	66.2
ART06203	34.2	53.0	59.6	66.3	70.8	68.7	71.9
ART06204	46.0	49.3	48.9	48.5	51.3	59.4	66.0
ART06205	34.3	53.1	59.6	66.2	70.8	69.8	72.0
ART06206	46.3	49.5	49.1	48.7	51.1	58.5	65.7

Summary of ARTI Test Run #1: Cooling Mode operation at DOE-A with system on leak
THS 6/20/95

		STD1	STD2	P#1	P#2	P#3	P#4	STD1	STD2	Notes:
ART06200	R32	21.03	0.05	21.39	21.36	21.37	19.55	21.03	0.05	System on; Full charge
	R125	25.67	74.79	26.24	26.21	26.20	24.83	25.73	74.64	
ART06201	R32	21.03	0.21	20.68	20.82	21.04	18.06	21.03	0.36	System on; 3/4 charge
	R125	25.73	74.72	25.78	25.80	25.97	23.45	25.73	74.47	
ART06202	R32	21.03	0.36	21.22	21.24	21.28	19.55	21.03	0.36	System on; refilled to full charge
	R125	25.73	74.47	26.25	26.13	26.18	24.81	25.73	74.47	
ART06203	R32	21.03	0.36	20.80	20.86	20.91	18.00	21.01	0.36	System on; 3/4 charge
	R125	25.73	74.47	25.73	25.90	25.87	23.38	25.72	74.06	
ART06204	R32	21.01	0.36	21.62	21.15	21.23	19.50	21.04	0.36	System on; refilled to full charge
	R125	25.72	74.06	26.49	26.12	26.16	24.74	25.73	73.93	
ART06205	R32	21.04	0.36	21.44	20.64	20.86	18.04	21.01	0.36	System on; 3/4 charge
	R125	25.73	73.93	26.52	25.71	25.85	23.39	25.71	74.06	
ART06206	R32	21.01	0.36	21.04	21.15	21.21	19.49	21.01	0.36	System on; refilled to full charge
	R125	25.71	74.06	25.99	26.05	26.10	24.70	25.71	74.06	
ART06207	R32	21.07	0.05	28.00	25.56	24.76	26.91	21.07	0.05	System off; full
	R125	25.70	74.18	32.66	29.44	28.50	30.97	25.70	74.18	

- more than 2% deviation in calculated compositions

		HX1	HX2	HX3	HX4	HX5	HX6	HX7	wt(lbs)	
ART06200	R32	16.95	16.56	15.81	14.23	21.67	21.43	21.44	6.4	=charge weight (lbs)
	R125	22.41	21.88	21.09	19.45	26.50	26.27	26.27	6.4	System on; Full charge
ART06201	R32	16.72	21.08	21.06	21.09	21.10	21.10	21.10	1.585	=charge removed (lbs)
	R125	21.75	26.02	25.97	25.99	26.00	26.00	26.00	4.815	System on; 3/4 charge
ART06202	R32	17.17	15.25	15.72	15.53	21.40	21.35	21.35	1.76	=charge added (lbs)
	R125	22.65	20.63	20.96	20.63	26.28	26.22	26.22	6.575	System on; refilled to full charge
ART06203	R32	16.25	20.92	20.95	20.98	21.02	21.00	21.02	1.57	=charge removed (lbs)
	R125	21.25	25.83	25.85	25.86	25.90	25.87	25.89	5.005	System on; 3/4 charge
ART06204	R32	16.69	15.99	15.34	16.74	21.17	21.26	21.28	1.75	=charge added (lbs)
	R125	22.12	21.30	20.58	21.78	26.05	26.11	26.13	6.755	System on; refilled to full charge
ART06205	R32	15.81	20.89	20.96	20.94	20.96	20.96	20.95	1.535	=charge removed (lbs)
	R125	20.81	25.77	25.82	25.79	25.81	25.80	25.79	5.22	System on; 3/4 charge
ART06206	R32	16.76	16.11	15.61	15.27	21.31	21.15	21.21	1.79	=charge added (lbs)
	R125	22.16	21.41	20.86	20.40	26.20	25.98	26.02	7.01	System on; refilled to full charge

Test 1 (6/20/95)

Sample Port #1 : Liquid from Condenser Exit
Sample Port #2 : Compressor Discharge
Sample Port #3 : Accumulator
Sample Port #4 : Liquid or 2 phase from Evaporator Inlet

		Liquid %		Vapor %		Total %					
Disch	wt (lbs)	R32	R125	R32	R125	R32	R125	Rechar	wt(lbs)	R32	R125
#1	1.59	15.01	20.29	24.31	28.99	20.22	25.1667	#1	1.76	20.43	25.31
#2	1.57	14.74	19.97	24.09	28.90	20.02	25.0129	#2	1.75	20.43	25.31
#3	1.535	14.42	19.56	24.47	29.41	20.28	25.2921	#3	1.79	20.43	25.31

charge composition

	R32	R125	R134a
startup	20.43	25.31	54.26
after d#	20.5	25.4	54.14
after r#1	20.5	25.3	54.17
after d#	20.63	25.45	53.92
after r#2	20.58	25.42	54.01
after d#	20.67	25.45	53.88
after r#3	20.61	25.42	53.98

circulating composition

	R32	R125	R134a
startup	21.37	26.22	52.41
after d#	20.84	25.85	53.3
after r#1	21.25	26.19	52.56
after d#	20.86	25.83	53.31
after r#2	21.33	26.26	52.41
after d#	20.75	25.78	53.47
after r#3	21.13	26.05	52.82

Fig. B.1.2-6 Heat Pump R407C Fractionation Test 1

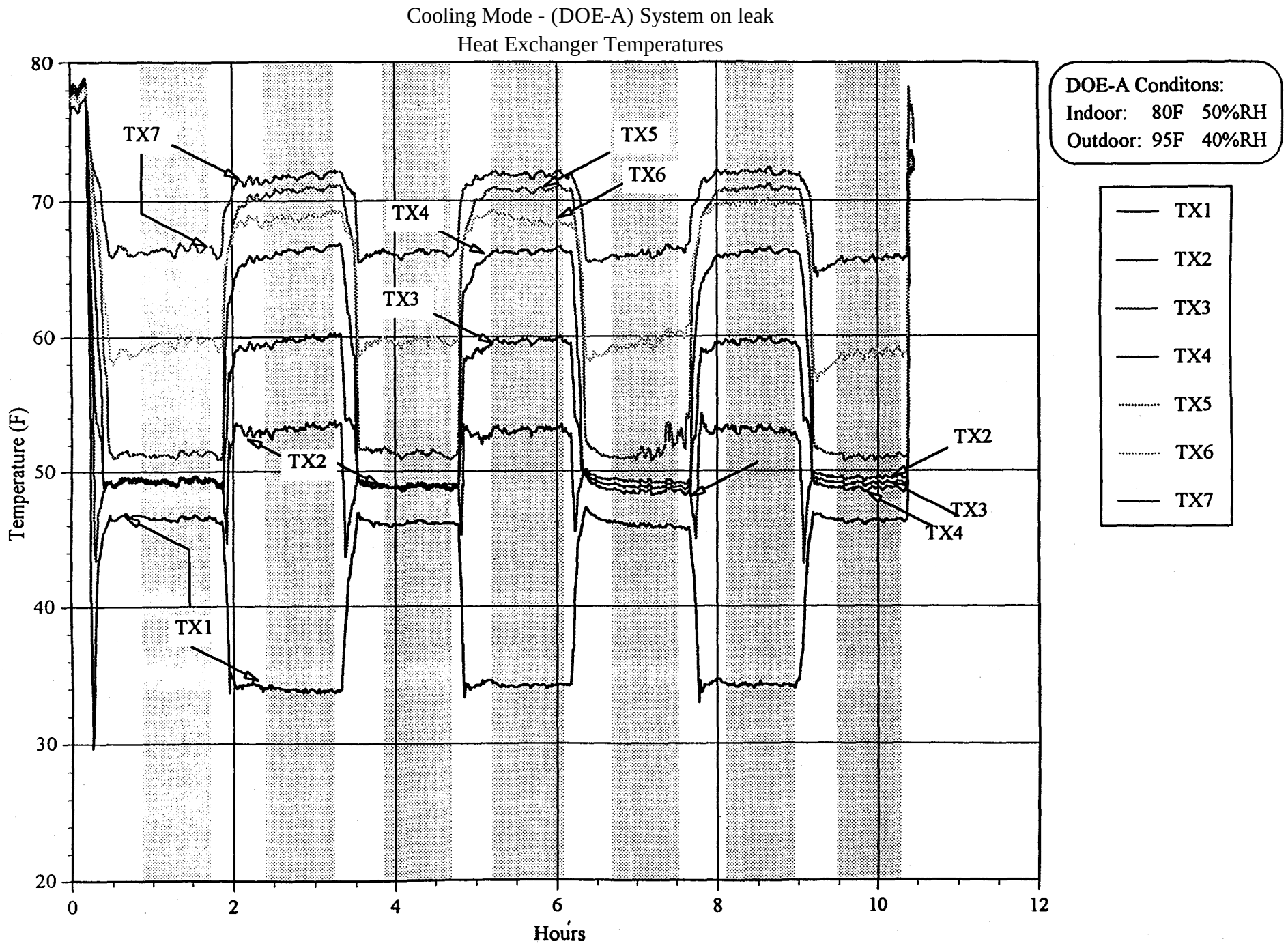

Fig. B.1.2-7 Heat Pump R407C Fractionation Test 1

Cooling Mode - (DOE-A) System on leak

Heat Exchanger Pressures

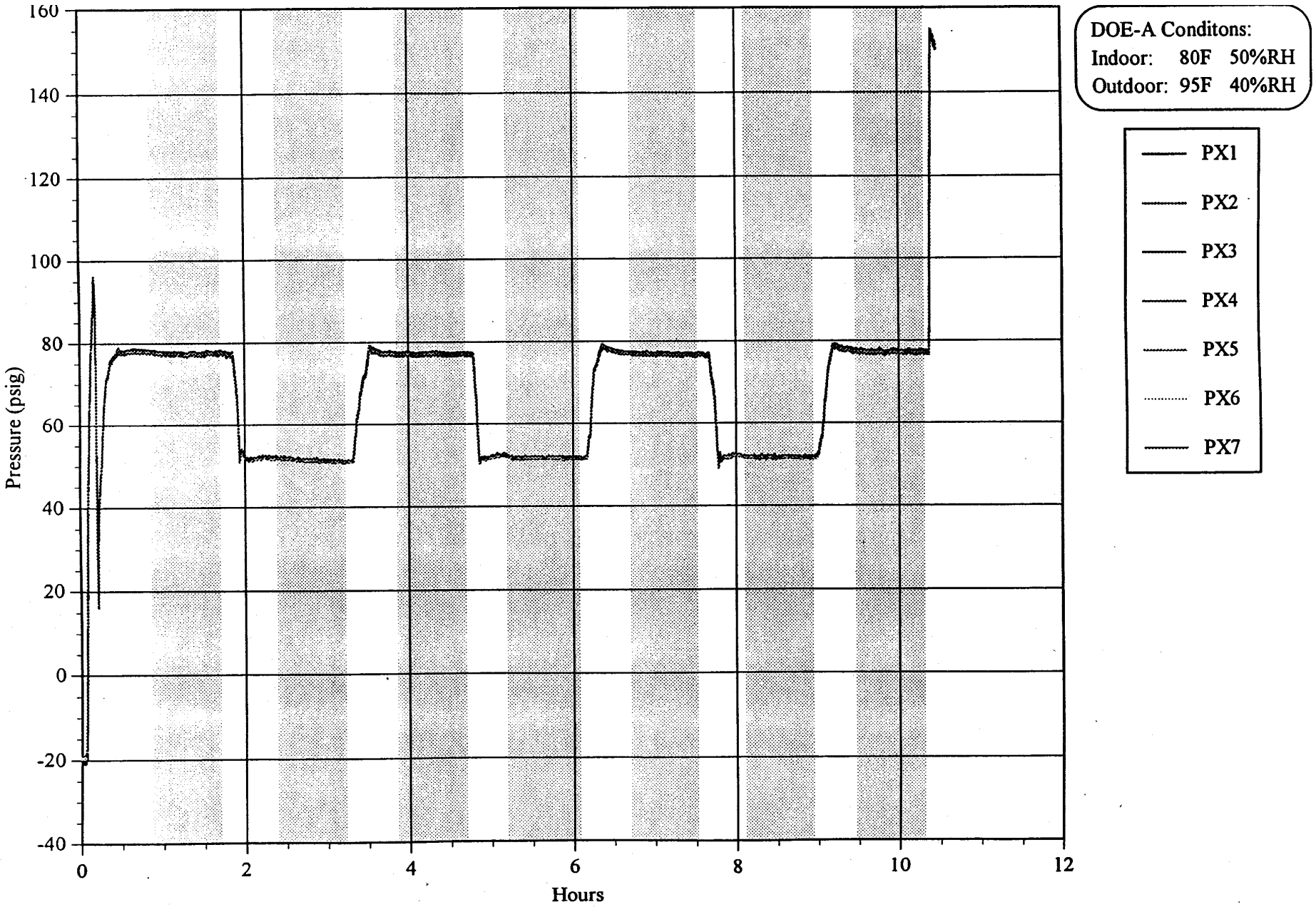

Fig. B.1.2-8 Heat Pump R407C Fractionation Test 1

Cooling Mode - (DOE-A) System on leak

Air Side Temperatures

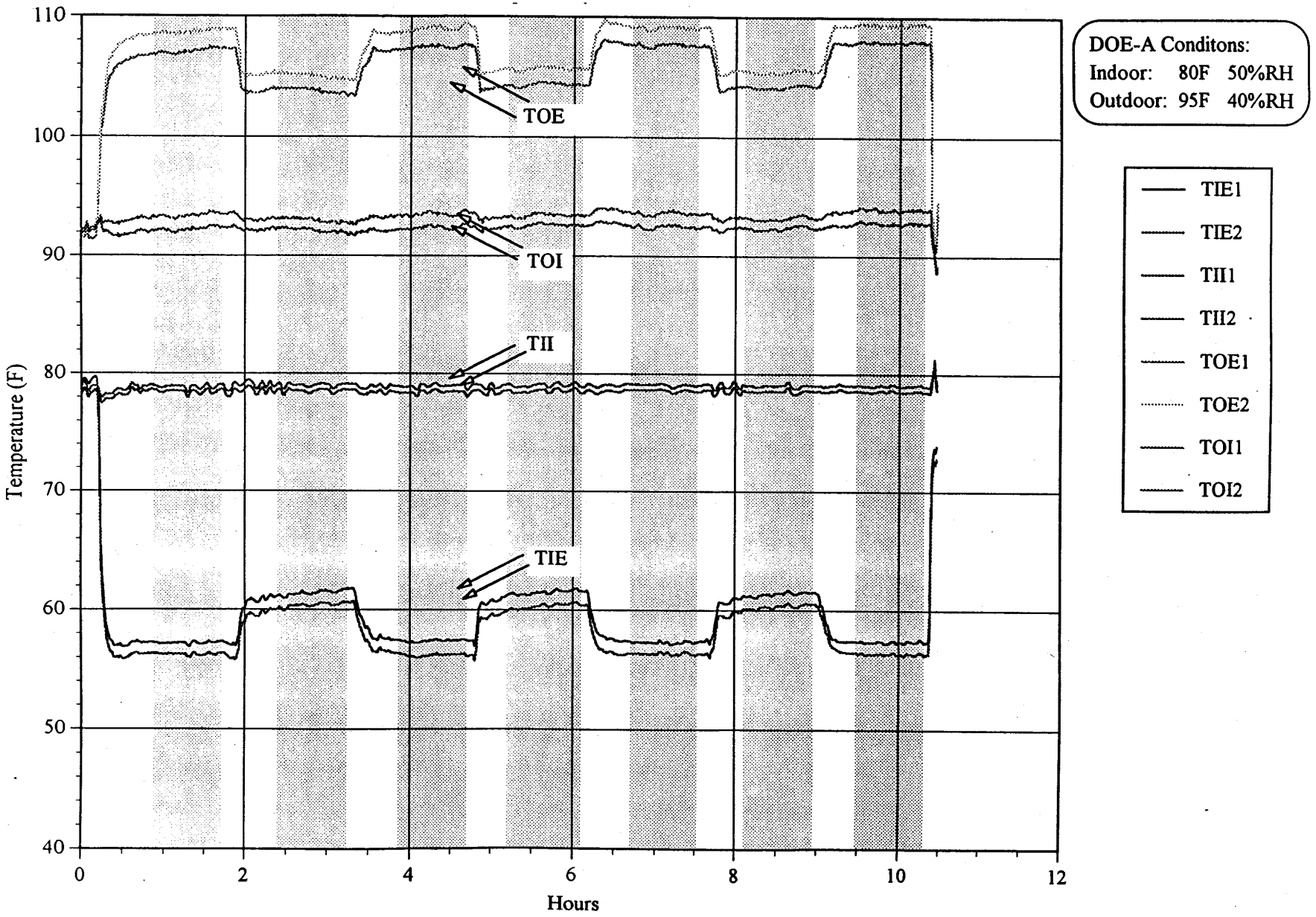

Table B.2-2. R407C - Test Data - Sequence #2

ARTI Run 2 (DOE E - System on leak)

Data Summaries:	start	finish	avg	time(sec)	POWER	SCALE	FLOW	htons	hkw/ton
ART06220	4109	7470	5789	5790	3502	27	-96	2.42	1.45
ART06221	9507	12620	11063	11070	2808	-8	-93	1.71	1.64
ART06222	14542	17741	16141	16140	3069	26	-96	1.75	1.76
ART06223	21876	25283	23579	23575	2740	60	-90	1.61	1.71
ART06224	27545	30673	29109	29114	2961	55	-96	1.71	1.73
ART06225	32972	36133	34552	34544	2630	33	-66	1.23	2.13
ART06226	38100	41396	39748	39764	2779	31	-82	1.35	2.07

	TIE1	TIE2	TII1	TII2	TOE1	TOE2	TOI1	TOI2
ART06220	95.8	94.9	68.2	68.8	41.7	42.2	45.6	45.6
ART06221	87.9	87.2	68.3	68.9	44.3	44.8	46.2	46.5
ART06222	88.3	87.6	68.3	68.9	44.7	45.1	45.9	46.3
ART06223	86.7	86.1	68.3	68.9	44.3	44.7	46.1	46.4
ART06224	87.9	87.3	68.3	68.9	44.8	45.3	46.0	46.3
ART06225	82.6	81.9	68.2	68.9	45.8	46.4	46.2	46.6
ART06226	83.8	83.0	68.2	68.8	45.1	45.9	46.0	46.3

	PS1	PS2	PS3	PS4	PS5	PS6
ART06220	284.6	284.9	279.8	62.3	40.7	37.8
ART06221	204.6	204.6	200.8	39.9	24.0	21.9
ART06222	219.6	219.3	215.7	42.8	25.1	22.1
ART06223	197.5	197.7	193.8	36.3	22.4	19.6
ART06224	210.5	210.5	206.7	40.6	24.4	21.2
ART06225	179.0	179.1	175.7	24.9	13.9	11.3
ART06226	187.6	187.5	184.1	29.5	16.3	13.2

	TS1	TS2	TS3	TS4	TS5	TS6	TS7	TS8
ART06220	205.0	180.5	96.9	32.1	38.3	40.4	40.8	81.1
ART06221	202.2	168.2	89.5	16.0	22.4	38.5	39.2	77.6
ART06222	163.6	137.4	88.0	17.5	5.6	6.0	6.6	62.9
ART06223	210.6	173.6	88.6	13.0	42.4	46.8	46.8	82.1
ART06224	175.0	146.5	88.3	15.9	5.7	6.1	6.1	71.0
ART06225	206.0	162.8	83.6	3.0	-1.2	27.3	28.6	87.7
ART06226	177.4	140.9	85.2	6.5	-3.3	-4.4	-3.1	74.1

	PX1	PX2	PX3	PX4	PX5	PX6	PX7
ART06220	282.4	282.2	282.8	282.4	282.9	282.8	282.8
ART06221	202.2	202.0	202.6	202.4	203.0	202.9	203.0
ART06222	217.3	216.9	217.3	217.3	217.8	217.8	217.8
ART06223	195.2	194.9	195.6	195.3	196.0	195.9	196.0
ART06224	208.2	207.9	208.6	208.3	208.9	208.8	209.1
ART06225	176.8	176.6	177.2	177.1	177.7	177.6	177.8
ART06226	185.4	185.1	185.7	185.6	186.2	186.1	186.3

	TX1	TX2	TX3	TX4	TX5	TX6	TX7
ART06220	96.0	91.9	93.2	95.4	109.2	113.5	117.3
ART06221	89.9	89.4	90.3	92.1	93.0	94.6	97.2
ART06222	88.1	87.4	88.8	92.7	94.9	96.6	99.3
ART06223	88.2	87.7	88.5	90.3	91.3	92.9	95.4
ART06224	88.5	88.3	89.7	92.1	93.5	95.1	97.6
ART06225	83.1	82.7	83.4	84.7	85.6	87.3	89.3
ART06226	84.8	84.3	85.0	86.3	87.3	88.9	90.8

Summary of ARTI Test Run #2: Heating Mode operation at DOE-E with system on leak
THS 6/22/95

		STD1	STD2	P#1	P#2	P#3	P#4	STD1	STD2	Notes:
ART06220	R32	21.04	0.05	29.13	21.00	21.00	20.97	21.05	0.05	System on; Full charge
	R125	25.68	74.77	32.56	25.85	25.85	25.81	25.68	74.74	
ART06221	R32	21.05	0.05	28.12	21.03	21.03	21.05	21.02	0.05	System on; 3/4 charge
	R125	25.68	74.74	31.85	25.86	25.84	25.87	25.66	74.72	
ART06222	R32	21.02	0.05	29.04	21.44	21.93	21.47	21.05	0.05	System on; refilled to full charge
	R125	25.66	74.72	32.54	26.25	26.74	26.25	25.68	74.75	
ART06223	R32	21.05	0.05	27.87	20.81	20.76	20.77	21.06	0.05	System on; 3/4 charge
	R125	25.68	74.75	31.62	25.62	25.54	25.57	25.67	74.75	
ART06224	R32	21.06	0.05	28.50	21.11	20.92	21.28	21.06	0.05	System on; refilled to full charge
	R125	25.67	74.75	32.06	25.86	25.70	26.03	25.67	74.76	
ART06225	R32	21.06	0.05	27.54	20.68	20.69	20.50	21.02	0.05	System on; 3/4 charge
	R125	25.67	74.76	31.40	25.44	25.43	25.29	25.64	74.74	
ART06226	R32	21.02	0.05	28.73	21.40	21.67	21.31	21.02	0.05	System on; refilled to full charge
	R125	25.64	74.74	32.33	26.12	26.39	26.05	25.64	74.74	
ART06227	R32	21.07	0.05	28.00	25.56	24.76	26.91	21.07	0.05	System off; full
	R125	25.70	74.18	32.66	29.44	28.50	30.97	25.70	74.18	

▒▒▒▒ - more than 2% deviation in calculated compositions

		HX1	HX2	HX3	HX4	HX5	HX6	HX7	wt(lbs)	
ART06220	R32	20.98	20.92	20.91	20.91	21.07	19.13	21.13	7.245	=charge weight (lbs)
	R125	25.82	25.78	25.76	25.75	25.87	24.38	25.95	7.245	System on; Full charge
ART06221	R32	20.85	20.69	20.43	20.27	20.20	17.81	21.52	1.55	=charge removed (lbs)
	R125	25.72	25.59	25.41	25.27	25.20	23.21	26.25	5.695	System on; 3/4 charge
ART06222	R32	21.50	21.49	21.53	21.15	21.19	19.34	23.62	1.745	=charge added (lbs)
	R125	26.29	26.29	26.32	26.07	26.12	24.76	28.18	7.44	System on; refilled to full charge
ART06223	R32	20.50	20.43	20.10	19.94	20.08	17.80	21.17	1.725	=charge removed (lbs)
	R125	25.37	25.31	25.08	24.95	25.03	23.10	25.87	5.715	System on; 3/4 charge
ART06224	R32	21.35	21.32	21.13	20.94	21.13	18.80	22.62	1.885	=charge added (lbs)
	R125	26.09	26.08	25.97	25.87	26.03	24.19	27.22	7.6	System on; refilled to full charge
ART06225	R32	20.26	20.21	20.07	20.07	20.05	17.90	20.46	1.815	=charge removed (lbs)
	R125	25.08	25.06	24.95	24.95	24.90	23.08	25.20	5.785	System on; 3/4 charge
ART06226	R32	21.04	20.92	20.73	20.56	20.88	18.49	21.40	0.93	=charge added (lbs)
	R125	25.85	25.77	25.60	25.47	25.70	23.73	26.10	6.715	System on; refilled to full charge

Test 2
(6/22/95)

Sample Port #1 : Liquid from Condenser Exit
Sample Port #2 : Compressor Discharge
Sample Port #3 : Accumulator
Sample Port #4 : Liquid or 2 phase from Evaporator Inlet

		Liquid %		Vapor %		Total %					
Disch	wt (lbs)	R32	R125	R32	R125	R32	R125	Rechar	wt(lbs)	R32	R125
#1	1.55	14.79	20.06	24.43	29.09	20.33	25.24	#1	1.745	20.43	25.31
#2	1.73	15.05	20.29	25.37	30.07	20.42	25.38	#2	1.885	20.43	25.31
#3	1.815	15.5	20.73	27.17	31.75	21.39	26.3	#3	0.93	20.43	25.31

charge composition

	R32	R125	R134a
startup	20.43	25.31	54.26
after d	20.5	25.3	54.21
after r#	20.5	25.3	54.22
after d	20.46	25.31	54.23
after r#	20.45	25.31	54.23
after d	20.16	25	54.85
after r#	20.19	25.04	54.76

circulating composition

	R32	R125	R134a
startup	20.99	25.84	53.17
after d	21.04	25.86	53.11
after r	21.61	26.41	51.98
after d	20.78	25.58	53.64
after r	21.1	25.86	53.03
after d	20.62	25.39	53.99
after r	21.46	26.19	52.35

Fig. B.1.2-9 Heat Pump R407C Fractionation Test 2

Heating Mode - (DOE-E) System on leak

System Temperatures

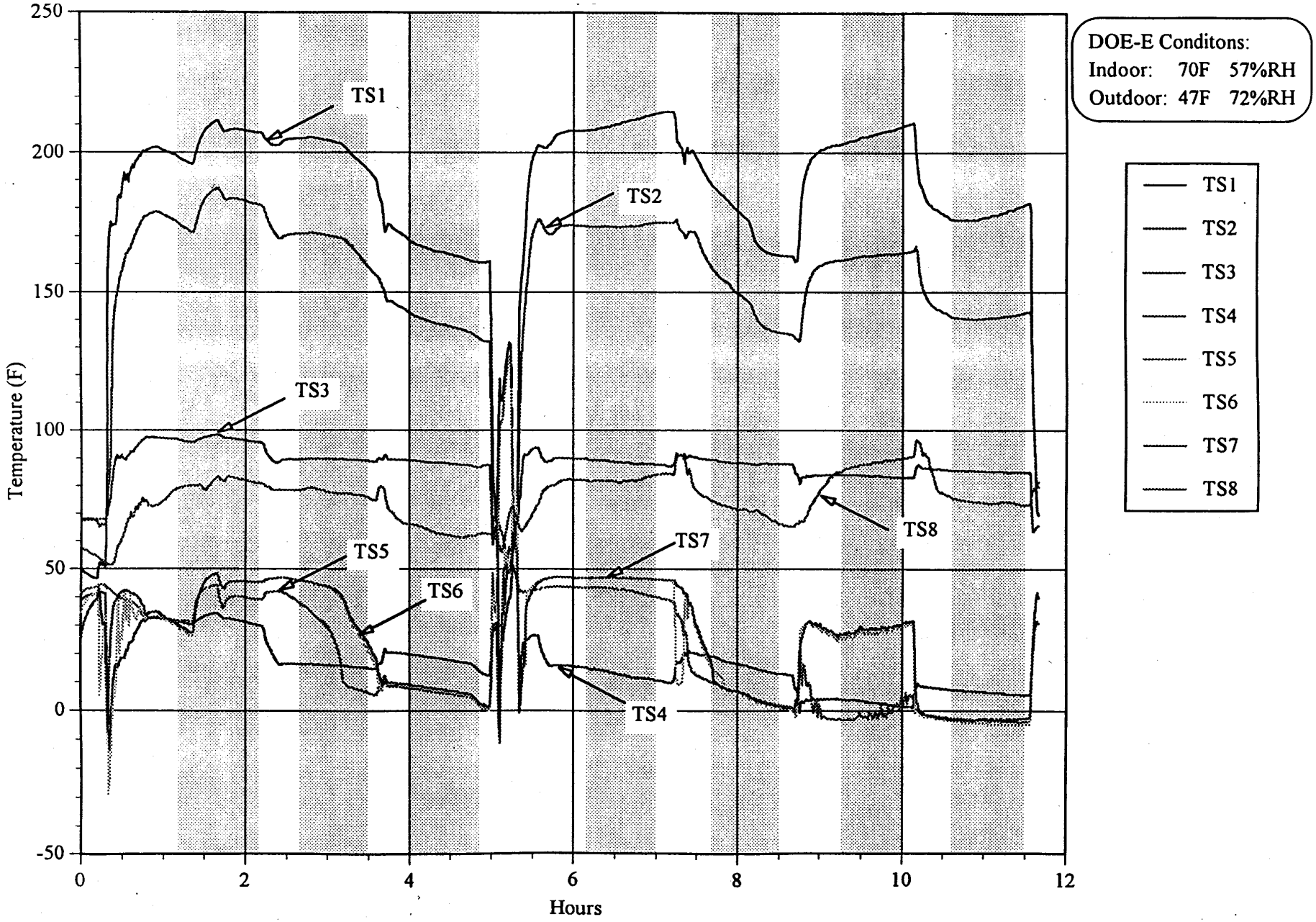

Fig. B.1.2-10 Heat Pump R407C Fractionation Test 2

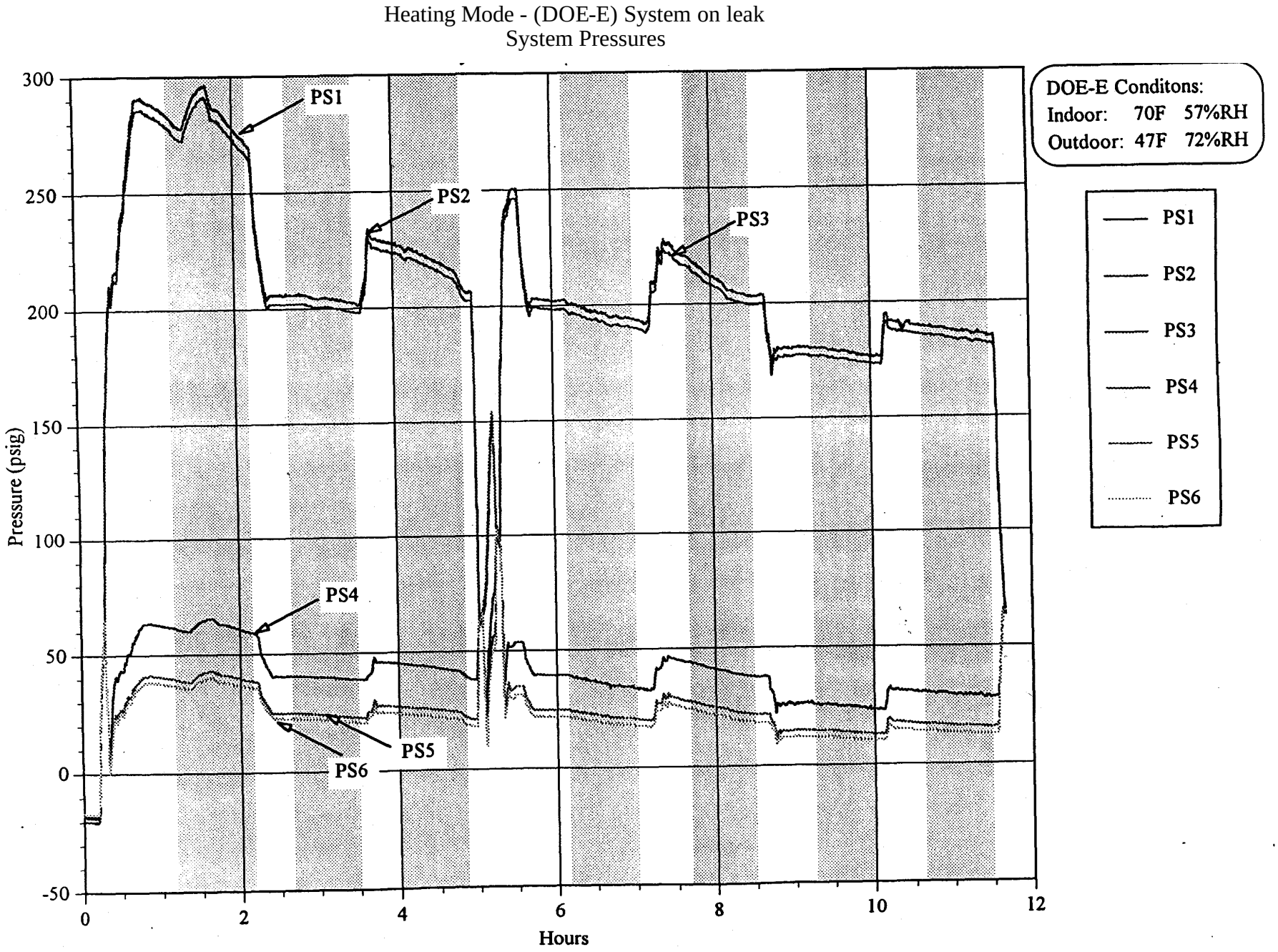

Fig. B.1.2-11 Heat Pump R407C Fractionation Test 2

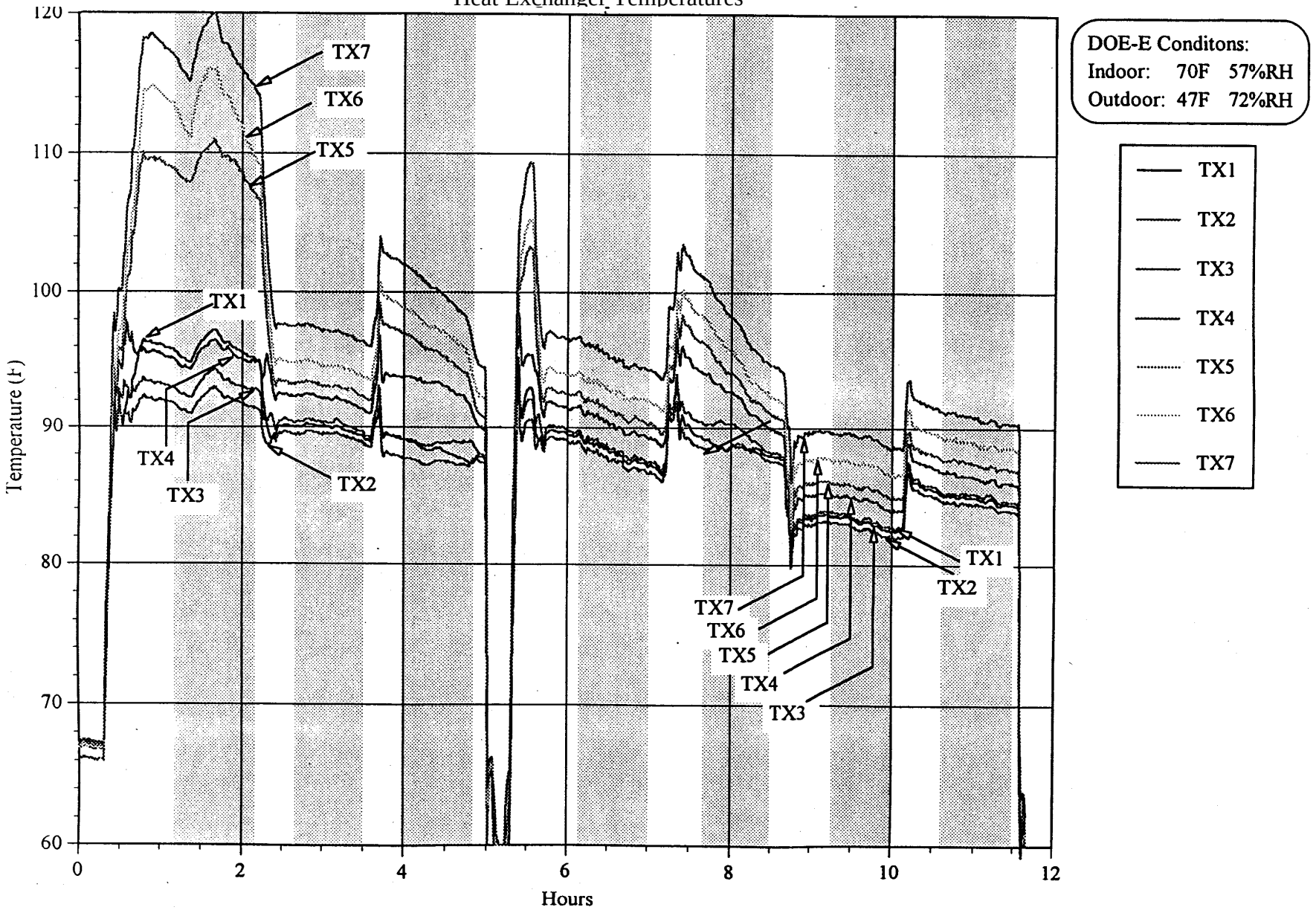

Fig. B.1.2-12 Heat Pump R407C Fractionation Test 2

Heating Mode - (DOE-E) System on leak

Heat Exchanger Pressures

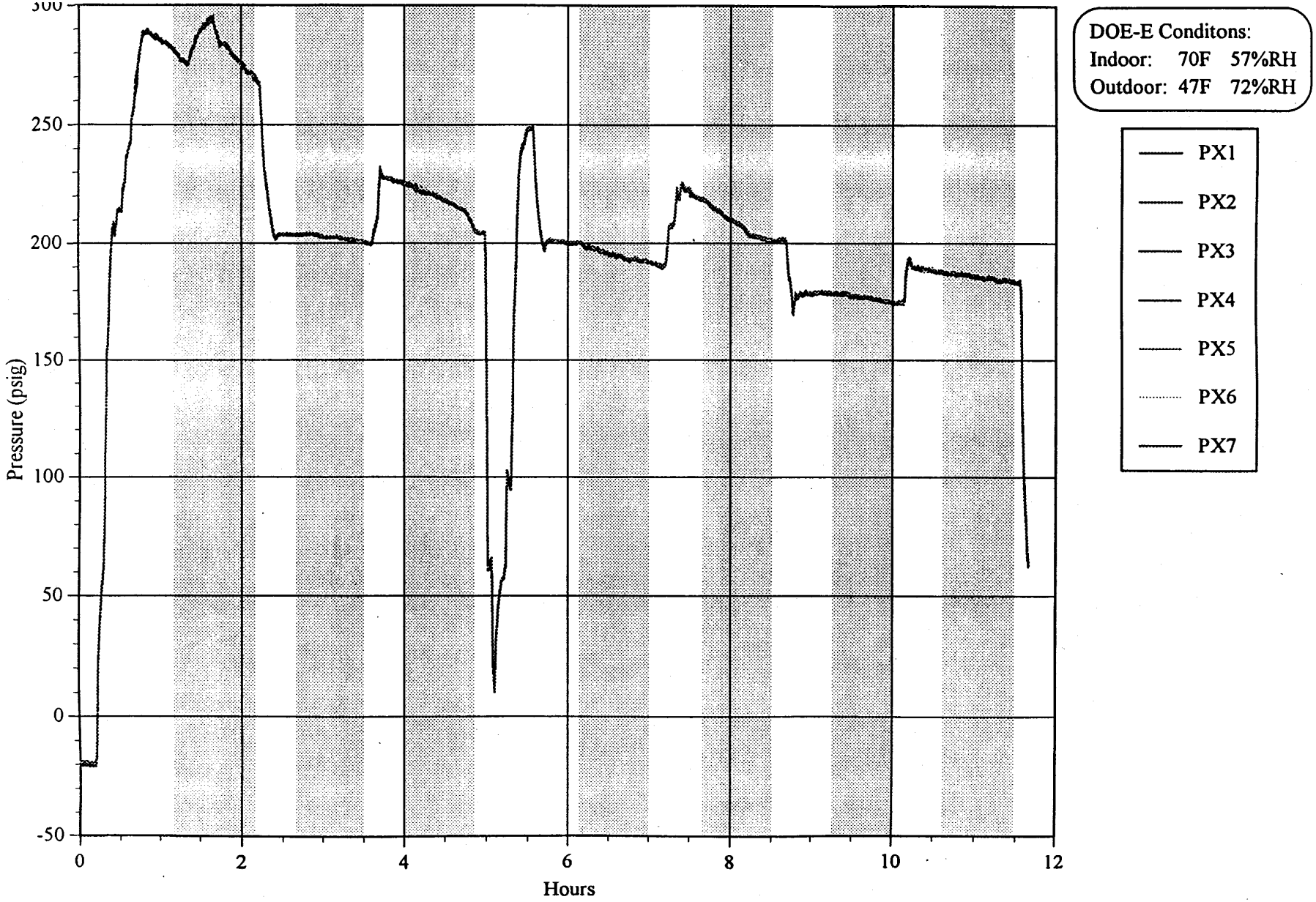

Fig. B.1.2-13 Heat Pump R407C Fractionation Test 2

Heating Mode - (DOE-E) System on leak

Air Side Temperatures

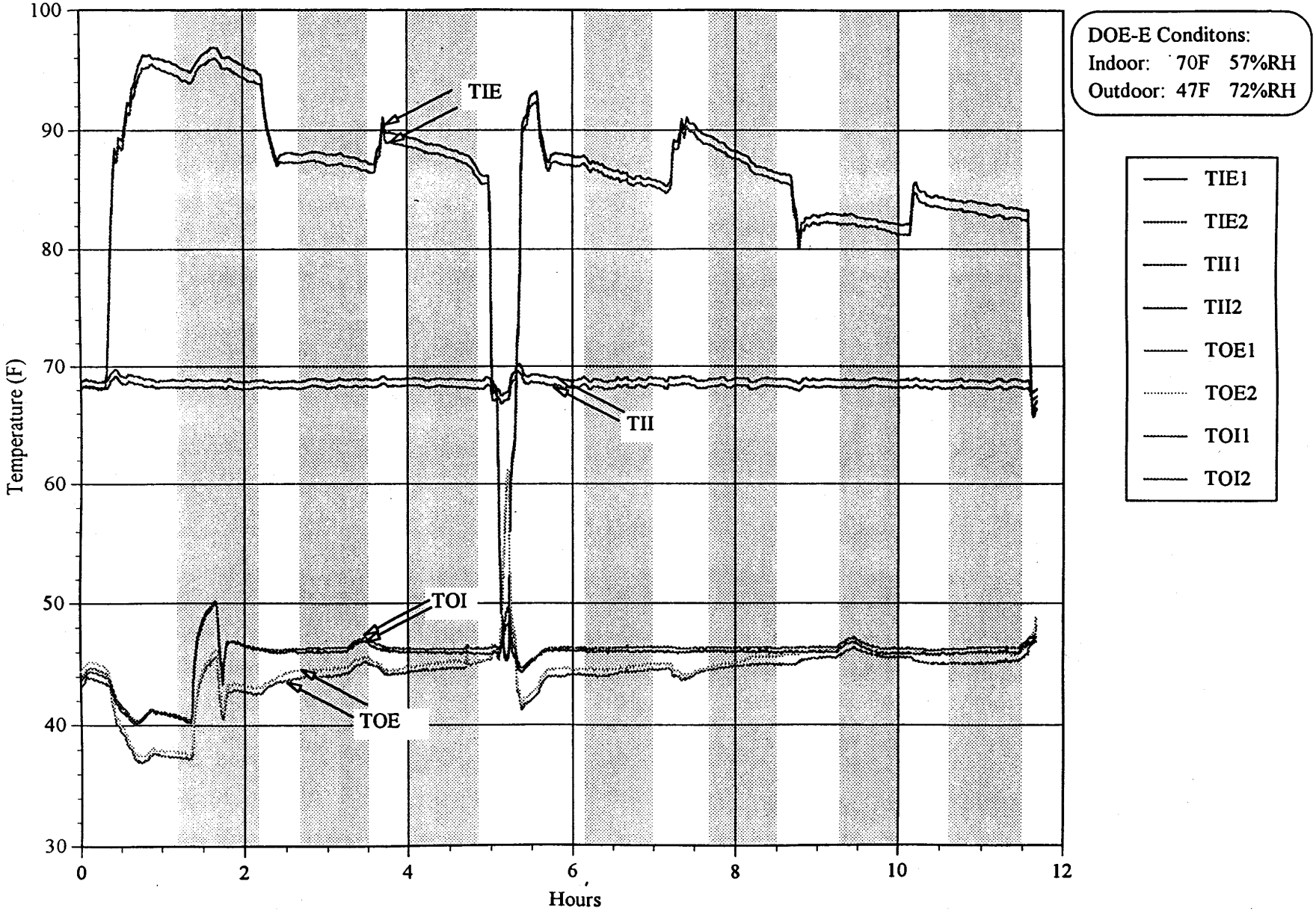

Fig. B.1.2-14 Heat Pump R407C Fractionation Test 2

Heating Mode - (DOE-E) System on leak

System Performance

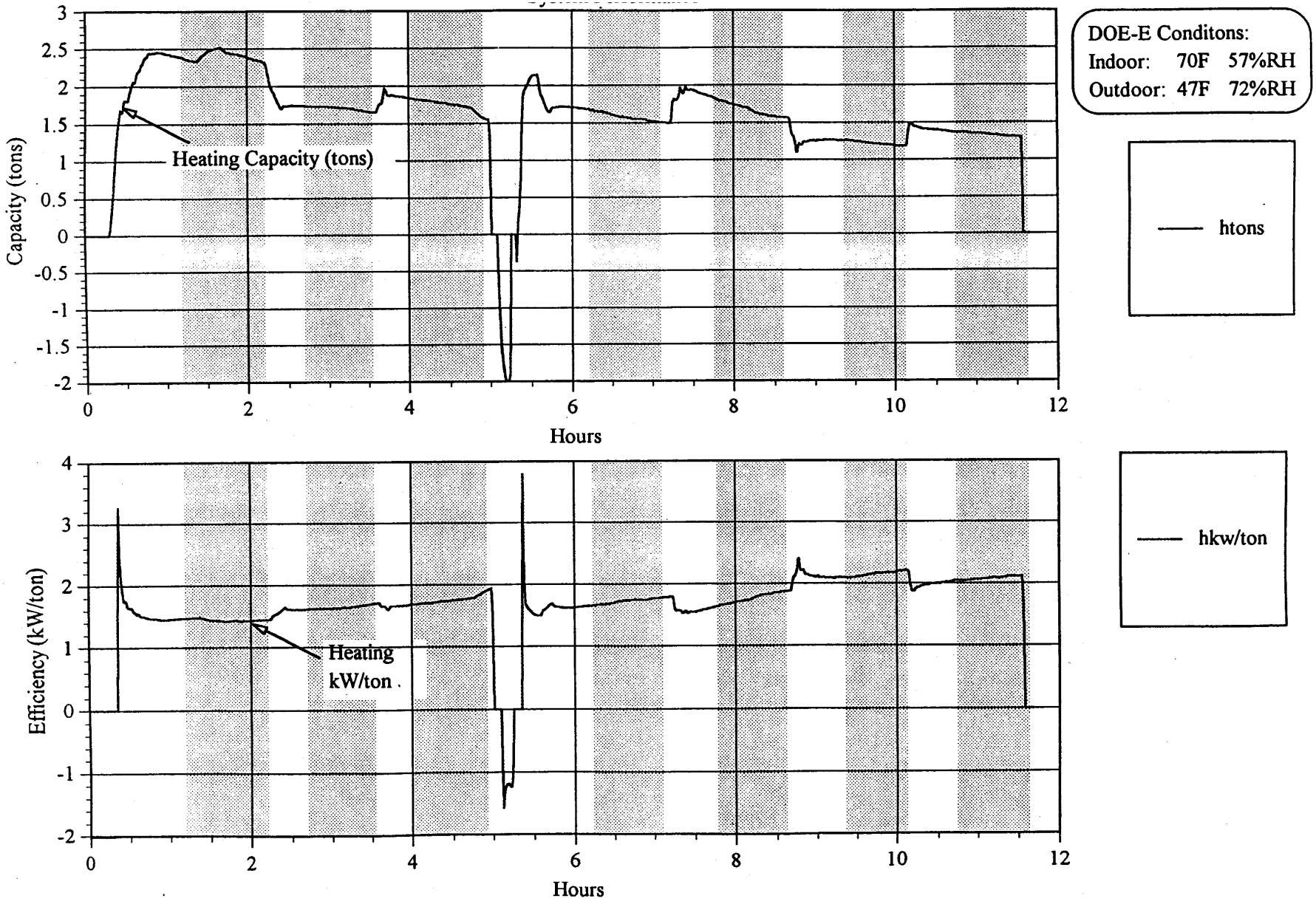

Fig. B.1.2-1 Heat Pump R407C Fractionation Test 2

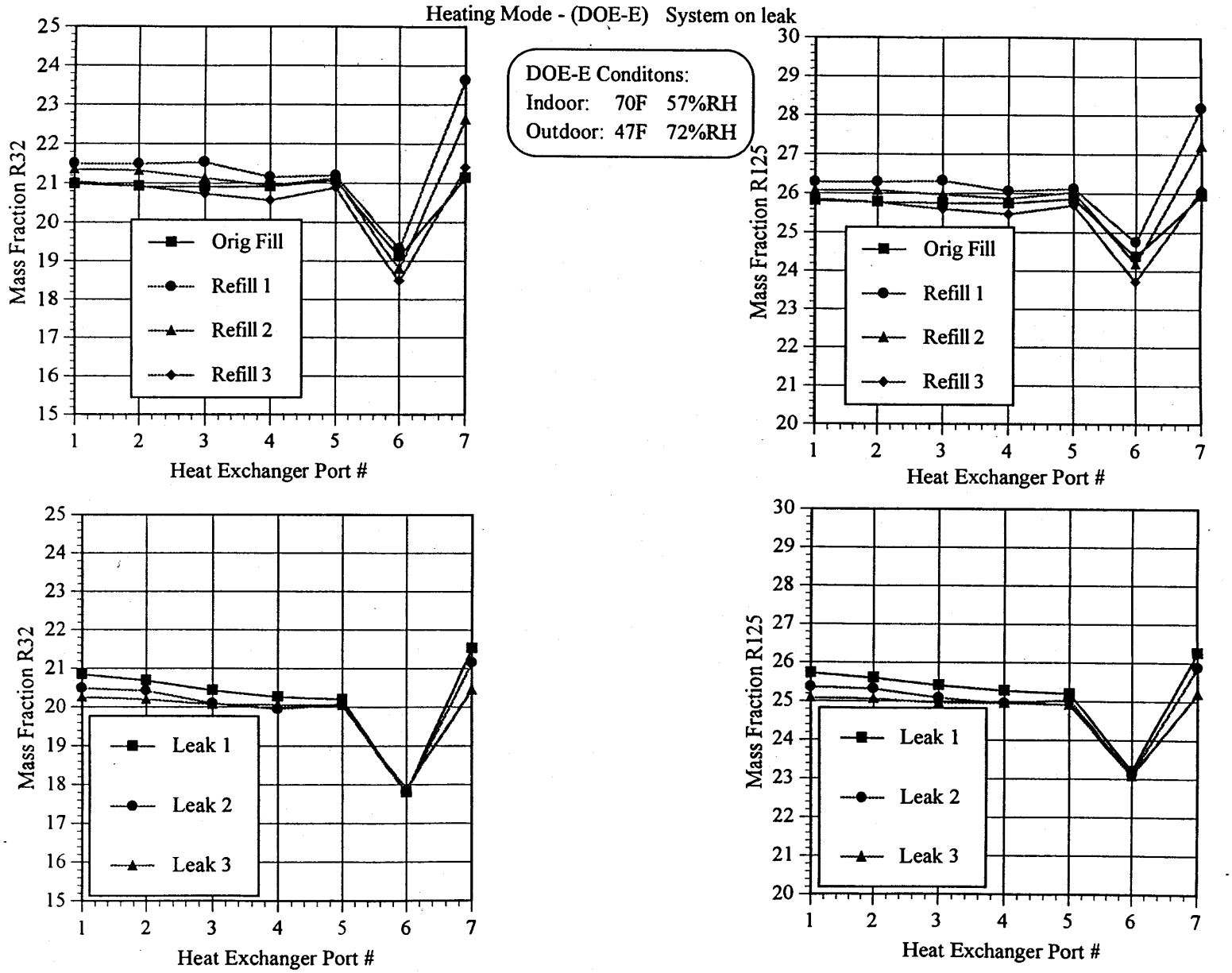

Fig. B.1.2-2 Heat Pump R407C Fractionation Test 2 & 4

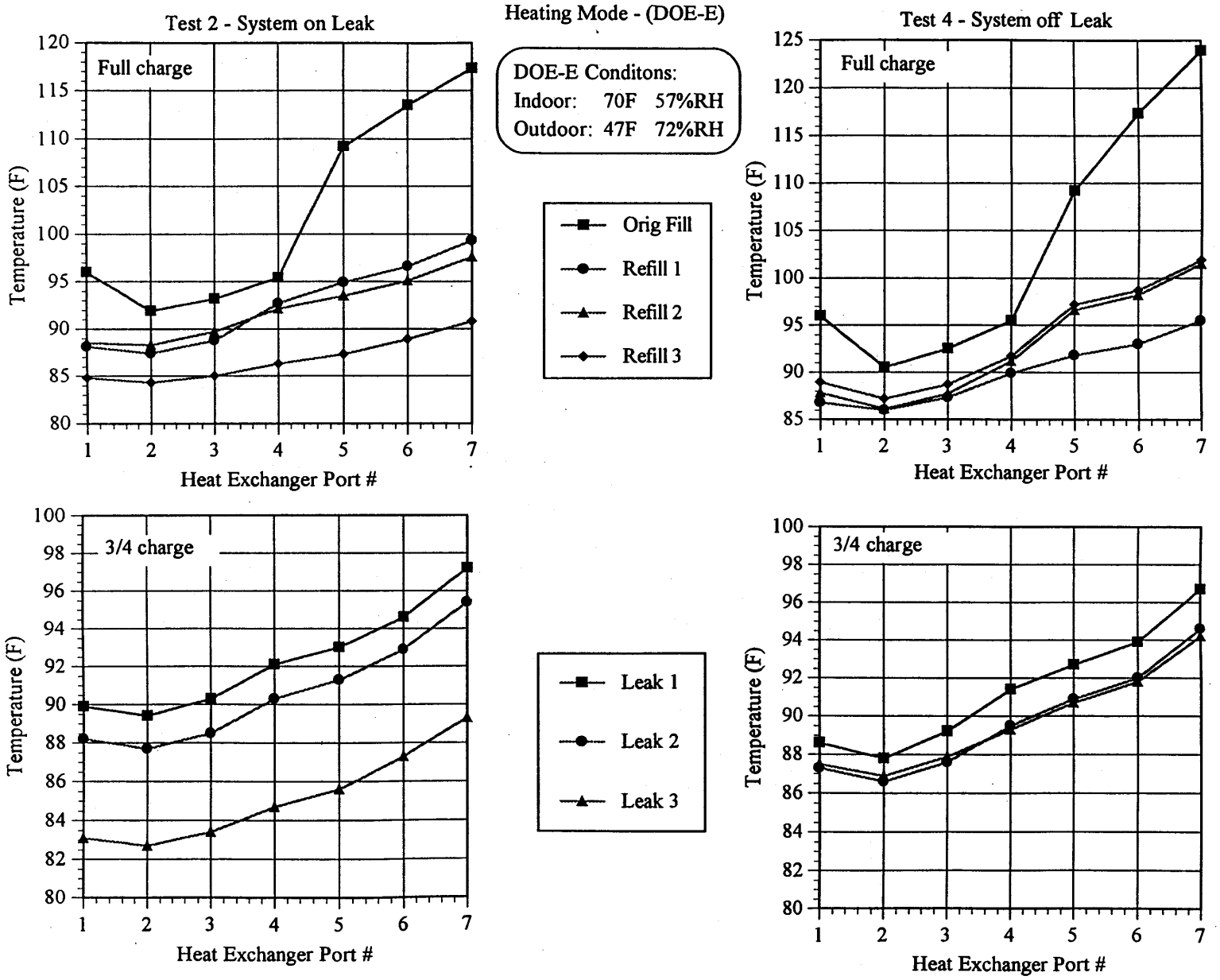

Table B.2-3. R407C - Test Data - Sequence #3

ARTI Run 3 (DOE A - System off leak)

Data Summaries:	start	finish	avg	time(se	POWE	SCALE	FLOW	ctons	htons	ckw/ton	hkw/ton
ART0627a	3693	6858	5276	5013	3907	-7	495	2.13	3.26	1.84	1.20
ART0627d	16363	19584	17974	17956	3350	51	107	1.52	2.57	2.20	1.31
ART0627e	21794	24914	23354	23517	3763	31	484	2.15	3.26	1.75	1.16
ART0627h	33591	37106	35349	35354	3251	49	-95	1.40	2.38	2.33	1.37
ART0627i	39578	42662	41120	41144	3731	47	476	2.06	3.22	1.81	1.16
ART0627l	52041	55041	53541	53526	3223	47	-96	1.36	2.31	2.37	1.40
ART0627m	57221	60233	58727	58746	3692	22	476	2.12	3.22	1.74	1.15

	TIE1	TIE2	TII1	TII2	TOE1	TOE2	TOI1	TOI2
ART0627a	57.9	56.5	78.5	79.1	106.6	107.8	91.7	92.5
ART0627d	62.1	61.1	78.6	79.1	102.3	103.3	90.6	91.2
ART0627e	57.6	56.5	78.5	79.1	105.6	106.7	90.7	91.5
ART0627h	63.6	62.6	78.6	79.1	101.3	102.2	90.5	91.1
ART0627i	58.1	57.1	78.6	79.2	105.8	106.9	91.1	91.9
ART0627l	63.9	62.8	78.4	79.0	101.3	102.3	90.9	91.4
ART0627m	57.7	56.6	78.5	79.0	105.9	106.9	91.1	92.0

	PS1	PS2	PS3	PS4	PS5	PS6
ART0627a	317.7	77.8	131.7	315.3	322.1	71.7
ART0627d	260.4	52.2	93.7	259.3	265.9	49.0
ART0627e	306.5	75.5	128.1	304.0	310.3	69.8
ART0627h	247.6	45.9	84.7	246.7	252.8	43.3
ART0627i	300.8	73.6	125.9	298.5	306.3	68.0
ART0627l	243.3	44.1	82.1	242.5	248.6	41.6
ART0627m	298.5	73.5	125.2	296.1	303.8	67.9

	TS1	TS2	TS3	TS4	TS5	TS6	TS7	TS8
ART0627a	191.9	50.2	68.7	109.4	186.4	53.4	55.2	124.4
ART0627d	224.4	73.8	53.1	108.5	214.6	79.6	81.0	135.9
ART0627e	192.1	50.3	68.2	108.6	186.4	57.2	58.9	122.4
ART0627h	228.8	74.3	49.9	106.8	217.8	80.7	82.0	137.0
ART0627i	191.5	49.7	68.1	109.0	185.8	56.5	58.2	122.3
ART0627l	229.5	74.1	49.2	106.3	218.5	81.0	82.2	138.0
ART0627m	191.9	50.6	68.0	108.6	186.5	58.9	60.5	122.1

	PX1	PX2	PX3	PX4	PX5	PX6	PX7
ART0627a	79.7	79.1	79.2	79.0	79.0	78.6	78.5
ART0627d	46.0	45.6	46.0	46.0	46.1	45.9	46.1
ART0627e	75.9	75.2	75.4	75.1	75.2	74.8	74.8
ART0627h	45.9	45.5	45.9	45.8	46.1	45.8	46.0
ART0627i	75.4	74.6	74.9	74.6	74.7	74.3	74.3
ART0627l	44.1	43.6	44.0	44.1	44.3	44.0	44.2
ART0627m	75.2	74.4	74.7	74.5	74.5	74.1	74.1

	TX1	TX2	TX3	TX4	TX5	TX6	TX7
ART0627a	46.7	49.5	48.9	49.1	50.9	57.6	65.3
ART0627d	32.2	56.2	63.1	68.3	71.8	70.9	72.9
ART0627e	46.5	49.8	49.4	49.6	55.9	62.5	68.2
ART0627h	32.2	56.3	63.2	68.4	71.9	71.0	72.9
ART0627i	46.2	49.5	49.2	49.4	57.8	63.3	68.7
ART0627l	31.4	56.8	63.3	68.6	71.9	70.9	72.8
ART0627m	46.1	49.2	48.8	49.0	51.1	60.0	66.6

Summary of ARTI Test Run #3: Cooling Mode operation at DOE-A with system off leak
THS 6/27/95

		STD1	STD2	P#1	P#2	P#3	P#4	STD1	STD2	Notes:
ART0627a	R32	21.05	0.07	21.95	21.55	21.60	19.91	21.05	0.05	System on; Full charge
	R125	25.68	74.75	26.71	26.31	26.35	25.06	25.69	74.74	
ART0627b	R32	21.05	0.05	22.65	23.47	21.73	29.70	21.06	0.05	System off; full charge
	R125	25.69	74.74	27.47	28.16	26.73	31.93	25.68	74.73	
ART0627c	R32	21.06	0.05	26.48	25.24	18.66	26.17	21.05	0.05	System off; 3/4 charge
	R125	25.68	74.73	30.57	28.64	24.23	30.31	25.68	74.75	
ART0627d	R32	21.05	0.05	19.54	20.38	20.37	17.53	20.99	0.05	System on; 3/4 charge
	R125	25.68	74.75	24.68	25.28	25.26	22.88	25.61	74.43	
ART0627e	R32	20.99	0.05	20.75	20.70	20.74	19.12	21.03	0.05	System on; refilled to full charge
	R125	25.61	74.43	25.78	25.62	25.65	24.35	25.66	74.17	
ART0627f	R32	21.03	0.05	22.20	21.92	20.08	27.89	21.12	0.05	System off; full charge
	R125	25.66	74.17	27.90	26.99	25.37	30.92	25.74	74.51	
ART0627g	R32	21.12	0.05	25.68	20.50	17.96	25.32	21.03	0.08	System off; 3/4 charge
	R125	25.74	74.51	30.28	24.94	23.44	29.89	25.65	74.36	
ART0627h	R32	21.03	0.08	19.07	19.39	19.39	16.39	20.94	0.09	System on; 3/4 charge
	R125	25.65	74.36	24.55	24.46	24.40	21.77	25.56	74.30	
ART0627i	R32	20.94	0.09	20.06	20.11	20.02	18.37	21.03	0.10	System on; refilled to full charge
	R125	25.56	74.30	25.52	25.08	24.97	23.62	25.66	74.19	
ART0627j	R32	21.03	0.10	22.27	21.76	20.01	28.37	21.05	0.05	System off; full charge
	R125	25.66	74.19	27.61	26.80	25.19	31.12	25.67	74.38	
ART0627k	R32	21.05	0.05	23.91	20.32	16.75	23.59	21.03	0.05	System off; 3/4 charge
	R125	25.67	74.38	29.05	24.59	22.31	28.30	25.64	74.42	
ART0627l	R32	21.03	0.05	18.32	18.61	18.64	15.53	20.96	0.05	System on; 3/4 charge
	R125	25.64	74.42	23.87	23.78	23.71	20.89	25.57	74.45	
ART0627m	R32	20.96	0.05	19.46	19.57	19.52	17.87	20.96	0.05	System on; refilled to full charge
	R125	25.57	74.45	24.96	24.64	24.51	23.13	25.57	74.45	
ART0628a	R32	21.06	0.06	26.50	23.07	22.78	27.12	21.03	0.05	System off; full
	R125	25.67	74.78	30.34	27.46	27.14	30.75	25.65	74.71	

- more than 2% deviation in calculated compositions

		HX1	HX2	HX3	HX4	HX5	HX6	HX7	wt(lbs)	
ART0627a	R32	17.08	16.43	16.13	17.87	22.08	21.63	21.64	6.53	=charge weight (lbs)
	R125	22.55	21.82	21.47	22.93	26.79	26.36	26.37	6.53	System on; Full charge
ART0627d	R32	14.84	20.41	20.40	20.43	20.42	20.43	20.43	1.52	=charge removed (lbs)
	R125	19.98	25.28	25.26	25.29	25.27	25.28	25.29	5.01	System on; 3/4 charge
ART0627e	R32	16.53	16.00	15.57	18.13	20.96	20.82	20.84	1.75	=charge added (lbs)
	R125	21.99	21.35	20.83	23.12	25.78	25.63	25.65	6.76	System on; refilled to full charge
ART0627h	R32	16.15	19.41	19.37	19.45	19.45	19.45	19.46	1.68	=charge removed (lbs)
	R125	21.10	24.36	24.32	24.39	24.39	24.39	24.39	5.08	System on; 3/4 charge
ART0627i	R32	15.91	15.18	14.44	19.86	20.09	20.14	20.14	1.95	=charge added (lbs)
	R125	21.31	20.47	19.64	24.75	24.96	25.01	25.02	7.03	System on; refilled to full charge
ART0627l	R32	15.77	18.67	18.69	18.71	18.74	18.73	18.77	1.73	=charge removed (lbs)
	R125	20.70	23.67	23.68	23.71	23.73	23.72	23.77	5.3	System on; 3/4 charge
ART0627m	R32	15.12	14.52	15.01	17.43	19.69	19.63	19.65	1.99	=charge added (lbs)
	R125	20.54	19.82	20.19	22.43	24.61	24.54	24.56	7.29	System on; refilled to full charge

Summary of ARTI Test Run #3: Cooling Mode operation at DOE-A with system off leak
THS 6/27/95

		STD1	STD2	P#1	P#2	P#3	P#4	STD1	STD2	Notes:
ART0627a	R32	21.05	0.07	21.95	21.55	21.60	19.91	21.05	0.05	System on; Full charge
	R125	25.68	74.75	26.71	26.31	26.35	25.06	25.69	74.74	
ART0627b	R32	21.05	0.05	22.65	23.47	21.73	29.70	21.06	0.05	System off; full charge
	R125	25.69	74.74	27.47	28.16	26.73	31.93	25.68	74.73	
ART0627c	R32	21.06	0.05	26.48	25.24	18.66	26.17	21.05	0.05	System off; 3/4 charge
	R125	25.68	74.73	30.57	28.64	24.23	30.31	25.68	74.75	
ART0627d	R32	21.05	0.05	19.54	20.38	20.37	17.53	20.99	0.05	System on; 3/4 charge
	R125	25.68	74.75	24.68	25.28	25.26	22.88	25.61	74.43	
ART0627e	R32	20.99	0.05	20.75	20.70	20.74	19.12	21.03	0.05	System on; refilled to full charge
	R125	25.61	74.43	25.78	25.62	25.65	24.35	25.66	74.17	
ART0627f	R32	21.03	0.05	22.20	21.92	20.08	27.89	21.12	0.05	System off; full charge
	R125	25.66	74.17	27.90	26.99	25.37	30.92	25.74	74.51	
ART0627g	R32	21.12	0.05	25.68	20.50	17.96	25.32	21.03	0.08	System off; 3/4 charge
	R125	25.74	74.51	30.28	24.94	23.44	29.89	25.65	74.36	
ART0627h	R32	21.03	0.08	19.07	19.39	19.39	16.39	20.94	0.09	System on; 3/4 charge
	R125	25.65	74.36	24.55	24.46	24.40	21.77	25.56	74.30	
ART0627i	R32	20.94	0.09	20.06	20.11	20.02	18.37	21.03	0.10	System on; refilled to full charge
	R125	25.56	74.30	25.52	25.08	24.97	23.62	25.66	74.19	
ART0627j	R32	21.03	0.10	22.27	21.76	20.01	28.37	21.05	0.05	System off; full charge
	R125	25.66	74.19	27.61	26.80	25.19	31.12	25.67	74.38	
ART0627k	R32	21.05	0.05	23.91	20.32	16.75	23.59	21.03	0.05	System off; 3/4 charge
	R125	25.67	74.38	29.05	24.59	22.31	28.30	25.64	74.42	
ART0627l	R32	21.03	0.05	18.32	18.61	18.64	15.53	20.96	0.05	System on; 3/4 charge
	R125	25.64	74.42	23.87	23.78	23.71	20.89	25.57	74.45	
ART0627m	R32	20.96	0.05	19.46	19.57	19.52	17.87	20.96	0.05	System on; refilled to full charge
	R125	25.57	74.45	24.96	24.64	24.51	23.13	25.57	74.45	
ART0628a	R32	21.06	0.06	26.50	23.07	22.78	27.12	21.03	0.05	System off; full
	R125	25.67	74.78	30.34	27.46	27.14	30.75	25.65	74.71	

- more than 2% deviation in calculated compositions

		HX1	HX2	HX3	HX4	HX5	HX6	HX7	wt(lbs)	
ART0627a	R32	17.08	16.43	16.13	17.87	22.08	21.63	21.64	6.53	=charge weight (lbs)
	R125	22.55	21.82	21.47	22.93	26.79	26.36	26.37	6.53	System on; Full charge
ART0627d	R32	14.84	20.41	20.40	20.43	20.42	20.43	20.43	1.52	=charge removed (lbs)
	R125	19.98	25.28	25.26	25.29	25.27	25.28	25.29	5.01	System on; 3/4 charge
ART0627e	R32	16.53	16.00	15.57	18.13	20.96	20.82	20.84	1.75	=charge added (lbs)
	R125	21.99	21.35	20.83	23.12	25.78	25.63	25.65	6.76	System on; refilled to full charge
ART0627h	R32	16.15	19.41	19.37	19.45	19.45	19.45	19.46	1.68	=charge removed (lbs)
	R125	21.10	24.36	24.32	24.39	24.39	24.39	24.39	5.08	System on; 3/4 charge
ART0627i	R32	15.91	15.18	14.44	19.86	20.09	20.14	20.14	1.95	=charge added (lbs)
	R125	21.31	20.47	19.64	24.75	24.96	25.01	25.02	7.03	System on; refilled to full charge
ART0627l	R32	15.77	18.67	18.69	18.71	18.74	18.73	18.77	1.73	=charge removed (lbs)
	R125	20.70	23.67	23.68	23.71	23.73	23.72	23.77	5.3	System on; 3/4 charge
ART0627m	R32	15.12	14.52	15.01	17.43	19.69	19.63	19.65	1.99	=charge added (lbs)
	R125	20.54	19.82	20.19	22.43	24.61	24.54	24.56	7.29	System on; refilled to full charge

Test 3 (6/27/95)

Sample Port #1 : Liquid from Condenser Exit
Sample Port #2 : Compressor Discharge
Sample Port #3 : Accumulator
Sample Port #4 : Liquid or 2 phase from Evaporator Inlet

		Liquid %		Vapor %		Total %					
Disch	wt (lbs	R32	R125	R32	R125	R32	R125	Recha	wt(lbs)	R32	R125
#1	1.52	16.28	21.58	27.41	31.67	22.72	27.42	#1	1.75	20.43	25.31
#2	1.68	16.74	22.02	27.41	31.67	22.29	27.05	#2	1.95	20.43	25.31
#3	1.73	17.81	23.41	29.54	33.82	23.92	28.84	#3	1.99	20.43	25.31

charge composition

	R32	R125	R134a
startup	20.43	25.31	54.26
after d	19.7	24.7	55.61
after r	19.9	24.8	55.26
after d	19.11	24.09	56.8
after r	19.48	24.43	56.09
after d	18	22.97	59.03
after r	18.67	23.61	57.72

circulating composition

	R32	R125	R134a
startup	21.7	26.45	51.85
after d	20.09	25.07	54.83
after r	20.73	25.68	53.59
after d	19.28	24.47	56.25
after r	20.06	25.19	54.75
after d	18.52	23.78	57.69
after r	19.52	24.7	55.78

Fig. B.1.2-15 Heat Pump R407C Fractionation Test 3

Cooling Mode - (DOE-A) System off leak

System Temperatures

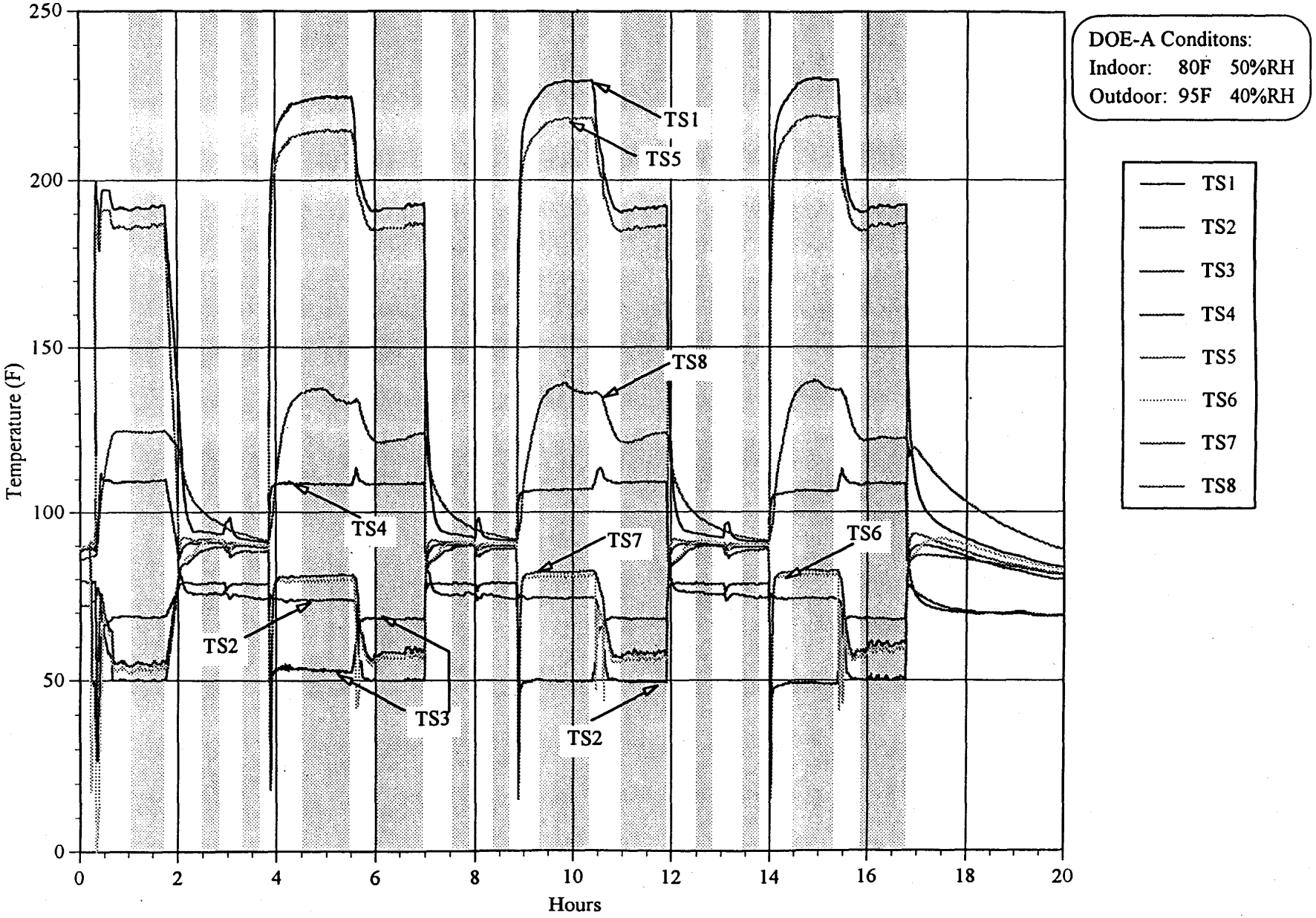

Fig. B.1.2-16 Heat Pump R407C Fractionation Test 3

Cooling Mode - (DOE-A) System off leak

System Pressures

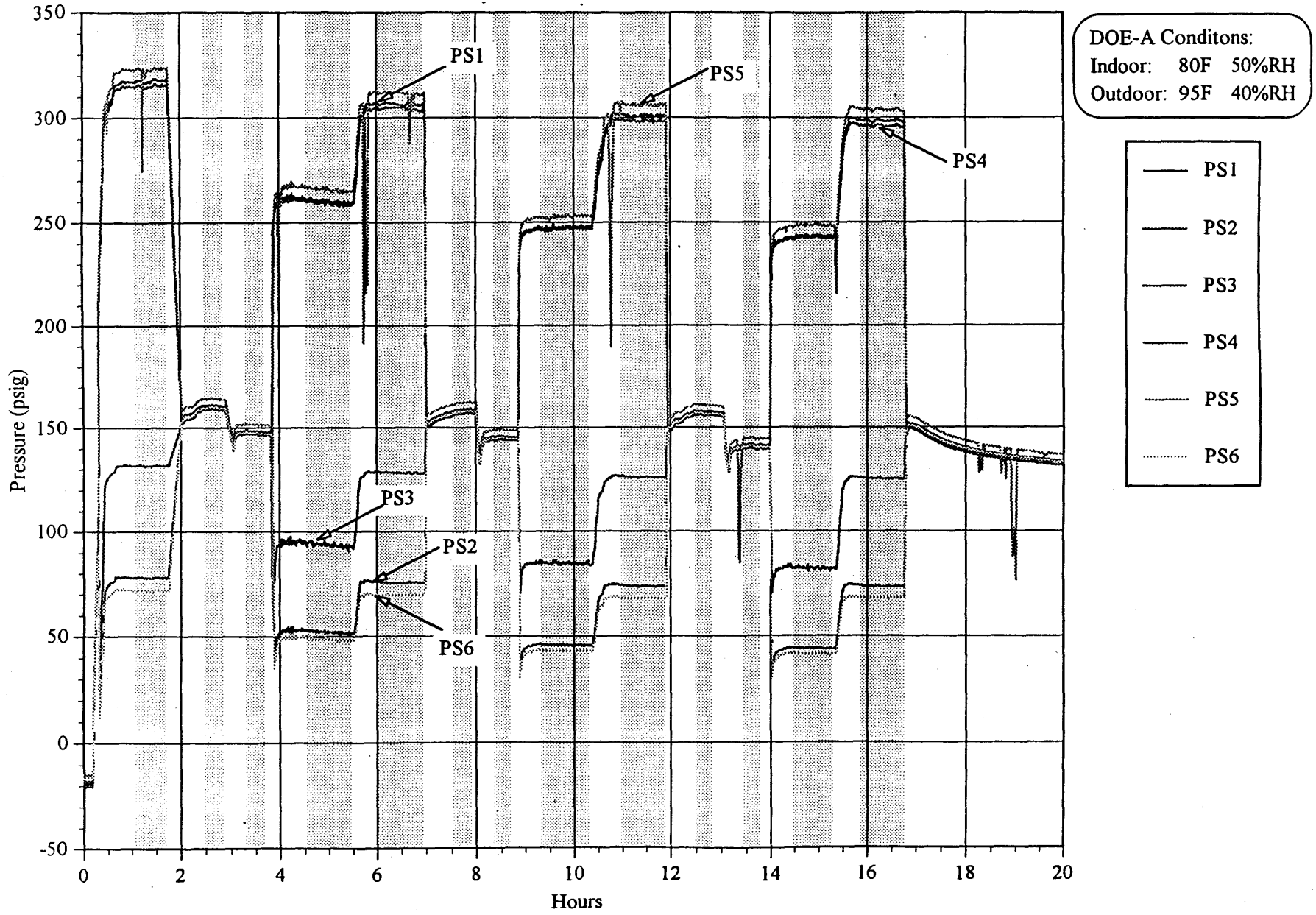

Fig. B.1.2-17 Heat Pump R407C Fractionation Test 3

Cooling Mode - (DOE-A) System off leak

Heat Exchanger Pressures

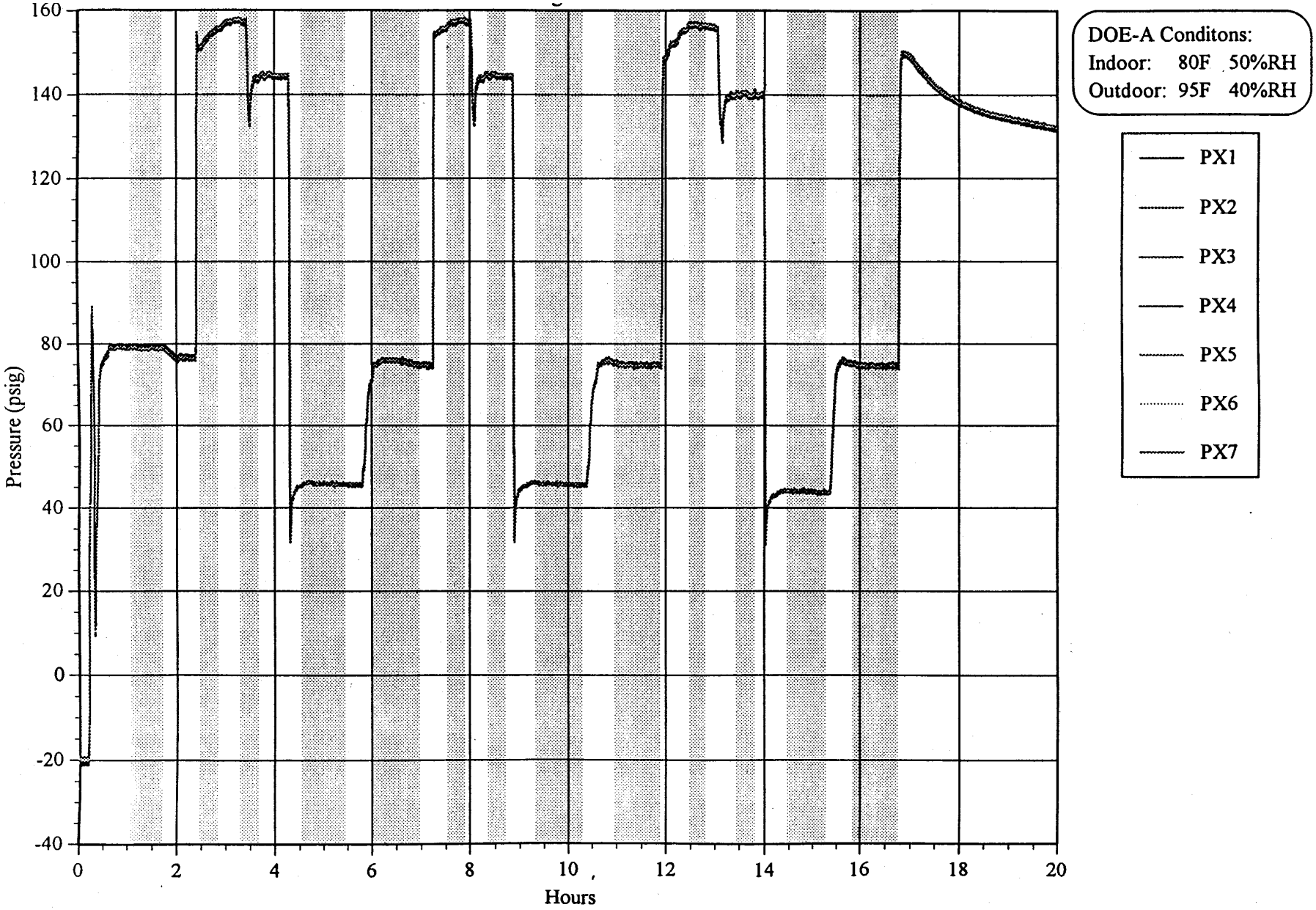

Fig. B.1.2-18 Heat Pump R407C Fractionation Test 3

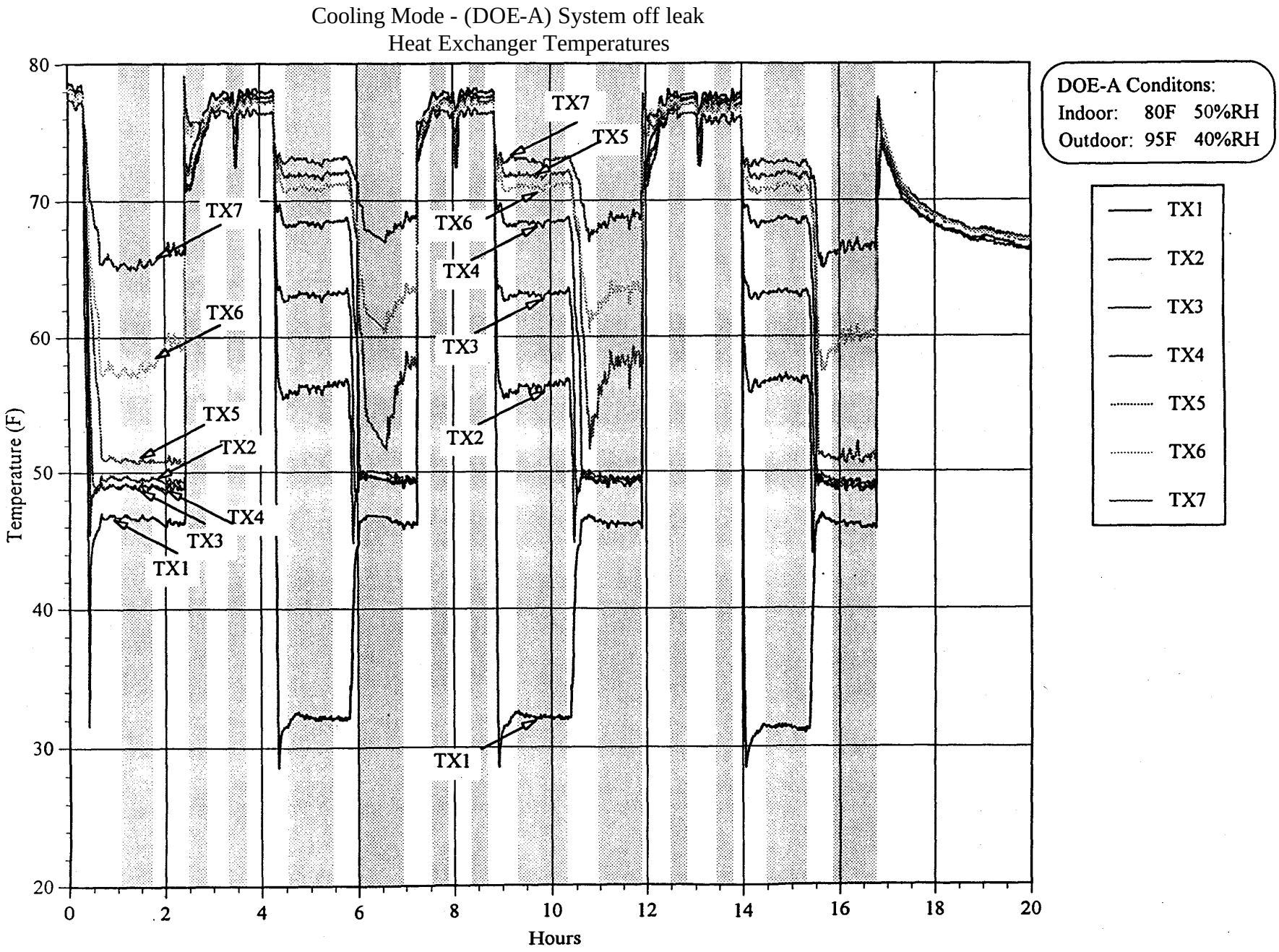

Fig. B.1.2-19 Heat Pump R407C Fractionation Test 3

Cooling Mode - (DOE-A) System off leak

Air Side Temperatures

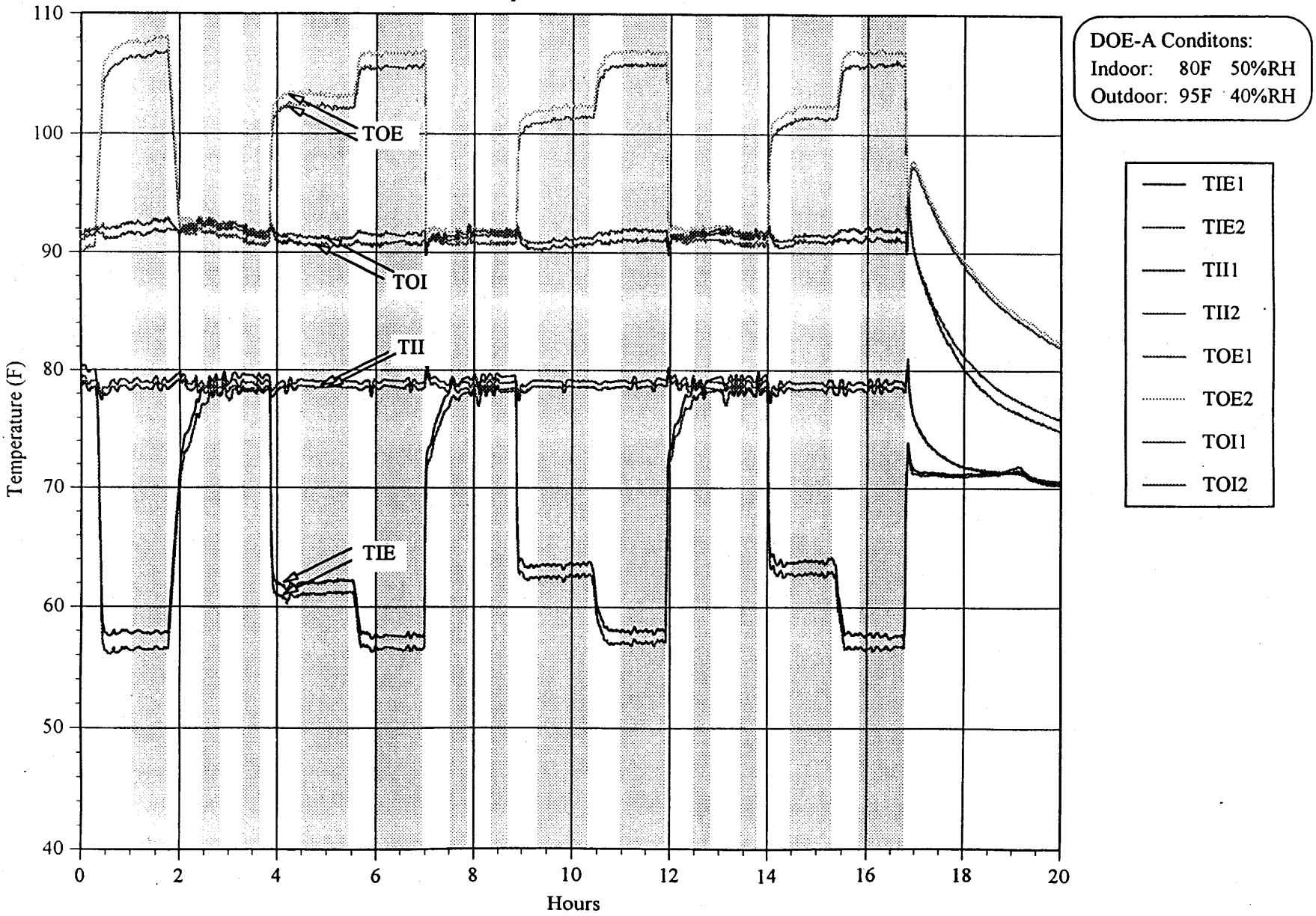

Fig. B.1.2-3 Heat Pump R407C Fractionation Test 3

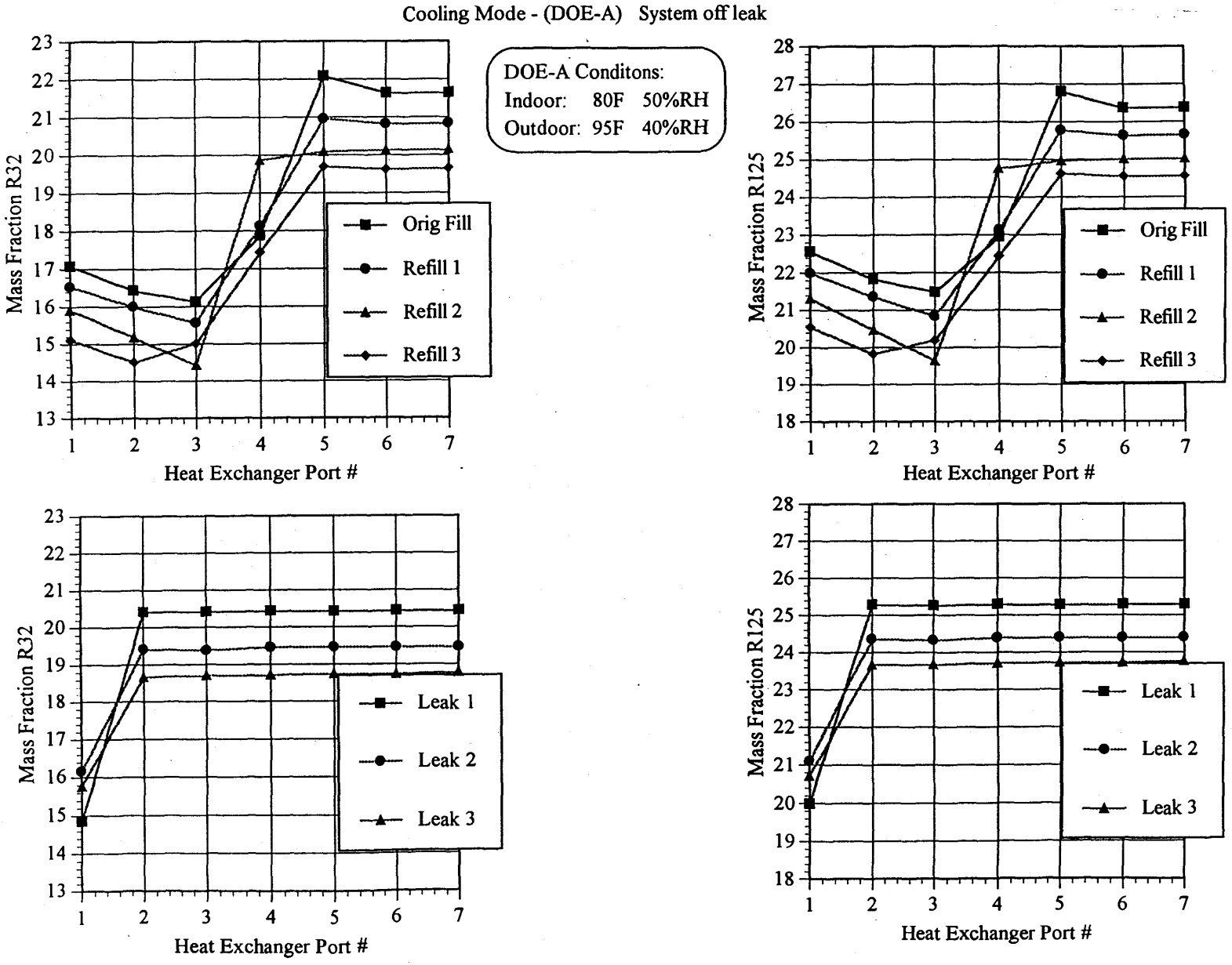

Table B.2-4. R407C - Test Data - Sequence #4

ARTI Run 4 (DOE E - System off leak)

Data Summaries:	start	finish	avg	time(sec	POWER	SCALE	FLOW	htons	hkw/ton
ART0629a	2665	5670	4168	4143	3903	58	-96	2.56	1.52
ART0629d	13458	16464	14961	14804	2893	47	-96	1.69	1.71
ART0629e	18854	21943	20399	20326	3074	33	-95	1.62	1.91
ART0629h	30612	33715	32164	32167	2731	22	-92	1.59	1.72
ART0629i	35922	39238	37580	37597	3090	56	-96	1.83	1.69
ART0629l	47762	50821	49292	49009	2678	6	-89	1.58	1.70
ART0629m	53019	56165	54592	54597	3062	19	-96	1.84	1.67

	TIE1	TIE2	TII1	TII2	TOE1	TOE2	TOI1	TOI2
ART0629a	97.2	96.8	68.3	69.0	41.6	41.5	45.6	45.7
ART0629d	87.6	87.1	68.3	68.9	43.7	44.1	45.7	46.1
ART0629e	86.8	86.1	68.2	68.9	44.8	45.3	45.8	46.2
ART0629h	86.4	85.7	68.2	68.8	44.2	44.7	45.9	46.3
ART0629i	89.2	88.2	68.1	68.8	44.4	44.8	46.0	46.5
ART0629l	86.6	85.2	68.1	68.7	44.3	45.1	46.3	46.8
ART0629m	89.5	88.2	68.2	68.7	44.4	45.0	46.3	46.7

	PS1	PS2	PS3	PS4	PS5	PS6
ART0629a	316.0	317.1	310.6	71.0	48.5	43.5
ART0629d	199.7	200.0	195.7	40.1	26.3	22.6
ART0629e	208.1	208.1	204.1	39.8	24.1	20.4
ART0629h	180.4	180.7	176.6	35.9	22.9	19.5
ART0629i	214.7	214.9	210.6	43.9	28.0	24.1
ART0629l	173.7	173.9	169.8	33.5	21.2	17.8
ART0629m	210.3	210.5	206.3	43.0	27.3	23.5

	TS1	TS2	TS3	TS4	TS5	TS6	TS7	TS8
ART0629a	206.2	185.3	98.4	37.1	40.8	35.7	36.2	84.3
ART0629d	203.4	172.4	88.1	16.7	42.5	46.5	46.5	79.2
ART0629e	169.5	142.4	86.7	14.4	4.5	3.2	4.6	69.3
ART0629h	198.8	167.4	87.3	16.8	43.6	47.0	47.1	80.7
ART0629i	177.9	152.4	88.1	21.5	12.0	13.7	14.1	70.9
ART0629l	198.9	166.8	87.5	17.1	44.1	47.6	47.6	81.3
ART0629m	178.2	153.0	89.0	22.6	12.9	15.1	15.6	72.1

	PX1	PX2	PX3	PX4	PX5	PX6	PX7
ART0629a	313.9	313.6	314.2	313.6	314.0	314.0	314.0
ART0629d	197.1	196.7	197.4	197.2	197.7	197.7	197.9
ART0629e	205.5	205.3	205.9	205.6	206.2	206.1	206.4
ART0629h	177.9	177.6	178.3	178.0	178.6	178.6	178.9
ART0629i	212.3	212.0	212.6	212.1	212.8	212.8	212.9
ART0629l	171.0	170.7	171.4	171.2	171.7	171.7	172.0
ART0629m	207.8	207.5	208.1	207.7	208.3	208.3	208.5

	TX1	TX2	TX3	TX4	TX5	TX6	TX7
ART0629a	96.0	90.5	92.5	95.5	109.2	117.3	123.9
ART0629d	88.6	87.8	89.2	91.4	92.7	93.9	96.7
ART0629e	86.8	86.0	87.3	89.9	91.8	93.0	95.5
ART0629h	87.3	86.6	87.6	89.5	90.9	92.0	94.6
ART0629i	87.8	86.1	87.7	91.2	96.6	98.2	101.5
ART0629l	87.5	86.9	87.9	89.3	90.7	91.8	94.2
ART0629m	88.9	87.2	88.7	91.7	97.2	98.7	101.9

Summary of ARTI Test Run #4: Heating Mode operation at DOE-E with system off leak
THS 6/29/95

		STD1	STD2	P#1	P#2	P#3	P#4	STD1	STD2	Notes:
ART0629a	R32	21.06	0.05	29.00	21.04	20.99	21.02	21.06	0.05	System on; Full charge
	R125	25.67	74.79	32.31	25.88	25.83	25.87	25.68	74.81	
ART0629b	R32	21.06	0.05	20.80	21.35	28.62	11.33	21.06	0.05	System off; full charge
	R125	25.68	74.81	25.64	26.39	31.83	16.84	25.67	74.75	
ART0629c	R32	21.06	0.05	18.28	27.86	20.90	23.10	21.05	0.05	System off; 3/4 charge
	R125	25.67	74.75	23.60	31.48	26.15	27.63	25.66	74.78	
ART0629d	R32	21.05	0.05	24.94	20.15	20.24	20.13	21.05	0.05	System on; 3/4 charge
	R125	25.66	74.78	29.33	25.19	25.28	25.18	25.65	74.78	
ART0629e	R32	21.05	0.05	26.15	21.26	16.02	22.12	21.06	0.06	System on; refilled to full charge
	R125	25.65	74.78	30.24	26.21	20.74	27.06	25.67	74.77	
ART0629f	R32	21.06	0.06	22.47	33.01	14.20	24.24	21.06	0.05	System off; full charge
	R125	25.67	74.77	28.24	34.84	19.20	29.10	25.67	74.76	
ART0629g	R32	21.06	0.05	20.68	24.10	13.67	22.68	21.06	0.08	System off; 3/4 charge
	R125	25.67	74.76	27.09	29.81	18.67	28.75	25.67	74.73	
ART0629h	R32	21.06	0.08	21.76	16.69	16.77	16.65	21.04	0.12	System on; 3/4 charge
	R125	25.67	74.73	26.98	22.13	22.23	22.10	25.65	74.73	
ART0629i	R32	21.04	0.12	23.59	18.15	18.05	18.23	21.06	0.13	System on; refilled to full charge
	R125	25.65	74.73	28.24	23.36	23.28	23.44	25.66	74.74	
ART0629j	R32	21.06	0.13	29.13	27.36	10.87	18.37	21.06	0.13	System off; full charge
	R125	25.66	74.74	32.56	31.29	15.35	23.57	25.67	74.75	
ART0629k	R32	21.06	0.13	20.83	23.36	15.18	19.82	21.06	0.13	System off; 3/4 charge
	R125	25.67	74.75	25.75	28.73	20.49	25.96	25.65	74.75	
ART0629l	R32	21.06	0.13	20.15	15.51	15.59	15.48	21.05	0.13	System on; 3/4 charge
	R125	25.65	74.75	25.42	20.90	20.98	20.87	25.65	74.75	
ART0629m	R32	21.05	0.13	20.25	17.47	16.95	17.57	21.06	0.13	System on; refilled to full charge
	R125	25.65	74.75	25.18	22.63	22.16	22.71	25.65	74.75	
ART0630a	R32	21.07	0.05	24.14	15.53	11.85	22.34	21.05	0.09	System off; full
	R125	25.65	74.80	28.96	21.17	16.24	26.72	25.66	74.74	

- more than 2% deviation in calculated compositions

		HX1	HX2	HX3	HX4	HX5	HX6	HX7	wt(lbs)	
ART0629a	R32	21.02	21.74	20.97	20.98	20.99	19.61	21.87	7.57	=charge weight (lbs)
	R125	25.87	26.48	25.82	25.88	25.84	24.80	26.54	7.57	System on; Full charge
ART0629d	R32	20.11	24.73	19.71	19.36	19.42	16.87	20.79	1.87	=charge removed (lbs)
	R125	25.17	29.28	24.88	24.72	24.60	22.42	25.73	5.7	System on; 3/4 charge
ART0629e	R32	22.17	22.49	22.10	21.78	22.92	20.18	23.98	1.675	=charge added (lbs)
	R125	27.12	27.47	27.21	27.06	27.93	25.77	28.71	7.375	System on; refilled to full charge
ART0629h	R32	16.46	21.93	16.46	15.92	16.11	13.50	17.16	1.925	=charge removed (lbs)
	R125	21.96	27.01	21.95	21.48	21.63	19.14	22.58	5.45	System on; 3/4 charge
ART0629i	R32	18.30	18.47	18.53	18.46	18.36	16.51	20.26	2.35	=charge added (lbs)
	R125	23.52	23.68	23.75	23.71	23.68	22.18	25.43	7.8	System on; refilled to full charge
ART0629l	R32	15.34	15.19	14.81	14.63	14.86	12.71	15.75	1.92	=charge removed (lbs)
	R125	20.75	20.62	20.28	20.11	20.29	18.18	21.11	5.88	System on; 3/4 charge
ART0629m	R32	17.61	17.81	17.87	17.77	17.93	15.84	19.71	2.495	=charge added (lbs)
	R125	22.77	22.97	23.03	22.97	23.21	21.46	24.85	8.375	System on; refilled to full charge

Test 4 (6/29/95)

Sample Port #1 : Liquid from Condenser Exit
Sample Port #2 : Compressor Discharge
Sample Port #3 : Accumulator
Sample Port #4 : Liquid or 2 phase from Evaporator Inlet

		Liquid %		Vapor %		Total %					
Disch	wt (lbs	R32	R125	R32	R125	R32	R125	Recha	wt(lbs)	R32	R125
#1	1.87	18.02	23.02	27.98	31.68	22.91	27.27	#1	1.675	20.43	25.31
#2	1.93	22.53	27.94	33.94	36.69	28.41	32.45	#2	2.35	20.43	25.31
#3	1.92	17.8	23.41	29.54	33.82	23.56	28.52	#3	2.495	20.43	25.31

charge composition

	R32	R125	R134a
startup	20.43	25.31	54.26
after d	19.6	24.7	55.72
after r	19.8	24.8	55.39
after d	16.72	22.09	61.19
after r	17.84	23.06	59.1
after d	15.95	21.25	62.8
after r	17.29	22.46	60.25

circulating composition

	R32	R125	R134a
startup	21.01	25.86	53.12
after d	20.17	25.21	54.61
after r	21.69	26.64	51.68
after d	16.7	22.16	61.14
after r	18.14	23.36	58.5
after d	15.53	20.92	63.55
after r	17.33	22.5	60.17

Fig. B.1.2-20 Heat Pump R407C Fractionation Test 4

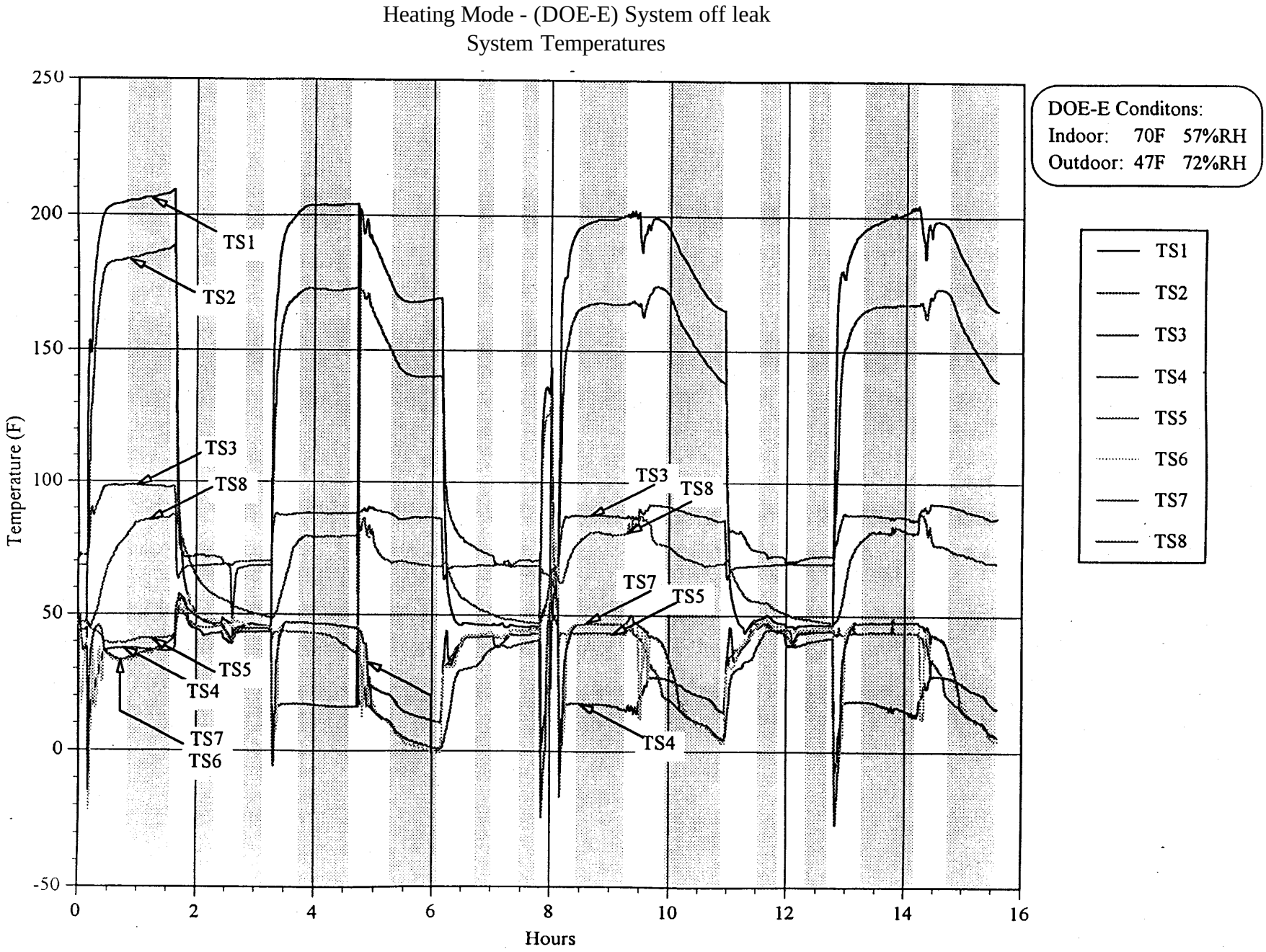

Fig. B.1.2-21Heat Pump R407C Fractionation Test 4

Heating Mode - (DOE-E) System off leak

System Pressures

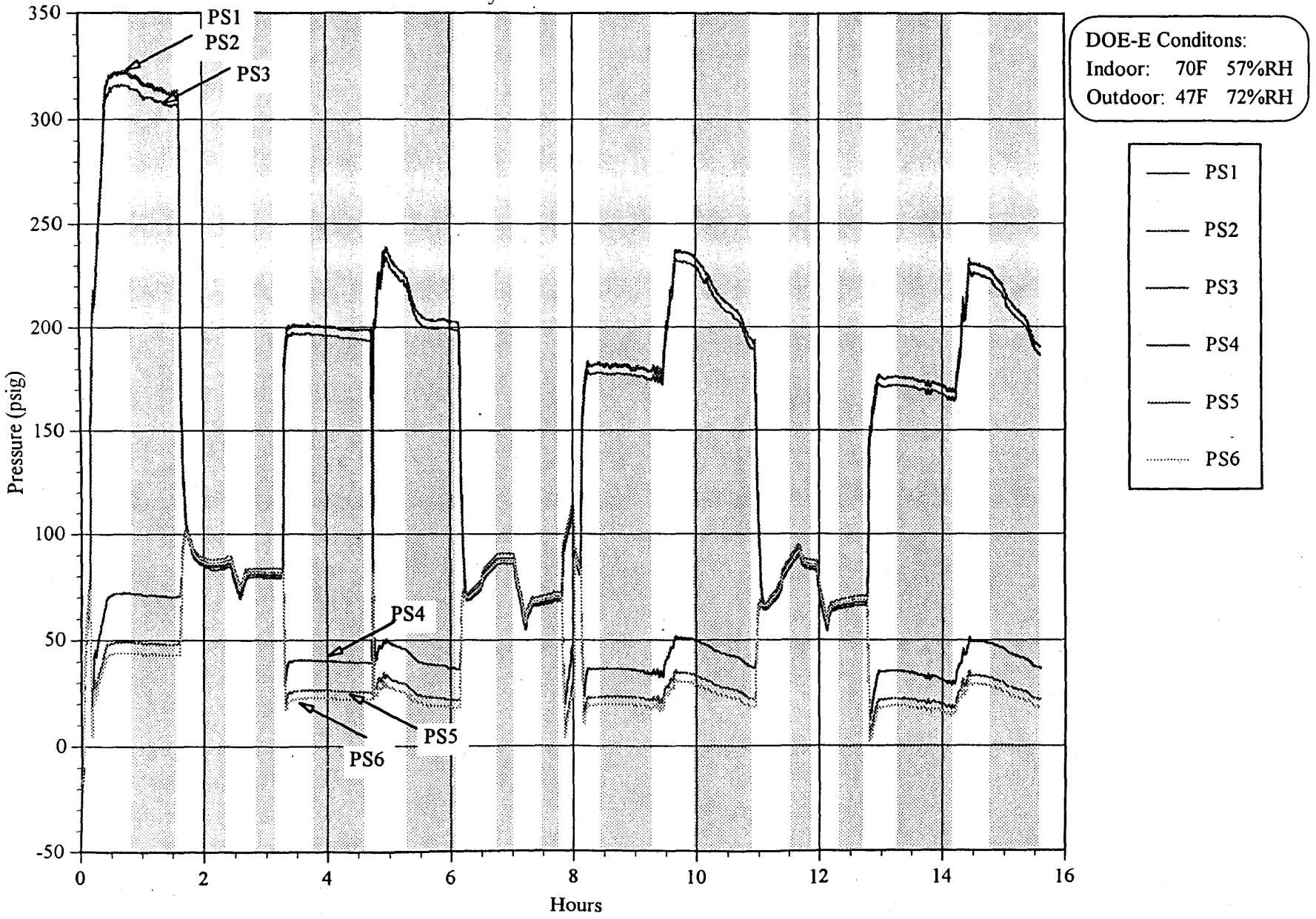

Fig. B.1.2-22 Heat Pump R407C Fractionation Test 4

Heating Mode - (DOE-E) System off leak

Heat Exchanger Temperatures

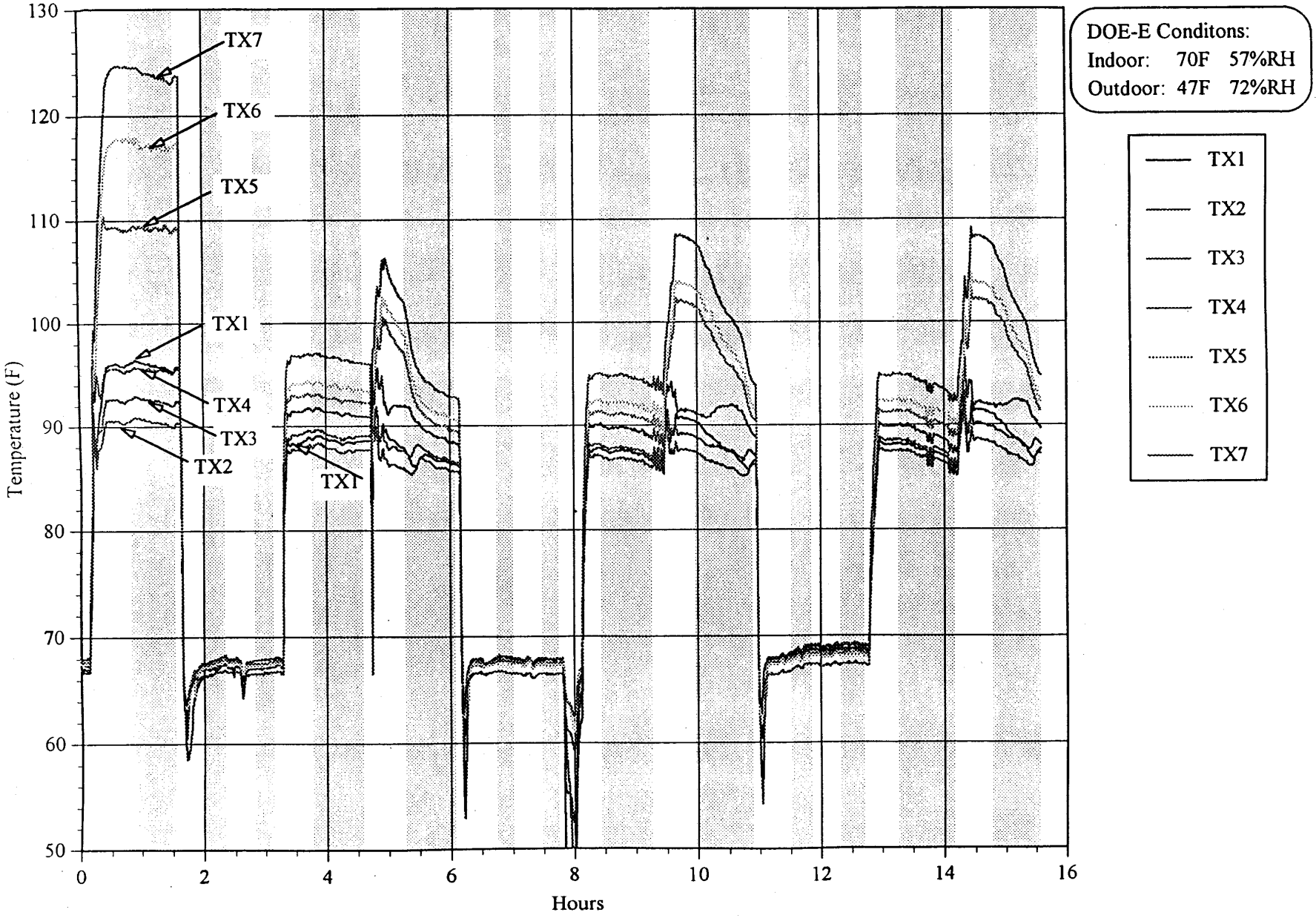

Fig. B.1.2-23 Heat Pump R407C Fractionation Test 4

Heating Mode - (DOE-E) System off leak

Heat Exchanger Pressures

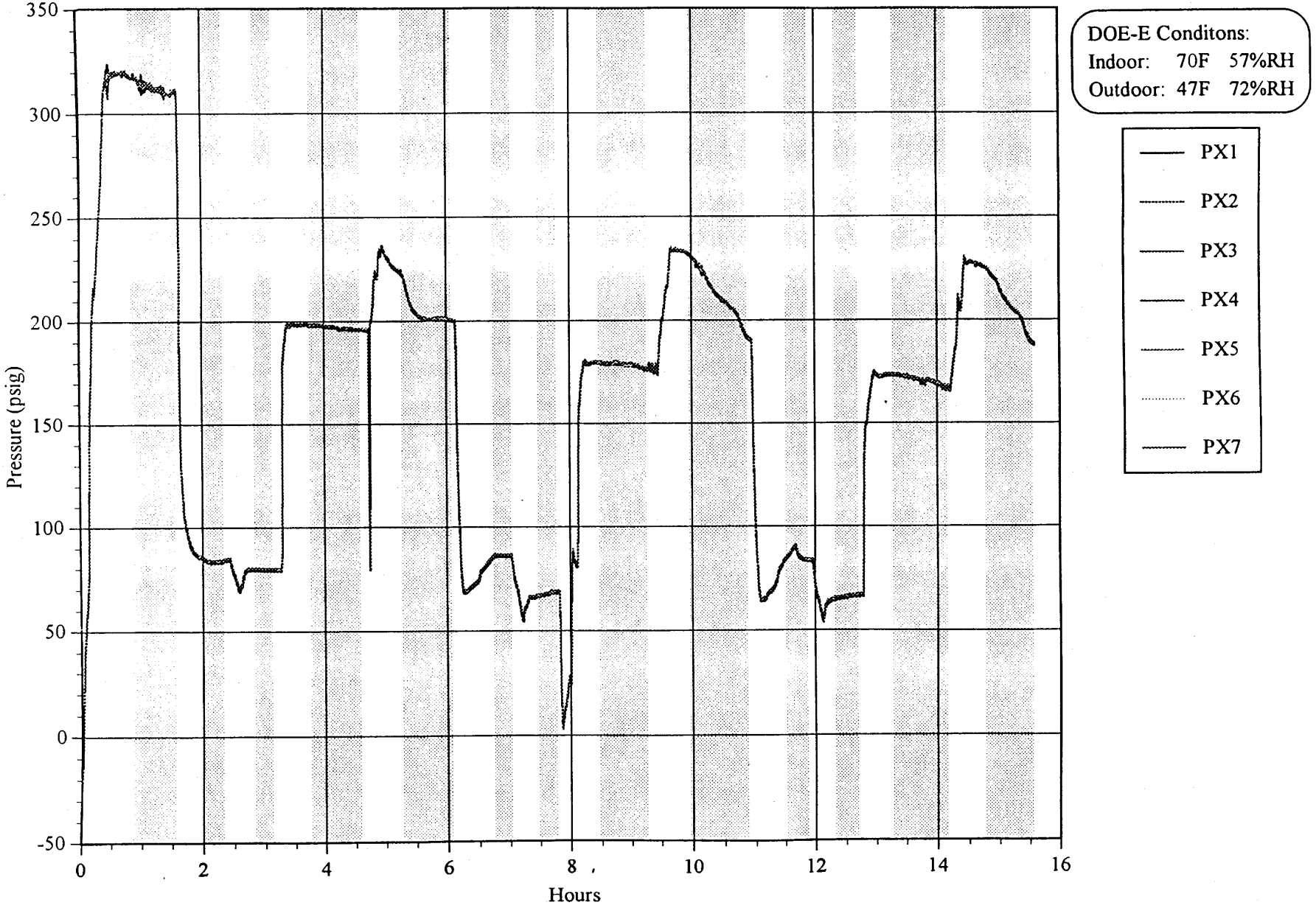

Fig. B.1.2-24 Heat Pump R407C Fractionation Test 4

Air Side Temperatures

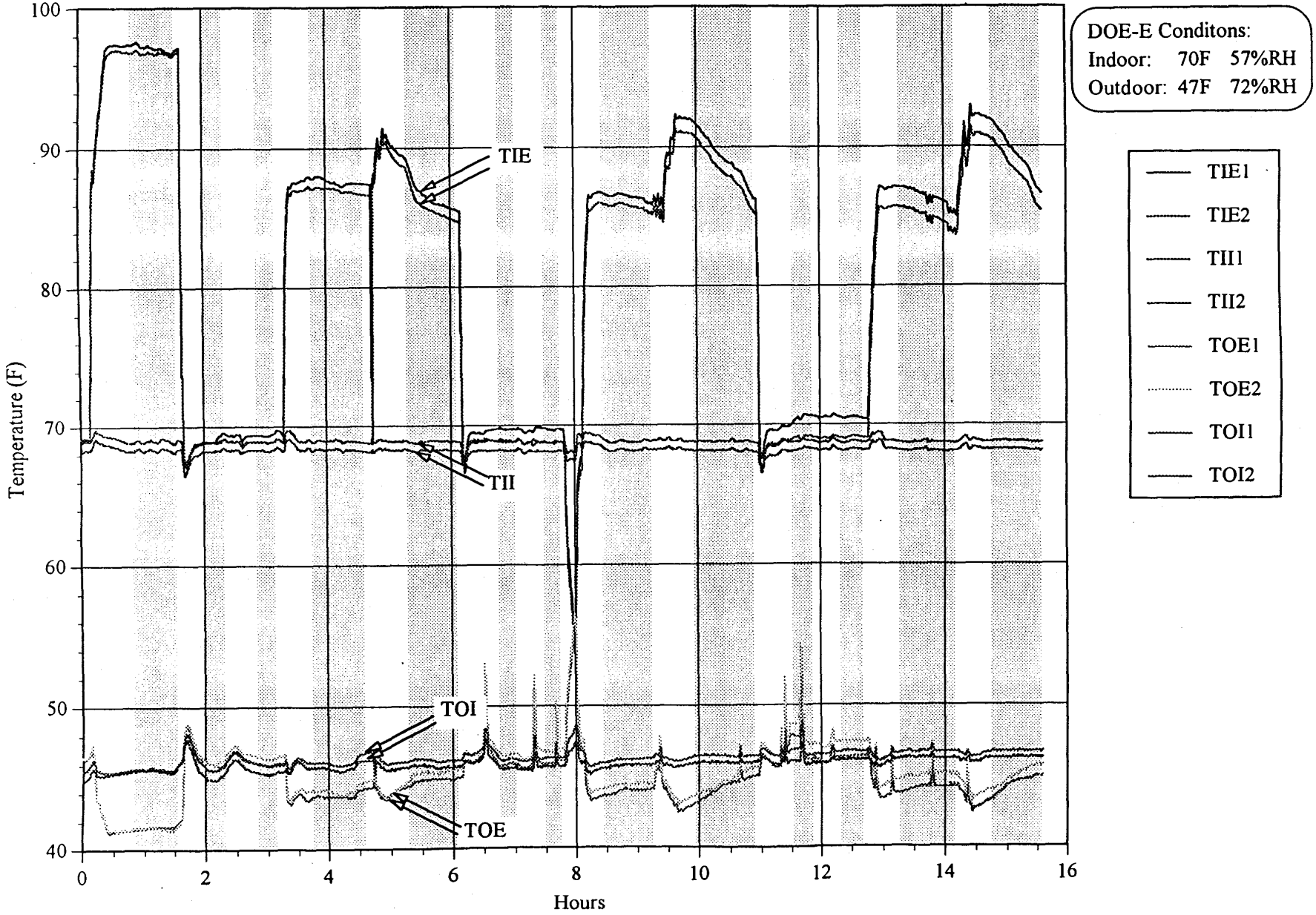

Fig. B.1.2-4 Heat Pump R407C Fractionation Test 4

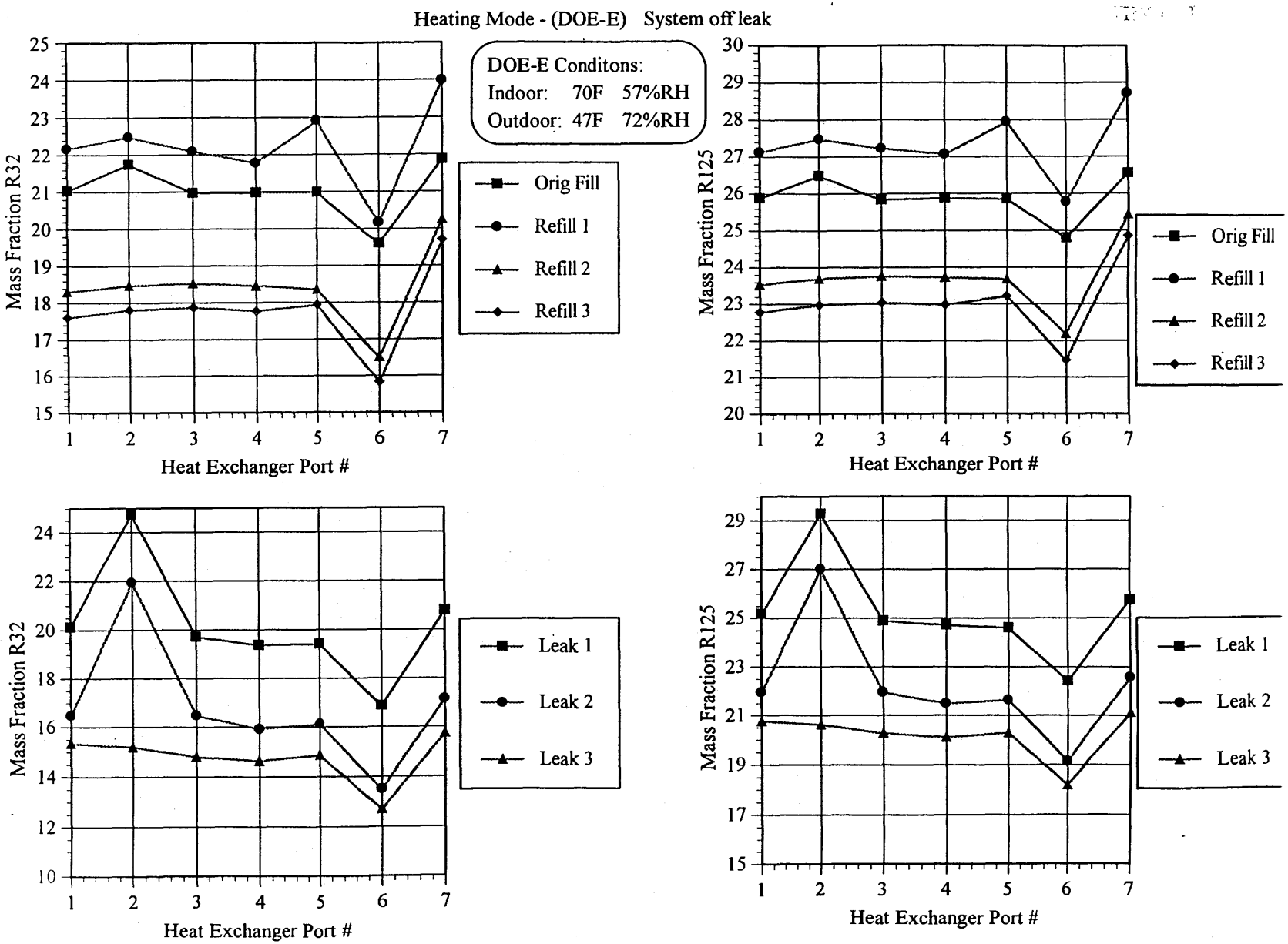

Summary of ARTI Test Run #5: Heating Mode operation at DOE-E with system on leak

THS 9/7/95

		STD1	STD2	P#1	P#2	P#3	P#4	STD1	STD2	Notes:
ART0907a	R32	21.06	0.05	29.13	20.91	20.68	20.88	21.06	0.09	System on; Full charge
	R125	25.68	74.82	32.45	25.74	25.54	25.68	25.67	74.75	
ART0907b	R32	21.06	0.09	28.56	20.77	20.76	20.81	21.06	0.12	System on; refilled to full charge
	R125	25.67	74.75	31.88	25.56	25.56	25.61	25.67	74.70	
ART0907c	R32	21.06	0.12	28.97	20.59	20.67	19.80	21.05	0.13	System on; refilled to full charge
	R125	25.67	74.70	32.29	25.38	25.47	24.77	25.65	74.68	
ART0907d	R32	21.05	0.13	28.67	20.59	20.73	20.61	21.06	0.13	System on; refilled to full charge
	R125	25.65	74.68	32.07	25.41	25.55	25.41	25.65	74.49	

- more than 2% deviation in calculated compositions

		HX1	HX2	HX3	HX4	HX5	HX6	HX7	wt(lbs)	leaked	added	circ
ART0907a	R32	20.84	20.81	20.82	20.80	20.89	19.10	20.04	7.47			20.83
	R125	25.65	25.61	25.62	25.60	25.65	24.32	24.96		1.915	1.915	25.63
ART0907b	R32	20.70	20.80	20.70	20.67	20.67	18.95	21.42	7.45			20.71
	R125	25.50	25.58	25.50	25.48	25.48	24.17	26.14		2.005	2.03	25.51
ART0907c	R32	20.63	20.64	20.65	20.63	20.62	18.75	19.64	7.455			20.64
	R125	25.44	25.44	25.46	25.44	25.43	23.98	24.61		2	2.105	25.44
ART0907d	R32	20.55	20.56	20.57	20.54	20.68	18.56	21.04	7.54			20.58
	R125	25.36	25.37	25.38	25.34	25.45	23.81	25.76				25.38

Test 5 (9/7/95)

OVERALL COMPOSITIONS

	R32	R125	R134a
initial charge =	20.45	25.22	54.33
after discharge 1 =	20.43	25.2	54.38
after refill 1=	20.39	25.19	54.42
after discharge 2 =	20.51	25.29	54.2
after refill 2=	20.48	25.28	54.23
after discharge 3 =	20.51	25.22	54.26
after refill 3=	20.4	25.17	54.43

circulating composition

	R32	R125	R134a
startup	20.82	25.65	53.52
after r	20.78	25.58	53.64
after r	20.35	25.21	54.44
after r	20.64	25.46	53.9

	R32	R125	R134a
initial charge	20.45	25.22	54.33
recharge 1 =	20.28	25.16	54.56
recharge 2 =	20.42	25.26	54.31
recharge 3 =	20.09	25.04	54.87
avg	20.31	25.17	54.52

	R32	R125	R134a
discharge 1 vapor=	26.2	30.37	43.43
discharge 1 liquid=	14.8	20.18	65.02
overall discharge 1=	20.52	25.29	54.19
discharge 2 vapor=	25.57	29.88	44.55
discharge 2 liquid=	15.12	20.43	64.44
overall discharge 2=	20.07	24.91	55.02
discharge 3 vapor=	26.24	30.66	43.1
discharge 3 liquid=	15.02	20.62	64.36
overall discharge 3=	20.41	25.44	54.15

Table B.2-5. R407C –Test Data – Sequence #5

ARTI Run 5 (DOE E - System on leak)

Data Summaries:	start	finish	avg	time(sec	POWER	FLOW	ctons	htons	ckw/ton	hkw/ton
ART0907a	7065	8739	7902	7893	3816	328	1.04	2.51	3.68	1.52
ART0907b	14226	15970	15098	15093	3754	322	1.01	2.50	3.71	1.50
ART0907c	21078	22913	21996	22033	3635	314	0.99	2.48	3.68	1.47
ART0907d	28145	29844	28994	29024	3584	308	0.95	2.45	3.79	1.46

	TIE1	TIE2	TII1	TII2	TOE1	TOE2	TOI1	TOI2
ART0907a	96.8	95.6	68.0	68.9	40.5	40.7	45.0	45.0
ART0907b	96.8	95.5	67.9	68.9	40.7	40.9	45.2	45.0
ART0907c	96.5	95.2	68.0	68.9	40.8	41.0	45.2	45.1
ART0907d	96.2	94.9	68.0	68.9	41.0	41.2	45.1	45.1

	PS1	PS2	PS3	PS4	PS5	PS6
ART0907a	301.8	301.8	296.2	67.6	47.0	41.2
ART0907b	296.1	296.6	291.3	66.2	46.4	40.7
ART0907c	289.2	289.8	284.3	64.6	45.2	39.5
ART0907d	283.2	283.5	278.3	63.1	44.2	38.6

	TS1	TS2	TS3	TS4	TS5	TS6	TS7	TS8
ART0907a	200.9	178.8	95.4	34.0	38.3	29.6	30.2	83.8
ART0907b	203.9	181.8	95.3	33.4	39.1	34.4	34.8	86.5
ART0907c	204.2	181.9	94.6	32.3	39.4	37.6	37.8	83.4
ART0907d	204.6	181.8	94.2	31.4	39.7	39.4	39.6	84.0

	PX1	PX2	PX3	PX4	PX5	PX6	PX7
ART0907a	299.4	299.1	299.5	299.5	298.6	299.5	299.6
ART0907b	294.0	293.7	294.7	294.9	293.7	294.1	294.6
ART0907c	287.4	287.0	287.5	287.5	286.6	287.4	287.6
ART0907d	281.1	280.7	281.1	281.1	280.3	281.1	281.4

	TX1	TX2	TX3	TX4	TX5	TX6	TX7
ART0907a	94.2	89.4	91.4	93.7	109.8	112.1	118.4
ART0907b	94.3	89.6	91.6	93.8	109.8	111.7	117.4
ART0907c	93.8	89.3	91.3	93.3	109.0	110.4	116.0
ART0907d	93.4	89.1	91.0	93.1	108.6	109.9	114.8

Fig. B.1.2-25 Heat Pump R407C Fractionation Test 5

Heating Mode - (DOE-E) System on leak

System Temperatures

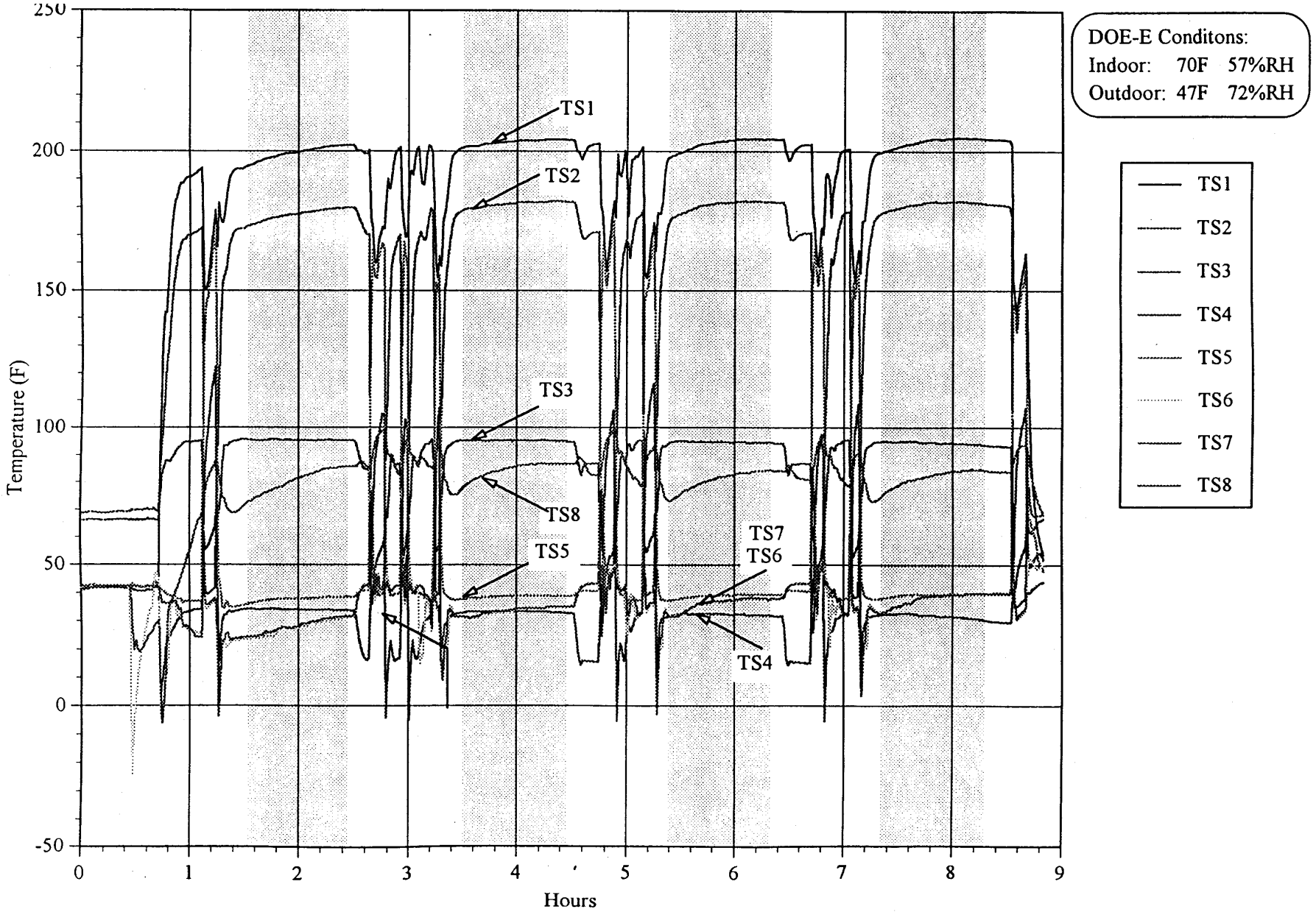

Fig. B.1.2-26 Heat Pump R407C Fractionation Test 5

Heating Mode - (DOE-E) System on leak

System Pressures

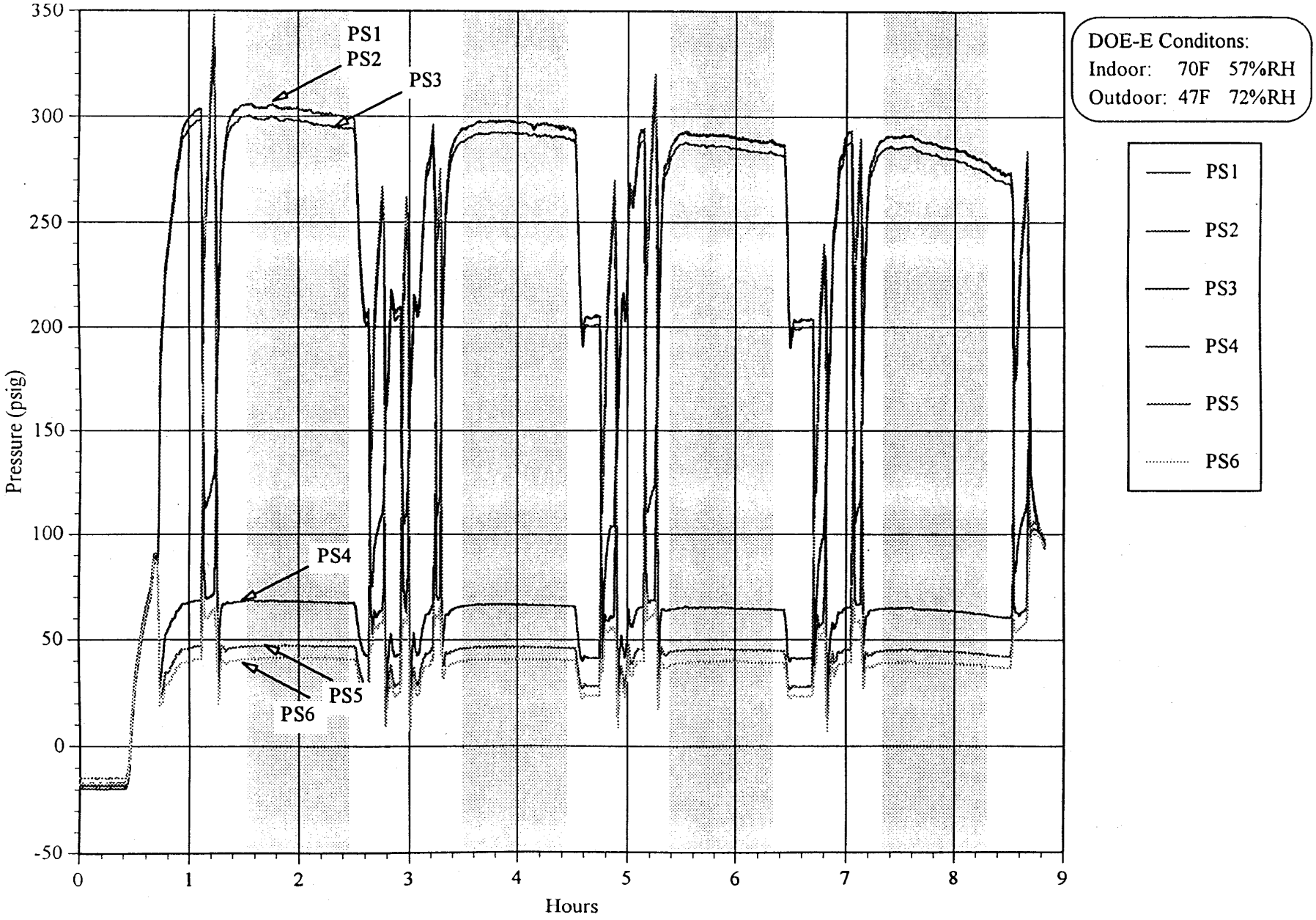

Fig. B.1.2-27 Heat Pump R407C Fractionation Test 5

Heating Mode - (DOE-E) System on leak

Air Side Temperatures

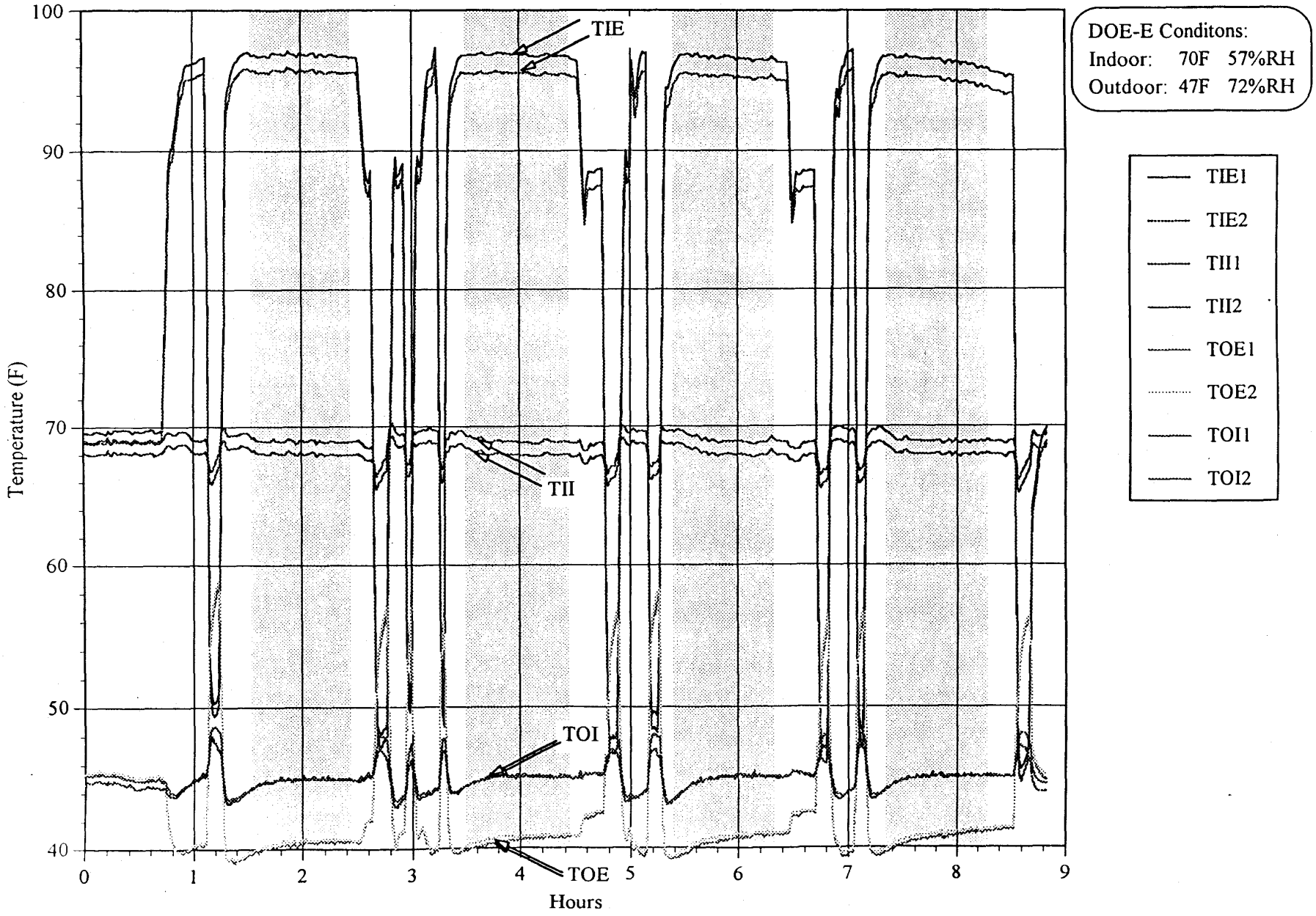

Fig. B.1.2-28 Heat Pump R407C Fractionation Test 5

Heating Mode - (DOE-E) System on leak

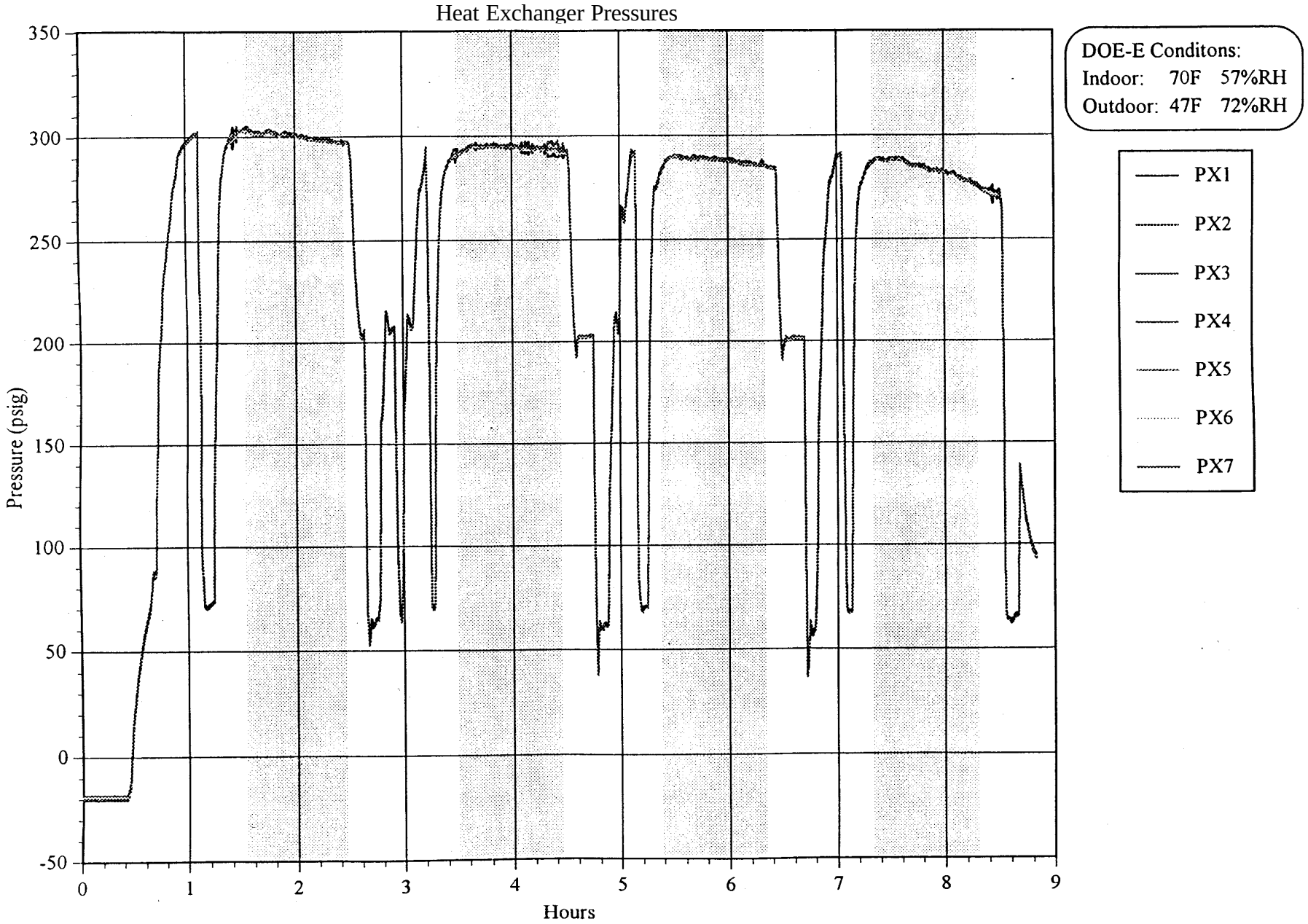

Fig. B.1.2-29 Heat Pump R407C Fractionation Test 5

Heating Mode - (DOE-E) System on leak

Heat Exchanger Temperatures

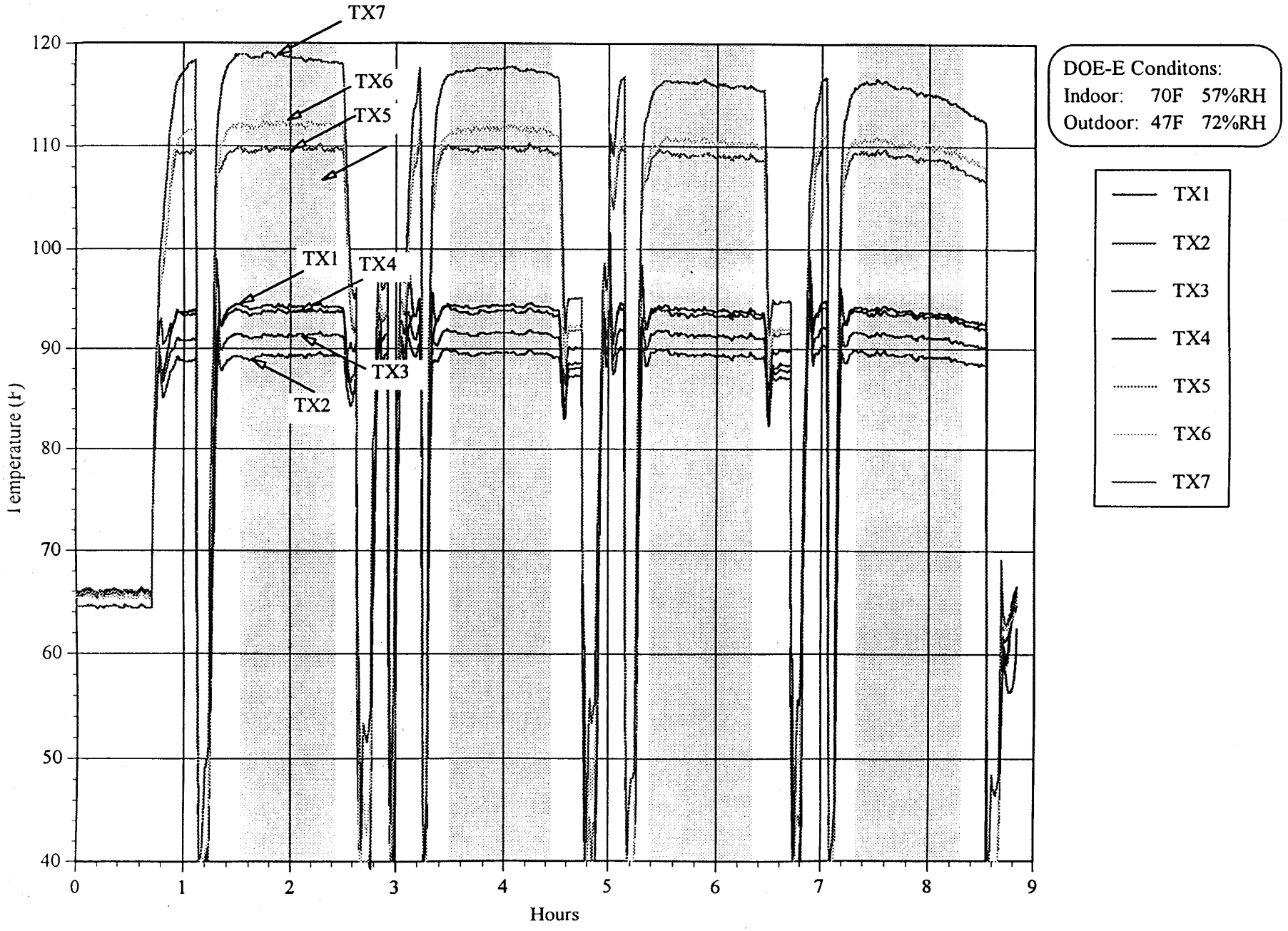

Fig. B.1.2-5 Heat Pump R407C Fractionation Test 5

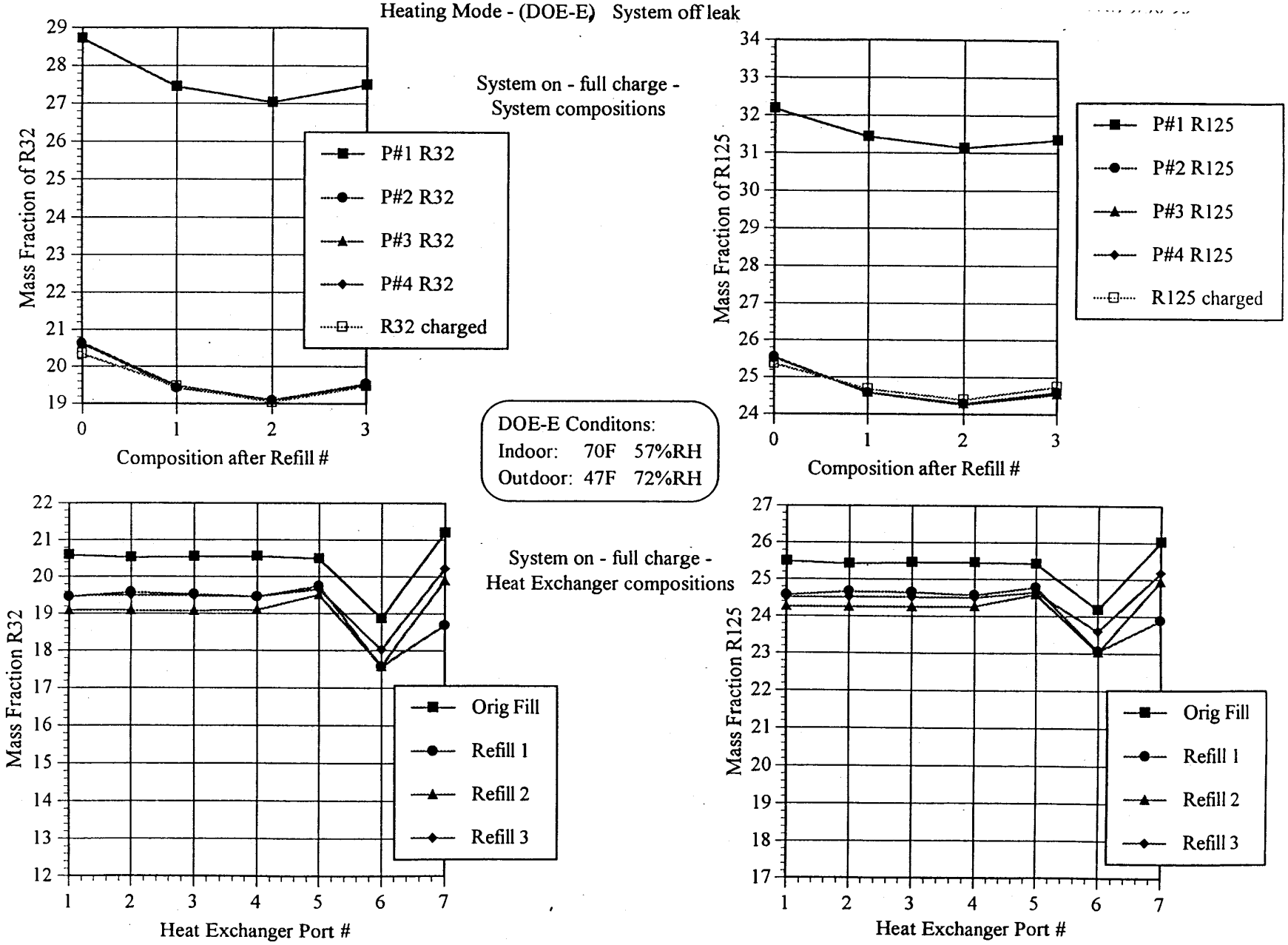

Summary of ARTI Test Run #6: Heating Mode operation at DOE-E with system off leak
THS 9/8/95

		STD1	STD2	P#1	P#2	P#3	P#4	STD1	STD2	Notes:
ART0908a	R32	21.06	0.09	28.71	20.62	20.60	20.64	21.05	0.11	System on; Full charge
	R125	25.67	74.61	32.17	25.54	25.53	25.54	25.66	74.56	
ART0908b	R32	21.05	0.11	27.45	19.42	19.48	19.46	21.05	0.11	System on; refilled to full charge
	R125	25.66	74.56	31.43	24.58	24.59	24.58	25.66	74.57	
ART0908c	R32	21.05	0.11	27.04	19.08	19.09	19.06	21.06	0.12	System on; refilled to full charge
	R125	25.66	74.57	31.14	24.29	24.29	24.25	25.66	74.56	
ART0908d	R32	21.06	0.12	27.50	19.54	19.50	19.48	21.04	0.13	System on; refilled to full charge
	R125	25.66	74.56	31.35	24.60	24.54	24.53	25.63	74.57	

▒▒▒▒ - more than 2% deviation in calculated compositions

		HX1	HX2	HX3	HX4	HX5	HX6	HX7	wt(lbs)	leaked	added
ART0908a	R32	20.59	20.52	20.55	20.55	20.49	18.87	21.20	7.425		
	R125	25.49	25.43	25.46	25.45	25.42	24.18	26.03		1.81	1.855
ART0908b	R32	19.45	19.58	19.53	19.45	19.74	17.57	18.69	7.45		
	R125	24.57	24.66	24.65	24.57	24.78	23.06	23.89		1.795	1.95
ART0908c	R32	19.09	19.09	19.08	19.10	19.51	17.58	19.90	7.585		
	R125	24.27	24.26	24.25	24.26	24.59	23.04	24.94		2.03	2.275
ART0908d	R32	19.48	19.50	19.49	19.46	19.65	18.02	20.22	7.81		
	R125	24.51	24.52	24.52	24.49	24.64	23.59	25.17			

Test 6 (9/8/95)

OVERALL COMPOSITIONS

	R32	R125	R134a
initial charge =	20.34	25.36	54.3
after discharge 1 =	19.2	24.5	56.3
after refill 1=	19.46	24.68	55.86
after discharge 2 =	18.46	23.99	57.55
after refill 2=	19.03	24.39	56.58
after discharge 3 =	18.88	24.37	56.75
after refill 3=	19.47	24.75	55.79

circulating composition

	R32	R125	R134a
startup	20.62	25.54	53.84
after r	19.45	24.58	55.97
after r	19.08	24.28	56.64
after r	19.51	24.56	55.94

	R32	R125	R134a
initial charge	20.34	25.36	54.30
recharge 1 =	20.25	25.23	54.53
recharge 2 =	20.70	25.55	53.75
recharge 3 =	20.90	25.68	53.42
avg	20.55	25.45	54

	R32	R125	R134a
discharge 1 vapor=	28.35	31.68	39.98
discharge 1 liquid=	18.52	23.63	57.86
overall discharge 1=	23.87	28.01	48.11
discharge 2 vapor=	28.24	31.57	40.19
discharge 2 liquid=	15.68	21.07	63.25
overall discharge 2=	22.58	26.84	50.59
discharge 3 vapor=	24.83	29.34	45.83
discharge 3 liquid=	14.78	20.23	64.98
overall discharge 3=	19.44	24.46	56.11

Table B.2-6. R407C - Test Data - Sequence #6

ARTI Run 6 (DOE E - System off leak)

Data Summaries:	start	finish	avg	time(sec	POWER	FLOW	ctons	htons	ckw/ton	hkw/ton
ART0908a	3525	7176	5351	5335	3797	328	1.02	2.50	3.72	1.52
ART0908b	12470	16493	14482	14499	3613	303	1.01	2.43	3.58	1.49
ART0908c	20948	24217	22583	22143	3582	314	1.03	2.41	3.50	1.49
ART0908d	28752	32534	30643	30133	3555	309	1.01	2.40	3.51	1.48

	TIE1	TIE2	TII1	TII2	TOE1	TOE2	TOI1	TOI2
ART0908a	96.8	95.8	68.1	69.0	40.5	40.5	44.8	44.8
ART0908b	95.9	95.1	68.1	69.0	40.4	40.4	44.8	44.7
ART0908c	95.8	94.8	68.1	69.1	40.4	40.5	44.8	44.7
ART0908d	95.4	94.6	68.0	68.9	40.4	40.5	44.8	44.7

	PS1	PS2	PS3	PS4	PS5	PS6
ART0908a	300.4	300.6	295.1	67.2	46.7	40.8
ART0908b	285.2	285.1	279.8	63.9	44.5	38.7
ART0908c	281.9	281.8	276.7	63.1	43.9	38.1
ART0908d	279.8	279.7	274.5	62.5	43.6	37.9

	TS1	TS2	TS3	TS4	TS5	TS6	TS7	TS8
ART0908a	198.3	176.4	95.1	33.6	38.6	27.4	27.9	82.2
ART0908b	197.5	175.7	94.2	32.8	38.8	32.5	33.0	80.5
ART0908c	197.6	175.7	94.2	32.8	38.9	33.9	34.3	78.9
ART0908d	200.1	177.8	93.7	31.8	39.2	36.9	37.2	80.3

	PX1	PX2	PX3	PX4	PX5	PX6	PX7
ART0908a	298.2	297.9	298.9	299.1	297.8	298.2	298.7
ART0908b	283.0	282.3	282.8	283.0	282.1	282.7	283.1
ART0908c	279.8	279.0	279.7	279.8	278.9	279.5	279.9
ART0908d	277.7	276.9	277.5	277.6	276.7	277.4	277.8

	TX1	TX2	TX3	TX4	TX5	TX6	TX7
ART0908a	93.9	89.0	91.0	93.5	109.6	111.6	118.0
ART0908b	93.2	88.8	90.7	93.3	109.1	110.2	116.2
ART0908c	93.2	88.7	90.6	93.2	108.8	110.0	115.9
ART0908d	92.8	88.3	90.3	93.0	108.5	109.6	115.1

Fig. B.1.2-30 Heat Pump R407C Fractionation Test 6

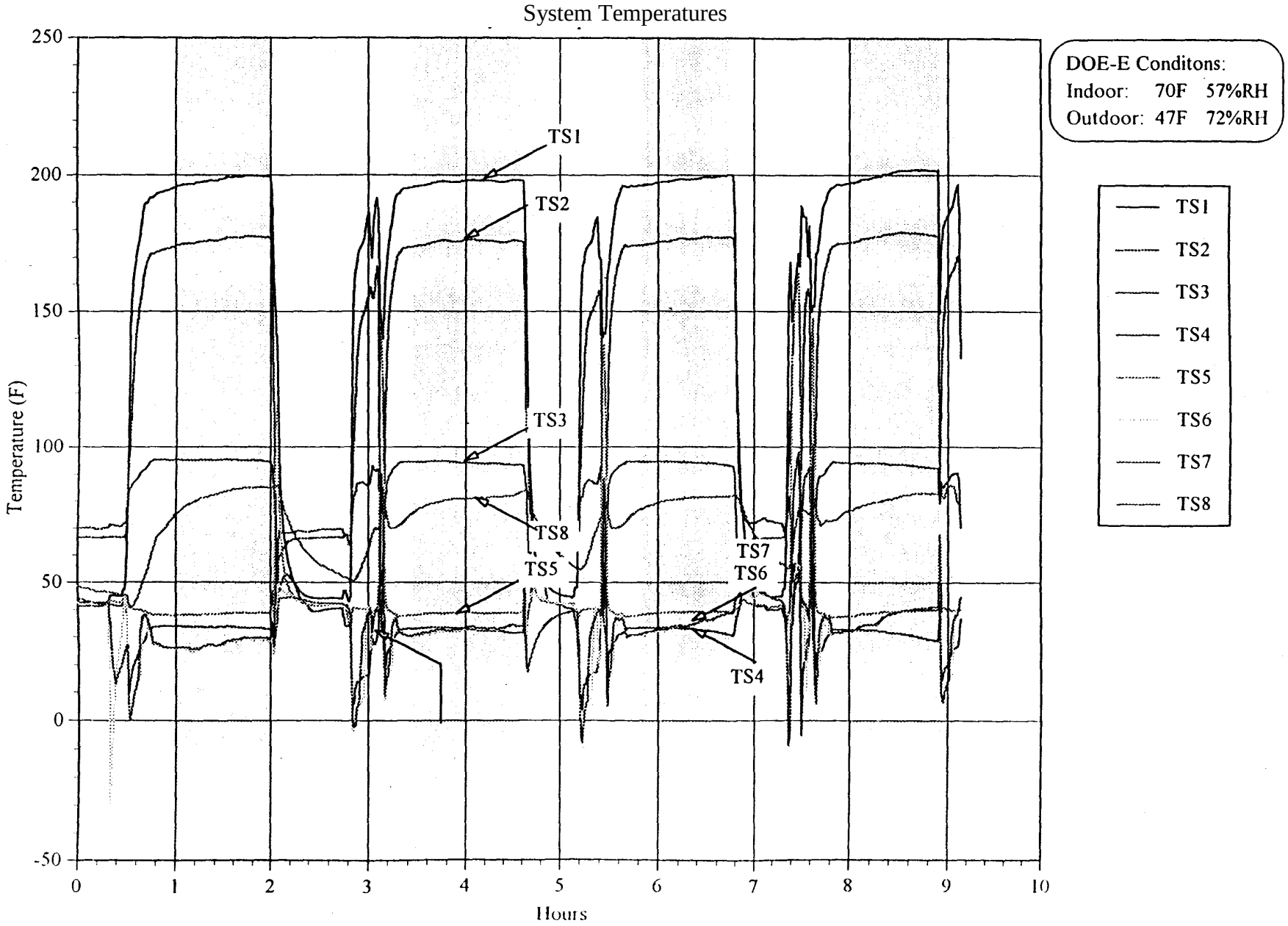

Fig. B.1.2-31 Heat Pump R407C Fractionation Test 6

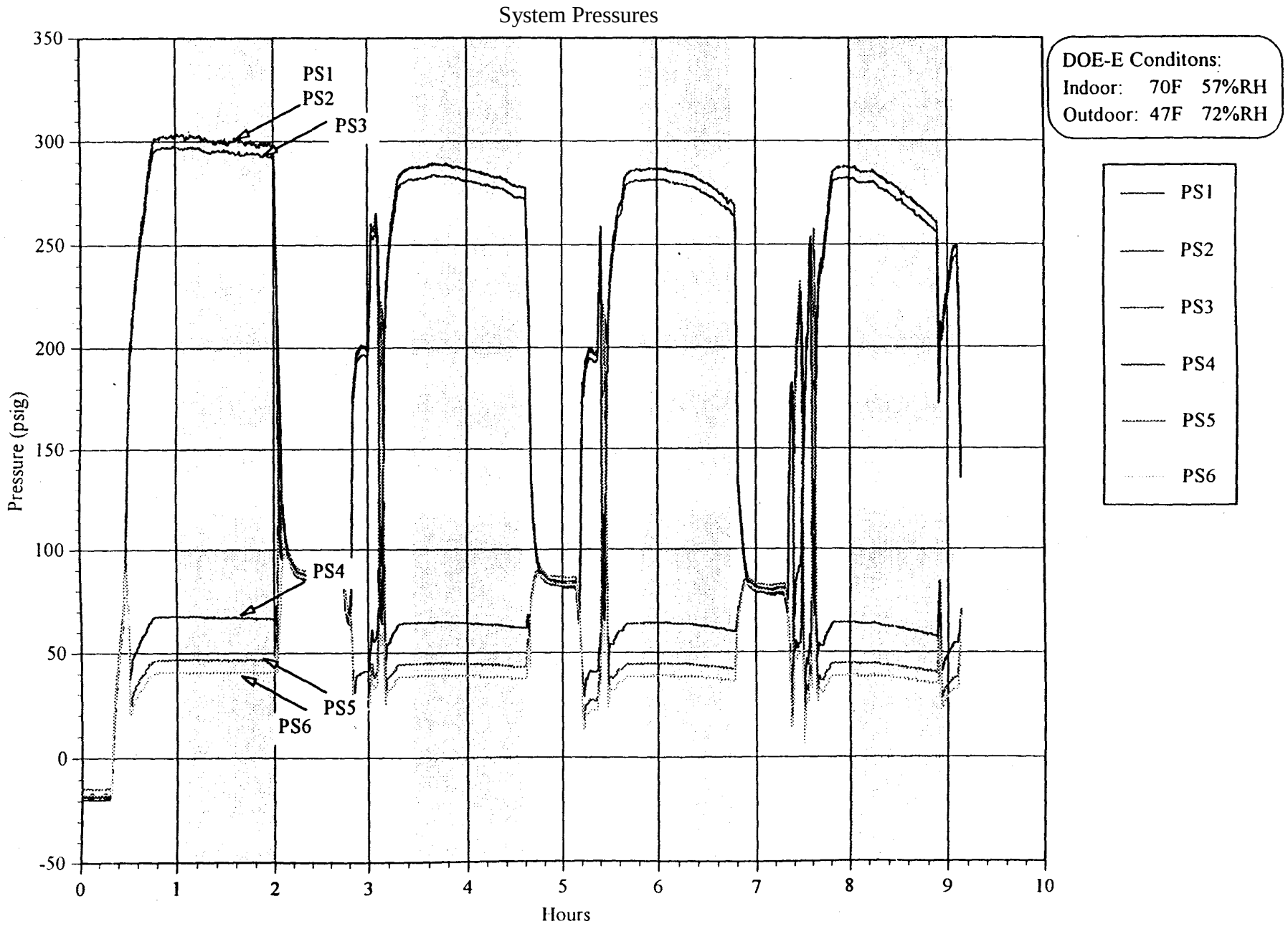

Fig. B.1.2-32 Heat Pump R407C Fractionation Test 6

Heating Mode - (DOE-E) System off leak

Air Side Temperatures

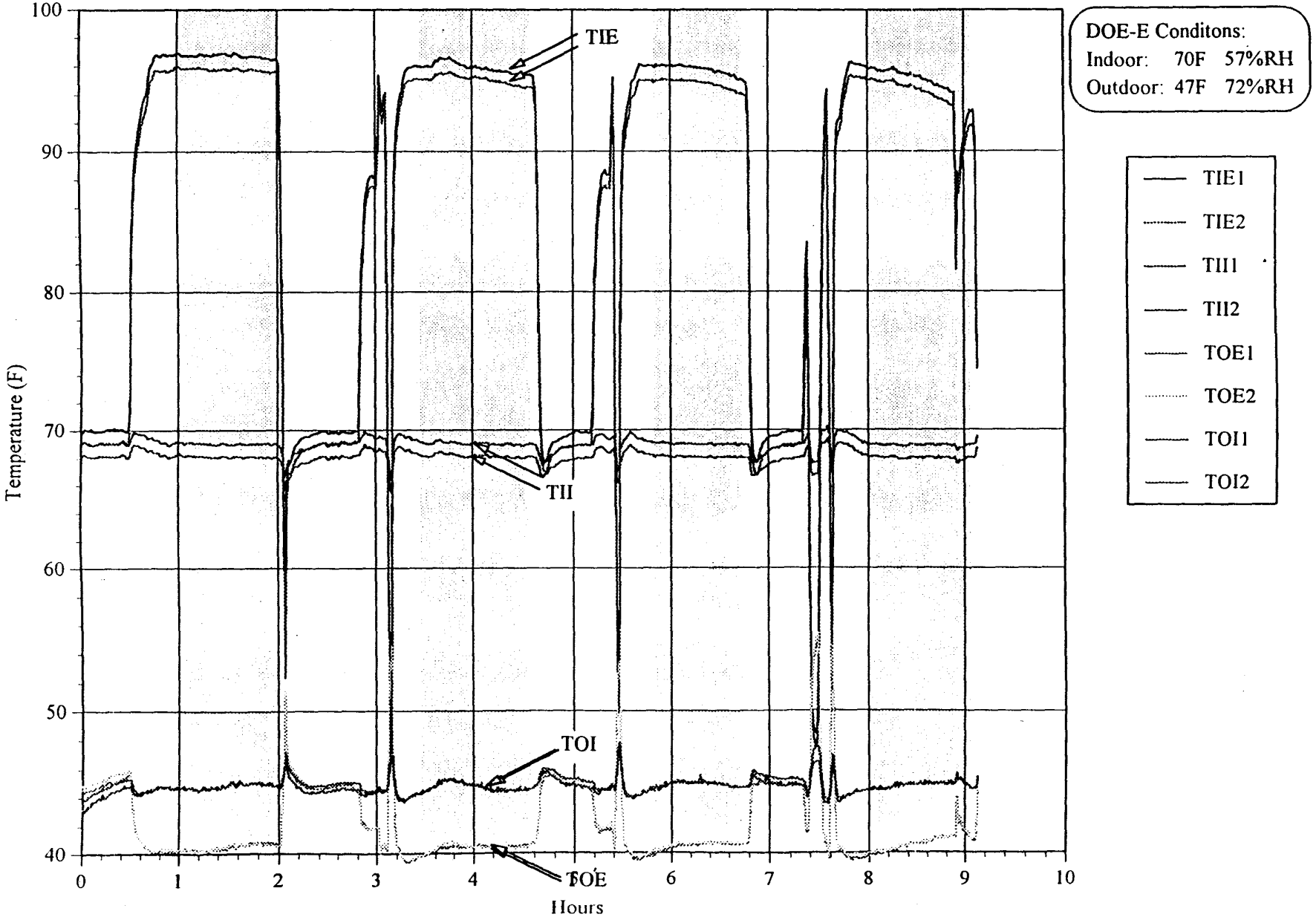

Fig. B.1.2-33 Heat Pump R407C Fractionation Test 6

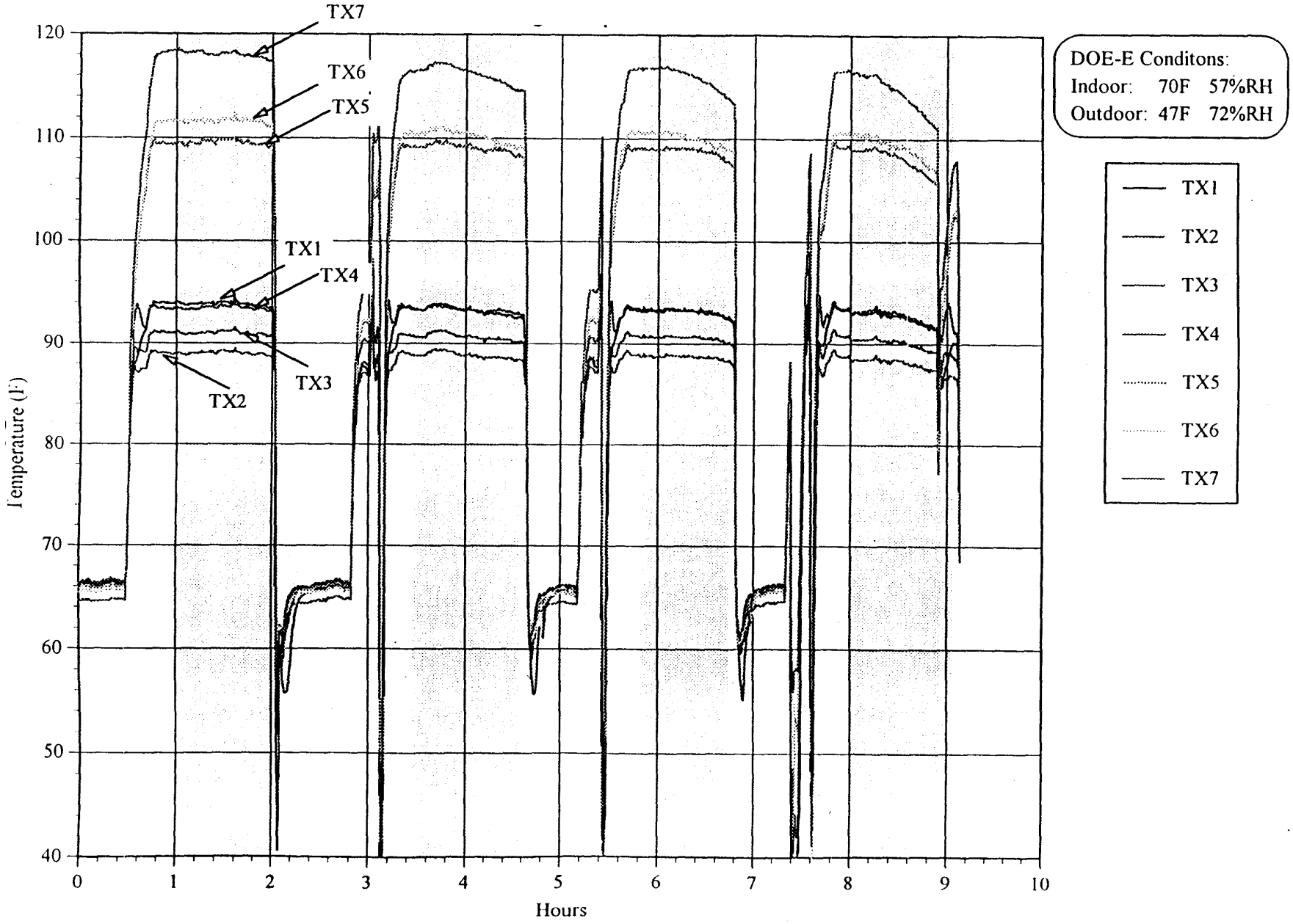

Fig. B.1.2-34 Heat Pump R407C Fractionation Test 6
Heating Mode - (DOE-E) System off leak